

INFORMATION TO USERS

This manuscript has been reproduced from the microfilm master. UMI films the text directly from the original or copy submitted. Thus, some thesis and dissertation copies are in typewriter face, while others may be from any type of computer printer.

The quality of this reproduction is dependent upon the quality of the copy submitted. Broken or indistinct print, colored or poor quality illustrations and photographs, print bleedthrough, substandard margins, and improper alignment can adversely affect reproduction.

In the unlikely event that the author did not send UMI a complete manuscript and there are missing pages, these will be noted. Also, if unauthorized copyright material had to be removed, a note will indicate the deletion.

Oversize materials (e.g., maps, drawings, charts) are reproduced by sectioning the original, beginning at the upper left-hand corner and continuing from left to right in equal sections with small overlaps.

Photographs included in the original manuscript have been reproduced xerographically in this copy. Higher quality 6" x 9" black and white photographic prints are available for any photographs or illustrations appearing in this copy for an additional charge. Contact UMI directly to order.

Bell & Howell Information and Learning
300 North Zeeb Road, Ann Arbor, MI 48106-1346 USA

UMI[®]
800-521-0600

MECHANICAL PERFORMANCE OF LANDFILL
LEACHATE COLLECTION PIPES

by

Richard W. I. Brachman

Graduate Program in Engineering Science
Department of Civil and Environmental Engineering

Submitted in partial fulfilment
of the requirements for the degree of
Doctor of Philosophy

Faculty of Graduate Studies
The University of Western Ontario
London, Ontario
April, 1999

© R.W.I. Brachman 1999



National Library
of Canada

Acquisitions and
Bibliographic Services

395 Wellington Street
Ottawa ON K1A 0N4
Canada

Bibliothèque nationale
du Canada

Acquisitions et
services bibliographiques

395, rue Wellington
Ottawa ON K1A 0N4
Canada

Your file Votre référence

Our file Notre référence

The author has granted a non-exclusive licence allowing the National Library of Canada to reproduce, loan, distribute or sell copies of this thesis in microform, paper or electronic formats.

The author retains ownership of the copyright in this thesis. Neither the thesis nor substantial extracts from it may be printed or otherwise reproduced without the author's permission.

L'auteur a accordé une licence non exclusive permettant à la Bibliothèque nationale du Canada de reproduire, prêter, distribuer ou vendre des copies de cette thèse sous la forme de microfiche/film, de reproduction sur papier ou sur format électronique.

L'auteur conserve la propriété du droit d'auteur qui protège cette thèse. Ni la thèse ni des extraits substantiels de celle-ci ne doivent être imprimés ou autrement reproduits sans son autorisation.

0-612-42503-7

Canada

المنارة للاستشارات


THE UNIVERSITY OF WESTERN ONTARIO
FACULTY OF GRADUATE STUDIES

CERTIFICATE OF EXAMINATION

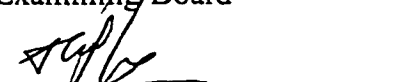
Chief Advisor



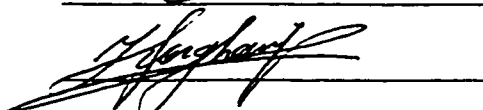
Advisory Committee



Examining Board







Dr. J.P. Carter


The thesis by
Richard W. I. Brachman

entitled

Mechanical Performance of Landfill Leachate Collection Pipes

is accepted in partial fulfilment of the
requirements for the degree of
Doctor of Philosophy

Date June 7, 1999


Chair of Examining Board

ABSTRACT

A laboratory study of the mechanical performance of perforated leachate collection pipes for use in municipal solid waste landfills was conducted. Although the use of uniformly-graded coarse gravel is desirable in landfill leachate collection systems to minimize the biologically induced clogging of the drainage layer, the extent to which the coarse gravel affects the mechanical performance of the pipe was previously unknown. It was also uncertain whether larger perforations – that are also needed to minimize the degree of clogging of the perforations – have a detrimental effect on the mechanical performance of the pipe. As a result of these uncertainties, finer gravel and smaller perforations have been used in landfills. This thesis describes a laboratory testing program conducted to assess the effects of coarse gravel backfill and large perforations on the structural response of high density polyethylene (HDPE) pipes for use in landfill leachate collection systems.

An approximate numerical technique employing Fourier Integrals is used to examine a shallow buried pipe under stiff plate loading, and it is shown that results obtained for a leachate collection pipe tested at Ohio University are substantially different from the response expected in a landfill. A new laboratory facility that simulates the biaxial earth pressures that act on a deeply buried pipe was therefore designed and developed to permit the measurement of the response of these pipes under controlled experimental conditions.

Pipe deflections with larger magnitudes and greater variations were caused by the coarse gravel backfill relative to those with a medium-dense sand backfill. For the 220 mm outside diameter, 25 mm thick HDPE pipes tested, the average vertical and horizontal diameter changes were approximately -1% and 0.8%, of the mean diameter at an applied

pressure of 250 kPa (representative overburden stresses for a medium size landfill with 20 to 25 metres of waste), and are less than allowable performance limits. Good agreement between measured and calculated deflections was obtained with an elastic arching solution.

The influence of 25 mm diameter perforations was found to be small on the strains measured at the crown, springline or invert compared to the dominant influence of the coarse gravel. It is shown that 25 mm diameter holes located at the quarter-points and at an axial spacing of 150 mm did not significantly increase stresses in the pipe or increase the likelihood of failure.

The maximum compressive hoop strain was measured at the interior springline; the maximum tensile hoop strain occurred at the interior invert. Both hoop and axial strains (and therefore stresses) were heavily influenced by local bending effects caused by the coarse gravel backfill. Maximum strains were approximately twice as large as the mean response. Tensile stresses estimated in the pipe are below the allowable long-term hydrostatic design stress for this material when subject to 250 kPa of vertical surcharge. Thus, despite the local bending stresses from the coarse gravel and stress redistribution from perforations, these pipes – for the specific conditions tested – are sufficiently thick to limit the potentially detrimental effect from the gravel and perforations and are therefore expected to perform well in a medium-size landfill (at least up to 250 kPa). Preliminary recommendations for the design of landfill leachate collection pipes when subject to larger pressures are provided.

KEYWORDS: landfill, leachate collection system, perforated pipes, high density polyethylene pipes, deeply buried pipes, pipe testing, three dimensional finite element analysis, soil structure interaction.

CO-AUTHORSHIP

This thesis contains material submitted for publication that has been co-authored by R.W.I. Brachman and his supervisors, I.D. Moore and R.K. Rowe. R.W.I. Brachman was the principal author for these manuscripts, and initiated and conducted the research reported in the thesis.

ACKNOWLEDGEMENTS

The laboratory testing reported in this thesis has been conducted in conjunction with the research work of Mr. Andrew Tognon. His original contributions to the techniques devised to permit strain measurements, the development of the diaphragm bladder, and the method used to minimize boundary friction were invaluable and enabled the laboratory testing for this thesis. For these, and his collaboration with conducting all of the laboratory tests, the author wishes to express his deepest appreciation.

This research has been conducted under the supervision of Drs. I.D. Moore and R.K. Rowe. The author is grateful for their guidance and contributions to this research project.

The assistance of: Dr. F.M. Bartlett; Messrs. Wilbert Logan, Gary Lusk, and Jon Southen; Ms. Trudy Laidlaw; and Messrs. Bob Stuart, Gord Debbert, and Dick Spencer are gratefully acknowledged. Financial support was received from the citizens of Canada and Ontario through the award of PGS-B Scholarship from the Natural Sciences and Engineering Research Council of Canada, and an Ontario Graduate Scholarship.

TABLE OF CONTENTS

CERTIFICATE OF EXAMINATION / ii

ABSTRACT / iii

CO-AUTHORSHIP / v

ACKNOWLEDGEMENTS / v

TABLE OF CONTENTS / vi

1. INTRODUCTION

1.1 DESCRIPTION OF PROBLEM / 1

1.2 CURRENT STATE OF PRACTICE / 3

1.3 RESEARCH OBJECTIVES AND METHODOLOGY / 5

1.4 SCOPE OF THESIS / 6

1.4.1 Interpretation of Ohio University Pipe Tests - Chapter 2 / 6

1.4.2 Hoop Compression Laboratory Testing - Chapter 3 / 6

1.4.3 Design of a New Laboratory Facility for Testing Small Diameter Buried Pipes - Chapter 4 / 7

1.4.4 Performance of a New Laboratory Facility for Testing Small Diameter Pipes Under Simulated Biaxial Earth Pressures - Chapter 5 / 8

1.4.5 Laboratory Investigation of the Effect of Coarse Gravel Backfill on the Mechanical Performance of Perforated Leachate Collection Pipes - Chapter 6 / 8

1.5 FORMAT OF THESIS / 9

1.6 REFERENCES / 9

2. ANALYSIS AND INTERPRETATION OF A BURIED PIPE TEST CONDUCTED IN THE OHIO UNIVERSITY FACILITY

2.1 INTRODUCTION / 11

2.2 DESCRIPTION OF OHIO UNIVERSITY TEST FACILITY / 13

2.3 METHOD OF ANALYSIS / 14

2.3.1 Finite Element Model / 15

2.3.2 Selection of Material Parameters / 16

2.4 THREE DIMENSIONAL ELASTIC ANALYSIS / 17

2.4.1 Description of Analysis / 18

2.4.2 Notation and Influence Matrix / 19

2.4.3 Calculation of Influence Coefficients Using Fourier Integrals / 21

2.4.4 Assembly of Final Solution / 23

2.4.5	Analysis of a Rectangular Rigid Footing on an Elastic Layer / 24
2.5	ANALYSIS OF A SHALLOW BURIED PIPE UNDER STIFF PLATE LOADING / 28
2.5.1	Calculated Contact Pressure / 28
2.5.2	Calculated Soil Stresses / 28
2.5.2.1	<i>Vertical Stresses / 29</i>
2.5.2.2	<i>Horizontal Stresses / 31</i>
2.5.2.3	<i>Axial Stresses / 32</i>
2.5.2.4	<i>Three-Dimensional Variation of Soil Stresses and Pipe Deflections / 32</i>
2.5.2.5	<i>Two-Dimensional Inelastic Stress Predictions / 32</i>
2.5.3	Interpretation of Pipe Deformations / 35
2.5.4	Interpretation of Thrusts and Moments / 37
2.6	SUMMARY AND CONCLUSIONS / 38
2.7	REFERENCES / 40
3.	HOOP COMPRESSION TESTING OF HDPE LEACHATE COLLECTION PIPE
3.1	INTRODUCTION / 59
3.2	HOOP COMPRESSION TESTING / 61
3.3	BACKFILL MATERIALS / 63
3.4	INSTRUMENTATION / 64
3.4.1	Pipe Deflections / 64
3.4.2	Pipe Strains / 64
3.5	RESULTS FOR TEST H1 - SAND BACKFILL / 67
3.5.1	Pipe Deformations / 67
3.5.2	Surface Strains / 67
3.5.3	Estimate of Strain Gauge Stiffening / 69
3.6	RESULTS FOR TEST H2a AND H2b RESULTS - COARSE GRAVEL BACKFILL / 70
3.6.1	Pipe Deformations / 71
3.6.2	Surface Strains / 71
3.6.3	Calculated Stresses / 74
3.7	PERFORATIONS / 76
3.7.1	Sand Backfill / 76
3.7.2	Coarse Gravel Backfill / 78
3.7.3	Estimate of Stresses Near Perforation / 79
3.8	SUMMARY / 81
3.9	REFERENCES / 82

- 4. THE DESIGN OF A LABORATORY FACILITY FOR EVALUATING THE STRUCTURAL RESPONSE OF SMALL DIAMETER BURIED PIPES**
- 4.1 INTRODUCTION / 103
- 4.2 LOADING CONDITIONS UNDER DEEP BURIAL / 105
- 4.3 SIMULATION OF VERTICAL EARTH PRESSURE / 106
- 4.4 SIMULATION OF LATERAL EARTH PRESSURE / 108
- 4.5 SELECTION OF TEST CELL DIMENSIONS / 109
- 4.6 INFLUENCE OF SIDE WALL FRICTION ON SOIL RESPONSE / 112
- 4.7 INFLUENCE OF SIDE WALL FRICTION ON SOIL AND PIPE RESPONSE / 116
- 4.7.1 Soil Stresses / 117
- 4.7.2 Pipe Response / 119
- 4.8 INFLUENCE OF LATERAL BOUNDARY STIFFNESS ON SOIL AND PIPE RESPONSE / 120
- 4.8.1 Soil Response / 121
- 4.8.2 Pipe Response / 123
- 4.9 TEST CELL DESIGN / 124
- 4.10 SUMMARY / 125
- 4.11 REFERENCES / 126
-
- 5. PERFORMANCE OF A NEW LABORATORY FACILITY FOR TESTING SMALL DIAMETER PIPES UNDER SIMULATED BIAXIAL EARTH PRESSURES**
- 5.1 INTRODUCTION / 147
- 5.2 DESCRIPTION OF LABORATORY FACILITY / 148
- 5.2.1 Laboratory Apparatus / 148
- 5.2.2 Simulation of Vertical and Horizontal Stresses / 148
- 5.2.2.1 *Vertical Pressures* / 148
- 5.2.2.2 *Horizontal Pressures* / 150
- 5.2.3 Limiting Boundary Friction / 151
- 5.3 DESCRIPTION OF LABORATORY TESTS / 152
- 5.3.1 Soil Materials Tested / 152
- 5.3.1.1 *Test P2a* / 152
- 5.3.1.2 *Test P2b* / 153
- 5.3.2 Details of Pipe Specimens / 154
- 5.3.3 Axial End Conditions / 155

5.3.4	Instrumentation / 157
5.3.4.1	<i>Pipe Strains / 157</i>
5.3.4.2	<i>Pipe Deflections / 158</i>
5.3.4.3	<i>Earth Pressure Cells / 158</i>
5.3.4.4	<i>Settlement Plates / 159</i>
5.4	RESULTS FOR TEST P2a / 160
5.4.1	Measured Surface Strains for Test P2a / 160
5.4.1.1	<i>Hoop Strains at Section C / 160</i>
5.4.1.2	<i>Axial Strains at Section C / 161</i>
5.4.1.3	<i>Variation of Strains Along Pipe / 162</i>
5.4.2	Pipe Deflections for Test P2a / 163
5.5	ASSESSMENT OF BOUNDARY CONDITIONS / 164
5.5.1	Soil Deformations / 165
5.5.2	Boundary Stress Measurements / 166
5.5.3	Test Cell Deflections / 167
5.6	RESULTS FOR TEST P2b / 170
5.6.1	Measured Surface Strains for Test P2b / 171
5.6.1.1	<i>Hoop Strains at Section C - P2b / 171</i>
5.6.1.2	<i>Axial Strains at Section C - P2b / 172</i>
5.6.1.3	<i>Comparison of Measured Strains Between Tests P2a and P2b / 172</i>
5.6.2	Pipe Deflections for Test P2b / 173
5.7	SUMMARY AND CONCLUSIONS / 176
5.8	REFERENCES / 177

6. LABORATORY INVESTIGATION OF THE EFFECT OF COARSE GRAVEL BACKFILL ON THE MECHANICAL PERFORMANCE OF PERFORATED LEACHATE COLLECTION PIPE

6.1	INTRODUCTION / 193
6.2	REVIEW OF PREVIOUS WORK / 195
6.3	DESCRIPTION OF LABORATORY TESTS / 196
6.3.1	Laboratory Apparatus / 196
6.3.2	Soil Materials Tested / 197
6.3.3	Details of Pipe Specimens / 199
6.3.4	Instrumentation / 200
6.3.5	The Calibration of Electrical Foil Strain Gauges on Polyethylene / 201
6.3.6	Testing Details / 202
6.4	MEASURED PIPE DEFLECTIONS / 202
6.4.1	Sand Backfill Versus Simulated Landfill Conditions / 203

6.4.2	Measured Deflections for Pipe P3 / 205
6.4.3	Influence of Perforations on Pipe Deflection / 206
6.4.4	Variation of Pipe Deflections / 208
6.4.4.1	<i>Diameter Changes at 250 kPa Vertical Surcharge / 208</i>
6.4.4.2	<i>Diameter Changes at Larger Vertical Surcharges / 209</i>
6.4.5	Summary of Deflection Measurements / 210
6.5	MEASURED SURFACE STRAINS FOR PIPE P3 / 211
6.5.1	Strain Response During Test / 212
6.5.2	Interior Pipe Strains / 213
6.5.2.1	<i>Interior Springlines / 214</i>
6.5.2.1	<i>Interior Crown and Invert / 216</i>
6.5.3	Exterior Pipe Strains / 218
6.5.3.1	<i>Exterior Springlines / 218</i>
6.5.3.2	<i>Exterior Crown and Invert / 219</i>
6.5.4	Interpretation of Statistical Testing / 220
6.6	VARIATION OF MEASURED SURFACE STRAINS FOR ALL TESTS / 221
6.6.1	Measured Hoop Strains at 250 kPa Vertical Surcharge / 221
6.6.1.1	<i>Springlines / 223</i>
6.6.1.2	<i>Crown / 224</i>
6.6.1.3	<i>Invert / 224</i>
6.6.1.4	<i>Shoulders and Haunches / 225</i>
6.6.2	Measured Axial Strains at 250 kPa Vertical Surcharge / 226
6.6.3	Measured Strains at Larger Vertical Surcharges / 228
6.7	CALCULATED PIPE STRESSES BASED ON MEASURED STRAINS / 229
6.7.1	Calculated Pipe Stresses at 250 kPa Vertical Surcharge / 231
6.7.2	Calculated Pipe Stresses at 900 kPa Vertical Surcharge / 232
6.7.3	Implications for Pipe Performance / 232
6.7.3.1	<i>Comparison With Short-Term Strength / 232</i>
6.7.3.2	<i>Long-Term Performance / 234</i>
6.8	COMPARISON OF PIPE DEFLECTIONS WITH DESIGN PROCEDURES / 237
6.8.1	Modified Iowa Equation / 238
6.8.2	Elastic Continuum Approach - Thin Tube Theory / 240
6.9	SUMMARY AND CONCLUSIONS / 241
6.10	REFERENCES / 245

7. SUMMARY AND CONCLUSIONS

7.1 INTERPRETATION OF LARGE SCALE PIPE TESTING / 266

7.2 DESIGN AND PERFORMANCE OF A NEW LABORATORY FACILITY FOR TESTING SMALL DIAMETER PIPES UNDER BIAXIAL EARTH PRESSURES / 267

7.3 LABORATORY INVESTIGATION OF THE EFFECT OF COARSE GRAVEL BACKFILL ON THE MECHANICAL PERFORMANCE OF PERFORATED LEACHATE COLLECTION PIPE / 268

7.4 SUGGESTIONS FOR FUTURE WORK / 271

7.5 REFERENCES / 272

APPENDIX I Numerical Integration During Fourier Integral Analysis / 273

APPENDIX II Constitutive Modelling of Soil Materials for Interpretation of Ohio University Test / 291

APPENDIX III Results from Laboratory Testing / 319

CHAPTER 1

Introduction

1.1 DESCRIPTION OF PROBLEM

Leachate collection systems are an important component of modern waste disposal facilities (e.g., municipal solid waste landfills). They are intended to control the hydraulic head acting on the liner and therefore a functional leachate collection system is important to minimize the contaminant migration from the waste disposal facility. It is known that both geosynthetic and geologic components of leachate collection systems (e.g., geotextiles, pipes and drainage gravel) can experience clogging because of particulate, chemical and biological effects (see Rowe et al. 1995). Clogging reduces the effectiveness of leachate collection and may lead to an increase in hydraulic head acting on the landfill liner system - resulting in greater contaminant transport from the facility (other factors being equal), higher temperatures at the base of the landfill, and reduced service life of geomembrane liners (Rowe 1998).

Design measures intended to minimize the potential for clogging of the leachate collection system can lead to service conditions for the pipe that are not experienced in typical buried pipe applications. For example, uniformly-graded gravel (e.g., nominal 40 - 50 mm crushed gravel) is now commonly used to minimize clogging in Ontario, Canada. The relatively large open void space and small surface area per unit volume provided by coarse gravel help to minimize biologically induced clogging (Rowe et al. 1995). However, there is a paucity of data that can be used to assess whether coarse gravel has a detrimental

effect on the mechanical performance of the pipe. Because the gravel particles are relatively large with respect to the size of the pipe (typical inside diameters from 150 mm to 250 mm), coarse gravel loads the pipe at discrete points around the outside surface rather than providing the more continuous support of other conventional backfill materials (e.g., sand, well-graded gravel). This effect is increased by the common use of angular gravel obtained by crushing rock such as dolomitic limestone. The effect of the coarse gravel backfill on the performance of the drainage pipes is presently unknown.

Further complicating the stress conditions within these pipes are stress concentrations arising from the presence of perforations. These holes in the wall of the pipe are essential for the purpose of leachate collection. However, these holes weaken the pipe compared to nonperforated pipe. Ideally, these holes should be sufficiently large to minimize the potential for clogging themselves and maximize the effectiveness of cleaning (from pressurised hydraulic jets that pass through the pipe). At the same time, they should not be so large and so numerous that they compromise the structural integrity of the pipe.

The magnitude of the stress concentrations from angular coarse gravel backfill and perforations, and their effect on the performance of the drainage pipes is presently unknown. One important issue to resolve is the extent and magnitude of tensile stresses within the pipe, since polyethylene materials may be susceptible to premature brittle failure at tensile stresses well below the ultimate stress (commonly referred to as stress cracking). Thicker polyethylene pipes are typically specified for use in landfill applications as a result of these uncertainties in pipe response.

1.2 CURRENT STATE OF PRACTICE

Current design practice for the structural performance of these landfill pipes is poor. Selection of the internal diameter of the pipes is normally based on maintenance requirements (e.g., large enough to permit video camera inspection and hydraulic flushing) since the hydraulic capacity of these pipes is rarely a controlling factor. Selection of an appropriate wall thickness (for plane pipes this is normally expressed as a ratio between the average external diameter and minimum wall thickness, SDR) is currently based on limiting the change in geometry of the pipe section to some value set in various codes of practice. In Canada for example, the change in vertical diameter for polyethylene pipes is specified to be less than 7.5% (CAN / CSA-b182.7-87).

Calculation of the change in the vertical diameter of the pipe is often undertaken using the Modified Iowa equation (e.g., Howard 1977). This semi-empirical equation was originally developed to estimate the horizontal diameter change for flexible metal culverts. Estimates of pipe deflection are a function of: soil support (characterised by the modulus of soil reaction, E'), pipe stiffness, and empirical deflection lag (D) and bedding constant (k) parameters. Calculated deflections are largely dependent on the empirical parameter E' , which is a function of soil modulus, pipe size, type of material, and ratio of horizontal to vertical stresses (Gumbel 1983). Koerner (1998) and Oweis and Khera (1998) recommend the use of this method, along with the E' values of Howard (1977) to estimate the pipe deflection for landfill pipes. Little guidance is provided in the literature for the selection of appropriate E' values that are representative of the soil stiffness for the coarse gravel now commonly used in landfills. Also, the Modified Iowa approach does not provide an

opportunity to calculate the stresses in the pipe, let alone consider issues such as the effect of perforations or discontinuous backfill support.

An alternate and more rational approach to the design of these deeply buried pipes is based on treatment of the ground around the pipe as an elastic continuum and pipe as an elastic tube (e.g., Moore 1993). There is a need to validate this approach for use with landfill pipes and adequately characterise the constitutive response of both the polyethylene pipe and coarse gravel backfill.

The current design rationale for perforations is varied. Zanzinger and Gartung (1995) suggest the use of long and narrow slotted perforations on the basis that they are hydraulically superior to round holes. However, since flow rates into the pipe may be very slow in landfills, the hydraulic performance of the perforation is not likely that important. Rather, concerns about the clogging of the perforation - which would be related to the size of the opening - are critical. It is postulated that a circular hole would clog less rapidly than a long and narrow slotted perforation of equivalent opening area. Selection of perforation size is arbitrary. Fleming et al. (1999) found that 10 mm diameter holes clogged after 1 to 5 years of exposure to landfill leachate. Clearly larger perforations than those currently used in practice are required to reduce the potential for biologically induced clogging. Chambers and McGrath (1981) state that the effect of perforations on the mechanical response of the pipe can be neglected if the holes are placed at or near the quarter points. This statement needs to be verified if larger perforations are to be used.

As a first step to improve the design methodology, there is a need to better understand how leachate collection pipes perform when subjected to loading conditions similar to that expected when deeply buried in a landfill.

1.3 RESEARCH OBJECTIVES AND METHODOLOGY

This thesis examines the mechanical performance of leachate collection pipes for use in municipal solid waste landfills. Emphasis is placed on understanding the effect of adverse service conditions on the collection pipes due to the coarse gravel backfill and relatively large perforations. The specific objectives of this research were to:

- design and construct a laboratory test facility that closely simulates the biaxial earth pressures experienced by a small diameter pipe when deeply buried in a landfill,
- describe how thick-wall high-density-polyethylene (HDPE) pipes perform under large overburden stresses,
- measure the response of HDPE pipes when surrounded by coarse gravel backfill,
- assess the effect of relatively large perforations on the local and global response of the pipe, and
- empirically establish whether coarse gravel and large perforations compromise the strength and serviceability of pipe typically used in landfills.

A research methodology was devised to achieve these objectives. Study of the important issues affecting the structural performance of these pipes was attained by performing large-scale laboratory tests in a setting that closely simulates the conditions experienced by a deeply buried small diameter pipe. Careful consideration of the measured laboratory results, guided by numerical analysis of the effects of the test cell boundary conditions, allowed inferences to be made regarding the structural response of leachate collection pipes.

1.4 SCOPE OF THESIS

The following sections summarize the original contributions described in this thesis.

1.4.1 Interpretation of Ohio University Pipe Tests - Chapter 2

A review of the literature pertinent to the testing of small diameter pipes was conducted prior to any new laboratory testing. Examination of published data from tests conducted by others elucidated major shortcomings of their testing methods. The results from a large-scale test conducted on a small diameter leachate collection pipe at Ohio University (Sargand 1993) were analysed and interpreted. This work showed that the boundary conditions of the Ohio facility imposed complex stress conditions on the pipe tested resulting from their attempt to simulate vertical overburden pressures by means of a stiff, rectangular load platform. A Fourier Integral analysis technique was implemented to facilitate the numerical analysis of the Ohio University tests (involving three dimensional geometry) to study the effect of the boundary conditions on the pipe response. It was found that the response of the pipe differed substantially compared to that expected in a landfill. The details of the numerical analysis and the interpretation of the Ohio University test are presented in Chapter 2. A study of the inversion of Fourier Integrals (critical for the successful application of this solution technique) is given in Appendix I.

1.4.2 Hoop Compression Laboratory Testing - Chapter 3

As a prelude to more elaborate testing, leachate collection pipes were tested under simplified boundary conditions in a facility similar to that developed by Selig et al. (1994). In these

tests, a uniform radial stress was applied to the soil and pipe to impart compressive hoop stresses in the pipe. Tests were conducted with both medium sand and coarse gravel backfill materials to represent two different loading conditions for the pipe. The sand backfill essentially provided continuous support for the pipe (relatively small particles in close contact with the pipe), while the coarse gravel backfill provided discontinuous support for the pipe (large particles randomly distributed around the exterior pipe circumference). Large variation in surface strains resulting from the coarse gravel backfill were measured. Also, strains were measured around a single perforation in the pipe to assess the mechanical response of the perforation.

1.4.3 Design of a New Laboratory Facility for Testing Small Diameter Buried Pipes - Chapter 4

A new facility was developed that closely simulates the biaxial (vertical and horizontal) stresses experienced by a pipe when deeply buried in a landfill. The development of the laboratory model required careful consideration of boundary conditions imposed during testing. This chapter reports on the design issues for the new laboratory facility. These issues included the selection of the size of the facility, the simulation of vertical and horizontal earth pressures, the implications of boundary friction and the significance of the boundary stiffness. Results from numerical analyses are presented to assess the effects of the boundary conditions of the test facility of the state of stress in the ground within the test cell as well as the mechanical response of the pipe.

1.4.4 Performance of a New Laboratory Facility for Testing Small Diameter Pipes Under Simulated Biaxial Earth Pressures - Chapter 5

This chapter reports on the performance of the new laboratory facility for testing small diameter buried pipes. Laboratory tests were performed in the new test facility to examine the appropriateness of the boundary conditions imposed during testing. The response of the pipe, the ground, and the test cell were examined to verify the effectiveness of the various techniques developed to: simulate vertical overburden loading by applying large uniformly distributed pressures, reduce sidewall friction in the laboratory facility, and limit the outward deflections of the test cell.

1.4.5 Laboratory Investigation of the Effect of Coarse Gravel Backfill on the Mechanical Performance of Perforated Leachate Collection Pipes - Chapter 6

Test results for three samples of high density polyethylene pipe with an average outside diameter of 220 mm and wall thickness of 25 mm conducted under simulated field conditions are reported in this chapter to examine the effect of coarse gravel and perforations on the structural response of leachate collection pipes. Vertical and horizontal diameter changes of the pipe are presented to examine the response of the pipe to the applied load. These measured deflections are compared with values obtained using available design procedures. Measured values of surface strain at locations around the pipe circumference are used to examine the response of the pipe and to investigate the effects of the coarse gravel backfill. Estimates of stresses in the pipe based on measured values of strain are compared with the short-term strength of the pipe. Factors important to the long-term performance of these pipes are considered. Preliminary recommendations for the design of leachate collection pipes are made.

1.5 FORMAT OF THESIS

This thesis has been prepared in accordance with the regulations for a Manuscript Format Thesis stipulated by the Faculty of Graduate Studies at The University of Western Ontario. Each chapter is presented in paper format without an abstract but with its own references. Tables and figures are given at the end of each chapter. References to chapters that have been published or accepted, submitted or are intended to be submitted for publication take the form “(Brachman et al. 1999; Chapter 5)” and refer to the paper by Brachman et al. that also appears as Chapter 5 in this thesis. Additional information is included in the appendices. Units of measurement corresponding to the S.I. system (Le Système International d’Unités) are used consistently throughout the thesis.

1.6 REFERENCES

- Chambers, R.E., and McGrath, T.J. 1981. Structural Design of Buried Plastic Pipe, Proceedings of the International Conference on Underground Plastic Pipe, Pipeline Division of the American Society of Civil Engineers, B.J. Schrock Ed., New Orleans LA, USA, ASCE, pp. 10-25.
- CSA (1987) CAN / CSA-b182.7-87 Plastic Drain and Sewer Pipe and Fittings, fourth edition, December 1987. Canadian Standards Association.
- Fleming, I.R., Rowe, R.K., and Cullimore, D.R. (1999) “Field Observations of Clogging in a Landfill Leachate Collection System”, Canadian Geotechnical Journal, (accepted).

- Gumbel, J.E. (1983) *Analysis and Design of Buried Flexible Pipes*, Ph.D. Thesis, Department of Civil Engineering, The University of Surrey, United Kingdom.
- Howard, A.K. (1977) "Modulus of Soil Reaction Values for Buried Flexible Pipe", *J. Geotech. Eng. Div.*, ASCE, Vol. 103, GT 1, pp. 33 - 43.
- Koerner, R.M. (1998) *Designing With Geosynthetics*, 4th Edition, Prentice Hall.
- Moore, I.D. (1993) "Structural Design of Profiled Polyethylene Pipe - Part I - Deep Burial", Geotechnical Research Centre Report GEOT-8-93, The University of Western Ontario, London, Canada.
- Oweis, I.S., and Khera, R.P. (1998) *Geotechnology of Waste Management*, 2nd Edition, PWS Publishing Company, Boston, USA.
- Rowe, R.K. (1998) "Geosynthetics and the Minimization of Contaminant Migration Through Barrier Systems Beneath Solid Waste", Sixth International Conference on Geosynthetics, Atlanta, GA, USA, IFAI, pp. 27-103.
- Rowe, R.K., Quigley, R.M., and Booker, J.R. (1995) *Clayey Barrier Systems for Waste Disposal Facilities*, E & FN Spon (Chapman & Hall), London.
- Sargand, S.M. (1993) "Structural Performance of an HDPE Leachate Collection Pipe", *31st Annual International Solid Waste Exposition*, San Jose, CA, USA, pp. 381 - 402.
- Selig, E.T., DiFrancesco, L.C., and McGrath, T.J. (1994) "Laboratory Test of Buried Pipe in Hoop Compression". *Buried Plastic Pipe Technology: 2nd Volume*, ASTM STP 1222, D. Eckstein, Ed., ASTM, Philadelphia, pp. 119-132.
- Zanzinger, H., and Gartung, E. (1995) "Large-scale Model Tests of Leachate Collection Pipes in Landfills Under Heavy Loads", *Advances in Underground Pipeline Engineering*, J.K. Jeyapalan and M. Jeyapalan (Eds.), ASCE, pp. 114 - 125.

CHAPTER 2

Analysis and Interpretation of a Buried Pipe Test Conducted in the Ohio University Facility ¹

2.1 INTRODUCTION

Large-scale testing is desirable to assess the structural performance of various culvert and sewer pipe products when subject to large loads associated with deep burial in the ground. Several test cells are available to the culvert and sewer pipe industry for proof testing new and existing products under high load levels. These cells are regularly used to examine the performance of metal, concrete and polymer pipe products. Facilities include test cells at Utah State University, Ohio University and the University of Massachusetts in the U.S.A.; and soil boxes like those at the Transportation Research Laboratory in the U.K. and LGA-Grundbauinstitut in Germany.

Testing conducted at these facilities may provide valuable insight into the performance of the pipe under simulated conditions. However, as with any laboratory investigation, it is essential to identify the boundary conditions of the test conducted and assess their implications for the practical problem being considered. Numerical analysis provides one means of determining the influence of the test facility boundary conditions upon the measured results.

¹ A version of this Chapter has been published.

Brachman, R.W.I., Moore, I.D., and Rowe, R.K., 1996. Interpretation of a buried pipe test: Small diameter pipe in the Ohio University facility. *Transportation Research Record*, 1541, pp. 64 - 70.

Results from a test conducted at the Ohio University facility on a small diameter high density polyethylene leachate collection pipe are analysed and interpreted. First, the details of the Ohio University facility are reviewed, with attention focussed on the testing boundary conditions.

Second, the details of the two and three dimensional finite element methods employed to interpret the test results are presented. This involves a brief description of the conventional two dimensional analysis performed. The details of an approximate numerical technique employing Fourier Integrals applied to the classical rigid footing problem are then presented. Results obtained for the simple rigid footing problem are compared with published solutions. The analysis is then used to calculate the response of a shallow buried pipe beneath a stiff rectangular footing.

Third, the results of the finite element analyses are used to examine the influence of the boundary conditions of the Ohio University facility, particularly focussing upon the implications of the loading system. The results of the finite element analyses are used to clarify the state of stress in the soil under loading conditions in the Ohio University test. The influence of the induced stress state upon the deformations, thrusts and bending moments of the pipe, and the behaviour of the soil mass are examined. Comparisons are made between the pipe response obtained in the Ohio facility and those expected to occur in a real field installation. Lastly, the manner in which these test results should be interpreted is also discussed.

2.2 DESCRIPTION OF OHIO UNIVERSITY TEST FACILITY

The results analysed in this chapter were obtained from a test conducted at the Ohio University load frame facility. Details of the testing apparatus have been described by Kastner et al. (1993) and Sargand et al. (1993). Essentially, two hydraulic cylinders are used to apply large vertical forces to the underlying soil and pipe through a stiff, rectangular loading platform (Fig. 2.1). The details of the particular test considered here, involving a small diameter pipe for use in landfill leachate collection systems, have been provided by Sargand (1993). Figure 2.1 shows the geometry through the central section of the test.

The 6 m long high density polyethylene pipe had an outside diameter of 152 mm, and a nominal wall thickness of 14 mm. The pipe was perforated with 13 mm diameter holes located 120° apart at the haunches, with an axial spacing of 127 mm. The pipe was buried within 25 mm crushed stone. Beneath the stone layer a compacted clay layer extended to shaley bedrock. Poorly graded granular material dumped in place was intended to simulate waste material (cover soil). A low stiffness woven geotextile was used to separate the stone from the clay and cover materials. The stiff *in situ* stiff clay formed the sidewalls of the trench parallel to the pipe axis.

A critical boundary condition for this particular test is the manner in which vertical load is applied to the ground and pipe below. The load platform used at the Ohio University test facility consists of eight steel beams welded together to form a 1.83 m × 2.74 m (6 ft × 9 ft) foundation.

A rectangular slab with dimensions $2a \times 2b$ can be considered as rigid if (Poulos and Davis 1974):

$$\frac{E_s}{1 - \nu_s^2} < \frac{8 D}{\pi (ab)^{3/2}} \quad (2.1)$$

where: a, b - half of footing width and length,
 D - flexural rigidity of platform, and
 E_s, ν_s - elastic soil parameters.

The flexural rigidities for the Ohio University load platform ($a=0.915$ m, $b=1.37$ m) were estimated to be 730 MN·m and 980 MN·m parallel and perpendicular to the pipe axis respectively. Based on the stiffness of the platform relative to the underlying soil, the load platform may be expected to behave as a rigid footing since the criterion of Equation 2.1 is satisfied for practical ranges of soil modulus (ie. $E_s/(1-\nu_s^2) < 1000$ MPa). Furthermore, observations during testing show the platform to uniformly deflect into the underlying soil (Goddard 1995), supporting the implication from Equation 2.1 that the load platform acts as a rigid foundation. A rigid footing prescribes a uniform displacement, producing a non-uniform surface pressure acting on the ground surface. This is different to the more uniform pressure expected from extensive overburden materials in the field.

2.3 METHOD OF ANALYSIS

Two dimensional elastic, two dimensional elasto-plastic and three dimensional elastic finite element analyses were conducted to interpret the test results from the Ohio University facility. Conventional two dimensional plane strain analysis was performed (e.g., Zienkiewicz and Taylor 1989), while the three dimensional analysis utilized the method described by Moore and Brachman (1994). The theoretical framework and implementation of the three dimensional elastic analysis is given in the Section 2.4.

Although the Ohio test involves complex three dimensional geometry and real soil materials, the use of two and three dimensional finite element techniques featuring elastic and elasto-plastic material response will demonstrate the significant effect of the testing boundary conditions upon the measured results. Comparison of the two dimensional and three dimensional elastic solutions provides an indication of the three dimensional nature of the response, while the comparison of two dimensional elastic and elasto-plastic solutions is used to investigate the significance of soil failure.

2.3.1 Finite Element Model

The finite element mesh used for the elastic analysis is shown in Figures 2.2. The pipe was modelled using twelve eight-noded rectangles, while seven-hundred and seventy-five six-noded triangles were used to model the surrounding soil materials. For the elastic analysis the lateral boundary of the mesh was located at a distance of twice the width of the platform from the pipe axis to sufficiently limit boundary effects (Fig. 2.2). In the case of the elasto-plastic analysis, the finite element results were more sensitive to the location of the lateral

boundary. This was a result of the shear failure induced in the silty clay native material. Consequently, the mesh width was extended to five times the platform width for the elastoplastic analysis. In all cases the lateral boundary and the line of symmetry along the centreline were modelled as smooth and rigid; the base was modelled as a rough and rigid.

The loading condition imposed by the rigid platform was modelled by prescribing a uniform displacement along the breadth of the platform. The effect of the surface roughness of the load platform was evaluated for the limits of a smooth rigid and a rough rigid load platform. It was found that the interface condition between the steel platform and ground surface has no significant effect on the resulting stress distribution (Brachman et al. 1995), consequently results for smooth interface only are presented in this chapter. An analysis was also performed simulating deep burial conditions, where a uniformly distributed load extended across the entire top surface of the mesh. In this case, the stiffness and density variations of any hypothetical overburden soil or waste were neglected.

The interaction condition between the pipe and the adjacent backfill was investigated for the limits of a rough and a smooth interface. Two-noded joint elements were used to model the soil-pipe interface.

2.3.2 Selection of Material Parameters

The selection of constitutive parameters for the materials tested is important for the analysis of the load test. Unfortunately, Sargand (1993) does not report any strength or stiffness data for the materials used in the test. The approach used to resolve this paucity of material parameters was two fold. First a range of elastic parameters was estimated based on published constitutive data from Selig (1990). Then sensitivity analysis was performed over

the identified range of values to ascertain the significance of key parameters. This approach permitted engineering decisions to be made regarding the selection of material properties. Detailed calculations of the sensitivity analysis are given in Appendix II. The values selected for use in the analyses are summarized in Table 2.1. For the elasto-plastic analyses, the strength of the ground materials were represented by a Mohr Coulomb failure criterion, characterized by cohesion c and angle of internal friction ϕ . The non-associated flow rule of Davis (1969) with angle of dilation ψ less than the angle of internal friction was also employed (see Appendix II).

The polyethylene pipe response was modelled with secant modulus of 470 MPa that was selected from data corresponding to the 2.5 hr time interval of the test (Moore and Hu 1994), and Poisson's ratio of 0.4. More sophisticated models are available to characterize the polyethylene response (e.g., Zhang and Moore 1997), but were not warranted in this simplistic assessment of the pipe test.

2.4 THREE DIMENSIONAL ELASTIC ANALYSIS

Accurate three dimensional finite element analysis by conventional means is neither simple nor inexpensive. First, it involves the generation of the three dimensional mesh of finite elements that is considerably more time consuming and more likely subject to undetected errors than its two dimensional counterpart. Second, a mesh that has sufficient refinement to produce reasonable predictions involves the formulation and solution of a huge number of equations. Alternatively, three dimensional semi-analytic approaches have been shown

to provide efficient and accurate solutions (Small and Wong 1988; Moore and Brachman 1994; Fernando and Carter 1998). These methods employ a two dimensional finite element mesh in conjunction with a Fourier transform to solve three dimensional problems. A semi-analytic procedure that uses a two dimensional finite element mesh across the buried pipe and a Fourier transform along the length of the pipe was therefore adopted to perform three dimensional analysis of the Ohio University test facility.

2.4.1 Description of Analysis

An approximate numerical technique employing semi-analytic finite-element analysis is used to examine the three-dimensional elastic response of a pipe structure under stiff plate loading. The contact pressure imposed on the ground surface by a rigid footing is first approximated by a number of regions of uniformly distributed loading, Figure 2.3. These pressures are the unknown quantities to be solved for. A relationship between the patch displacements and patch forces is then assembled and used to solve for the unknown contact pressures for a uniform prescribed displacement across the footing. Once the contact pressures are known, the response of the elastic medium to the pressure distribution imposed by the stiff plate can be found.

Selvadurai (1979) cites the early work of Zemochkin and Sinitsyn, who used this basic premise to analytically solve for the response of beams and plates on elastic foundations. Many investigators have since used this approach to solve various problems involving circular, elliptical and rectangular rigid plates subject to symmetric and asymmetric loading. A collection of these solutions have been compiled by Poulos and Davis (1974) and Selvadurai (1979).

Past approaches have typically used known analytical solutions (e.g., Boussinesq's or Mindlin's solution, or numerical integration of the biharmonic equation) to relate patch displacements and forces to enable calculation of the unknown surface pressure. However, the presence of a buried structure beneath the loaded plate precludes the use of such solutions. Fourier Integral analysis was therefore adopted to calculate the relationship between displacements and forces. This approach explicitly considers the soil-structure interaction (between the pipe and surrounding soil) and also permits analysis of different materials.

2.4.2 Notation and Influence Matrix

Figures 2.3a and 2.3b show a rectangular footing divided into a series of $2m \times 2n$ patches of equal size. Only one-quarter of the platform need be considered (Fig. 2.3c) as the problem of a rigid plate subject to a vertical force is doubly symmetric about the footing centrelines (ie. the lines $x=0$ and $z=0$). The patches are labelled according to the indices i and j , where i varies from 1 to m along the x direction, and j varies from 1 to n along the z direction. The variables m and n quantify the respective number of patches in the x and z directions.

A flexibility relationship between the pressure applied to a patch and the corresponding displacements for each and every patch may be established such that,

$$[F_{k,l}] P_l = D_k \quad (2.2)$$

where: $[F_{k,l}]$ is a flexibility or influence matrix $[(m \times n) \times (m \times n)]$,

P_l is a vector of patch pressures $[(m \times n) \times 1]$,

D_k is a vector of patch displacements $[(m \times n) \times 1]$,
 k refers to the location of the displacement, and
 l refers to the location of the loaded patch.

Expansion of Equation 2.2 for $m \times n$ regions of uniform pressure gives:

$$\begin{bmatrix} f_{1,1} & f_{1,2} & f_{1,3} & \dots & f_{1,mxn} \\ f_{2,1} & & & & \\ f_{3,1} & & & & \\ \cdot & & & & \\ \cdot & & & & \\ \cdot & & & & \\ f_{m \times n, 1} & \dots & & & f_{m \times n, m \times n} \end{bmatrix} \begin{bmatrix} p_1 \\ p_2 \\ p_3 \\ \cdot \\ \cdot \\ \cdot \\ p_{m \times n} \end{bmatrix} = \begin{bmatrix} d_1 \\ d_2 \\ d_3 \\ \cdot \\ \cdot \\ \cdot \\ d_{m \times n} \end{bmatrix} \quad (2.3)$$

where: $f_{k,l}$ = average displacement of patch k with a unit pressure on patch l ,
 p_l = average pressure on patch l ,
 d_k = average displacement of patch k ,
 $k = n(i_k - 1) + j_k$
 $l = n(i_l - 1) + j_l$

Consider the case with the contact pressure approximated by 216 regions of uniform pressure ($m=6$, $n=9$, Figure 2.3) to illustrate the adopted nomenclature. Two regions are shaded in Figure 2.3c. The first is located at $i=2$ and $j=3$, giving $k=12$; the second patch with

$i=5$ and $j=7$, has $l=43$. Coefficient $f_{12,43}$ then corresponds to the displacement of patch 12 ($i=1, j=3$) with a uniform pressure applied at patch 43 ($i=5, j=7$).

The elements in the first column of the flexibility matrix can be obtained by applying a unit pressure at patch 1 and evaluating the average displacement at each of the $m \times n$ patches, yielding influence coefficients $f_{1,1}, f_{2,1}, f_{3,1}, \dots, f_{m \times n,1}$. This procedure can then be repeated for a unit pressure applied at each and every patch to obtain the entire influence matrix. Recognizing that the influence matrix [F] is symmetric reduces the computational effort required for solution. Only $\frac{1}{2} nm(m+1)$ influence coefficients need to be calculated to formulate the $m^2 n^2$ terms of the influence matrix if symmetry is used. For the case shown in Figure 2.3c (ie. $m=6, n=9$) application of symmetry reduces the computational effort by a factor of fifteen. Provided that the influence coefficients can be determined efficiently and accurately, the formulation of the influence matrix is straightforward.

2.4.3 Calculation of Influence Coefficients Using Fourier Integrals

Three-dimensional semi-analytic finite element analysis is used to calculate the influence coefficients relating patch pressure and displacement. Semi-analytic finite element approaches featuring integral transforms have been used by Small and Wong (1988), Moore and Brachman (1994), Brachman et al. (1995), Fernando et al. (1996) and Fernando and Carter (1998) to obtain efficient and accurate solutions to three dimensional elastic problems. These methods employ a two dimensional finite element mesh in conjunction with a Fourier transform to solve three dimensional problems.

The Fourier integral approach removes the dependence upon the longitudinal spatial coordinate (ie. z in Fig. 2.3) in lieu of a transform variable, α . The Fourier cosine integral of any function $g(\xi)$ is given by:

$$F_c(\alpha) = \int_0^{\infty} g(\xi) \cos(\alpha\xi) d\xi \quad (2.4)$$

where: $F_c(\alpha)$ is the Fourier cosine integral of $g(\xi)$,

α is the transform variable, and

ξ is the variable being transformed.

Vertical applied loads, displacements and stresses can be expressed in transformed coordinates through Equation 2.4. Harmonic finite element analysis can then be performed using a two-dimensional mesh discretized in the x-y plane (e.g., Fig. 2.2) to solve for the transformed quantities of displacements and stresses for specific harmonic values of α . Inverse integrals with the form:

$$g(z) = \frac{2}{\pi} \int_0^{\infty} F_c(\alpha) \cos(\alpha z) d\alpha \quad (2.5)$$

are used to convert the computed harmonic response back to the Cartesian coordinate system. The integrand of Equation 2.5 is a function of the transform variable α , and can be evaluated for any particular value of z . Brachman and Moore (1998) [Appendix I] have discussed the nature of these inverse integrals and numerical techniques to successfully evaluate them.

2.4.4 Assembly of Final Solution

The next step, once the influence matrix has been formulated is to calculate the surface pressure distribution arising from a prescribed uniform displacement across the footing. The average pressure for each patch can be found by solving Equation 2.2 for P_l ,

$$P_l = [F_{k,l}]^{-1} D_k \quad (2.6)$$

with $[F_{k,l}]$ as calculated for the particular case being examined and with $D_k = [1, 1, \dots, 1]^T$ corresponding to a uniform displacement at each patch beneath the platform.

The response of the underlying materials (e.g., soil and pipe) subject to loading from the rigid footing can then be calculated by applying the regions of uniform pressure (P_l) that approximate the contact pressure. Fourier Integral analysis was also used to calculate this response.

Linear superposition was used to assemble the response from all of the patches for the multi-step loading depicted in Figure 2.3b. The response of each patch of width b/n located distance $b(j-1)/n$ from the footing centreline could have been analysed. However, the Fourier Integral for a relatively narrow patch of loading separated from the centre by a large distance (e.g., patch $j=n$ located $b(n-1)/n$ from the centre) is a complex function requiring substantial numerical effort for successful inversion. (e.g., see Brachman and Moore 1998; Appendix I). Analysis featuring simple patches with uniform pressure along the z direction yield much simpler Fourier Integrals that require less numerical effort to invert. The multi-step loading of Figure 2.3b was therefore modelled by considering patches

of uniform pressure of width $2b$ and magnitude p_n less patches of width jb/n and magnitude $(p_{j+1} - p_j)$, repeated for $j=1$ to $n-1$.

2.4.5 Analysis of a Rectangular Rigid Footing on an Elastic Layer

The simple case of a rigid, rectangular footing ($2a \times 2b$) on an elastic layer (E_s, ν_s) of finite depth (h) and subject to vertical force P is now solved to illustrate the use of the semi-analytic finite-element technique. Figure 2.4 shows a portion of the two-dimensional mesh used for the analysis, consisting of two-hundred and forty-six six-noded triangular elements. The portion of the mesh shown in Figure 2.4 extended both laterally and vertically a distance of six times the footing half width ($6a$), and boundaries were modelled as smooth and rigid. Additional cases were analysed for the boundaries extending further from the footing, and also with the bottom boundary modelled as rough and rigid. In all cases, symmetry was employed along the footing centreline ($x=0$).

The contact pressures imposed by the rigid rectangular footing, evaluated using the semi-analytic finite element method, are examined in Figure 2.5. These results are for a rectangular footing with $b=1.5a$, and are shown for two values of Poisson's ratio ($\nu_s=0.3$ and 0.49), and for two different thicknesses of the elastic layer ($h=1.5a$, and $h>6a$).

Figures 2.5a and 2.5b plot contours of equal contact pressure beneath the rigid footing. One-quarter of the footing is shown and the results are normalized by the average surface pressure (ie. p / p_{av} , where $p_{av} = P / 4ab$, and P is the total vertical force applied to the footing). Figures 2.5c and 2.5d are plots of the normalized contact pressure for sections taken along the lines $z=0$ and $x=0$, respectively.

The rigid footing imposes a nonuniform surface pressure distribution on the ground surface. Load is shed from the centre and is attracted towards the edges as a result of the rigid nature of the platform. The surface pressure towards the middle of the platform depends on the thickness and the Poisson's ratio of the compressible layer. For example near the centre of the footing (ie. $x=0, z=0$), the contact pressure is roughly 50% of the average surface pressure for $h/a > 6$ (Fig. 2.5a).

Figure 2.5a is nearly identical to that presented by Butterfield and Banerjee (1971) for the solution of a rigid rectangular raft ($b=1.5a$) upon an incompressible (ie. $\nu_s=0.5$) elastic half space. Their solution also involved approximating the contact pressures with a series of uniform pressures, featuring integration of Mindlin's embedded point-load solution. Comparison with their solution is shown in Figures 2.5c and 2.5d. Very good agreement was found using the semi-analytic finite element method with Fourier Integral analysis ($h/a > 6$ and $\nu=0.49$).

Decreasing the thickness of the compressible layer results in an increase in contact pressure. For example with $h/a = 1.5$, the contact pressure is 1.35 times larger than for $h/a > 6$ (for $\nu=0.49$). When the finite depth has as noticeable effect, Poisson's ratio also influences the contact pressure as increasing Poisson's ratio results in larger contact pressures. These observations are consistent with those results reported by Poulos and Davis (1974) for the solution of a rigid circular footing on an elastic layer of finite depth.

Increasing the thickness of the elastic layer had little effect on the contact pressure for $h/a > 6$ (ie. approaching half space conditions). Also, the contact stresses are essentially independent of Poisson's ratio for $h/a > 6$ shown by the solutions for $\nu_s=0.3$ and 0.49 .

Dividing the footing into $m=10$ and $n=15$ patches provided acceptable results, since further increases in m and n had little effect on the results near the middle of the footing. Increasing the number of patches does give a slightly better solution near the edges of the footing where there is a large change in stress over a relatively small area. However, greater refinement of patches does not appear to be warranted, especially for the analysis of a pipe under stiff plate loading (reported in the next section), where the response beneath the middle of the plate is considered.

Milovic (1992) also reports a solution for the contact stresses for this problem obtained using a double power series expansion for the contact stress between the footing and the elastic medium. This solution for a rigid rectangle ($b=1.5a$) on an elastic half space is also plotted in Figures 2.5c and 2.5d. These results are larger than the contact stresses reported in this chapter and those by Butterfield and Banerjee (1971) for most of the footing, and are smaller near the edges (ie. for $x/a > 0.9$ and for $z/a > 1.4$). It appears that the double power series expansion is incapable of describing the contact pressure distribution (at least with the number of terms in the expansion considered by Milovic), with a relatively flat distribution for $x/a < 0.5$ and a very large gradient for $x/a > 0.8$. As a result, the solution of Milovic produces greater contact stresses near the centre and smaller stresses near the edges compared with the actual elastic stress distribution.

Milovic and Tournier (1973) have published solutions for a rough rigid footing on an elastic layer of finite depth, underlaid by a rough rigid boundary. They solved this problem using a double Fourier Series formulation for the displacements of the elastic medium. The contact stresses for a rectangular rigid footing ($b=2a$) on a layer of thickness $h=6a$, with $\nu_s=0.3$ are shown in Figure 2.6. The contact pressures calculated using the semi-

analytic finite element method with Fourier Integral analysis (given by the square symbols) are only slightly larger ($\sim 2\%$) than those calculated for a footing with $b=1.5a$. This is similar to the results reported for increasing the length of the rectangle on an elastic half space by Butterfield and Banerjee. Increasing the aspect ratio of the rectangle (ie. b/a) results in an increase in the contact pressure to the limit of a rigid strip footing. Solutions are shown in Figure 2.6 for both a smooth rigid and rough rigid strip. The interface conditions between the strip and the elastic medium has little influence on the contact pressure.

The contact stresses calculated by Milovic and Tournier are roughly 1.3 times larger than those calculated from the semi-analytic finite element analysis. The fact the semi-analytic finite element analysis considered only a smooth rigid footing is unlikely to account for the discrepancy between the two solutions, given the limited effect of the footing interface roughness on the contact stresses for a strip. Milovic and Tournier's contact pressures for $b=2a$ are larger than for the limiting case of a strip footing, and are even larger for $b/a=5$. It appears that the double Fourier series formulation also does not properly represent the contact stresses. The solutions of Milovic (1992) and Milovic and Tournier (1973) would at least be conservative for simple engineering calculations (e.g., calculation of stress increments beneath the centre of the footing to estimate settlement), but do not appear to be suitable for comparison with other solutions (ie. as a basis to validate other analyses).

2.5 ANALYSIS OF A SHALLOW BURIED PIPE UNDER STIFF PLATE LOADING

The results from the finite element analyses are now used to clarify the state of stress in the soil arising from the rigid, finite sized load platform used in the Ohio University tests. The influence of the induced stress state upon the pipe deformations, thrusts and moments is examined. Comparisons are also made between the pipe response induced in the test facility, and that which is likely to occur in a real field installation.

2.5.1 Calculated Contact Pressure

The contact pressure imposed on the ground surface by the stiff plate is plotted in Figure 2.7. Contours of normalized surface pressure (p / p_{av}) are shown for one-quarter of the loaded area. There is significant variation of contact stresses in both transverse (x) and longitudinal (z) directions. Stress redistribution occurs, again as load is attracted towards the edges of the stiff plate. The distribution towards the centre also varies because of the non-uniform materials beneath the plate (crushed stone and cover soil materials, see Fig. 2.1). Less than 50% of the average surface pressure acts near the centre of the plate, with only 43% calculated at $x=0, z=0$. Thus the combination of load spreading in the x and z directions coupled with non-uniform material stiffness results in a complex pressure distribution imposed on the ground by the plate.

2.5.2 Calculated Soil Stresses

Contours of vertical σ_y^* , horizontal σ_x^* and axial stress σ_z^* calculated at z equal to zero, and normalized by the average surface pressure (ie. $\sigma^* = \sigma / p_{av}$) are plotted in Figure 2.8.

2.5.2.1 Vertical Stresses

Contours of vertical stress (Figure 2.8a) show that the normalized contact stress varies from less than 0.5 near the centre to values greater than 1.3 closer to the edge of the plate. As a result, the soil above the pipe experiences a vertical stress of approximately 50% of the average surface pressure. The finite width of the load platform leads to attenuation of stresses as load spreads out through the ground. The rigid nature of the plate lead to stress redistribution towards the perimeter of the plate, further reducing the vertical stress reaching the pipe.

Redistribution of vertical stress around the pipe (ie. arching) because of the difference in pipe stiffness relative to that of the zone of soil it replaces is evident from Figure 2.8a. This results in increases of vertical stress near the shoulder ($\theta = 45^\circ$) and haunch ($\theta = -45^\circ$) areas of the pipe, and decreases at the crown ($\theta = 90^\circ$), invert ($\theta = -90^\circ$) and springline ($\theta = 0^\circ$). (Note: θ is the angle around the pipe, with $\theta = 0^\circ$ oriented parallel to the positive x direction, and counter-clockwise angles as positive). These local stress changes occur largely within a region of soil one diameter around the pipe. Overall, the pipe experiences much lower stresses because of the load spreading that occurs, which is attributed to the finite size and large rigidity of the loading plate.

The resulting non-uniform vertical stress distribution at the surface makes interpretation of the equivalent total load applied during the test difficult. Sargand (1993) estimates an equivalent height of fill for the test load assuming that the average stress (p_{av}) acts across the surface of the platform. This was claimed by Masada et al. (1996) to be conservative. However, Figure 2.8a shows that this approach would over estimate the equivalent height of fill by a factor of nearly two.

Figure 2.9a presents the calculated elastic vertical stress increment with depth along the line $x=0.3\text{m}$, which corresponds to the location where the material directly beneath the load platform changes from stone to cover soil. The clay layer extends from $y=0$ at the base to $y=0.91\text{ m}$, where it is overlain by the stone layer which extends up to the surface ($y=1.78\text{ m}$). The three dimensional (3D) analysis (Fig. 2.9a - curve i) predicts a relatively constant value with depth of $\sigma_y^* = 0.5 p_{av}$. Using conventional two dimensional (2D) plane strain elastic analysis, the vertical stress with depth is about $\sigma_y^* = 0.7$, roughly 1.4 times greater than the 3D prediction (Fig. 2.9a ii). The 2D prediction is greater than the 3D prediction, since it neglects the load spreading that occurs along the pipe axis for the 3D case. Figure 2.9a (curve iv) illustrates the expected deep burial response with an extensive uniformly distributed load. For that case, the vertical stress at the surface is $0.94 p_{av}$ and increases to $1.0 p_{av}$ with depth. This illustrates the significant effect of the finite size and rigidity of the load platform; the 3D prediction (i) is only about one half of the stress increment predicted for deep burial (iv). This discrepancy arises due to the non-uniform applied pressure distribution together with the load spreading under the finite sized platform.

It could be argued that despite the non-uniform surface distribution over the entire platform, the region directly above the central section experiences an almost uniform surface pressure of roughly 50% of the average applied pressure. However, it is shown subsequently, that the test facility produces horizontal stress conditions and pipe response that deviate significantly from deep burial conditions, and hence one cannot simply factor the applied load to get a better estimate of the equivalent fill height.

2.5.2.2 Horizontal Stresses

Calculated horizontal stress contours (σ_x^*) are shown in Figure 2.8b. The horizontal stress varies with depth from $0.5 p_{av}$ near the surface to zero just above the pipe crown. Figure 2.8b shows a large region near the base of the stone layer that experiences tensile stresses if the stone material is assumed to be elastic. This implies that the stone layer experiences bending type stresses (ie. greater compression near the surface and tensile stresses near the bottom of the layer).

Trial analyses were performed to validate the observed bending in the x-y plane. The analysis showed that if the stone and clay materials had uniform stiffness with depth (ie. $E_{stone} = E_{clay}$) the tensile region would not develop, Figure 2.9b (curve iii). The relative difference in stiffness between the crushed stone and the clay (E_{stone} / E_{clay}) was examined for a range of expected values reported by Selig (1990). Tensile stresses were calculated for all practical ratios of stone to clay modulus (Brachman et al. 1995; Appendix II). The presence of the compressible clay layer below the relatively stiffer stone is therefore one factor leading to bending stresses in the stone.

Furthermore, if the load was applied over a more extensive region on the ground surface, this tension region would not exist, Figure 2.9b (curve iv), even with the a difference in material properties between the stone and the clay. Therefore this bending occurs because of the difference in stiffness between the stone and clay materials and the finite surface loading.

2.5.2.3 Axial Stresses

In addition to the bending in the transverse (x-y) plane, bending also occurs along the axis of the pipe (ie. y-z plane) as illustrated by the axial stress contours in Figure 2.8c. This bending arises as the load platform is of finite size along the z direction. Three-dimensional elastic σ_z^* stress contours, Figure 2.8c, reveal that longitudinal bending creates a significant tensile region in the stone material, if assumed to be elastic. The axial stress varies from $0.2 p_{av}$ close to the surface to $-0.2 p_{av}$ near the bottom of the stone layer. This axial bending is consistent with observations made during the test by Sargand (1993) who stated that "the pipe deflected similar to a beam under the loaded area." This type of bending would not be expected under deep burial conditions as the overburden load would likely extend a great distance along the pipe axis.

2.5.2.4 Three-Dimensional Variation of Soil Stresses and Pipe Deflections

Variation of vertical, horizontal and axial stresses in the longitudinal direction are examined in Figure 2.10. Stresses are reported for two points: Point A is located one pipe diameter above the crown; Point B was located one pipe diameter away from the springline. Vertical stresses at both A and B increase as z increases, reaching a maximum value near the end of the plate, and then rapidly decrease to zero for locations not beneath the loaded region. Zones of tension calculated at location B extend beneath the plate.

Vertical displacements calculated at the ground surface δ_{surf} , and the crown δ_{cr} and δ_{in} invert of the pipe are plotted in Figure 2.11 for increasing distance along the longitudinal direction. These values are normalized by the deflection of the plate (δ_{surf}). The

displacement prescribed on the ground surface by the stiff plate loading is evident. Pipe deflections vary along the pipe showing the axial bending induced by the finite loading.

2.5.2.5 Two-Dimensional Inelastic Stress Predictions

Real stone would not be expected to experience the tension predicted by the elastic analysis; rather the material would likely yield. The 2D elasto-plastic analysis of the test facility predicted a plastic region adjacent to the pipe starting at low load levels, as shown in Figure 2.12a for $P=52$ kN. This zone of plastic (yielded) material is in the location of the "tensile" region predicted by the elastic analyses. The low confining pressures which develop under the influence of bending induced in the granular layer lead to this shear failure. Also in Figure 2.12a, local yield can be observed beneath the edge of the platform and along the trench wall in the cover soil. The plasticity in the soil results in a redistribution of stresses, and consequently in the loads that reach the pipe. To further examine the influence of yield upon the state of stress, vertical and horizontal stress contours obtained from the 2D elasto-plastic analysis are presented in Figure 2.13. The results are again normalized with respect to p_{av} and are presented for the load level of $P=1400$ kN ($p_{av}=280$ kPa).

Figure 2.13a plots the vertical stress state (σ_y^*). It can be seen that the maximum vertical stress does not occur at the edge of the platform as found for the elastic analysis, but rather occurs closer toward the platform centreline with a value of $\sigma_y^*=1.6$. This redistribution can be explained by considering the extent of the soil failure for this load level, shown in Figure 2.12b. The yielded soil beneath the edge of the platform can support no further increase in load, and the load is redistributed to the unyielded soil. Soil failure induced by the rigid load platform further complicates the surface pressure distribution

imposed by the platform, and makes the task of interpreting the equivalent height of fill even more difficult.

Figure 2.12b shows that the plastic region has almost fully engulfed the pipe. This results in a decrease in lateral support for the pipe as illustrated by the 2D elasto-plastic horizontal stress (σ'_x) contours plotted in Figure 2.13b. The horizontal stress in the soil adjacent to the pipe is only $\sigma'_x=0.2p_{av}$ as a result of the soil failure. Larger pipe deflections would be expected as a result of the decrease in lateral support for the pipe.

Figure 2.12b also indicates that the plastic region has propagated through the clay layer. The shear failure observed in the clay soils develops into a collapse mechanism, Figure 2.12c, which is analogous to bearing capacity failure under the rigid load platform. This observation can be supported by examining the non-linear behaviour of the measured load deflection response of the platform Figure 2.14. Conventional bearing capacity analysis for the clay foundation, reasonable for this geometry (Rowe and Soderman 1987), treating the granular material as a surcharge and with a shape factor of 1.1, yields bearing capacity of $P=2200$ kN ($p_{av}=440$ kPa) consistent with the loads in Figure 2.14. Furthermore, Goddard (1995) reports on "soil failure" and observes that "the adjacent soil moves up and away from the loading plate." These observations support the interpretation that at high load levels, the response for this particular test is governed by the soil failure induced in the compacted clay foundation.

2.5.3 Interpretation of Pipe Deformations

Now that the state of stress induced by the load platform for this particular test has been clarified, the influence upon the pipe and soil response can be investigated. The effect upon

the observed pipe deflection is examined first.

The change in vertical and horizontal diameter calculated by the 2D elastic, 3D elastic and 2D elasto-plastic analyses are presented in Table 2.2, along with the measured values reported by Sargand (1993). Also recorded in Table 2.2 are the predicted pipe diameter changes for a 2D elasto-plastic analysis simulating the deep burial problem. This extensive overburden case corresponds to a uniformly distributed pressure across the entire surface. The values are all reported for the same magnitude of total force applied to the platform of $P=1400$ kN ($p_{av}=280$ kPa).

The elastic results in Table 2.2 are presented for the case of a bonded pipe-backfill interface condition. Results with both bonded and smooth pipe-backfill interface conditions are given for the elasto-plastic analysis of the load platform and extensive overburden cases. There is a 3.6% increase in ΔD_v and 12.4% increase in ΔD_h when the pipe is modelled with a smooth interface. The influence of the interface condition is more pronounced for the extensive overburden case, yielding 30% and 64% increases in ΔD_v and ΔD_h respectively when modelled as smooth instead of bonded. The shear failure that engulfs the pipe for the load platform case (see Figure 2.12) limits the transfer of shear stresses at the pipe interface and thus modelling the interface as purely smooth does not result in a large increase in pipe deflections. However, for the extensive overburden case shear failure is not as prevalent and there is a marked increase in deflections, particularly in ΔD_h , when the pipe interface is smooth.

The 2D elastic solution predicts slightly greater deflections than the 3D solution. This illustrates the effect of analysing a 3D problem with a 2D technique. The 3D predictions of deflections are smaller as the load reaching the pipe is reduced due to the variation of surface

pressure along the axis of the pipe seen earlier. The significance of shear failure in the stone is demonstrated as the 2D elasto-plastic solution predicts deflections that are nearly three times greater than for the 2D elastic solution. The yielded soil (shown in Fig. 2.12b) provides much less support and much larger pipe deflections result.

The calculated horizontal and vertical diameter changes from the 2D elasto-plastic analysis are plotted with the measured values in Figure 2.15. The calculated change in horizontal diameter (ΔD_h) compares reasonably with the measured values, with only slight scatter around the measured points. The calculated ΔD_v results closely match the measured values up to a load of $P=1100$ kN. For load levels greater than $P=1100$ kN the 2D elasto-plastic results underestimate the considerable softening response that was observed. Overall the prediction provides good agreement with the measured values, indicating that the constitutive parameters used in the analysis are reasonable (see Appendix II for the extensive parametric study conducted).

Comparison of load platform and extensive overburden cases in Table 2.2 show the dominant influence of the finite sized, rigid loading platform. The anticipated ΔD_v value for the extensive overburden case is roughly 22% of the value measured in the test cell. More substantial however, is the effect upon the horizontal diameter change. The horizontal diameter change in the test cell is 17 times greater than the value expected for the extensive overburden case. These values show that not only the magnitude, but more significantly, the mode of pipe deflection produced in the test facility is different to that expected in a landfill. The large ΔD_h values measured in this facility are a direct result of the influence of the rigid load platform and are significantly different to the conditions expected in a landfill.

2.5.4 Interpretation of Thrusts and Moments

The circumferential thrusts and moments in the pipe calculated for the load level of $P=1400$ kN are presented in Figures 2.16 a and b, respectively. Solutions are shown for the 2D elasto-plastic load platform (curves i and ii) and extensive overburden (curves iii and iv) cases for both a rough and smooth pipe-backfill interface. The presented values are plotted versus the angular position in the pipe (θ), with $\theta=0^\circ$ at the springline and counter clockwise angles positive.

The interface condition has a substantial influence upon the distribution of thrusts in the pipe. The smooth case results in a more uniform thrust distribution, tending to the average value of the rough case, for both the load platform and extensive burial cases. Figure 2.16a implies that the Ohio University test facility produces thrusts that underestimate those expected under extensive overburden conditions. First of all, the thrusts for the load platform case (curve i) are roughly zero at both the crown and the invert. This arises because of the soil failure induced by bending in the x-y plane which leads to low horizontal stresses around the pipe (Fig. 2.13b). For the extensive overburden case, significant thrusts are experienced at the crown and the invert. Secondly the springline thrust for the load platform case (curve i) is only 70% of the extensive burial value (curve iii). Also, the average thrust induced in the test facility is only one half of the extensive overburden case as shown by the smooth interface solutions (curves ii and iv). Therefore it appears that unconservative thrust values occur due to induced soil failure and the finite size of the load platform. The difference in thrust predicted in the pipe may be particularly significant if the perforations are critical to the performance of the pipe.

The moments expected in the pipe are largely unaffected by the pipe-backfill

interface condition as displayed in Figure 2.16b. However the test facility conditions result in a very different moment distribution than that expected in a landfill. Figure 2.16b shows that the moments at the crown, springline, and invert for the load platform case are approximately 3 times greater than the values for extensive overburden conditions. This shows that the soil failure greatly increases the circumferential bending moments that the pipe experiences, as the difference between vertical and horizontal stresses increases for the load platform case. Only small moments arise in the pipe for the extensive overburden condition.

2.6 SUMMARY AND CONCLUSIONS

The analysis and interpretation of a buried pipe test conducted on a 150 mm diameter HDPE leachate collection pipe at the Ohio University facility were presented. The boundary conditions of the test facility were identified, with particular attention placed on the method of load application.

The details of an approximate numerical technique used to examine the three dimensional elastic response of a shallow buried pipe under stiff plate loading were presented and discussed. The contact pressure imposed on the ground surface by the stiff plate was approximated by a number of regions of uniform pressure. A relationship between the uniform pressures and resulting surface displacements was used to solve for the contact pressure distribution. Fourier Integral analysis was used to calculate the influence coefficients and to compute the response of the elastic medium to the contact pressure.

Results agreed with the published solution of Butterfield and Banerjee (1971) for a simple rectangular rigid footing problem. It was found that solutions featuring either the double power series or double Fourier series expansions were incapable of capturing the contact pressure distribution and yield larger values of contact stress and stress with depth beneath the centre of the footing compared with the actual stresses.

The results from the two and three dimensional finite element analyses of full scale tests of leachate collection pipes demonstrated that the boundary conditions of the Ohio testing facility are complex, and the results derived from the tests require careful interpretation before reliable decisions are made about pipe performance under landfills. In the particular case analysed, the Ohio University load frame produces pipe response that is different to that expected under deep burial conditions. Firstly, the non-uniform stress distribution imposed by the finite, rigid loading platform is significantly different to the stresses resulting from the extensive and more uniform distribution expected in a landfill. Secondly, at low load levels, a region of the backfill adjacent to the pipe yields as the granular layer behaves like a beam in bending. This greatly reduces the lateral support of the pipe, increases the magnitude of the pipe deformations and alters the mode of pipe deflection. Lastly, at high load levels the test is governed by soil failure, producing conditions not expected in a landfill environment.

The measured deflections in the Ohio University facility are greater than those expected in a landfill situation as are the circumferential moments. Thrusts are expected to be lower than those in a landfill situation. It is difficult to conclude whether the Ohio University test facility produces conservative results relative to those in a real installation, as the mechanism of deformation is different to the field loading case. The results of

Sargand (1993) must be viewed with considerable caution in relation to their application to the design of pipes in landfills. The boundary conditions of the Ohio University facility are expected to have a significant but different effect on large diameter pipe.

2.7 REFERENCES

- Brachman, R.W.I., and Moore, I.D. (1998). "Numerical integration during Fourier Integral Analysis." *International Journal for Numerical and Analytical Methods in Geomechanics*, In Press, Accepted 7/16/98.
- Brachman, R.W.I., Moore, I.D., and Rowe, R.K. (1995). "Analysis of pipe structures in soil test cells - Ohio University facility." *Geotechnical Research Centre Report GEOT-14-95*, The University of Western Ontario, London, Canada.
- Brachman, R.W.I., Moore, I.D., and Rowe, R.K. (1996). "Interpretation of a buried pipe test: Small diameter pipe in the Ohio University facility." *Transportation Research Record*, 1541, 64-70.
- Butterfield, R. and Banerjee, P.K. (1971). "A rigid disc embedded in an elastic half space." *Geotechnical Engineering, Journal of the Southeast Asian Society of Soil Engineering*, Vol. 2, No. 1, 35-52.
- Fernando, N.S.M., and Carter, J.P. (1998). "Elastic analysis of buried pipes under surface patch loading." *Journal of Geotechnical and Geoenvironmental Engineering*, Vol. 124, No. 8, ASCE, 720-727.

- Fernando, N.S.M., Small, J.C., and Carter, J.P. (1996). "Elastic analysis of buried structures subject to three-dimensional surface loading." *International Journal for Numerical and Analytical Methods in Geomechanics*, Vol. 20, 331-349.
- Goddard, J.B. (1995). "A comparison of the Utah State and Ohio University soil cell tests." ORTEC Conference, Ohio.
- Kastner, R.E., Sargand, S.M., and Mitchell, G.F. (1993). "Structural performance of PVC leachate collection pipe." *Structural Performance of Pipes*, Sargand, Mitchell and Hurd (Eds.), Balkema, Rotterdam, 83-95.
- Masada, T.M., Sargand, S.M., and Hazen, G.A. (1996). "Discussion of: Interpretation of a buried pipe test: Small diameter pipe in the Ohio University facility." *Transportation Research Record*, 1541, 70-71.
- Milovic, D. (1992). *Stresses and Displacements for Shallow Foundations*. Elsevier, Amsterdam.
- Milovic, D.M., and Tournier, J.P. (1973). "Stresses and Displacements due to rigid rectangular foundation on a layer of finite thickness." *Soils and Foundations*, Japanese Society of Soil Mechanics and Foundation Engineering, Vol. 13, No. 4, 29-43.
- Moore, I.D. and Brachman, R.W.I. (1994). "Three dimensional analysis of flexible circular culverts." *Journal of Geotechnical Engineering*, Vol. 120, No. 10, 1829-1844.
- Moore, I.D. and F. Hu. 1994. *Analysis and design of buried high density polyethylene gravity flow pipe*, Geotechnical Research Centre Report GEOT-17-94, The University of Western Ontario, London, Canada.

- Moore, I.D. 1993. Structural design of profiled polyethylene pipe - Part I - Deep burial, Geotechnical Research Centre Report GEOT-8-93, The University of Western Ontario, London, Canada.
- Poulos, H.G., and Davis, E.H. (1974). Elastic solutions for soil and rock mechanics. John Wiley & Sons, Inc., New York.
- Rowe, R.K., and Soderman, K.L. (1987). Stabilization of very soft soils using high strength geosynthetics: the role of finite element analyses, Geotextiles & Geomembranes, Vol. 6, pp 53-80.
- Sargand, S.M. (1993). "Structural performance of an HDPE leachate collection pipe." Proceedings of the 31st Annual International Solid Waste Exposition, August 2-5, 1993, San Jose, CA, 381-402.
- Sargand, S.M., Hazen, G.A., Fernando, M.E.R. and Hurd, J.O. (1993). "Field performance of a corrugated HDPE pipe." Transportation Research Board, 72nd Annual Meeting, January 10-14, 1993, Washington D.C.
- Selvadurai, A.P.S. (1979). Elastic Analysis of Soil-Foundation Interaction. Elsevier Scientific Publishing Company, New York.
- Selig, E.T. (1990). "Soil properties for plastic pipe installations." Buried Plastic Pipe Technology, ASTM STP-1093, Buczala and Cassady (Eds.), ASTM, Philadelphia, 141-158.
- Small, J.C., and Wong, W.K. (1988). "The use of integral transforms in solving three dimensional problems in geomechanics." Computers and Geotechnics, 6(3), 199-216.

Zhang, C., and Moore, I.D. (1997). "Finite element modelling of inelastic deformation of ductile polymers." *Geosynthetics International*, Vol. 4, No. 2, 137-163.

Zienkiewicz, O.C., and Taylor, R.L. (1989). *The finite element method. Fourth Edition, Volume 2*, McGraw-Hill Book Company (UK) Limited, London.

TABLE 2.1 Constitutive Soil Parameters Used in the Study

	Stone	Cover Soil	Clay	In situ Clay
E (MPa) / ν	50 / 0.25	20 / 0.20	10 / 0.35	10 / 0.35
c (kPa) / ϕ°	0 / 48	0 / 36	60 / 0	60 / 0

TABLE 2.2 Vertical (ΔD_v) and Horizontal (ΔD_h) Diameter Change for Load Platform and Extensive Overburden Cases with $P=1400$ kN, $p_{av}=280$ kPa.

	Load Platform		Extensive Overburden	
	Calculated	Measured	Calculated	Measured
Soil Model	2D EI ^a	3D EI ^b	2D EI-PI ^c	2D EI-PI ^c
Soil Pipe Interface	Bonded	Bonded	Bonded	Bonded
			Smooth	Smooth
ΔD_v (mm)	-1.02	-0.93	-2.80	-2.90
			-3.44	-3.44
ΔD_h (mm)	0.82	0.62	2.58	2.90
			2.67	2.67
			-0.74	-1.06
			0.16	0.44

^a Two Dimensional Elastic Analysis.

^b Three Dimensional Elastic Analysis.

^c Two Dimensional Elasto-Plastic Analysis.

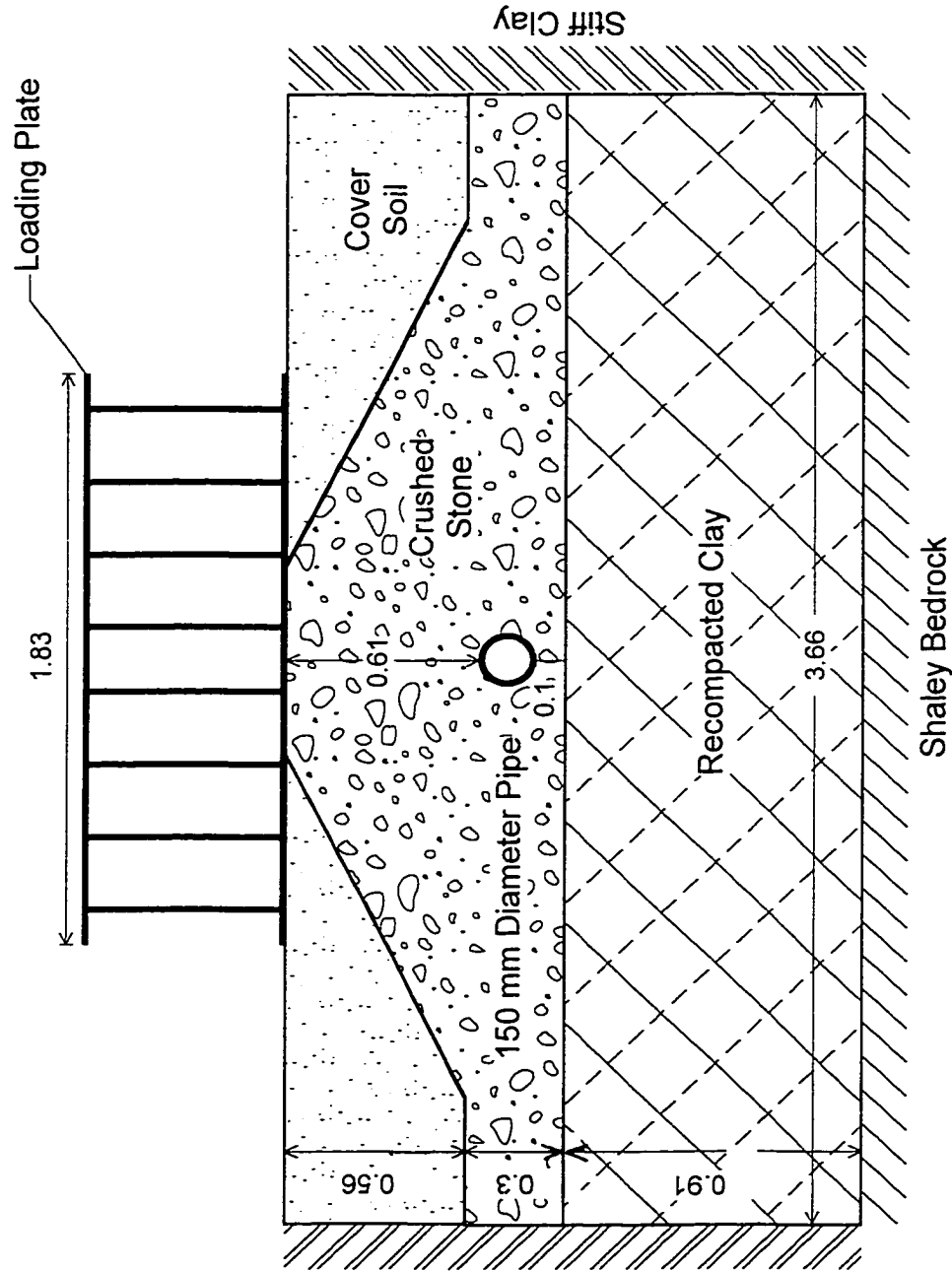


FIGURE 2.1 Cross section through Ohio University test facility showing stiff loading plate (modified from Sargand 1993). (Dimensions in metres).

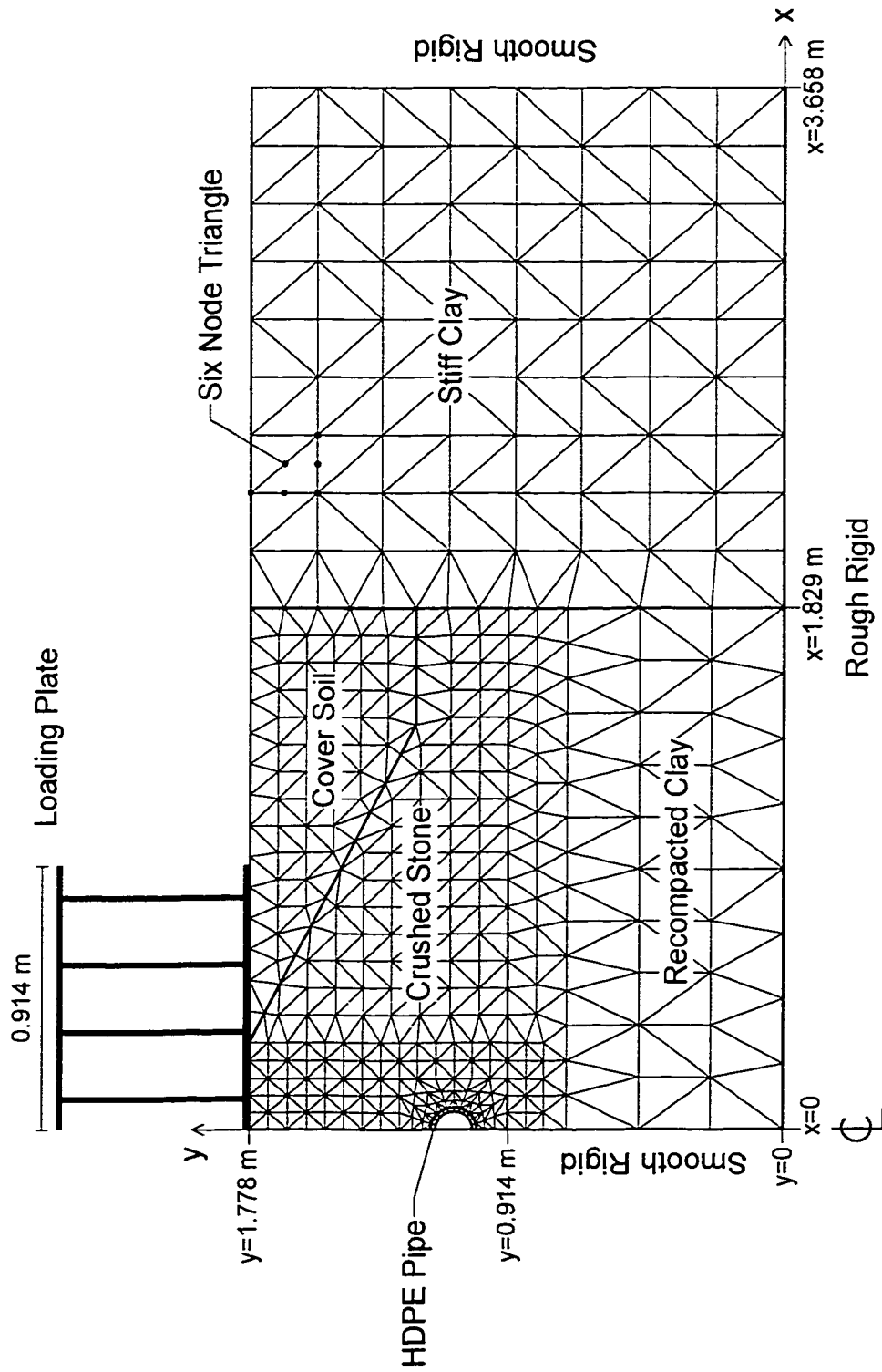


FIGURE 2.2 Cross section through Ohio University test facility showing two-dimensional finite element mesh.

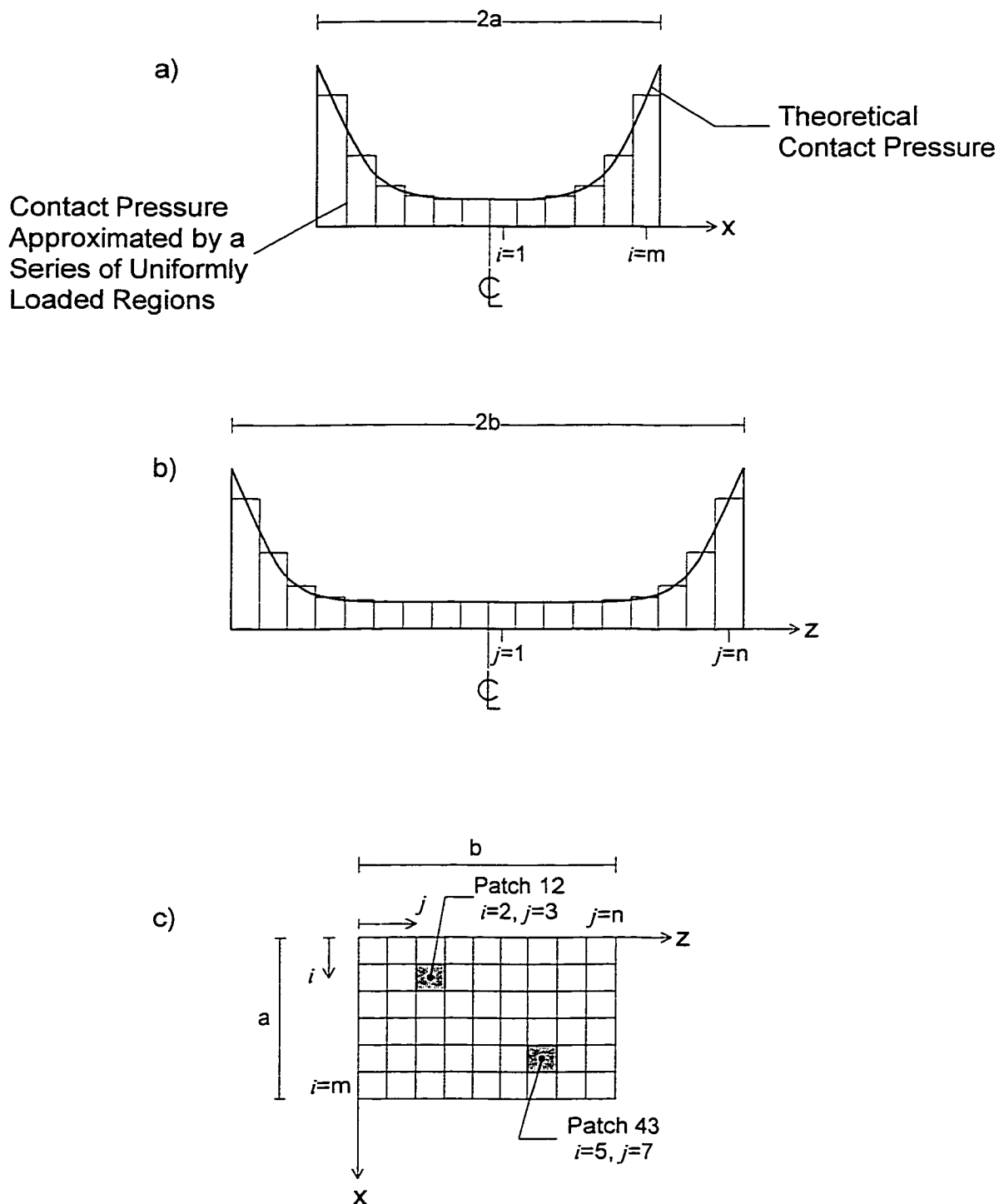


FIGURE 2.3 Contact pressure distribution beneath a rigid, rectangular footing on an elastic medium when subject to vertical force P approximated by $2m \times 2n$ regions of uniformly distributed pressure.

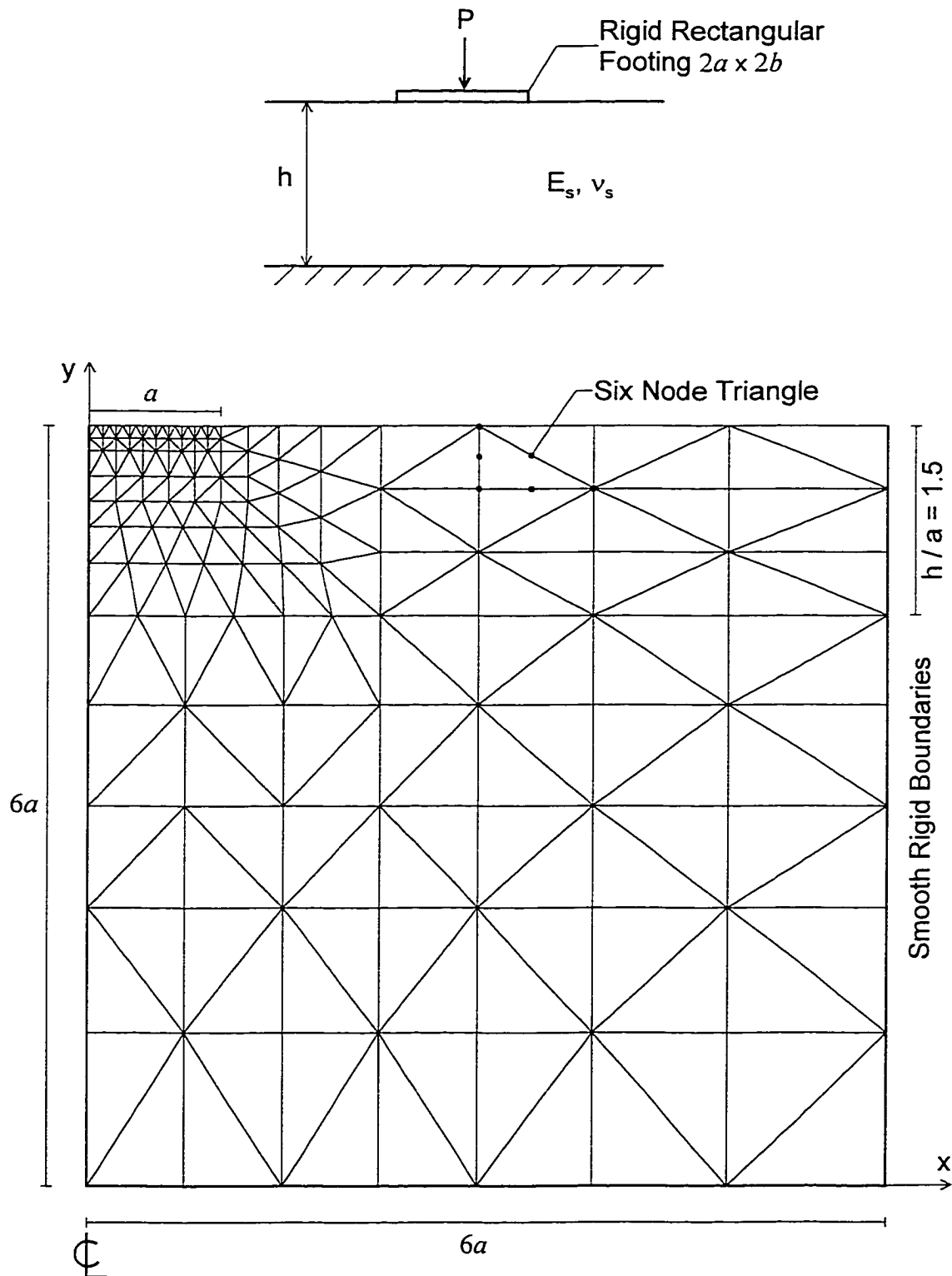


FIGURE 2.4 Finite element mesh used to solve for the response of a rectangular rigid footing ($2a \times 2b$) on an elastic layer (E_s, ν_s) of finite depth (h) subject to vertical force P .

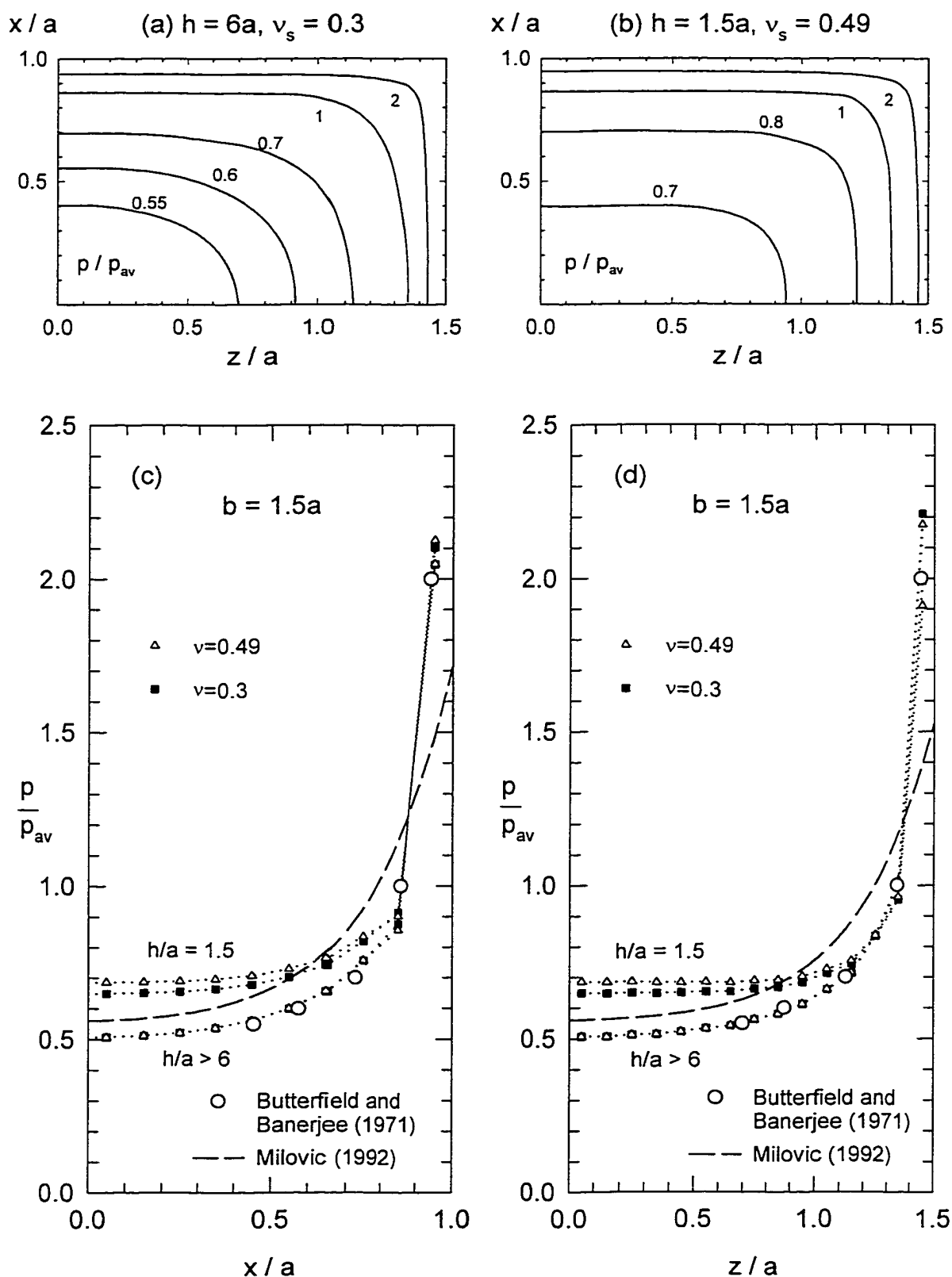


FIGURE 2.5 Calculated contact pressure for a rigid-rectangular footing ($2a \times 3a$) on an elastic layer of finite depth subject to vertical force ($m=10$, $n=15$). Solutions are given for h/a equal to 1.5 and h/a greater than 6.

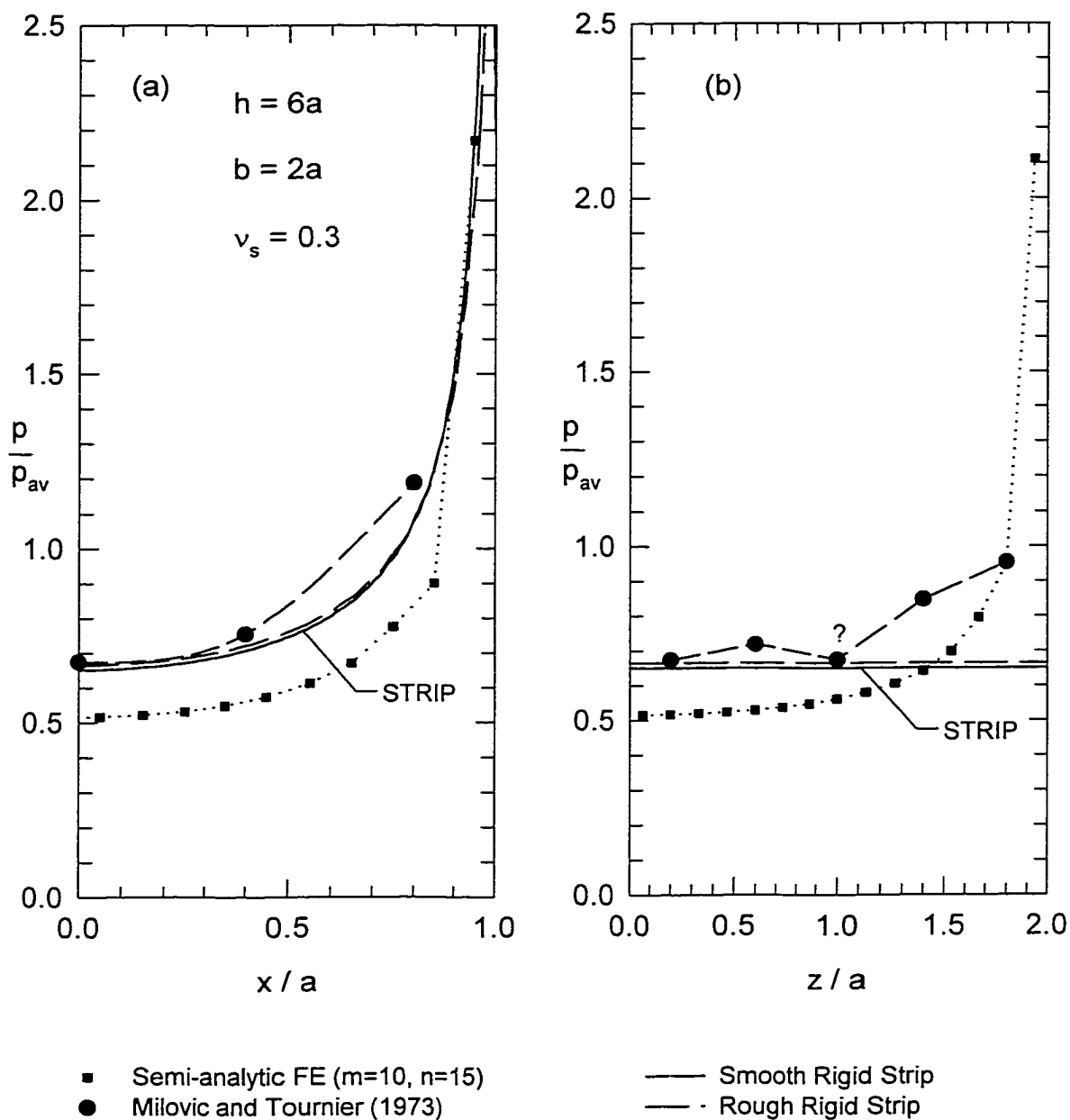


FIGURE 2.6 Contact pressure for a rigid rectangular footing ($2a \times 4a$) on an elastic layer ($\nu_s = 0.3$) of depth $h = 6a$ underlaid by a rough rigid layer ($m=10, n=15$). Solution of Milovic and Tournier (1973) for the same problem also shown. Limits for a rough rigid and smooth rigid strip (ie. $b \gg a$) are also given.

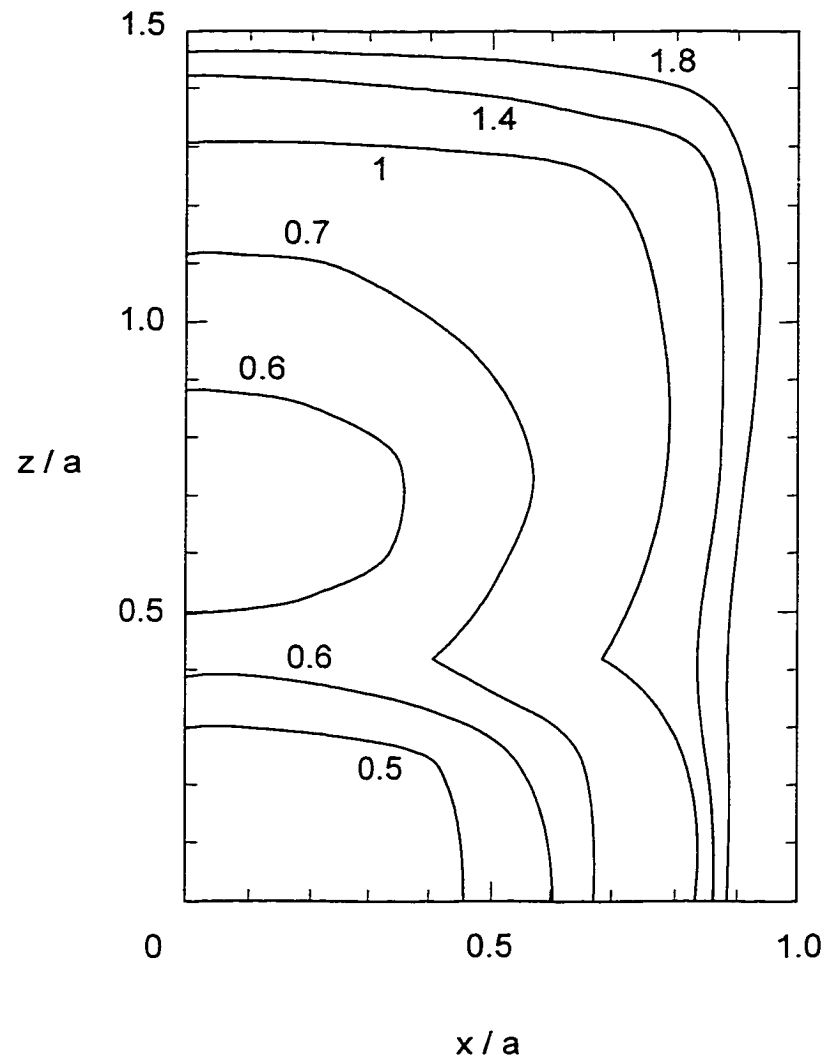


FIGURE 2.7 Calculated contact stresses imposed by the stiff plate ($b=1.5a$). Values normalized by the average surface pressure.

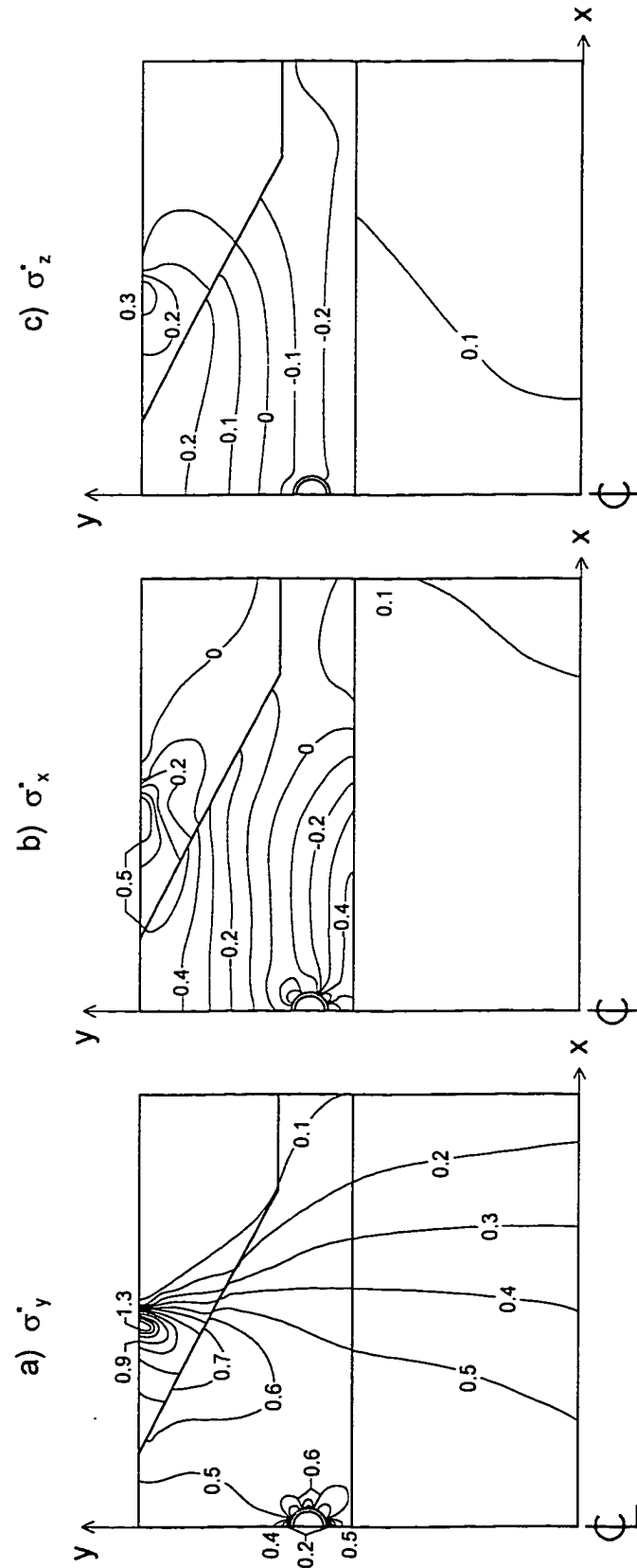


FIGURE 2.8 Contours of vertical σ_y^* (a), horizontal σ_x^* (b) and axial σ_z^* (c) stresses beneath stiff load plate. Calculated at $z=0$. Stresses are normalized by the average contact pressure ($\sigma^* = \sigma/p_{av}$).

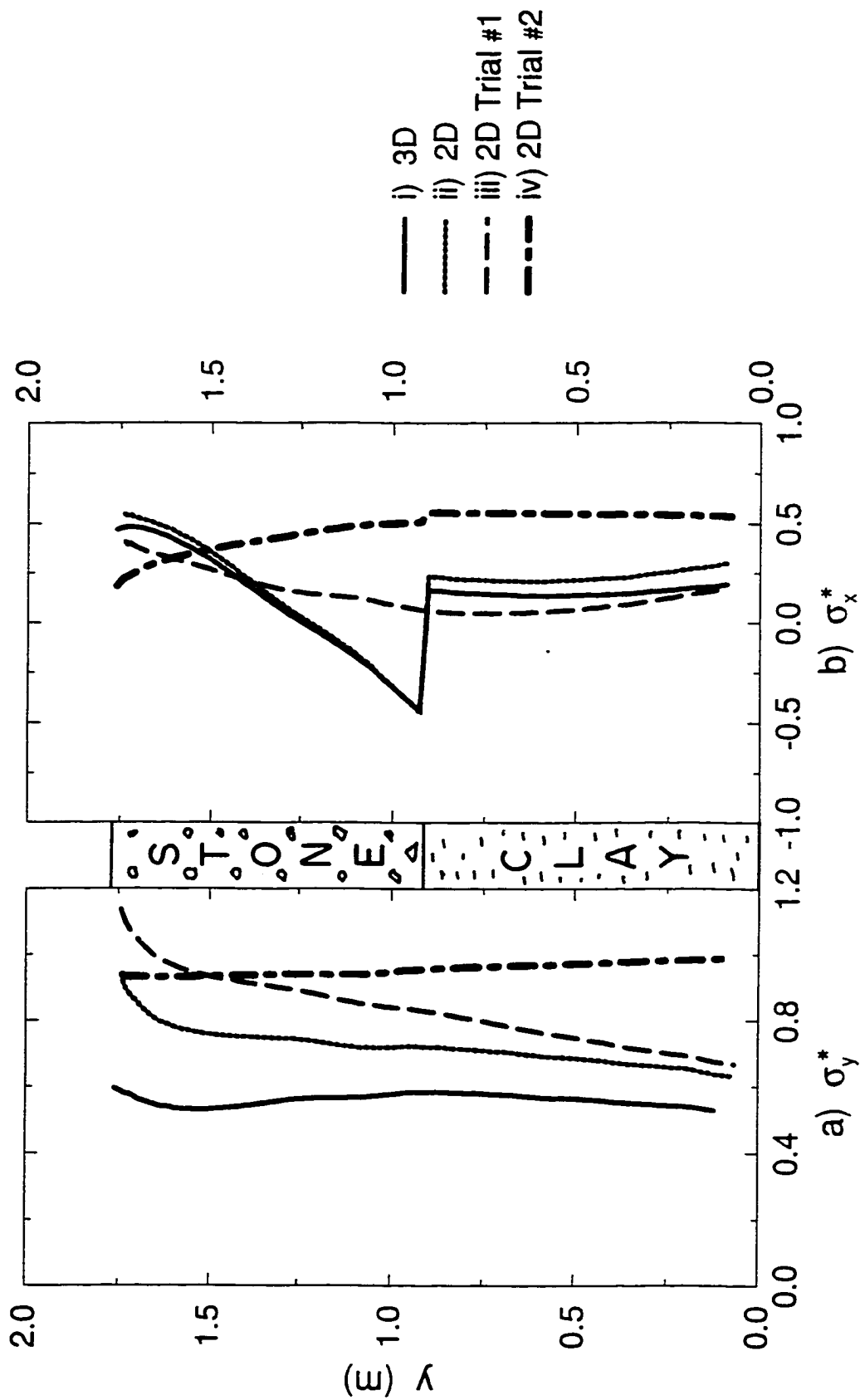


FIGURE 2.9 Normalized vertical (a) and horizontal (b) elastic stress predictions along the line $x=0.3$ m.

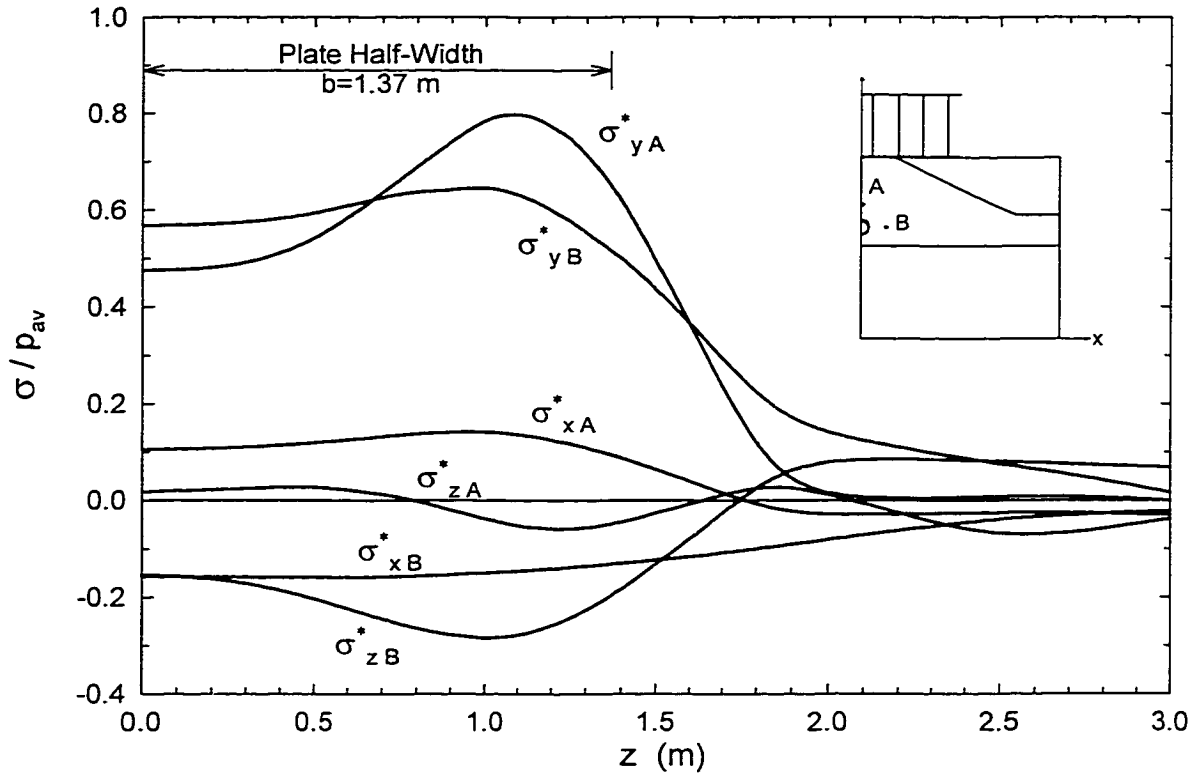


FIGURE 2.10 Variation of vertical, horizontal and axial stresses along pipe axis at points A and B.

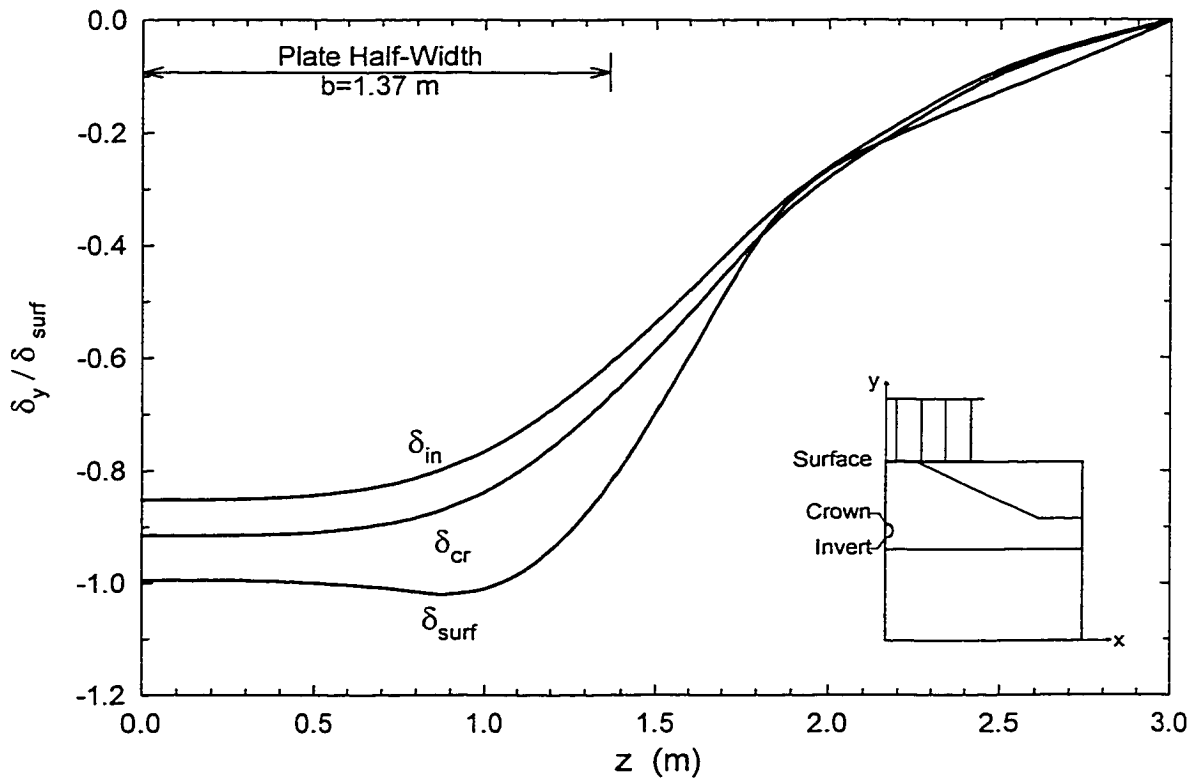


FIGURE 2.11 Variation of vertical deflections along pipe axis at the ground surface, pipe crown and pipe invert.

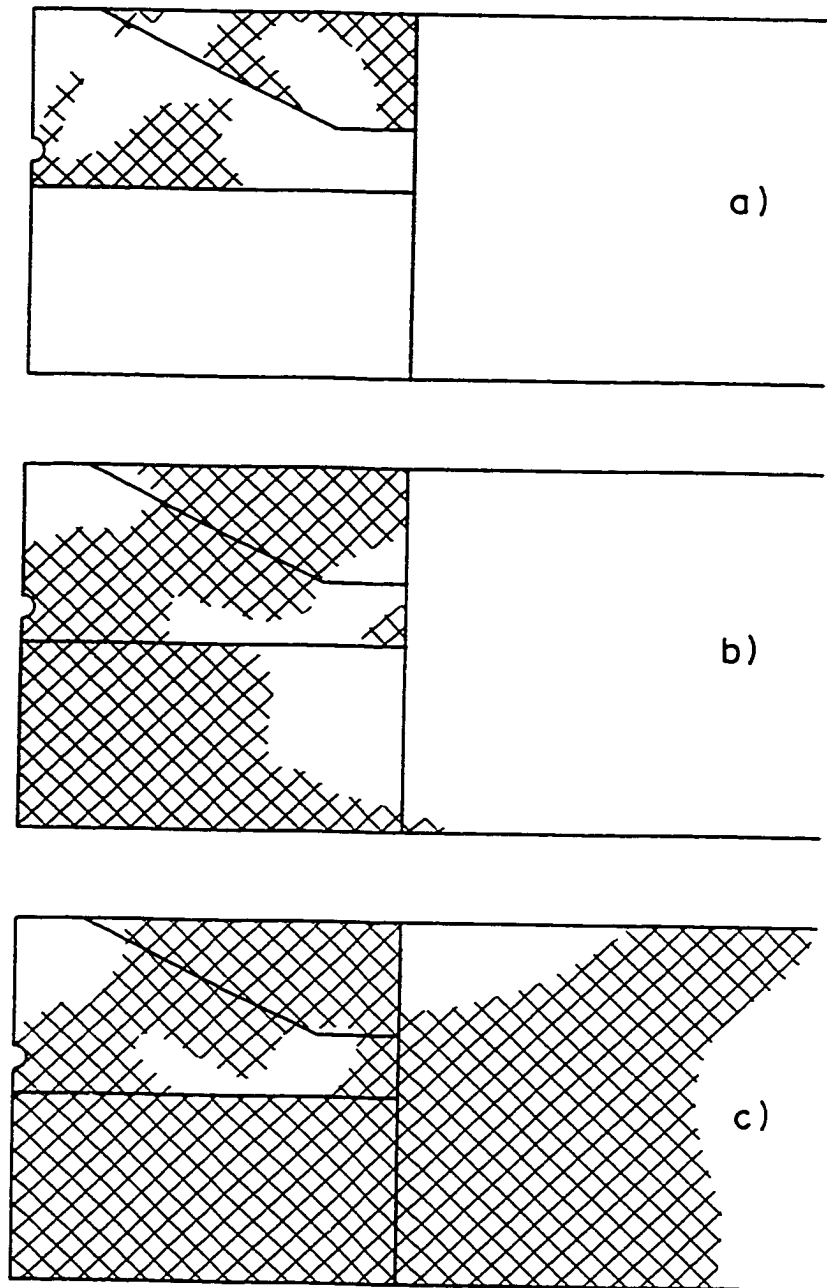


FIGURE 2.12 Predicted plastic zones for P equal to: (a) 52 kN, (b) 1400 kN, and (c) 2100 kN.

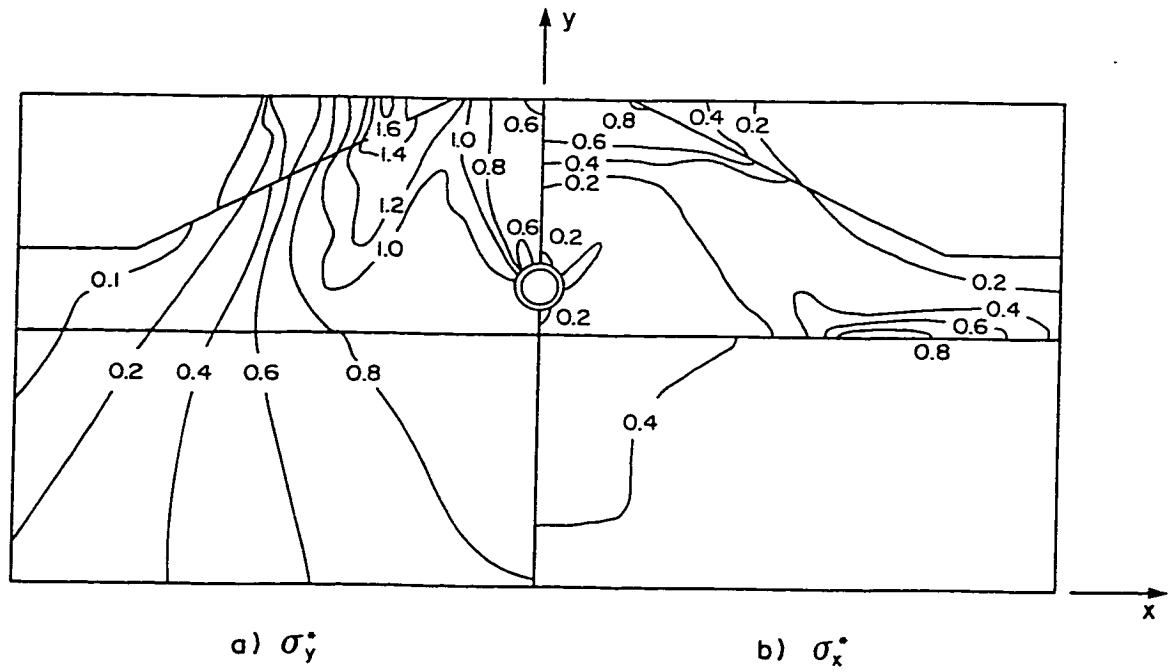


FIGURE 2.13 Normalized two-dimensional elasto-plastic stress contours at z equal to zero for P equal to 1400 kN: (a) σ_y^* and (b) σ_x^* .

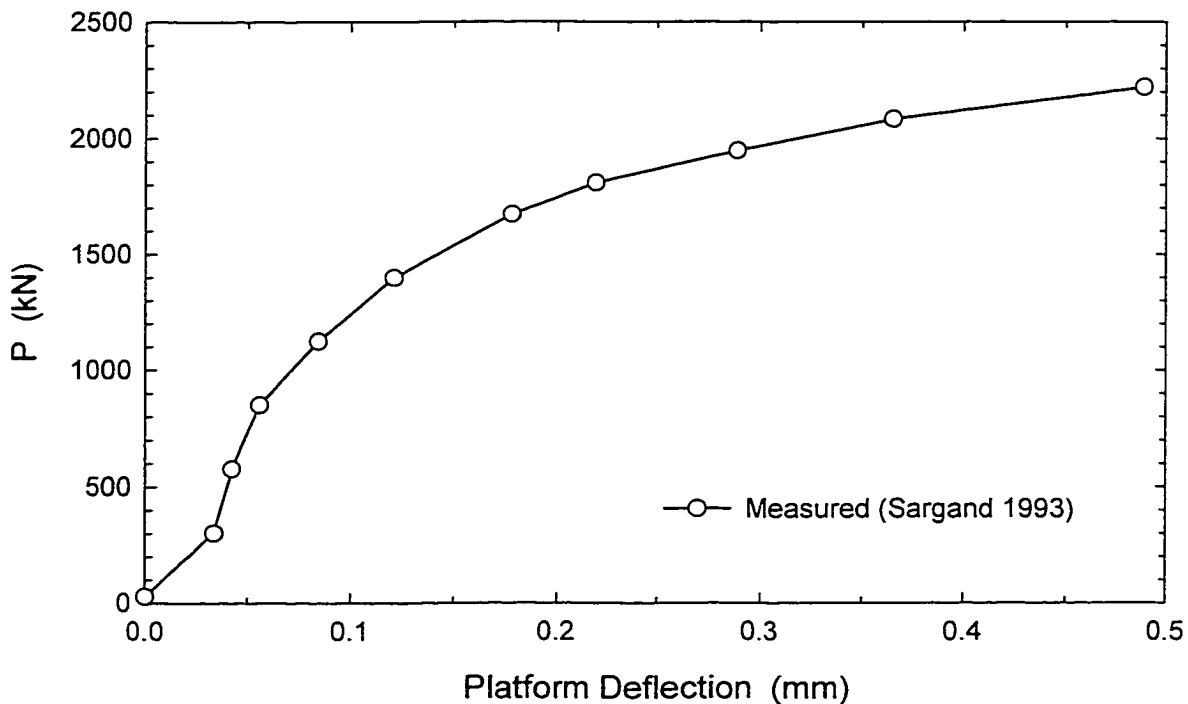


FIGURE 2.14 Measured load deflection response of load platform.

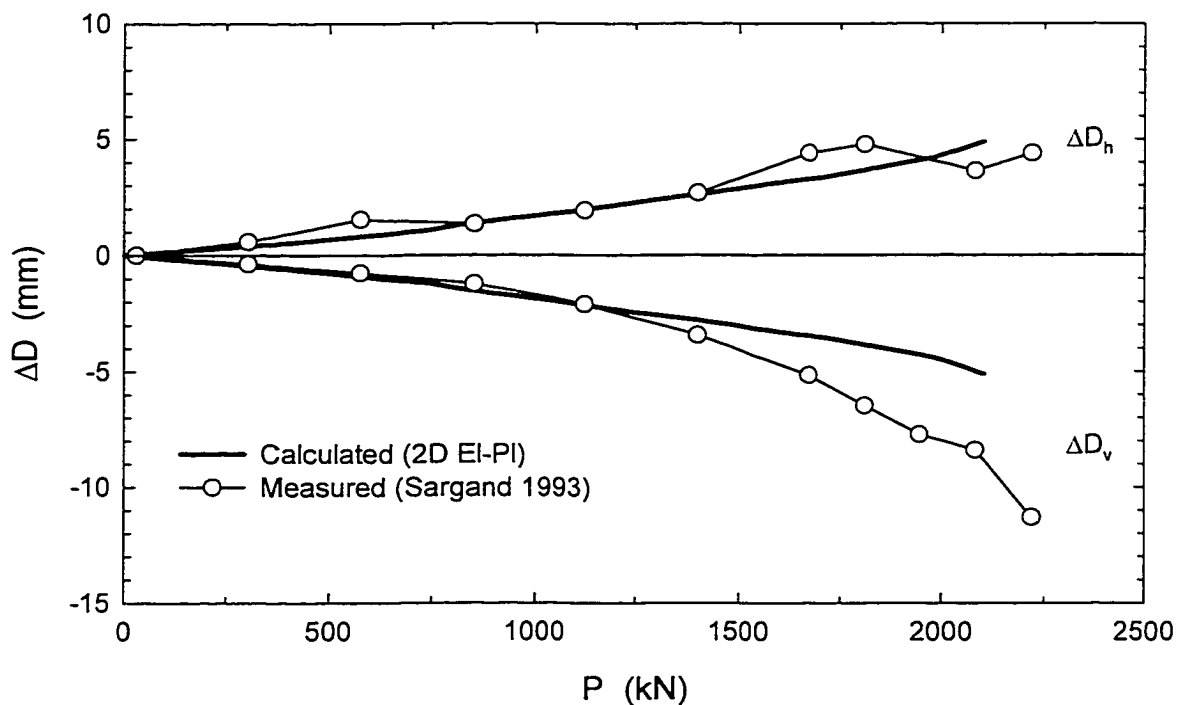


FIGURE 2.15 Measured and calculated change in vertical ΔD_v and horizontal ΔD_h pipe diameter from two dimensional elasto-plastic analysis.

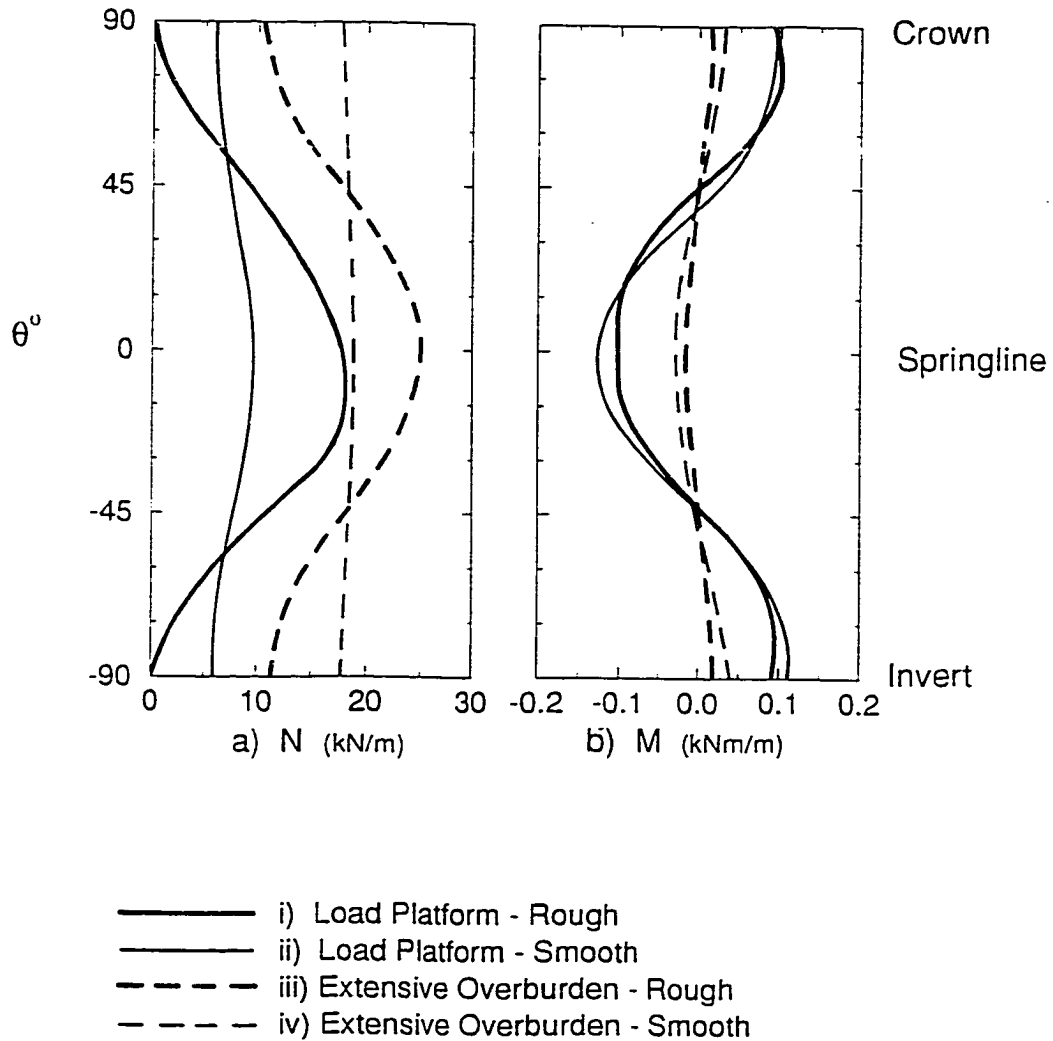


FIGURE 2.16 Two-dimensional elasto-plastic calculated (a) thrust N and (b) moment M distributions for both load platform and extensive burial cases. Rough and smooth pipe interface solutions shown at P equal to 1400 kN.

CHAPTER 3

Hoop Compression Testing of HDPE Leachate Collection Pipe

3.1 INTRODUCTION

High density polyethylene (HDPE) drainage pipes serve the vital role of collecting, transporting and removing contaminants from modern waste containment facilities. Ensuring their structural stability is an important consideration in the design of the leachate collection system.

Design measures intended to minimize the potential of particulate, chemical and biological clogging of the leachate collection system (see Rowe et al. 1995) can lead to adverse service conditions for the pipe that are not experienced in typical buried pipe applications. For example, coarse uniformly-graded gravel (e.g., crushed stone) is often specified as the backfill material surrounding the pipe, Figure 3.1. The large open void space and small surface area provided by the gravel help to minimize biologically induced clogging (Rowe et al. 1995). However, when the pipe is surrounded by coarse gravel it will be supported at discrete points around the circumference rather than the more continuous support provided by other backfill materials (e.g., sand, well graded gravel). Local bending stresses arising from the discontinuous support could potentially affect the structural performance of the drainage pipe. Thus it may be hypothesised that the use of coarse gravel may be detrimental to the structural performance of the pipe because of this discontinuous support.

Further complicating the stress conditions within these pipes are stress concentrations arising from the presence of perforations. These holes in the walls of the pipe, which are essential for the purpose of leachate collection, weaken the pipe compared to nonperforated pipe. Ideally, these holes should be sufficiently large to minimize the potential for clogging themselves and maximize the effectiveness of cleaning. However, at the same time, they should not be so large and so numerous that they compromise the structural integrity of the pipe. The magnitude of the stress concentrations from coarse gravel backfill and perforations, and their effect on the mechanical performance of the drainage pipes is presently unknown. Thicker polyethylene pipes are typically specified for use in landfill applications as a result of this uncertainty.

The performance of these geosynthetic materials is a function of both the soil backfill and the pipe. Previous studies (e.g., Moore 1993) have demonstrated that the behaviour of polyethylene pipes is different to that of conventional piping materials like steel, aluminum, polyvinyl chloride or fibreglass. Unlike thin polyethylene pipes, these other materials are stiff in the hoop direction and do not experience circumferential shortening. The response of a thick polyethylene pipe is also likely to be different to that of a thin pipe since radial stresses may not be negligible with respect to circumferential stresses, and variation of stress through the thickness of the pipe may become important as the thickness of the pipe increases. Laboratory testing of thick high density polyethylene pipes is warranted to identify how these geosynthetic materials are likely to perform when deeply buried in a landfill.

Results from laboratory tests of HDPE drainage pipes (320 mm outside diameter, OD SDR 11, where SDR is the ratio of outside diameter to the minimum wall thickness)

surrounded by two different backfill materials and loaded under axisymmetric radial pressures are reported in this chapter. The nature of the loading and the details of the test facility are briefly discussed. The materials involved in the tests are summarized. The instrumentation used to measure deformations and surface strains of the pipe are described. Results from three tests are then presented to examine the performance of HDPE drainage pipes under axisymmetric hoop compression. Measurements of surface strain around an isolated 32 mm diameter perforation are compared with values measured away from the hole to study the effect of the hole on the performance of the pipe under the simplified laboratory conditions.

3.2 HOOP COMPRESSION TESTING

Leachate collection pipes are typically surrounded by a select backfill material (e.g., coarse stone) and subject to loading from the solid waste overburden. The performance of the pipe is a function of both the stiffness of the pipe and the soil (ie. soil-pipe system). Deep burial of a pipe leads to vertical σ_v and horizontal σ_h stresses that act on the soil at some distance away from the pipe. A preliminary approach used to simulate deep burial loading in the laboratory is to consider the response of the soil-pipe system when subject to the mean of the distant boundary stresses σ_m (Fig. 3.2), where $\sigma_m = \frac{1}{2}(\sigma_v + \sigma_h)$. Compressive hoop stresses develop in the pipe when the surrounding soil is subjected to the uniform, radial stress σ_m . This idealization does not model the biaxial earth pressures σ_v and σ_h that are expected to prevail under field conditions. While test facilities capable of simulating biaxial

compression loading on a pipe do exist (e.g., Chapter 4), the simple approximation of hoop compression loading is considered to be a useful prelude to more elaborate testing and analysis. Hoop compression tests involve simple boundary conditions, require a small volume of soil, and provide results that are relatively straightforward to model and interpret.

The laboratory tests were conducted in a facility similar to the one developed by Selig et al. (1994). The particular details of the hoop compression test cell used have been reported by Moore et al. (1996). Figure 3.3 shows plan and elevation sections through the test cell. Figure 3.4 is a photograph showing a plan view of the pipe, coarse gravel backfill, bladder and steel test cell. Essentially, a test specimen of pipe 1.4 m long was placed inside a 0.9 m diameter cylindrical steel test cell with the longitudinal axis of the pipe oriented in the vertical plane. The pipe was surrounded by the backfill soil. Once the lid of the cell was placed, a pressurized air bladder was used to apply a radial stress to the soil pipe system. The bladder was made from nylon-reinforced chlorosulphunated polyethylene (1 mm thick) that was chemically seamed around the perimeter to form a sealed bag. The pressure applied by the bladder is close to the free field uniform stress σ_m (the soil zone absent beyond the air bladder has a small effect on the stress condition). The pipe response (deformations and surface strains) were recorded as the bladder pressure was applied.

Three tests were conducted in the hoop compression cell, denoted as tests H1, H2a and H2b. Table 3.1 summarizes the important details for these tests. Two specimens of 320 mm outside diameter SDR 11 pipe were tested and are referred to as pipes H1 and H2. These pipes were made with a polyethylene material with cell classification PE 345434C in accordance with ASTM D3350, and Class PE 3408 according to the Plastic Pipe Institute.

3.3 BACKFILL MATERIALS

Two different backfill materials were used in the testing. The grain size distribution curves for these two materials are shown in Figure 3.6. The material used for test H1 was a poorly graded medium sand (SP) while the uniformly (or poorly) graded 50 mm coarse gravel (GP), consisting of crushed dolomitic limestone was used for tests H2a and H2b. This 50 mm coarse gravel is now commonly specified as the drainage medium for leachate collection systems in Ontario, Canada. The two different backfill materials represent different loading conditions for the pipe. The support provided by the sand backfill will tend to be more uniform (the small sand particles provide almost continuous support around the pipe circumference), whereas the coarse gravel will provide nonuniform support (discontinuous support from much fewer contact points randomly distributed around the circumference). Figures 3.4 and 3.5 show the point loading conditions arising from the coarse gravel backfill.

Backfilling procedures were selected to obtain uniform densities within the sand. The material was dumped in place, with the height of the fall constant for each lift. The material was placed in 150 mm thick lifts and was compacted imparting the same energy to each lift (dropping a 7 kg mass a distance of 300 mm with three passes of compaction made for each lift). The densities were measured with a nuclear density meter that was calibrated with sand cone density tests to compensate for the close proximity of the steel and polyethylene. The sand was placed at an average bulk density of 1790 kg/m^3 , and an average water content of 3.4%. As in typical field applications, the stone was dumped into the cell with no attempt made to compact the stone. The stone was placed at an average bulk density

of 1410 kg/m^3 . This was obtained by recording the net weight of the stone in the cell and estimating the volume occupied by the stone.

3.4 INSTRUMENTATION

3.4.1 Pipe Deflections

The deflections of the pipe were measured using a laser analog sensor. The laser was mounted on a linear motion block and rail system capable of translating in the vertical (z) direction. Rotation in the circumferential (θ) direction of the entire assembly was achieved using two flange bearings located at the lid and base of the cell. This arrangement was intended to allow the deflection to be measured at any point inside the pipe. The error associated with the laser sensor was $\pm 0.1 \text{ mm}$. However, greater errors arose from repositioning the laser to take readings at multiple locations. Better precision was obtained with the laser when targets affixed to the pipe surface were used.

3.4.2 Pipe Strains

The surface strains of the pipe were measured using electrical foil strain gauges. Stacked rosettes with a gauge length of 2 mm (Showa type N32-FA-2-120) were selected to provide a measure of strain over a small region (important when investigating the effect of coarse gravel backfill).

The layout of gauges for Test H1 was selected to measure the variation of strain in the pipe with the more continuous backfill support provided by the medium sand. Four

rosettes were placed on the inside surface around the circumference at $\theta = 0^\circ, 90^\circ, 180^\circ$ and 270° , and two were placed on the outside at $\theta = 0^\circ$ and 270° at Section A ($z = 845$ mm) as shown in Figure 3.3. Two single gauges (also 2 mm gauge length) were oriented in the circumferential direction at $\theta = 225^\circ$ and 315° at this section.

The objective of Test H2a and H2b was to observe the effect of the coarse gravel backfill on surface strains of the pipe. A grid of rosettes located on a small portion of the inside surface of the pipe was selected to monitor the variation of strains beneath one stone contact point. Figure 3.7 shows the gauge layout at Section A for pipe H2. The centre of the grid corresponds to the location $\theta = 270^\circ$ and $z = 845$ mm, where a stone was placed on the outside of the pipe. A grid marking the location of the gauges was used to position the stone contacts in this region (Figure 3.5). Note that the circles drawn on the grid represent the location of gauges on the interior surface of the pipe. Carbon was paper placed on the outside surface of the pipe and was used for recording the location and spacing of the contact points. The rosettes were placed at 22.5 mm centre to centre spacings in the z direction (locations A, B, C, D and E) and at 18 mm spacing in the θ direction (locations F, G, C, H and I). This grid allowed the variations in circumferential and axial strains to be observed both in the z and θ directions beneath one (hand-placed) stone contact point. Two rosettes were also located at opposite points B and D on the exterior surface of the pipe.

Both pipes H1 and H2 contained a single 32 mm diameter perforation located at Section B-B ($z = 555$ mm, Figure 3.3). Figure 3.8a shows the location of the perforation. Strain gauges were positioned around the hole on both the inside and outside surfaces of the pipe. Three gauges were placed on the inside located at $0, 45$ and 90° from the circumferential direction (α), Figure 3.8b, while two gauges were placed on the outside

surface, opposite to those on the inside at $\alpha=0$ and 90° . The centre of each gauge was located 4 mm from the edge of the perforation.

Strain gauging the interior of a small diameter pipe is not a trivial task. Attaching the strain gauges to the polyethylene surface involved the following steps. First the location of the gauge was clearly marked. A mirror was used to see the inside surface of the pipe. The surface was then cleaned with isopropyl alcohol. Next the gauge was aligned with the marks and temporarily secured in place with clear tape. At this time, the location and orientation of the gauge were checked, and adjustments were made if necessary. Part of the tape was then peeled back to expose the bottom of the gauge and the bonding surface. The bonding surface was then abraded using 320 grit emery cloth and cleaned once again with the isopropyl alcohol. Next, the surface was cleaned with a neutralizing solution. Adhesive was then sparingly applied to the back of the gauge. The gauge (supported by the tape) was rolled back into place. Last, firm pressure was applied by hand for two minutes, and the adhesive was allowed to cure as specified by the manufacturer.

The potential that the strain readings can be affected by the presence of the gauge itself is acknowledged (e.g., Beatty and Chewning 1979). This arises as the stiffness of the gauge (metal foil, polymer backing and glue) is similar to that of the polyethylene. Comparisons between measured strains (using strain gauges) and calculated strains (based on measured deflections) will be made to provide a preliminary estimate of the stiffening effect on local strain readings.

3.5 RESULTS FOR TEST H1 - SAND BACKFILL

The load path followed for Test H1 is shown in Figure 3.9, plotting the applied bladder pressure against the elapsed time of the test. The 50 kPa increments of pressure were rapidly applied and kept constant for a 10 minute duration. Pipe deformations, surface strains, and gauge stiffening results from Test H1 are now examined.

3.5.1 Pipe Deformations

The deflected shape of the pipe when tested in the sand backfill is plotted in Figure 3.10a for the central section ($z = 700$ mm). Values are shown for applied bladder pressures of 250 and 500 kPa, and are magnified by a factor of twenty. These plots are presented to observe the mode of deformation of the pipe when subjected to hoop compression loading. The diameter decreases as pressure is applied. There is a shift in the position of the pipe as it translates down and to the right (relative to Figure 3.10a). Excluding the rigid body translation, essentially radially symmetric deformations were experienced by the pipe. At an applied pressure of 500 kPa, the average diameter change (ΔD) is -1.5 mm, with a 15% difference between the largest (-1.6 mm) and smallest (-1.4 mm) measured values across diameters 0° - 180° and 90° - 270° , respectively.

3.5.2 Surface Strains

The circumferential (ϵ_θ) and axial (ϵ_z) surface strains of the pipe are now examined. The strain values are plotted against time, with compressive strains negative. Strain values are expressed as microstrain ($\mu\epsilon$), where $1000 \mu\epsilon$ is 0.1% strain.

Figure 3.11a plots the measured circumferential strains on the interior surface of the pipe at Section A ($z=845$ mm). Values are shown for ϵ_{θ} measured at four circumferential positions ($\theta=0^{\circ}$, 90° , 225° , and 270°). The circumferential gauges located at $\theta=180$ and 315° did not provide readings (damaged lead wire connections). The strain rapidly increased when the bladder pressure was applied followed by a small creep component of strain for the remainder of each increment. The measured values of ϵ_{θ} became increasingly negative under hoop compression loading, and reached an average value of $-4350 \pm 100 \mu\epsilon$ (where $\pm 100 \mu\epsilon$ is the 95% confidence interval of the mean) at a time of 112 minutes, which corresponds to an applied bladder pressure of 500 kPa. These four readings agree quite well with each other, having a standard deviation of $90 \mu\epsilon$. This corresponds to a coefficient of variation (ie. mean \div standard deviation) of 2% at this load level. Only a 4% difference was observed between the maximum value (measured at 270°) and the minimum value (recorded at 90°) for this load level. The measured values are summarized in Table 3.2. Overall the strain readings in the circumferential direction were uniform, as expected for the medium sand backfill.

The axial strains measured on the inside surface at Section A are plotted in Figure 3.11b. Values of ϵ_z are shown for locations $\theta=0^{\circ}$, 90° , 180° , and 270° . The axial strains feature a similar response with time as ϵ_{θ} , with a rapid increase in strain followed by a small component of creep. The measured ϵ_z values increase to an average value of $2900 \pm 500 \mu\epsilon$ at 112 minutes (500 kPa applied pressure). These strains are positive implying extension of the pipe in the axial direction.

The positive axial strains measured in this test result from a small degree of confinement in the axial direction. The deflection of the lid of the cell was estimated to be

3 mm at a bladder pressure of 500 kPa, which corresponds to an axial strain of roughly 2100 $\mu\epsilon$. The hoop compression cell was originally designed for testing large diameter profiled wall polyethylene pipes which feature a small cross-sectional area (e.g., Moore et al. 1996). However, for thick pipes that feature a large cross-sectional area, coupled with the high Poisson's ratio for polyethylene ($\nu=0.46$), large axial forces are generated during testing. The stiffness of the steel lid and insert plate were not sufficiently large enough to obtain the plane strain conditions ($\epsilon_z = 0$) that could occur at many locations in the field. The end restraint conditions for this test are probably closer to plane stress conditions ($\sigma_z = 0$), which are also relevant for the leachate collection pipe problem (e.g., near thermal expansion joints). Another component of the observed axial strains arises from longitudinal bending of the pipe because the load is not applied across the entire pipe length (see Fig 3.3).

The axial strains vary more than the circumferential strains. There is a 20% difference between the minimum and maximum values measured at $\theta = 0^\circ$ and 90° . The standard deviation was 300 $\mu\epsilon$ at an applied bladder pressure of 500 kPa, yielding a coefficient of variation of 10%. This variation arises because of bending in the axial direction that tends to reduce the axial strains at $\theta = 0^\circ$ and 270° and increase the values at $\theta = 90^\circ$ and 180° . This bending is consistent with the deformations depicted in Figure 3.10a.

3.5.3 Estimate of Strain Gauge Stiffening

The effect of the gauge stiffness upon the local strain readings may be observed by comparing circumferential strain values measured using the strain gauges with values of strain calculated from measured deflections. For axisymmetric conditions, where there is no variation of circumferential deflection in the circumferential direction (ie. $\partial \rho_\theta / \partial \theta = 0$), the

strains on the inside surface of the pipe can be expressed as $\epsilon_{\theta} = \Delta D / D_i$, where D_i is the inside diameter of the pipe. Figure 3.12 shows that the average strain measured with the strain gauges ($\epsilon_{\theta_{avg}}$) is consistently smaller in magnitude than the strain computed from the average diameter change ($\Delta D_{avg} / D_i$). Apart from some scatter of the values based on deflections at pressures of 150 kPa and 450 kPa, the two curves exhibit similar trends. At an applied bladder pressure of 500 kPa the strain gauges measure only 73% of the circumferential strain calculated based on deflections. The strain gauge readings are consistently smaller because of a reinforcing effect provided by the gauge itself. The stiffness of the gauge is similar to that of the polyethylene, resulting in a local perturbation in the strain field beneath the gauge. Surface strain readings on polyethylene obtained from conventional strain gauges should be corrected for this stiffening effect especially when stress resultants are obtained from measured strains. For the remainder of this chapter, comparisons are made based on measured (uncorrected) strain values for studying the variations induced by the stone. Estimates of pipe stresses (based on measured strains) are corrected for this effect.

3.6 RESULTS FOR TEST H2a AND H2b RESULTS - COARSE GRAVEL BACKFILL

The load paths followed for Test H2a and H2b (Figure 3.9) were similar to that for Test H1. The maximum pressure obtained in Test H2a was 250 kPa and 350 kPa for test H2b, both limited because the bladder failed. The deformations and surface strains for Test H2a and H2b are now presented.

3.6.1 Pipe Deformations

The deflected shapes of the pipe during test H2a are plotted in Figure 3.10b for three pressure levels (50, 100 and 200 kPa), again with the deformations magnified by a factor of 20. The deflected shape is roughly circular for the first load increment to 50 kPa. For the next and all subsequent load levels, the deflected shape is nonuniform with a large radial deflection observed at $\theta=45^\circ$. At a pressure of 200 kPa, the diameter change is -2.2 mm across the $45^\circ - 225^\circ$ diameter, while it is equal to -1.6, -1.5 and -1.2 for diameter lines $0^\circ - 180^\circ$, $90^\circ - 270^\circ$, and $135^\circ - 315^\circ$, respectively. It is challenging to physically account for the large deflection observed at 45° . The possibility that this is a result of a laser error was ruled out because of the consistency of deflection readings at this point for all load levels in this test. Similar nonuniform deflections were observed at other sections in this and another test. Figure 3.10c plots the deformed shapes of the pipe for test H2b illustrating the nonuniform deformations measured in this test, with relatively large deflections at $\theta=90^\circ$. These nonuniform deflected shapes are therefore attributed to the discontinuous support provided to the pipe from the coarse gravel backfill.

3.6.2 Surface Strains

The variations of surface strains from test H2a provide a measure of the effect that the discontinuous support provided by the coarse gravel backfill has on the structural response of the pipe. A summary of the measured values is presented in Table 3.3. Since the strain measurements were made with a stacked rosette gauge, the principal strains could be computed directly from the three strain measurements at each point. For each location the major and minor principal strains were oriented in the circumferential and axial directions.

This fact was important to verify since rosette gauges are more expensive and require the recording of greater number of readings than a biaxial gauge (where the two gauges are perpendicular to each other). For the more detailed laboratory study reported in Chapters 5 and 6, biaxial gauges oriented in the circumferential and axial directions were predominantly used.

The variation of ϵ_{θ} in the circumferential direction is plotted in Figure 3.13a showing strain measured at points F, G, C, H, and I of the strain gauge grid (Figure 3.7). The sudden decrease in strain at 59 minutes corresponded to the failure of the bladder. The strains increase to an average value of $-2000 \pm 500 \mu\epsilon$ at 58 minutes (250 kPa) with a coefficient of variation of 16%. A 38% difference in ϵ_{θ} between the maximum G and the minimum I compressive strains was found at 250 kPa. Since the circumferential strain readings from the sand test (H1) demonstrated that consistent strain readings could be reproduced under axisymmetric conditions (with only a 2% coefficient of variation), the observed variation in circumferential strain recorded during Test H2a is therefore attributed to the discontinuous loading conditions imposed by the coarse gravel backfill.

Variation of ϵ_{θ} in the axial direction is plotted in Figure 3.14a for points A, B, C, D, and E of the grid (Figure 3.7). At a load level of 250 kPa, there is a 27% difference between the measured maximum and minimum values recorded at points B and E, respectively. These values are summarized in Table 3.3.

The following observations can be made regarding the variation of circumferential strain on the inner surface of the pipe:

- the maximum ϵ_{θ} values were measured in between closely spaced contacts (Points B, F, and G),

- the next highest values were measured at points directly beneath stone contacts (Points C and A),
- the lowest values measured were at points between widely spaced contacts.

The variation of axial strains in the circumferential direction are examined in Figure 3.13b and 3.14b. Figure 3.13b shows a 40% variation in ϵ_z between points C and F at 250 kPa. Likewise, a 60% difference was found between the maximum and minimum values in Figure 3.14b. These variations are also attributed to the point loading of the coarse gravel on the pipe, as they occurs over a small section of the pipe interior.

Considering the ten strains measurements of the grid together yields a mean circumferential strain of $-1900 \pm 200 \mu\epsilon$ at 250 kPa. A coefficient of variation of 16% was found for these measurements. The maximum recorded strain was near 1.3 times the mean value, similar to the ratio of mean to the minimum value. Axial strains varied more than the hoop strains with the ten measurements yielding a mean of $1300 \pm 300 \mu\epsilon$, and a coefficient of variation of 30%.

The same pipe specimen was tested again (H2b) with conditions identical to test H2a. Fewer gauges of the grid shown in Figure 3.7 were monitored to permit measurements of strain around the perforation (reported in the next section). The results between tests H2a and H2b were not statistically different at the 95% significance level (using a t-test distribution), thus permitting a valid comparison of measured values between the two tests.

The strains recorded during test H2b are also reported in Table 3.3, at an applied pressure of 250 kPa. Results similar to those of test H2a were obtained since for both tests, the stones opposite the grid of strain gauges (Figure 3.5) were hand placed in a nearly

identical manner. If the stones were placed in a random manner in each test, then the results from different tests would be expected to be different. For the fewer number of measurements during test H2b, the mean circumferential strain was $-1900 \pm 300 \mu\epsilon$ with a coefficient of variation of 16%, while the mean axial strain was $1450 \pm 300 \mu\epsilon$ (20% coefficient of variation), both at a pressure of 250 kPa.

The strains measured at Section A during test H2b are plotted in Figure 3.15 against the applied bladder pressure. Also shown on these plots are the measured strains at Section A from test H1. Overall, the response of both backfill materials and the pipe are essentially linear over the applied pressures tested. The variation in hoop strains due to the gravel backfill is evident from the data in Figure 3.15. The hoop strains with gravel backfill are 16% smaller, on average, than those for the sand backfill. At 350 kPa, the mean hoop strain from six readings was $-2600 \pm 400 \mu\epsilon$ with gravel backfill, while $-3100 \pm 160 \mu\epsilon$ was recorded for the sand backfill. This difference between the two means is statistically significant at the 95% level. However, this comparison indicates only a slightly stiffer response of the gravel when tested in hoop compression relative to the sand at this particular density.

3.6.3 Calculated Stresses

The variation in pipe stresses resulting from the gravel backfill are of practical interest to the engineering community. However, the computation of stresses from measured values of surface strain is not trivial. Issues such as the strain gauge stiffening effect and the selection of a modulus value for polyethylene complicate the computations of stress from values of surface strain.

An estimate of the pipe stresses can be obtained based on the measured surface strains using Hooke's Law for plane stress in the radial direction (ie. $\sigma_r = 0$, which is valid on the inside surface of the pipe tested). An important consideration in estimating the pipe stresses based on measured strains is the selection of appropriate constitutive parameters for polyethylene. In general, the mechanical response of polyethylene is highly nonlinear and time dependent. The viscoplastic constitutive model of Zhang and Moore (1997) - developed from samples taken from the same pipe material - was used to estimate Young's modulus for the appropriate strain levels and time. Secant moduli of 470, 440 and 400 MPa were used based on measured strains corresponding to applied bladder pressures of 250, 350 and 500 kPa, respectively. Poisson's ratio of 0.46 and a strain gauge correction factor of 1.4 were used in all calculations.

The hoop and axial stresses calculated from the measured strains at Section A for tests H2a and H2b are summarized in Table 3.4 at an applied bladder pressure of 250 kPa. Compressive stresses are taken as negative values. Similar values of pipe stresses are obtained for the two tests. The mean hoop stress from test H2a was -1.1 ± 0.2 MPa, with values varying from the -0.7 MPa to -1.4 MPa. While the local bending stresses arising from the gravel backfill cause these variations (50% difference between maximum and minimum), the pipe is sufficiently thick (for this particular coarse gravel and pipe diameter) such that tensile stresses do not exist in the hoop direction when subject to the axisymmetric radial stresses applied by the bladder. Tensile stresses are typically a greater concern for polyethylene pipes, related to the long term potential for stress cracking. When the pipe is subject to biaxial earth pressures (ie. where the vertical pressure is greater than the horizontal

pressure), tensile stresses may occur in the pipe. In this case, local bending effects imposed by the coarse gravel backfill will likely lead to larger tensile stresses at some locations.

Axial stresses are tensile with a mean of 0.3 ± 0.2 MPa at 250 kPa pressure. These tensile stress are well below allowable working stresses of 4.3 MPa (hydrostatic design stress) for these pipe materials. However, these results do show that tensile axial stresses can occur in the pipe if little axial restraint is provided to the pipe. Axial tensile stresses are increased by the local bending effects from the coarse gravel. The effects of the local bending stresses on the hoop and axial stresses in the pipe when subject to the more realistic case of biaxial earth pressures are investigated in Chapter 6.

3.7 PERFORATIONS

Results of measured surface strains are now presented to study the redistribution of strains around a single perforation located at Section B (see Figures 3.3 and 3.8). First, distributions of strain measured tangential and normal to the hole are examined. Comparisons are then made between the strains measured near the hole and those occurring distant from the perforation. Results are presented for both sand and gravel backfills. The sand backfill results are examined prior to the more complex case involving coarse gravel backfill.

3.7.1 Sand Backfill

Strain distributions measured around a single perforation are presented in Figure 3.16 for an applied pressure of 500 kPa. These plots show the variation of strain tangential and normal

to the hole for different locations around the hole (α as defined in Figure 3.8b). Results are shown for both inside and outside surfaces of the pipe (Section X-X of Figure 3.8a).

Figures 3.16a plots the strain measured tangential to the hole on the interior surface of the pipe. Values are given for locations $\alpha=0$ and 90° around the hole that were oriented in the axial and circumferential directions, respectively. The gauge at $\alpha=45^\circ$ did not provide a reading (broken lead wire). The strains of Figure 3.16a are indicative of oval-type deformations of the circular hole, with tensile strains recorded at $\alpha=0^\circ$ and compressive strains at $\alpha=90^\circ$. Strains normal to the hole (Figure 3.16c) also vary around the hole with similar magnitude but opposite sign of those tangential to the hole.

Strains tangential to the perforation measured on the exterior surface of the pipe are plotted in Figure 3.16b. There is a similar distribution in strain compared to the values of Figure 3.16a (ie. tensile strains at $\alpha=0^\circ$ and compressive strains at $\alpha=90^\circ$), however the magnitudes are substantially different. The strain at $\alpha=0^\circ$ is a much greater tensile value on the exterior surface, while the compression at $\alpha=90^\circ$ is smaller than that measured on the inside surface. The variation in strain through the pipe thickness is a noteworthy observation suggesting that any interpretation should involve a consideration of three dimensional geometry. Analysis of perforations using a simple approximation of a hole in a thin plate or cylindrical shell (for which solutions do exist) may not capture the mechanics of this particular problem.

The maximum compressive strain was recorded tangential to single perforation on the inside surface at $\alpha=90^\circ$. This value is plotted versus the applied bladder pressure in Figure 3.17 (hollow circles). Here it is compared with the strain measured distant from the perforation (solid circles). The circumferential strain distant from the perforation was

obtained by averaging the four values measured at Section A. The disturbance to the local strain field caused by a single perforation is demonstrated by the increase in strains recorded tangential to the hole relative to the Section A. The strain at $\alpha=90^\circ$ near the hole is consistently larger than the strain distant from the hole with a maximum value of $-6700 \mu\epsilon$ compared to the average distant circumferential strain of $-4350 \mu\epsilon$, both at an applied pressure of 500 kPa . This corresponds to a strain concentration around the perforation 1.6 times the undisturbed value.

3.7.2 Coarse Gravel Backfill

Strains tangential and normal to the perforation for the case of coarse gravel backfill are presented in Figure 3.18 at a bladder pressure of 350 kPa. The results of Figure 3.18 are similar to those obtained with sand backfill (Figure 3.16), again with the maximum compressive strain located at $\alpha=90^\circ$ on the inside surface and tangential to the hole. Also, the distribution of strains around the hole are consistent with the pattern observed for sand backfill conditions. The tensile strains measured at $\alpha=0^\circ$ are smaller than those for the sand test, especially on the inside surface.

Comparison of the strains around the perforation with values measured away from the hole is not as straightforward as for the case with sand backfill. The strains inherently vary because of the discontinuous nature of the backfill-support provided by the coarse gravel. For this reason, six values of circumferential strain opposite one contact zone at Section A were averaged to characterize the strains distant from the perforation, yielding an average strain of $-2600 \pm 400 \mu\epsilon$ at a bladder pressure of 350 kPa.

The average circumferential strains distant from the perforation are also plotted in Figure 3.17 (solid triangles). These coarse gravel strains are slightly smaller than those measured for sand backfill conditions, reflecting a small difference in soil modulus between the two backfill materials. Overall, the response is linear over the pressure range tested for both materials. The strain measured near the perforation (hollow triangles) is 10% larger than the sand value. It is likely that the value measured around the perforation may also involve variations like those measured at Section A because of the discontinuous backfill-support. The measured value near the perforation was $-5500 \mu\epsilon$ at 350 kPa. This value is 2.1 times the average distant value strain. As might be expected, it appears that the coarse gravel backfill further complicates the strain response around the perforation.

3.7.3 Estimate of Stresses Near Perforation

An estimate of the maximum stresses based on measured strains was made using the viscoplastic constitutive model of Zhang and Moore (1997). The maximum compressive stress around the perforation occurs on the interior surface and tangential to the hole (ie. in circumferential direction) at $\alpha=90^\circ$, while the maximum tensile stress occurs on the exterior surface at $\alpha=0^\circ$ and oriented in the axial direction.

For the sand test, the maximum compressive stress was estimated to be -4.2 MPa, which is roughly 1.9 times the hoop stress distant from the perforation (ie. at Section A), at 500 kPa bladder pressure. Also at this pressure, the maximum tensile stress near the perforation is nearly 2.7 MPa. It is more difficult to define a stress concentration factor given only two measurements of strain on the exterior surface of the pipe. Based on the

limited data, the tensile stresses near the perforation are approximately 1.5 times those away from the hole.

When tested with the sand backfill, the maximum compressive stress was estimated to be -3.6 MPa at a bladder pressure of 350 kPa. This value is approximately 2.7 times the average of the six measurements made at Section A. Clearly, the coarse gravel backfill complicates the response around the perforation, leading to a larger stress concentration factor than that found with the sand backfill. A maximum tensile stress of 1.8 MPa was calculated on the exterior surface near the hole. No attempt is made to estimate the exterior stresses at Section A based on measurements of strain at two locations only.

Chambers and McGrath (1981) have suggested the use of strain (and stress) concentration factors of 2.3 for a circular hole in a smooth-wall pipe (like that considered here) in bending, and 3.0 for a circular hole in uniform tension. The stress concentration factor of 3.0 is the maximum value that can be obtained from the solution for a hole in a plate. Based on the limited measurements it appears that a stress concentration factor of approximately 3.0 can be used for preliminary design purposes which includes the influence of the coarse gravel.

The single perforations tested here are subject to both compressive and tensile stresses (in the circumferential and axial directions, respectively). A good design practice would be to place the perforations at the quarter points which are close to the points of inflection (ie. where the hoop stresses are the smallest) when subject to the biaxial earth pressures expected under field conditions.

3.8 SUMMARY

The results of hoop compression tests for 320 mm OD, SDR 11 HDPE drainage pipes tested with medium sand and coarse gravel backfill materials were presented. The loading conditions, test cell features and instrumentation were described. When tested with the sand backfill the thick polyethylene pipe response was largely axisymmetric. The measured diameter changes of the pipe were relatively uniform, although some translation was observed. The measured circumferential strains closely matched each other demonstrating that consistent readings could be obtained. A stiffening effect of strain readings using electrical foil strain gauges was observed and a simple correction factor of 1.4 based on measured deformations was proposed. Tensile axial stresses occurred in the pipe because the load was not placed along the entire length of the pipe and since axial restraint provided by the test cell was closer to plane stress conditions. Improvements in bladder design since this work (e.g., see Chapter 5) and axial stiffening of the test cell would result in better loading conditions for future laboratory tests conducted with this facility.

The results of the tests conducted with coarse gravel backfill demonstrated that nonuniform pipe deflections occur because of the discontinuous nature of support provided to the pipe by the stone. Circumferential and axial strains on the inside surface of the pipe varied over 40% beneath one stone contact. Comparison of tests with medium sand and coarse gravel backfill materials demonstrated the adverse conditions a leachate collection pipe experiences when deeply buried in a leachate collection system. Additional testing is warranted to better characterize the thick polyethylene pipe response under more realistic biaxial earth pressures. This is the subject of Chapter 6.

Measurements of surface strain around a 32 mm diameter perforation in a 320 mm diameter, 32 mm thick, high density polyethylene pipe were presented. These values were compared with strains measured distant from the perforation to study the effect of an isolated hole on the pipe strains. Strain concentration factors of 1.6 and 2.1 were measured near the perforation with sand and coarse gravel backfills, respectively. The maximum compressive strain occurred tangential to the perforation oriented in the circumferential direction on the pipe interior surface, while the maximum tensile strain was recorded on the exterior of the pipe oriented in the axial direction. These locations are also where the maximum compressive and tensile stresses were calculated. Stress concentration factors up to 3.0 were found around the perforation when tested with the coarse gravel backfill. Strains and stresses also varied between the inside and outside surfaces of the pipe. These test results reported in this chapter served as a useful prelude to the more elaborate testing conducted under simulated landfill conditions presented in Chapter 6.

3.9 REFERENCES

- Beatty, M.F., and Chewning, S.W. 1979. Numerical analysis of the reinforcement effect of a strain gauge applied to a soft material, *International Journal of Engineering Science*, Vol. 17, pp. 907 - 915.
- Chambers, R.E., and McGrath, T.J. 1981. *Structural Design of Buried Plastic Pipe*, Proceedings of the International Conference on Underground Plastic Pipe, Pipeline

Division of the American Society of Civil Engineers, B.J. Schrock Ed., New Orleans LA, USA, ASCE, pp. 10-25.

Moore, I.D., Laidlaw, T.C., and Brachman, R.W.I. 1996. Test cells for static pipe response under deep burial, 49th Canadian Geotechnical Conference of the Canadian Geotechnical Society, September 23 to 25, St. John's NF, Canada, pp. 737 - 744.

Moore, I.D. 1993. Structural design of profiled polyethylene pipe - Part I - Deep burial, Geotechnical Research Centre Report GEOT-8-93, The University of Western Ontario, London, Canada.

Rowe, R. K., Quigley, R.M., and Booker, J.R. 1995. Clayey Barrier Systems for Waste Disposal Facilities, E & FN Spon (Chapman & Hall), London.

Selig, E.T., DiFrancesco, L.C., and McGrath, T.J. 1994. Laboratory Test of Buried Pipe in Hoop Compression. Buried Plastic Pipe Technology: 2nd Volume, ASTM STP 1222, pp. 119-132.

Zhang, C., and Moore, I.D. (1997) "Nonlinear Mechanical Response of High Density Polyethylene. Part I: Experimental Investigation and Model Evaluation", *Polymer Engineering and Science*, Vol. 37, No. 2, pp. 404-413.

TABLE 3.1 Summary of hoop compression tests on 320 mm diameter SDR 11 HDPE pipe.

Test	Pipe	Backfill Soil	Maximum Applied Pressure (kPa)	Average Temperature (°C)
H1	H1	uniformly-graded medium-sand	500	21
H2a	H2	uniformly-graded coarse-gravel	250	23
H2b	H2	uniformly-graded coarse-gravel	350	23

TABLE 3.2 Measured strains at Section A during test H1, reported at an applied bladder pressure of 500 kPa.

	Angular Position Around Pipe θ°					Mean	Coefficient of Variation
	0	90	180	225	270		
ϵ_θ ($\mu\epsilon$)	-4400	-4250	-	-4300	-4400	-4350	2%
ϵ_z ($\mu\epsilon$)	2500	3150	3100	-	2800	2900	10%

TABLE 3.3 Summary of strains opposite instrumented stone contact zone measured during tests H2a and H2b, reported at an applied bladder pressure of 250 kPa.

Location	Test H2a		Test H2b	
	ϵ_{θ} ($\mu\epsilon$)	ϵ_z ($\mu\epsilon$)	ϵ_{θ} ($\mu\epsilon$)	ϵ_z ($\mu\epsilon$)
A	-1850	1800	-1850	1700
B	-2100	1450	-2200	1500
C	-1950	1000	-2150	1200
D	-1800	900	-	-
E	-1500	700	-2000	1000
F	-2350	1750	-	-
G	-2400	1500	-	-
H	-1800	1250	-1700	1500
I	-1500	1300	-1400	1700
J	-2000	1000	-	-
Mean	-1900	1300	-1900	1400
Coefficient of Variation	16%	29%	16%	20%

TABLE 3.4 Estimates of hoop and axial stresses calculated from measured strains opposite instrumented stone contact zone measured during tests H2a and H2b. Secant modulus of 470 MPa, Poisson's ratio of 0.46 and a gauge correction factor of 1.4 were used in the calculations. Stresses are reported for an applied bladder pressure of 250 kPa. Compressive stresses are negative.

Location	Test H2a		Test H2b	
	σ_{θ} (MPa)	σ_z (MPa)	σ_{θ} (MPa)	σ_z (MPa)
A	-0.8	0.8	-0.9	0.7
B	-1.2	0.4	-1.2	0.5
C	-1.2	0.1	-1.3	0.2
D	-1.1	0.1	-	-
E	-1.0	0	-1.3	0
F	-1.3	0.6	-	-
G	-1.4	0.3	-	-
H	-1.0	0.3	-0.8	0.6
I	-0.7	0.5	-0.5	0.9
J	-1.3	0.1	-	-
Mean	-1.1	0.3	-1.0	0.5
Confidence Level 95%	± 0.2	± 0.2	± 0.3	± 0.3
Coefficient of Variation	20%	80%	16%	20%

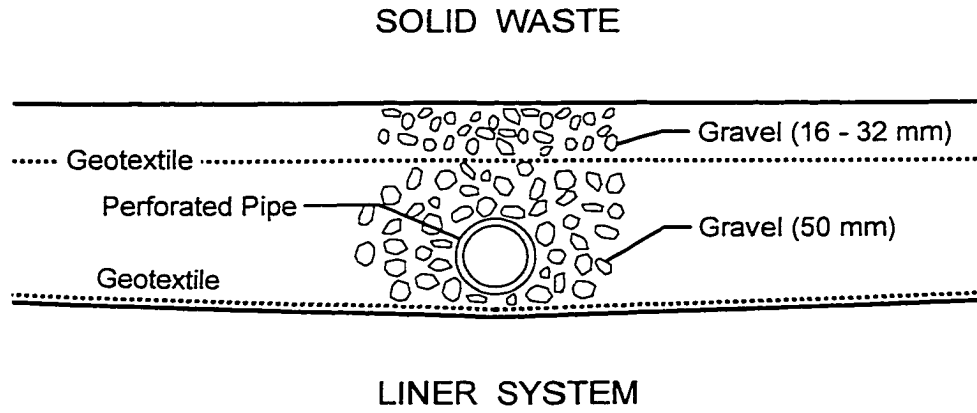


FIGURE 3.1 Cross section through a typical primary leachate collection system in a municipal solid waste landfill.

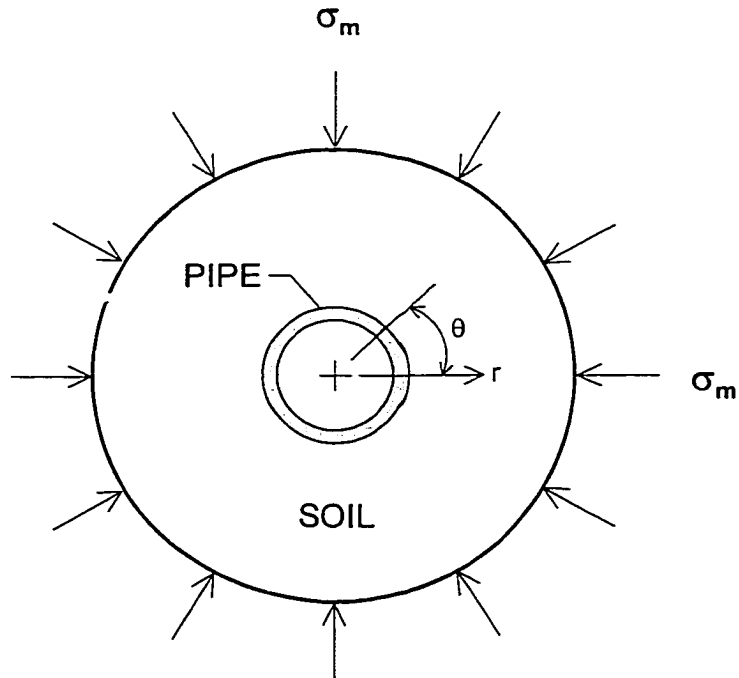


FIGURE 3.2 Idealized loads acting on soil-pipe system with distant boundary stress σ_m .

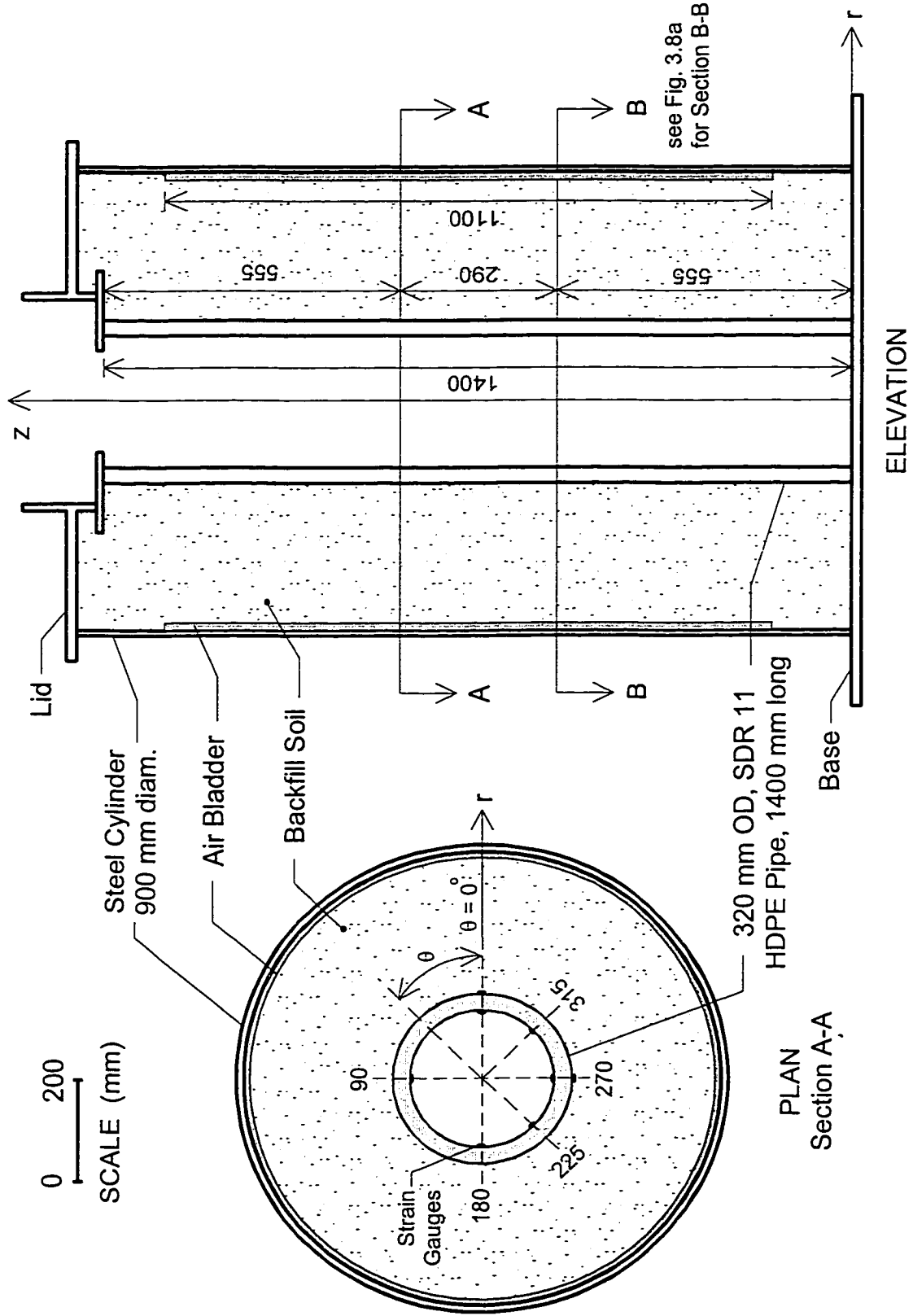


FIGURE 3.3 Plan and elevation view of hoop compression test facility showing location of instrumentation for pipe sample H1. Dimensions in mm.



FIGURE 3.4 Plan view of test cell showing pipe, coarse gravel backfill and bladder.



FIGURE 3.5 Discontinuous support provided by coarse gravel backfill.

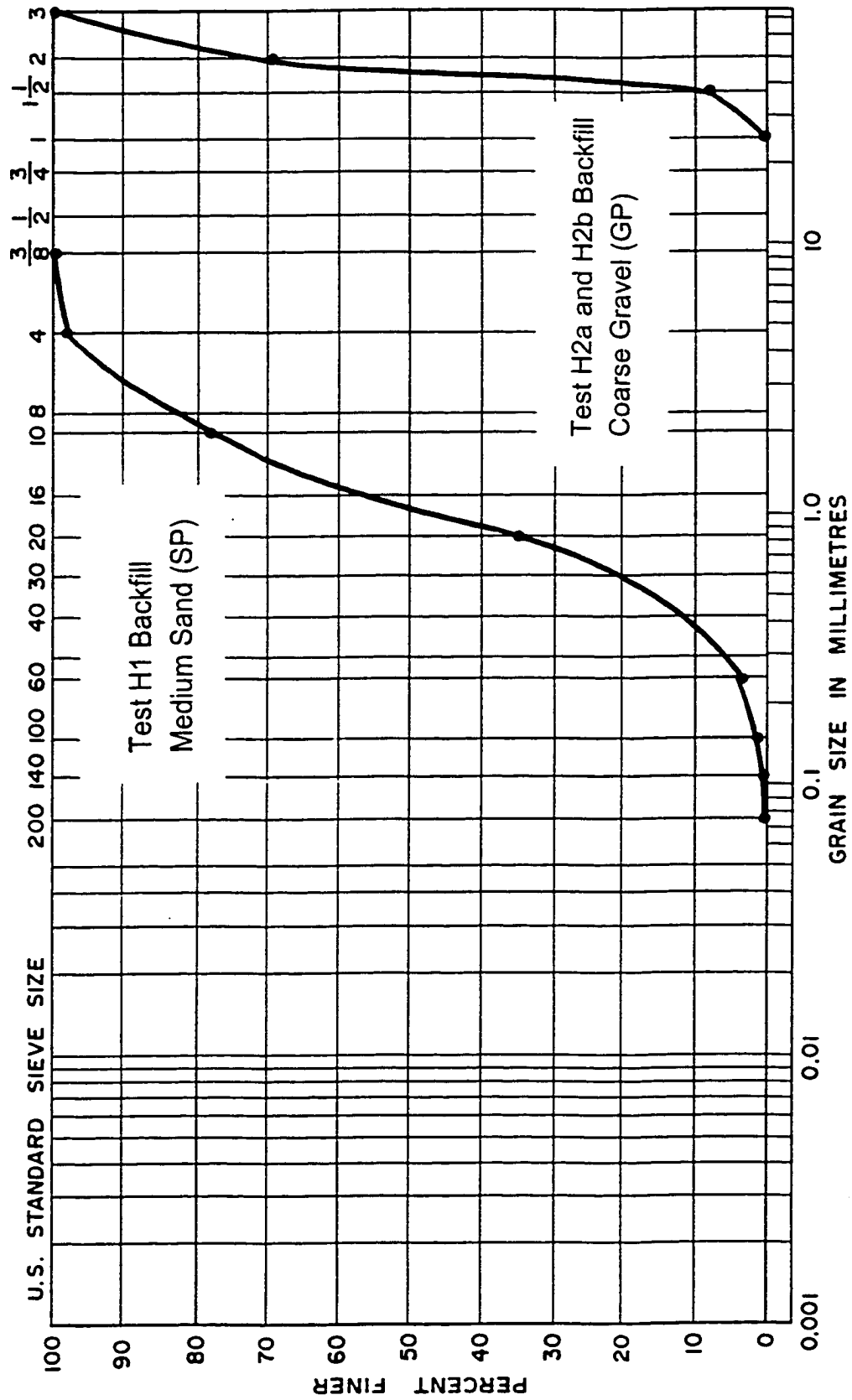


FIGURE 3.6 Grain size distribution curves for medium sand (SP) and coarse gravel (GP).

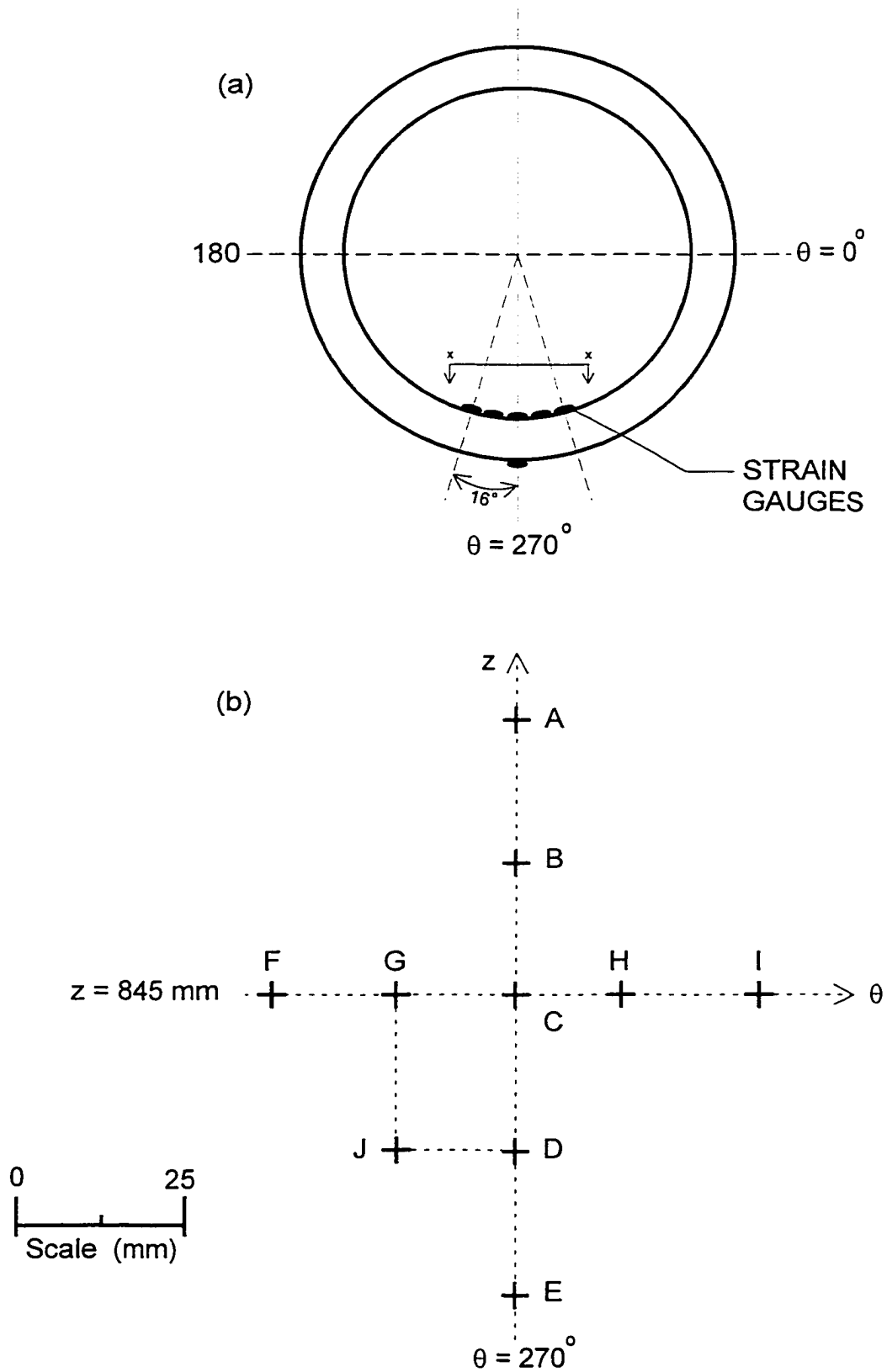
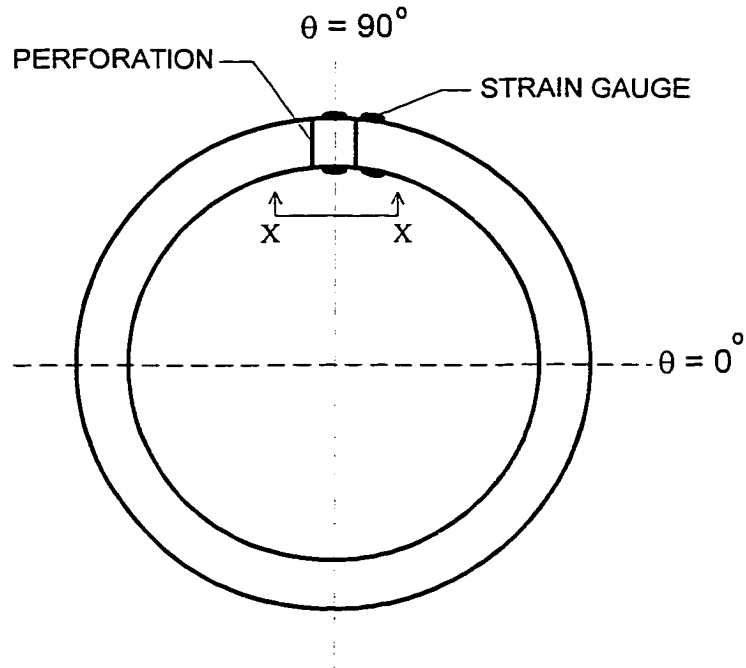
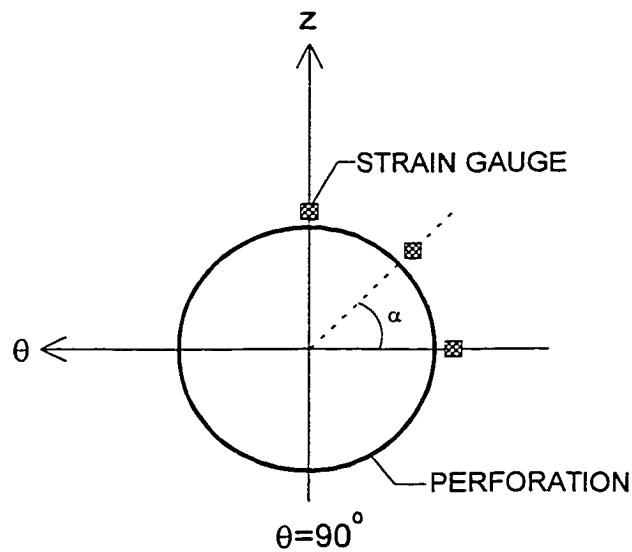


FIGURE 3.7 (a) Location of strain gauges for pipe H2 at Section A.
 (b) Strain gauge placement opposite stone contact zone (Section x-x).



(a) Section B-B showing location of 32 mm diameter perforation.



(b) Section X-X - Position of strain gauges around perforation on inside surface ($r=129$ mm).

FIGURE 3.8 Location of strain gauges around a single 32 mm diameter perforation for both pipes H1 and H2.

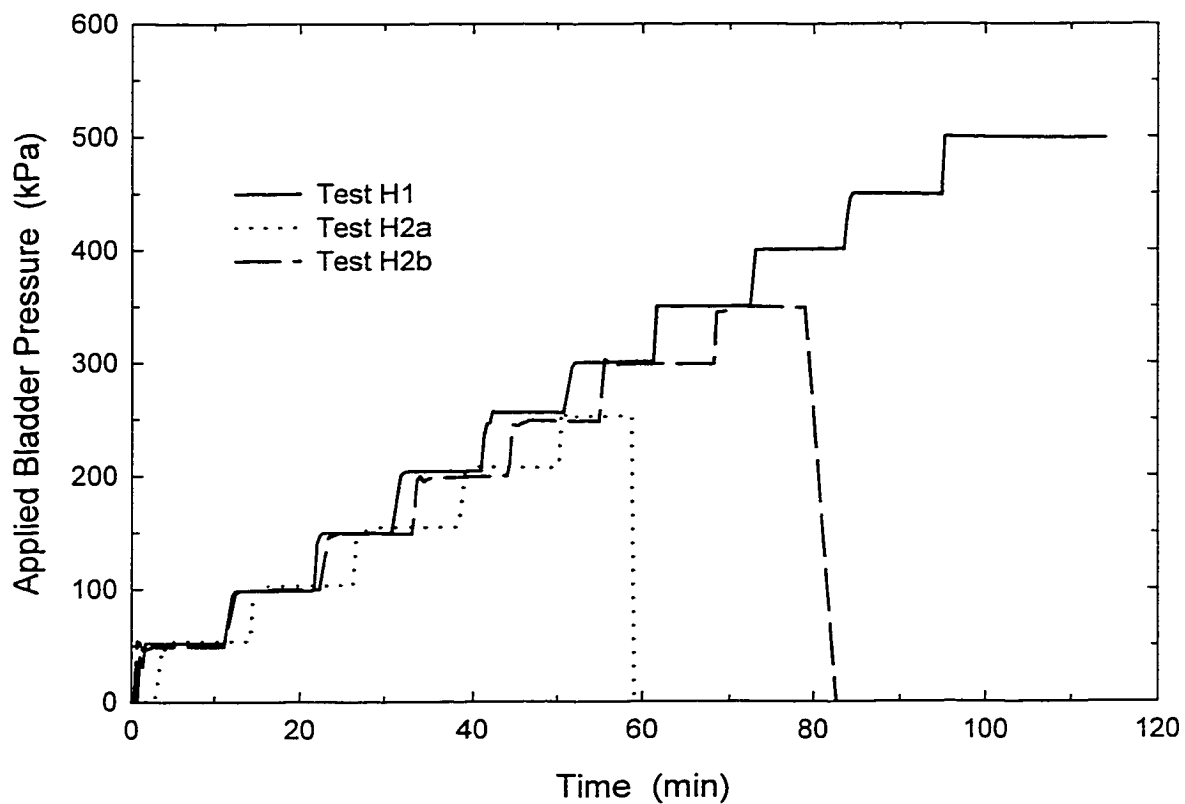


FIGURE 3.9 Applied bladder pressure versus time for tests H1, H2a and H2b.

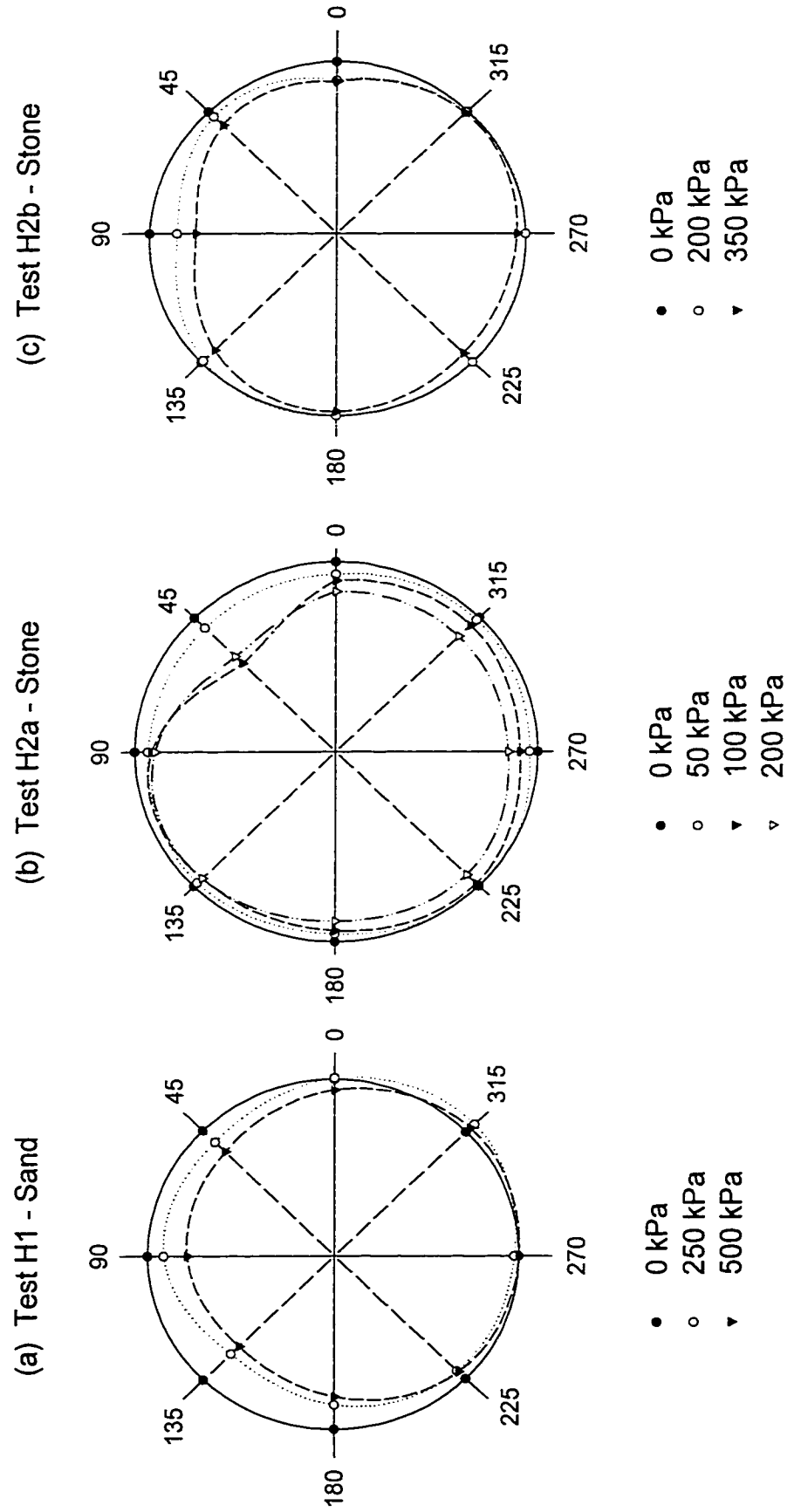


FIGURE 3.10 Deflected shape (x 20) at central section for tests: (a) H1, (b) H2a and (c) H2b.

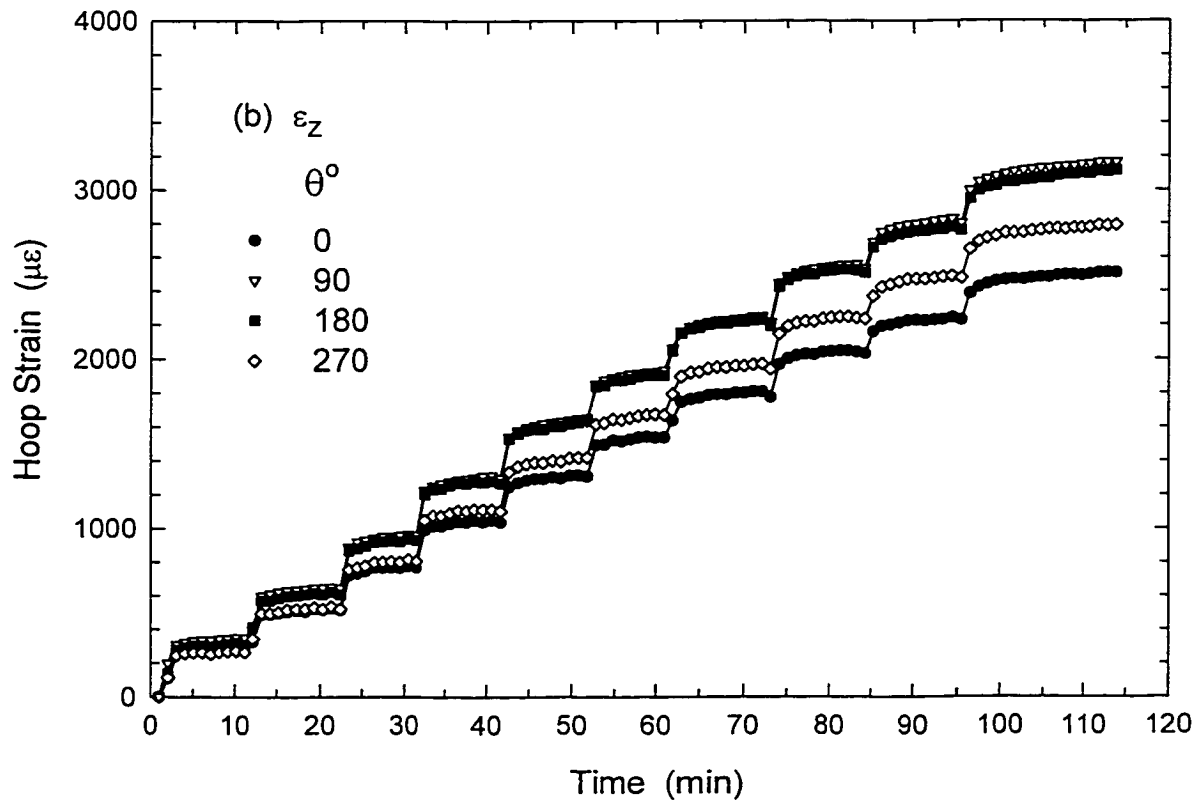
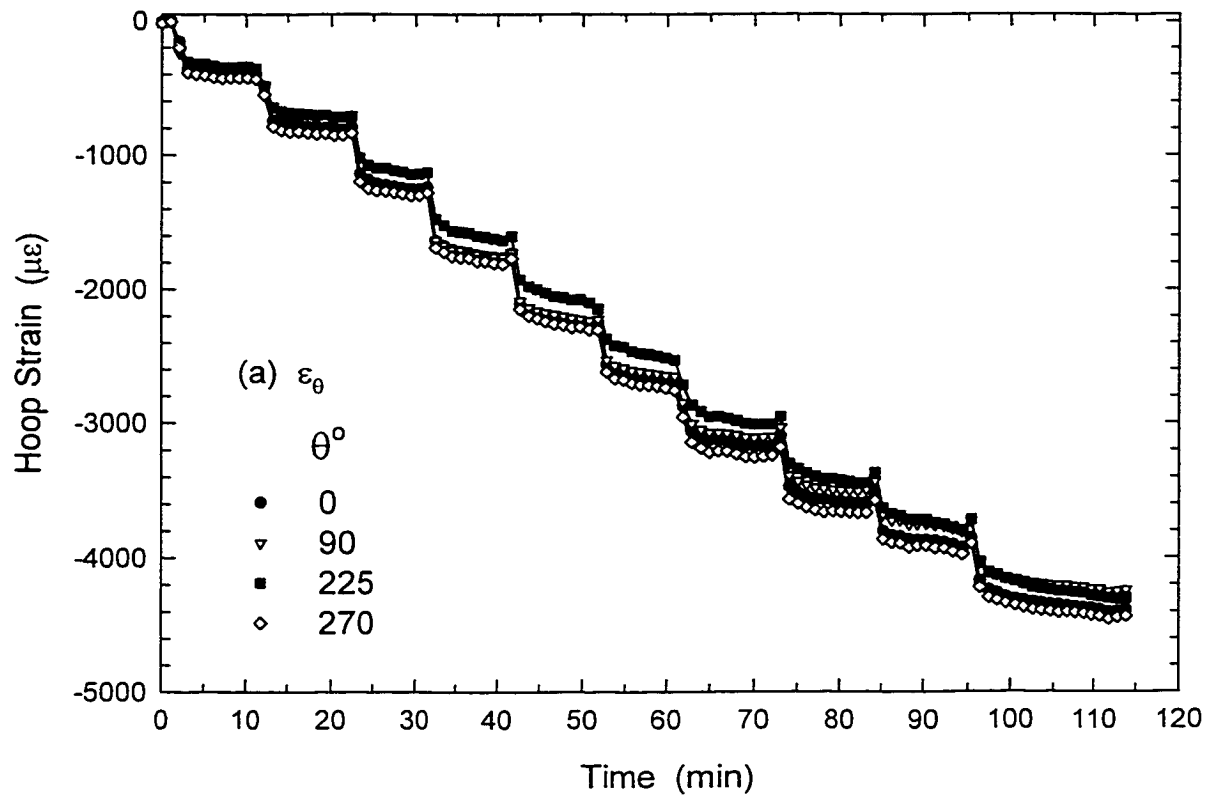


FIGURE 3.11 Variation of (a) hoop ϵ_{θ} and (b) axial ϵ_z strains measured in the circumferential direction at Section A during Test H1.

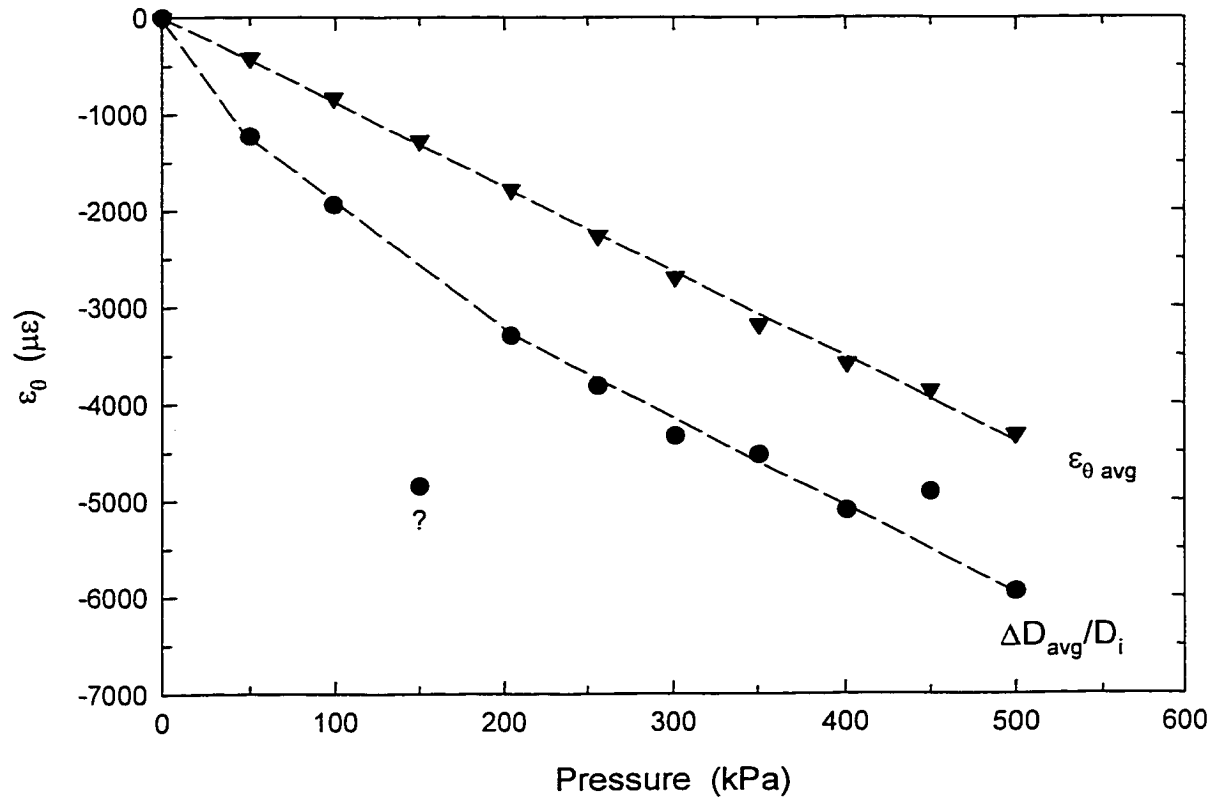


FIGURE 3.12 Average circumferential strains measured with strain gauges compared with circumferential strains calculated based on measured deflections for Test H1.

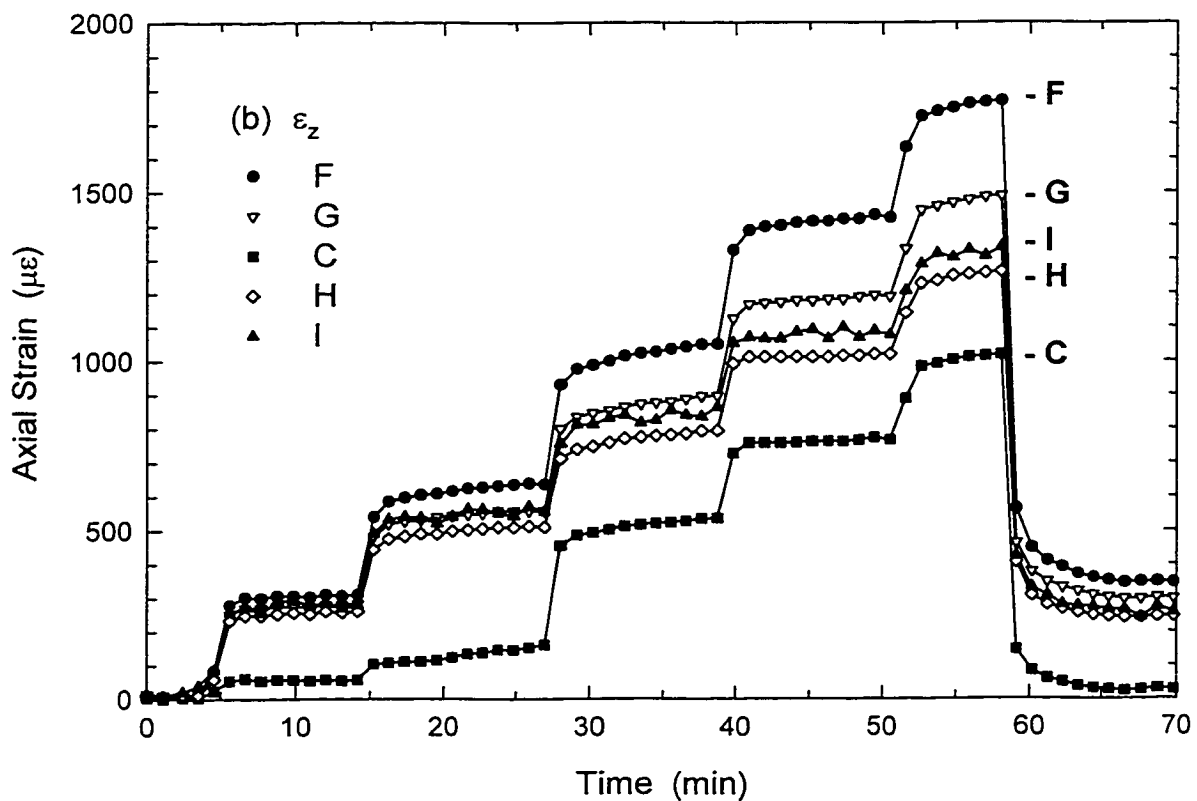
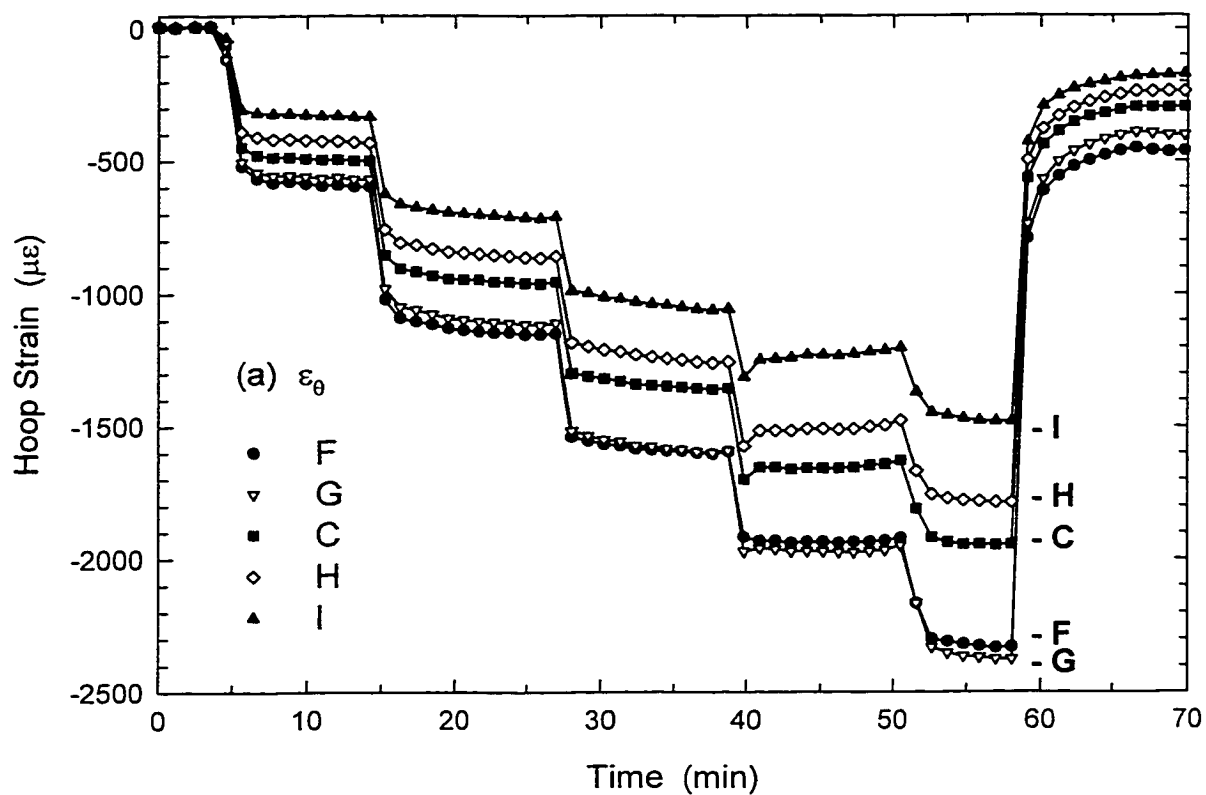


FIGURE 3.13 Variation of (a) hoop ϵ_{θ} and (b) axial ϵ_z strains measured in the circumferential direction at Section A during Test H2a.

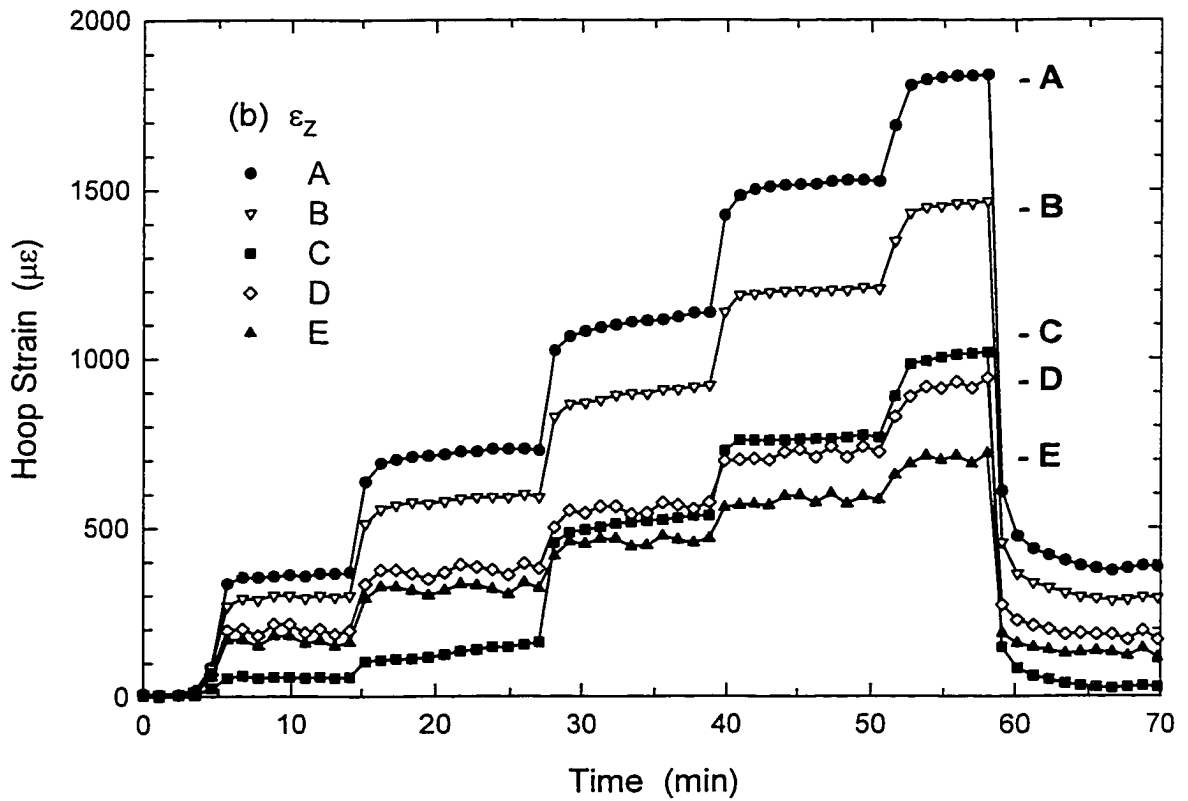
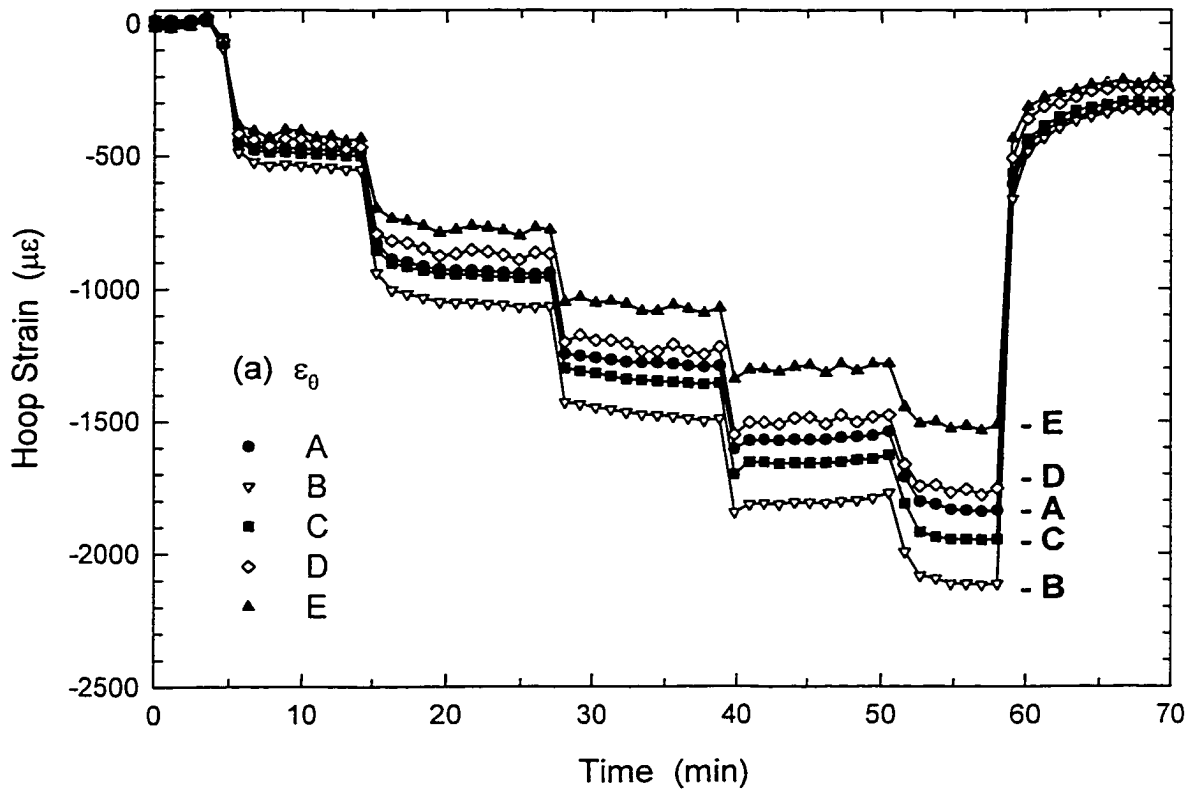


FIGURE 3.14 Variation of (a) hoop ϵ_{θ} and (b) axial ϵ_z strains measured in the axial direction at Section A during Test H2a.

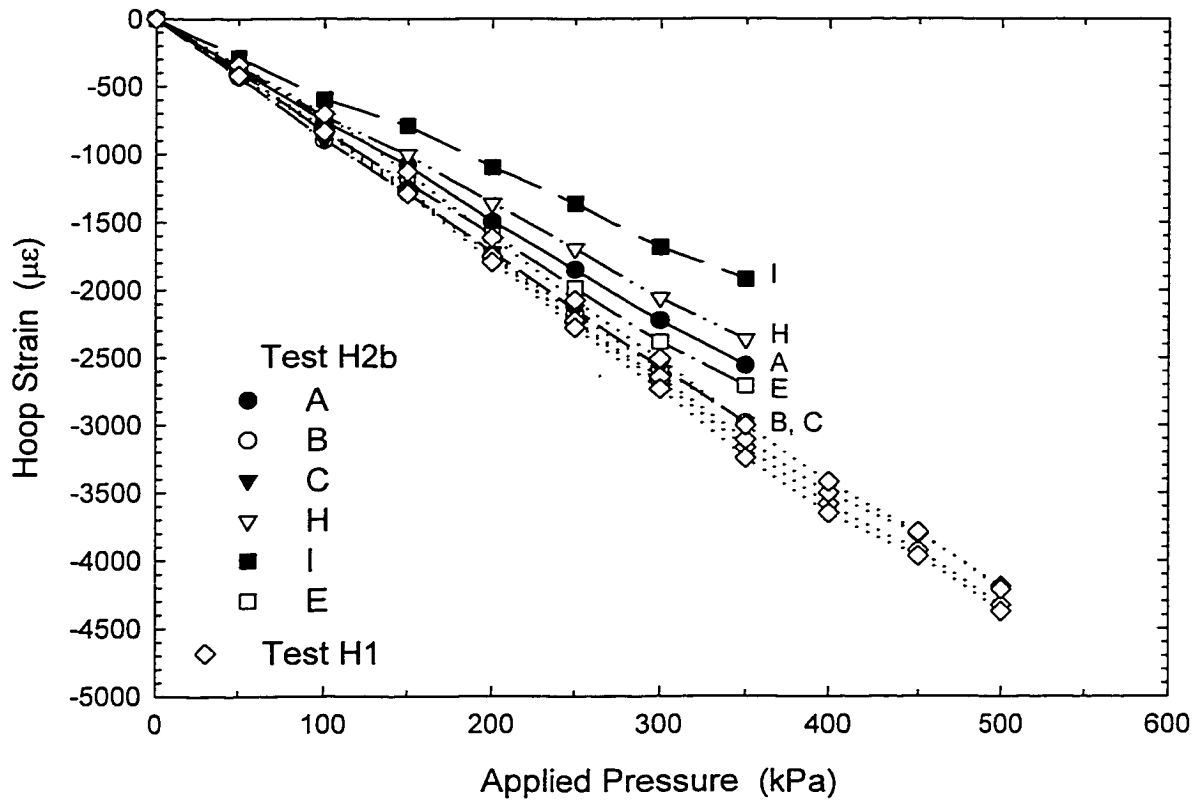


FIGURE 3.15 Hoop strains measured at Section A during tests H1 (sand) and H2b (gravel).

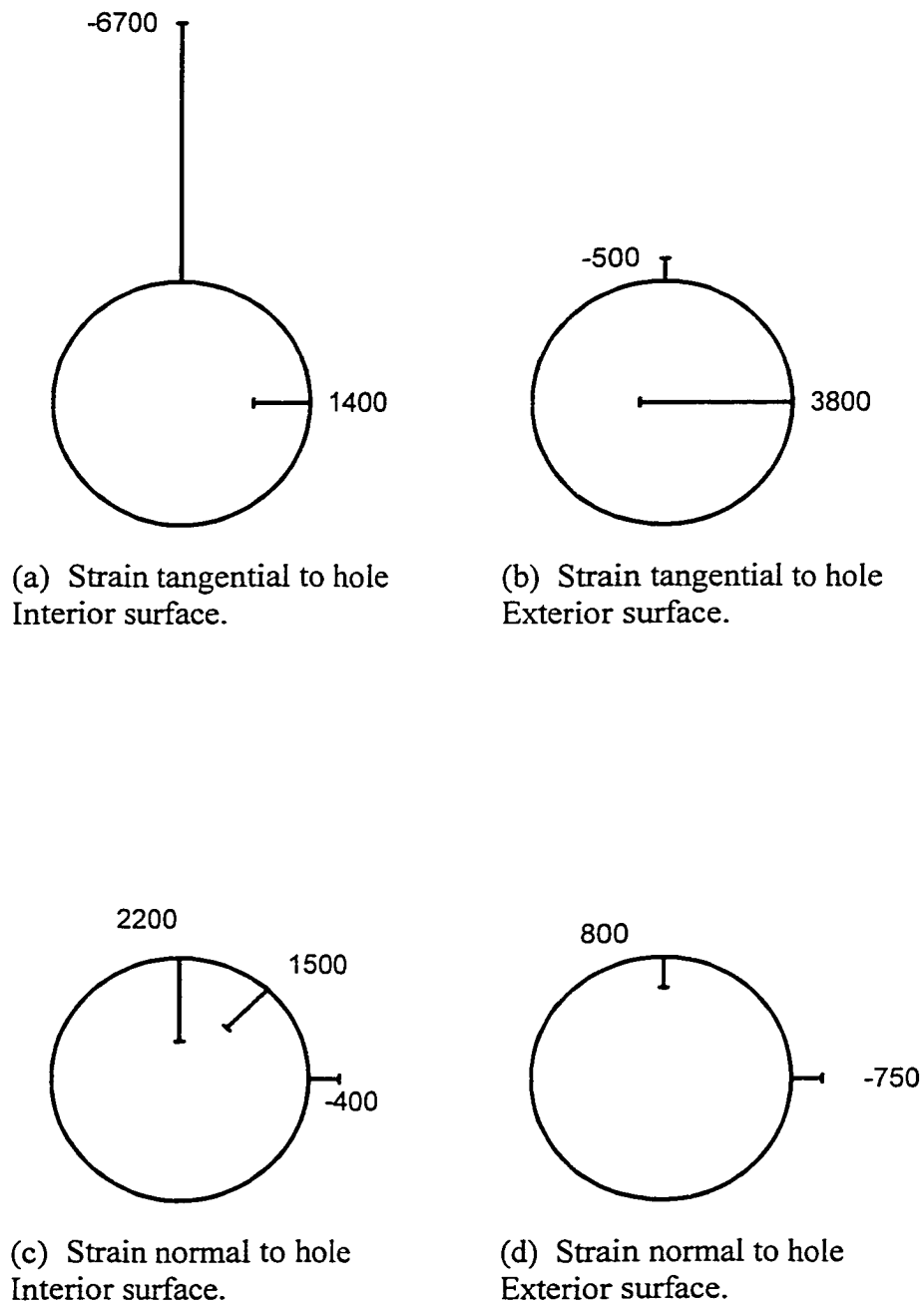


FIGURE 3.16 Measured strain values ($\mu\epsilon$) tangential and normal to the perforation on the interior and exterior surfaces of the pipe for Test H1 with sand backfill at an applied bladder pressure of 500 kPa.

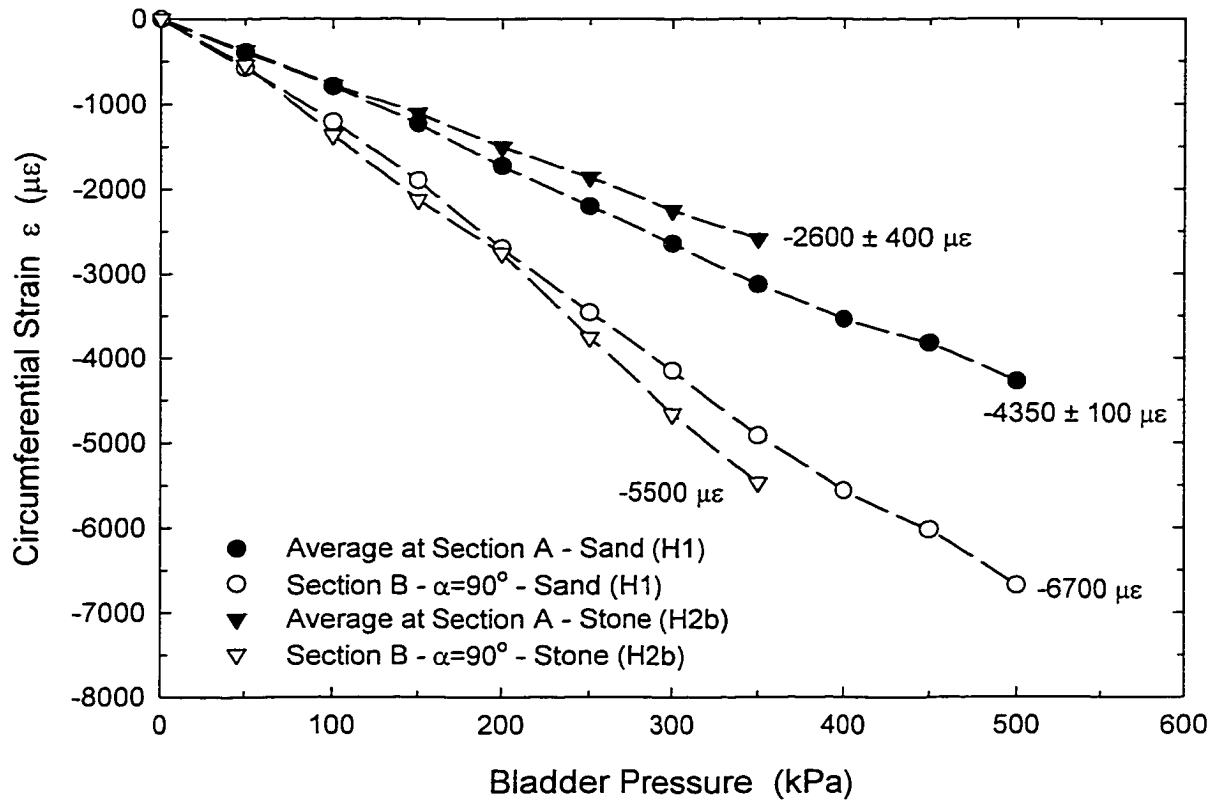
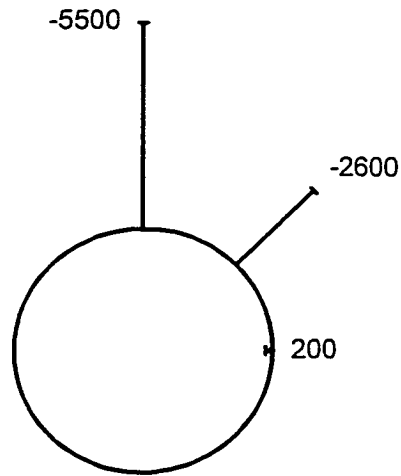
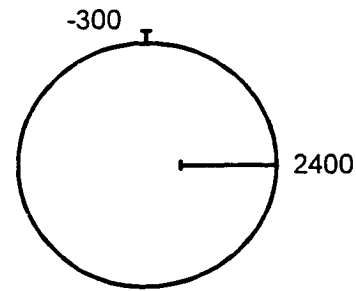


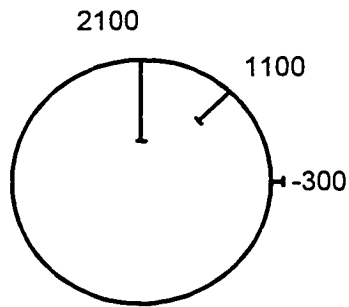
FIGURE 3.17 Circumferential strain measured distant from and near perforation for both sand (H1) and coarse gravel (H2b) backfill.



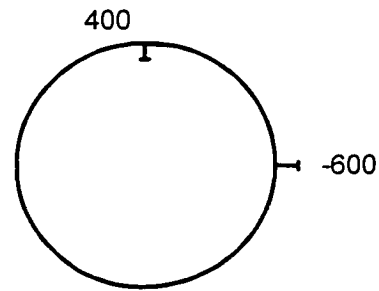
(a) Strain tangential to hole
Interior surface.



(b) Strain tangential to hole
Exterior surface.



(c) Strain normal to hole
Interior surface.



(d) Strain normal to hole
Exterior surface.

FIGURE 3.18 Measured strain values ($\mu\epsilon$) tangential and normal to the perforation on the interior and exterior surfaces of the pipe for Test H2b with stone backfill at an applied bladder pressure of 350 kPa.

CHAPTER 4

The Design of A Laboratory Facility for Evaluating the Structural Response of Small Diameter Buried Pipes

4.1 INTRODUCTION

Large scale testing of buried pipes is useful for evaluating the structural response expected under field conditions. Such facilities include the test cells at Utah State University, University of Massachusetts at Amherst, and Ohio University in the United States; The University of Western Ontario in Canada; and LGA Geotechnical Institute in Germany.

As with most laboratory investigations, the boundary conditions of the testing apparatus may significantly influence the results derived from the test. The boundary conditions of the facilities for testing pipe include the method of load application, as well as the geometry of the testing conditions. The state of stress in the soil around the pipe and, consequently, the structural response of the pipe are significantly influenced by these boundary conditions.

Each of the existing facilities has limitations related to the boundary conditions in the facility. Both the Utah State and Ohio facilities attempt to simulate the deep burial response of a pipe. However, the Utah State cell essentially applies hydrostatic stress conditions to the soil around the pipe (Kastner et al. 1993) that differ from the biaxial stresses expected to occur in the field. Also, no effort is made to control friction that can mobilize along the sidewalls of the facility. The soil and pipe response when tested in the Ohio facility differs substantially to that expected to occur in a typical field installation (Brachman et al. 1996;

Chapter 2). A complex response is produced because the overburden pressure is simulated by applying load through a stiff, rectangular plate.

Hoop compression cells at the University of Massachusetts (Selig et al. 1994) and the University of Western Ontario (Moore et al. 1996) provide a simple idealization of the pressures acting on the soil near a buried pipe by explicitly modelling the earth pressures as a uniform radial pressure. This considerably simplifies the laboratory conditions required for testing and provides a useful measure of pipe response under simplified soil pressures. The main shortcoming of this approach, however, is that the biaxial response (ie. vertical pressures greater than horizontal pressures) that occurs in the field is not simulated by the axisymmetric applied radial pressure.

None of the existing facilities can closely approximate the expected field conditions with respect to the stress state associated with deep and extensive burial in a zone of soil surrounding a pipe. There is a need for a facility that would allow a laboratory assessment of the performance of small diameter pipes under expected service conditions (e.g., a deeply buried leachate collection pipe in a landfill).

The objective of this chapter is to discuss the design of a new laboratory facility for evaluating the performance of small diameter pipes when buried under deep and extensive overburden material. The facility involves a prism of soil with a pipe buried within, subject to large vertical pressures while allowing only small horizontal deflections along the lateral boundaries. Attention is focussed on the influence of the boundary conditions in the new facility and how reasonably the test cell represents the field conditions for a buried pipe. Issues such as the loading conditions under deep burial, simulation of vertical earth

pressures, development of lateral earth pressure, selection of test cell dimensions, and the influence of sidewall friction and boundary stiffness on soil and pipe response are examined.

4.2 LOADING CONDITIONS UNDER DEEP BURIAL

The first step considered in the design of the laboratory facility involved identifying the boundary conditions experienced by the pipe when buried in the field. Figure 4.1a shows an idealized installation of a deeply buried small diameter pipe. The pipe is typically surrounded by a select backfill material and is subjected to pressures from the overburden above. For example, these conditions could represent a pipe buried under an earth embankment, or within a leachate collection system in a deep landfill. The buried pipe does not act as an isolated structural element with clearly defined applied loading, but rather acts as a component of the soil-pipe system. The structural performance of the pipe is a function of both the soil and pipe stiffness, and the resulting soil-structure interaction. Consequently, to simulate the expected field conditions the soil-pipe system must be modelled in the laboratory.

A region of soil around the pipe is isolated in Figure 4.1b showing idealized earth pressures acting distant from the pipe. Pressures arise at the boundaries of the soil-pipe system from deep burial. These pressures have a vertical component σ_v arising from the weight of the overlying materials above the pipe and a horizontal component σ_h associated with the restraint against lateral soil movement within the embankment. Horizontal stresses are often expressed as $K\sigma_v$, where K is the coefficient of lateral earth pressure. Provided that

these biaxial stresses can be simulated in a laboratory model, a reasonable idealization of field conditions should be attained.

4.3 SIMULATION OF VERTICAL EARTH PRESSURE

The vertical stress from the weight of the overburden material may be reasonably represented by applying a uniformly distributed pressure σ_{vo} at the surface of the soil in the test cell, Figure 4.1c. This pressure corresponds to some equivalent height of overburden material. For extensive and prismatic geometry, and where earth pressures are invariant in the horizontal direction, the applied pressure may be considered to be equivalent to the weight of the column of soil of height d per unit area (Fig. 4.1a). For other cases where overburden stresses vary in the horizontal direction, various analytical or numerical solutions may be employed to estimate the stresses in the vicinity of the pipe for a given embankment geometry.

The stiffness of the overburden above the backfill material used in the cell is neglected in this idealization. Burial under extensive and uniform stratigraphy does produce uniform vertical stresses at some distance above the pipe. Provided that the uniform stress boundary is placed sufficiently far above the pipe in the laboratory model (distance largely controlled by pipe diameter), a reasonable approximation for deeply buried pipes is obtained. Further, in some deep burial applications (e.g., landfills) most of the fill stiffness comes from the drainage stone placed around the pipe (which is present in the laboratory

test) and the waste above this stone will typically be expected to have a much lower stiffness than the stone.

Conditions encountered by pipes buried within a trench could also be simulated in the new laboratory facility. In this case a proportion of overburden stress is attenuated by shear stresses mobilized along the sides of the trench. This paper however, focuses only on the case of deep burial within extensive soil materials.

Other investigators have used a variety of approaches to attempt to simulate the earth pressures expected under deep burial. For example, both testing facilities at Utah State and Ohio University use hydraulic cylinders to apply forces to steel plates that in turn apply pressures to the soil. At Utah State, many steel plates are used, whereas one large (1.83 m × 2.74 m) platform is used in the Ohio facility. Finite element analysis of the Ohio University facility (Brachman et al. 1996; Chapter 2) has shown that this method of load application gives rise to a complex stress state which is quite different to that expected in the field.

Another approach involves the use of pressurized bladders to apply a uniformly distributed pressure. This approach has been used by many investigators. Höeg (1968) appears to be the first to report the use of a vulcanized neoprene rubber bag to simulate large applied pressures. DiFrancesco et al. (1994) and Rogers et al. (1996) also used bladders but at much lower pressures (207 to 380 kPa and 150 kPa, respectively). Zanzinger and Gartung (1995, 1998) report on the use of water filled flat jacks pressurized up to 1000 kPa.

Pressurized air bladders were selected to simulate the vertical stresses acting on the soil-pipe system. Several types of bladder construction were tried. The first involved seamed sheets of 1.14 mm thick nylon-reinforced chloro-sulphunated polyethylene. This

economical design was used for several tests (e.g., Brachman 1997 [Chapter 3]; Moore and Laidlaw 1997; Brachman et al. 1998) and worked well for lower pressures ranging from 250 kPa to 500 kPa. Rupture of these bladders at higher pressures resulted from material failure, usually near the edge seams. An alternative design using a diaphragm-type arrangement, involving a 3 mm thick Buna N rubber membrane with a mechanical seal around the perimeter, proved more reliable, especially at high pressures (see Chapter 5).

A design pressure of 1000 kPa was selected for the test cell facility. This pressure level corresponds to the deep burial case of roughly 50 m in an embankment soil ($\gamma \approx 20$ kN/m³) or from 77 to 125 m in a municipal solid waste facility ($\gamma \approx 8$ to 13 kN/m³), and was considered to cover most practical situations.

4.4 SIMULATION OF LATERAL EARTH PRESSURE

Horizontal stresses could be simulated in a similar manner by applying lateral pressures equivalent to the horizontal stresses generated in the field σ_h . Unfortunately the magnitude of the horizontal stress relative to the vertical stress (ie. K) is not well defined for many backfill materials (it is a complex function of particle size, shape, gradation, density, and stress history). An alternate approach of controlling the displacement at the lateral boundary of the soil-pipe system was therefore adopted. Here, lateral stresses are developed by limiting the outward deflection of the side walls (ie. by simulating $\delta_x \approx 0$ or K_0 conditions, Fig. 4.1c). Hence the soil will generate horizontal stresses close to those expected in the field for the backfill and lateral earth pressures conditions responding under zero lateral

strain. To achieve this, the lateral boundary must be sufficiently stiff to minimize outward deformations of the soil and be located far enough from the pipe so that the behaviour of the pipe is not significantly altered.

The boundary condition perpendicular to the pipe axis is also idealized as a small displacement boundary ($\delta_z \approx 0$ in Fig. 4.1c). Axial stresses σ_z will also develop at these boundaries in a manner similar to the horizontal stresses σ_x . Stiff side walls should reasonably represent the plane strain axial conditions of the pipe that would be expected to prevail for a long pipe buried in the field. Axial restraint conditions other than plane strain could also be simulated in the test cell.

4.5 SELECTION OF TEST CELL DIMENSIONS

Another important idealization of the field problem involved the selection of a finite region of the soil-pipe system for modelling in the laboratory. Two important issues controlled the selection of cell dimensions (ie. breadth B, length L and height H shown in Fig. 4.1c). First, it is recognised that the vertical and horizontal stresses in the embankment are disturbed locally around the pipe, since the pipe has different stiffness to the volume of soil it replaces. The proximity of the top surface of the cell must therefore be sufficiently remote from the pipe so that vertical stresses are close to uniform. Similarly, the bottom surface of the cell must be sufficiently remote so that a stiff boundary does not induce non-uniform vertical stresses. The regions above and below a buried pipe where stress is attenuated are of approximately equal size, and controlled by the pipe diameter. Reasonable physical

modelling of soil stresses is attained provided that the pipe is located no closer to the surface or the base than a distance equal to the pipe diameter.

Secondly, friction mobilized on the vertical side walls of the test cell is inevitable. Shear stresses acting on the lateral boundaries differs from the idealized soil block shown in Figure 4.1b. Control of the roughness of the side walls is important to limit this effect. Furthermore, the side walls must be located far enough away from the pipe so that most of the pressure applied to the top surface of the soil block reaches the pipe. This establishes a relationship between lateral test cell dimensions B and L with the pipe diameter.

The magnitude of interface friction mobilized in the laboratory test cell depends on the surface roughness of the side walls. For rough steel in contact with the soil, the ratio of the side wall interface friction angle to internal angle of friction of the soil (ϕ_{sw}/ϕ) may range from 0.8 to 0.9, while for smooth steel ϕ_{sw}/ϕ may be 0.5 to 0.7 (Perloff and Baron 1976). Consequently, for granular backfill materials with ϕ between 30° and 55° the friction angle for an untreated surface may vary from 15° to 50° .

The degree to which friction acts on the side walls may be reduced by treatment of the soil-steel interface. The need to reduce the friction on a boundary has been previously examined in other laboratory investigations. For example, Bathurst and Benjamin (1988) reported that side wall friction could be reduced to 15° by using sheets of polyethylene layered between sand and a plexiglass side wall. Direct shear tests conducted to assess the effectiveness of different interface treatments (Tognon et al. 1999) found side wall friction angles ϕ_{sw} between 16° to 21° (depending on backfill soil) for minimal interface treatment (geotextile / polyethylene sheet), while 5° was found for layered polyethylene sheets lubricated with silicone grease.

An estimate of the proportion of the applied pressure that reaches the soil within the test cell can be obtained by modifying classical arching theory to consider the three dimensional geometry of the laboratory test cell. The vertical stress at depth h below the surface in a cell of width B and length L , subjected to an applied surface pressure of σ_{vo} (Fig. 4.1c), can be estimated by:

$$\sigma_v = \frac{\gamma}{2K\mu w} (1 - e^{-2K\mu wh}) + \sigma_{vo} e^{-2K\mu wh} \quad (4.1)$$

where: $w = \text{geometry coefficient} = 1/B + 1/L$,

$K = \text{coefficient of lateral pressure}$,

$\mu = \text{coefficient of side wall friction} = \tan \phi_{sw}$,

$\phi_{sw} = \text{angle of side wall friction}$, and

$\gamma = \text{unit weight of the soil}$.

The vertical stress at mid-depth in the test cell calculated using Equation 4.1 is plotted in Figure 4.2 for increasing width of the test cell B and for a range of interface friction angles ϕ_{sw} . Compressive stresses are taken as positive. The results shown are for the specific case of a square cell (ie. $B=L$) of height 1.6 m (ie. $h=0.8$ m) with a pressure of 1000 kPa applied at the surface (also taking $\gamma=18$ kN/m³, and $K=0.33$).

The results in Figure 4.2 provide an initial estimate of the influence of the distance to the lateral boundary coupled with the effect of boundary roughness. As the distance to the boundary increases, the proportion of the vertical stress reaching mid-depth increases.

Theoretically if the boundary is sufficiently remote (ie. for large values of B) there is negligible loss in applied pressure with depth. However once B becomes sufficiently large, further increases result in only slight improvements in the stresses acting within the ground. With a test cell width B equal to 2 m, a good approximation is achieved for side wall friction less than 10° , as 99%, 95% and 91% of the applied vertical stress is calculated at this location for ϕ_{sw} of 1, 5 and 10° , respectively.

Based on the calculations from Equation 4.1, and also considering the cost of test cell fabrication (recognising that larger dimensions require stiffer side walls) and the logistics of test cell use (e.g., volume of soil required for testing), dimensions with height of 1.6 m, breadth of 2.0 m and length of 2.0 m were selected.

4.6 INFLUENCE OF SIDE WALL FRICTION ON SOIL RESPONSE

The simple arching model of Equation 4.1 provides a good indication of the significance of the proximity and roughness of the lateral boundary. The results of finite element analysis of a test cell with the selected dimensions (B=2 m) were studied to further investigate the effect of side wall friction and lateral stiffness on the soil and pipe response.

The case of the test cell backfilled only with a soil material ($E=80$ MPa, $\nu=0.25$, $\phi=40^\circ$, $\psi=\phi/4$, $c=0$, $\gamma=18$ kN/m³) was analysed first to assess the stress redistribution within the soil for various levels of side wall friction. Two-dimensional, plane-strain, elasto-plastic finite element analysis with a Mohr-Coulomb failure criterion and the nonassociative flow rule of Davis (1969) was employed. The finite element mesh is shown in Figure 4.3. Two

hundred and seventy four six-noded triangular continuum elements were used to model the soil. Symmetry along the centreline of the test cell was used. Side wall friction was simulated with fifty three two-noded joint elements with interface friction angle ϕ_{sw} .

Figure 4.4 plots vertical σ_y and horizontal σ_x stresses with depth near the centreline of the test cell with a 1000 kPa pressure uniformly applied across the surface. Results are shown for the limits of a smooth ($\phi_{sw}=0^\circ$) and rough ($\phi_{sw}=\phi$) side wall, as well as two intermediate values of $\phi_{sw}=5^\circ$ and 20° .

When the side walls are perfectly smooth ($\phi_{sw}=0^\circ$), the stresses are uniform in the lateral direction (ie. x) and increase linearly with depth because of the soil self weight (ie. $\sigma_y=\sigma_{vo}+\gamma h$, where: $\sigma_{vo}=1000$ kPa and h is the depth below the surface). At the surface ($y=1.6$ m) the vertical stress is equal to the applied stress, 1000 kPa; at the base the vertical stress is equal to 1028.8 kPa. Horizontal stresses equal to $K\sigma_v$, where $K=v/(1-v)=0.33$, are developed. Real soil materials are expected to have other K values, but the results calculated here should still be a good indicator of the impact of the boundary condition.

The stress redistribution along the centreline caused by shear stresses mobilized along the side walls is evident from the other results presented in Figure 4.4. As the angle of side wall friction increases, the vertical stresses decrease with depth. For example, at mid-depth ($y=0.8$ m) the proportion of vertical stress relative to smooth side walls is 99%, 94% and 87% for ϕ_{sw} of 5, 20 and 40° .

These values are slightly larger than those calculated using the modified arching theory from Equation 4.1 (e.g., 4% difference for ϕ_{sw} of 5°). The differences arise as the finite element analysis models arching in the x and y directions only, thus overestimates stress with depth relative to three dimensional conditions. This difference will be minimal

for interface friction angles of 5° . The modified arching solution, however, simplistically assumes full mobilization of the interface shear stresses and no rotation of principal stresses, whereas the finite element analysis models both progressive shear mobilization along the interface and allows lateral redistribution of stresses, both of which are likely to occur in the laboratory facility. Thus despite the limitation imposed by using two dimensional geometry, the finite element results provide a more reasonable assessment of the influence of side wall friction than does the modified arching solution.

Contours of vertical stress σ_y with ϕ_{sw} equal to 20° (associated with minimal surface treatment) are given in Figure 4.5a. The transfer of stresses to the side wall is evident from the large decrease in σ_y , particularly near the side wall and close to the base of the cell where the vertical stresses reduce to 650 kPa.

Horizontal stresses σ_x are also no longer uniform in the lateral direction and are not proportional to σ_y with one particular K value if shear stresses are allowed to develop along the side wall. Figure 4.4 shows that horizontal stresses along the centreline increase near the surface and then decrease with depth (relative to $\phi_{sw}=0^\circ$) as ϕ_{sw} increases. At mid-depth there is 97%, 89% and 85% of the horizontal stress with smooth side walls for ϕ_{sw} of 5° , 20° and 40° .

Contours of horizontal stress σ_x are shown in Figure 4.5b for ϕ_{sw} equal to 20° , and appear to be quite complex. Close to the surface there are zones of increasing σ_x towards the centre of the test cell (also apparent in Fig. 4.4) and decreasing σ_x closer to the side wall (both relative to $\phi_{sw}=0^\circ$). This stress distribution is attributed to the deformation of the soil mass (Fig. 4.6) as the soil near the centreline experiences greater compression in the horizontal direction. This effect becomes more pronounced for greater levels of friction

mobilized along the interface (see Fig. 4.4). Close to the side wall and near the surface, lateral soil deformations are away from the boundary (ie. towards the centre of the soil block), yielding smaller horizontal stresses.

At greater depths, the horizontal stress contours illustrate the transfer of stresses to the side walls. Associated with this redistribution are rotations of principal stresses. Figure 4.7 plots vectors of principal stress (σ_1 and σ_3 are major and minor principal stresses) for ϕ_{sw} equal to 20° . Also shown in Figure 4.7 are contours of principal stress rotation α that refers to the counter clockwise rotation of the orientation of the major principal stress from the vertical. A maximum rotation of principal stresses of 12° occurs in the lower corner of the test cell.

Treatment of the lateral boundary with lubricated polyethylene sheets reduces side wall friction to less than 5° (Tognon et al. 1999). The vertical stress contours with ϕ_{sw} equal to 5° are plotted in Figure 4.8a. Note that a much smaller contour interval of 20 kPa is used compared with the 50 kPa contour interval of Figure 4.5a. Less than 2% difference in vertical stresses occurs throughout most of the stress field. Vertical stresses are still somewhat reduced in the lower corner of the test cell (6% reduction), however this region of soil is remote from the centre of the cell (ie. location of the pipe).

Horizontal stresses for ϕ_{sw} of 5° are plotted in Figure 4.8b. Again a finer contour interval was used to illustrate the stress field. The pattern of horizontal stresses is similar to that with ϕ_{sw} equal to 20° , however the magnitude of the stress changes are substantially smaller for the lower interface friction angle of 5° . There is only a small (less than 3%) effect on stresses at mid-depth (ie. pipe location). The rotation of principal stresses is

substantially reduced for side wall friction of 5° (Fig. 4.9). Principal stress rotation is less than 1° for over half of the soil mass and is only 2° adjacent to the side wall.

4.7 INFLUENCE OF SIDE WALL FRICTION ON SOIL AND PIPE RESPONSE

The previous section illustrated the impact of side wall friction on the response of a block of soil within the test cell. The effect of side wall friction on a pipe buried within soil inside the test cell is now considered.

Figure 4.10 shows the finite element mesh used to assess the impact of cell boundaries on the soil stress distributions and the pipe response. The base boundary was modelled as rigid, and the side walls as rigid with angle of surface friction ϕ_{sw} . Ninety-seven two-noded joint elements were used to model surface friction. The soil was modelled using seven hundred and eighty-four six-noded triangles, while one hundred and thirty-six six-noded triangles were used to model the pipe. As in the previous section, the soil was modelled with modulus 80 MPa, Poisson's ratio of 0.25 and internal angle of friction 40° . A high-density polyethylene pipe of outside diameter 320 mm, wall thickness 32 mm, and located in the middle of the test cell was modelled with elastic modulus 500 MPa and Poisson's ratio 0.4. More sophisticated constitutive models are being used to characterize the response of plastic pipe (e.g., Moore and Hu 1995; Zhang and Moore 1997) but are not warranted in this preliminary assessment of pipe-soil-test cell interaction. Plane strain analysis of the pipe-soil-cell system was undertaken which neglects the impact of wall

friction and wall rigidity in the third dimension (along the pipe axis). Shear stresses along the interface between the soil and the pipe were limited by the friction angle ϕ of 40° .

4.7.1 Soil Stresses

Figure 4.11 shows the distribution of vertical stress σ_y and horizontal stress σ_x along a vertical section through the soil 0.2 m away from the pipe centreline. Solutions are given for side wall friction angles ϕ_{sw} of 0° , 5° , 10° , 24° and 35° . These results are similar to those obtained for the cell filled with soil only (no pipe), but in addition to the stress redistribution because of friction on the lateral boundary there is a local perturbation in the stress field arising from the difference in stiffness of the pipe and volume of soil it replaces.

For small friction angles (less than or equal to 5°), the impact on stresses near the pipe is negligible. As expected, impact increases with depth, and for friction angle associated with minimal surface treatment ($\sim 24^\circ$) the vertical stresses decrease by approximately 12% at the base of the cell. Stress decrease at the pipe location is roughly 6% for wall friction of 24° .

The impact of the pipe on stresses adjacent to the side wall (along $x=0.925$ m) can be examined from the results in Figure 4.12. For the case of smooth side walls ($\phi_{sw}=0^\circ$), a slight decrease in vertical stress and an increase in horizontal stress towards mid-height ($y=0.8$ m) occurs relative to values with soil only in the cell (Fig. 4.4). These trends indicate that near this location (2.6 pipe diameters) away from the pipe, the impact of pipe on horizontal stresses is of the order of 10%, and less than 1% for vertical stresses (both relative to soil only in the cell). The magnitude of these changes will have minimal influence on the overall soil-pipe response. This indicates that the lateral boundary is located sufficiently far

from the 320 mm diameter pipe. The proximity to the stiff side wall will become more important as pipe diameter increases. Pipes with a diameter greater than 500 mm may be significantly affected by the proximity of the side wall.

As wall roughness increases, the vertical stress decreases with depth. For a high interface friction angle of 35° , roughly one third of the overburden stress reaches the cell base at this location adjacent to the wall. Wall friction also decreases the horizontal stress values towards the upper ground surface. This is similar to what is predicted if the pipe is absent, where the mode of ground deformation affects lateral stresses at this location. Impact for expected range of wall friction (5° to 24°) is clearly seen. These stress changes are related to the horizontal stress increases near the cell centreline close to the ground surface seen in Figure 4.11, which are also largely independent of the pipe.

Figure 4.13 shows contours of vertical and horizontal stress in the ground with side wall friction of 5° . The redistribution of stresses in the soil arising from the difference in the pipe stiffness to that of the volume of soil it replaces (ie. arching) is evident. The vertical stress field of 1000 kPa (Fig. 4.13a) shows zones of both increasing and decreasing stress near the pipe. Vertical stresses decrease above the crown, below the invert and directly adjacent to the springline of the pipe. Zones of soil near the shoulder (between crown and springline) and haunch (between springline and invert) of the pipe experience increases in vertical stress. The stress redistribution occurs largely within one pipe diameter away from the pipe and the vertical and horizontal boundaries have little effect on the arching around the pipe. Horizontal stresses (Fig. 4.13b) increase above the crown, below the invert and adjacent to the springline. Regions of lower horizontal stress occur near the shoulder and haunch locations around the pipe.

Limits of soil arching (Moore 1993) exist for stiff pipes where the pipe attracts load from the surrounding soil (negative arching) and flexible pipes where load is shed to the surrounding soil (positive arching). This thick-wall polyethylene pipe experiences some positive arching (with ground stiffness $E=80$ MPa and $\nu=0.25$) but not to the extent for profile-wall polyethylene pipe (for the same soil stiffness) because of the larger hoop stiffness for the thick pipe.

4.7.2 Pipe Response

Side wall friction also has an impact on pipe deflections. The results from the finite element analysis are summarized in Table 4.1, for various side wall friction angles. Increases in ϕ_{sw} result in a decrease in magnitude of vertical deflection at both the crown and invert (δ_{cr} and δ_{in}) of the pipe because of reductions in the stresses that reaches the pipe. The horizontal deflection at the springline (δ_{sp}) of the pipe increases with greater boundary friction resulting from reduced lateral confinement provided to the pipe as stress is redistributed towards the side wall. For example, the magnitude of the vertical diameter change ($\Delta D_v = \delta_{cr} - \delta_{in}$) is 3% smaller for ϕ_{sw} of 24° compared to smooth side walls. The horizontal diameter change ($\Delta D_h = 2 \times \delta_{sp}$) increases relative to smooth side walls by 8% for ϕ_{sw} equal to 24° . Overall, the pipe deflections are not greatly sensitive to levels of side wall friction mobilized on the lateral boundaries.

The results from both the simplified arching analysis and the finite element results indicate that although the side wall friction does affect the soil and pipe response, the influence over the range of values expected in the laboratory with successful boundary treatment is relatively small. Thus levels of side wall friction less than 5° would not be

expected to introduce a significant deviation from expected field conditions. It is also notable that the effort to obtain very low ϕ_{sw} (ie. $\phi_{sw} \ll 5^\circ$) does not result in a substantial improvement in the laboratory idealization.

4.8 INFLUENCE OF LATERAL BOUNDARY STIFFNESS ON SOIL AND PIPE RESPONSE

All preceding analysis of the influence of the proximity and roughness of the lateral boundary of the test cell has assumed rigid side walls. Outward movements of the lateral boundary may alter the stress conditions within the ground and the pipe.

Outward lateral deformations of the side walls are expected to result in similar reductions in horizontal stresses that occur in the ground behind a retaining wall when subject to outward deformation. Lambe and Whitman (1969) report that approximately 0.5% lateral strain is sufficient to mobilize active stresses for a sand tested under triaxial extension conditions. Also, the impact of lateral deformations increases as the soil stiffness increases.

Results from two-dimensional finite element analysis are examined to obtain a measure of the impact of lateral deformations on the soil and pipe response. The finite element mesh of Figure 4.10 was used with the same soil and pipe constitutive parameters. Side wall friction of 5° was considered. The normal stiffness of the joint elements along the lateral boundary was varied to provide different magnitudes of outward lateral movement (δ_x in Fig. 4.1c). The influence of these boundary deformations on resulting soil and pipe response are presented.

4.8.1 Soil Response

Figure 4.14 shows the effect of lateral boundary stiffness on soil stresses. Vertical σ_y and horizontal σ_x stresses near the pipe ($x=0.2\text{m}$, $y=0.8\text{ m}$) and close to the side wall ($x=0.925\text{m}$, $y=0.8\text{ m}$) are reported for different magnitudes of lateral deflection δ_{sw} calculated at mid-depth along the side wall (ie. $x=1.0\text{ m}$, $y=0.8\text{ m}$). Results are shown for deflections ranging from 0 to 7.5 mm of outward movement (0 to 0.75% lateral strain) when subject to a uniform 1000 kPa surcharge.

The vertical stresses calculated at mid-depth ($y=0.8\text{ m}$) and near the wall are not greatly influenced by the magnitude of side wall deflection. At this location, the horizontal stresses are more sensitive to increases in lateral deflections, as horizontal stresses decrease with increasing side wall deflection. Near the side wall, horizontal stresses are 370 kPa for a rigid boundary, and decrease to 225 kPa for boundary deflections of 7.5 mm, where active stress conditions are nearly mobilized. For larger deflections, horizontal stresses are limited by $K_a\sigma_y$, where K_a is Coulomb's active earth pressure coefficient. For ϕ equal to 40° , side wall friction of 5° and using the one-dimensional vertical stress results in the active limit of approximately 213 kPa. The results from the finite element analysis tend towards this limit. Lateral deflection of 1 mm leads to a 16% decrease in σ_x at this location (relative to rigid walls). For soil modulus of 50 MPa, the horizontal stress near the wall is reduced by 10% relative to rigid walls for side wall deflections of 1 mm. Impacts of boundary deformation are therefore more pronounced as the soil tested is stiffer. Selection of modulus of 80 MPa likely represents an upper estimate of ground materials (ie. well compacted granular material) to be tested in the facility. For tests involving ground materials to simulate burial

conditions in a landfill (like those reported in Chapter 5 and 6), soil modulus is expected to be less than 50 MPa.

The decrease in lateral stresses adjacent to the pipe produces differences in the stresses that occur around the pipe. For rigid side walls horizontal stresses near the pipe are 620 kPa (Fig. 4.14). Again, for δ_{sw} greater than 7.5 mm, horizontal stresses are close to active pressure conditions. There is little change in the vertical stress closer to the wall at this location. The selection of soil modulus has a greater effect on the stresses calculated near the pipe (compared with values near to the wall) given the close proximity of the zone of stress redistribution around the pipe which is influenced by the soil modulus.

Zones of soil failure within the ground also depend on the lateral boundary stiffness. Figure 4.15 shows the location of zones of shear failure in the soil calculated for different magnitudes of side wall deflection. When the lateral boundaries are rigid, two local regions of soil failure occur near the pipe located at the shoulder and the haunch. This local plastic region occurs as the ratio of σ_1/σ_3 reaches N_ϕ at these locations (where $N_\phi = [1 + \sin\phi] / [1 - \sin\phi]$ for the frictional material modelled). Such soil failure is consistent with that described by Moore and Booker (1987), and leads to stress redistribution from the plastic to elastic material, and increased stresses and deflections of the pipe. This is expected to occur under field conditions and is important to be able to simulate in the laboratory model. However, as the outward lateral deformation increases, these plastic regions extend further out from the pipe, and extend towards the surface and base for deflections larger than 2 mm. Another local zone of soil failure appears near the outer top surface for lateral boundary deflections larger than 1 mm. When active conditions are approached (ie. $\delta_{sw} = 7.5$ mm), there is a significant region of soil failure corresponding to the large boundary deformations. It is

important to limit the boundary deflections to limit the deviation in ground response from that expected to occur in the field.

4.8.2 Pipe Response

Clearly, there is a pronounced effect of lateral boundary stiffness on the soil response. Consequently the pipe response (deflections and stresses) is also significantly impacted by these outward deflections.

Calculated pipe deflections are plotted in Figure 4.16 against the side wall deflection at a surcharge pressure of 1000 kPa. Crown deflections δ_{cr} increase while invert δ_{in} deflections decrease for increases in δ_{sw} . This leads to an overall increase in the vertical diameter change ($\Delta D_v = \delta_{cr} - \delta_{in}$). Horizontal deflections at the springline also increase for larger δ_{sw} producing greater horizontal pipe diameter change ($\Delta D_h = 2 \times \delta_{sp}$). For boundary deformation of 1 mm at a vertical surcharge of 1000 kPa, ΔD_v is 1.14 times larger than for rigid walls, while ΔD_h is 1.6 times larger. For soil modulus of 50 MPa, increases in vertical and horizontal diameter change of 1.09 and 1.3 relative to rigid walls were calculated.

As the side wall deflections increase, the decrease in lateral support for the pipe alters the mode of pipe deflection. This leads to greater bending stresses within the pipe relative to those calculated for rigid walls. The pipe experiences greater tensile stresses at the interior crown and invert locations, while there are greater compressive stresses at the interior springline.

Small boundary deformations produce pipe deflections and stresses in the pipe that are larger than those expected for rigid walls. Limiting boundary deflections to 1 mm at a

vertical surcharge of 1000 kPa results in a reasonable representation of deep burial conditions.

4.9 TEST CELL DESIGN

The analyses reported in this paper assessing the effects of proximity, roughness and stiffness of the lateral boundary were used to establish design limits for a new laboratory facility for testing small diameter pipes when deeply buried under large overburden stresses.

A schematic drawing of the test cell is shown in Figure 4.17. Inside dimensions are 2.0 m wide, 2.0 m long, and 1.6 m high. The test facility is self equilibrated under the 4 MN applied force acting over 4 m² by tying the lid and base units together with twelve 25 mm diameter steel rods. The stiff side walls consist of four frames welded to 40 mm thick steel plates. This arrangement limits lateral deflections to 1 mm under 1000 kPa surcharge pressure in the bladder and for K of 0.5. Over a length of 2 m, this represents lateral deflections less than two one-thousandths of the span (lateral soil strain $\epsilon_z < 0.2\%$).

Side wall friction treatment consisting of layers of polyethylene sheets lubricated with silicone grease is employed, limiting side wall friction to less than 5°. Protection of the interface is necessary and achieved with a 2 mm thick polyethylene sheet with horizontal slots (5 mm wide) to permit progressive shear failure to mobilize from the top downwards during testing (see Tognon et al. 1999).

4.10 SUMMARY

Design issues for a new laboratory facility for testing of small diameter deeply buried pipes have been presented. Based on a series of finite element analyses, it is concluded that the test cell provides a reasonable simulation of the stress state expected to prevail for a pipe deeply buried under an embankment or landfill.

Vertical stresses from overburden pressures are simulated by the application of uniformly distributed vertical pressure. Horizontal stresses are developed like those expected in the field by limiting the lateral deflection of the side walls. Selection of cell geometry was made such that the stresses within the ground surrounding the pipe are similar to those expected when deeply buried under overburden material.

Potential boundary effects arising from the proximity, roughness and stiffness of the lateral boundary were assessed using finite element analysis. Surface friction mobilized along the cell boundaries may alter the stress conditions within the soil and the pipe, leading to less of the applied pressure reaching the pipe. Reduction of side wall friction to less than 5° (by inclusion of sheets of polyethylene lubricated with silicone grease) results in minimal (less than 5%) changes relative to frictionless conditions. Lateral boundary deformations may reduce the horizontal stresses acting in the soil and increase the deformations of the pipe. Limiting the boundary deformation to 1 mm at an applied surcharge of 1000 kPa (by suitable structural stiffness) provides a reasonable idealization of field conditions.

4.11 REFERENCES

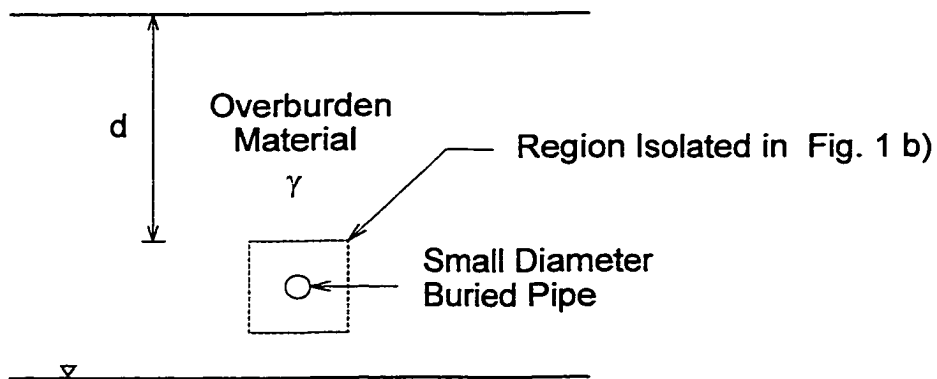
- Bathurst, R.J. and Benjamin, D.J. 1988. Preliminary assessment of side wall friction on large scale models in the RMC test facility. P.M. Jarrett and A. McGown (eds.), *The Application of Polymeric Reinforcement in Soil Retaining Structures*, Kluwer Academic Publishers, pp. 181-192.
- Brachman, R.W.I. 1997. Hoop Compression Testing of HDPE Leachate Collection Pipe, *Geosynthetics '97*, IFAI, Long Beach, CA, USA, pp. 337-350.
- Brachman, R.W.I., Moore, I.D. and Rowe, R.K. 1996. Interpretation of a buried pipe test: Small diameter pipe in the Ohio University facility, *Transportation Research Record*, 1541, pp. 64-70.
- Brachman, R.W.I., Rowe, R.K., Moore, I.D., Tognon, A. 1998. Laboratory investigation of the performance of leachate collection pipe with coarse stone, *Sixth International Conference on Geosynthetics*, Atlanta, GA, USA, pp. 191-196.
- Davis, E.H. 1969. Theories of Plasticity on the failure of soil masses. *Soil Mechanics Selected Topics*. I.K. Lee (Ed.), London: Butterworth, pp. 341-374.
- DiFrancesco, L.C., Selig, E.T. and McGrath, T.J. 1994. Laboratory testing of high density polyethylene drainage pipes. *Geotechnical Report No. CPP93-412F*, Department of Civil Engineering, University of Massachusetts at Amherst, 134 pages.
- Höeg, K. 1968. Stresses Against Underground Structural Cylinders, *J. Soil Mech. Fdn. Div.*, ASCE SM4, pp. 833-858.

- Kastner, R.E., Sargand, S.M. and Mitchell, G.F. 1993. Structural performance of PVC leachate collection pipe. Structural Performance of Pipes, Sargand, Mitchell and Hurd (eds.), Balkema, Rotterdam, pp. 83-95.
- Lambe, T.W. and Whitman, R.V. 1969. Soil Mechanics, Wiley, New York.
- Moore, I.D. 1993. Structural Design of Profiled Polyethylene Pipe - Part I Deep Burial, Geotechnical Research Centre Report GEOT-8-93, The University of Western Ontario, London, ON, Canada, March 1993.
- Moore, I.D. and Booker, J.R. 1987. Ground Failure Around Buried Tubes, Rock Mechanics and Rock Engineering, 20, pp. 243-260.
- Moore, I.D. and Hu, F. 1995. Response of HDPE pipe under hoop compression. Transportation Research Record. No. 1514, Design and Performance of Underground Pipe, pp. 29-36.
- Moore, I.D. and Laidlaw, T.C. 1997. Corrugation buckling in HDPE pipes - measurements and analysis, 76th Annual Meeting, Transportation Research Board, Washington D.C., January 11-15, Preprint No. 97-0565.
- Moore, I.D., Laidlaw, T.C. and Brachman, R.W.I. 1996. Test cells for static pipe response under deep burial, 49th Canadian Geotechnical Conference, September 23-25, St. John's NF, pp. 737-744.
- Perloff, W.H. and Baron, W. 1976. Soil Mechanics Principles and Applications, John Wiley & Sons, New York, 745 p.
- Rogers C.D.F., Fleming, P.R. and Talby, R. 1996. Use of visual methods to investigate the influence of installation procedure on pipe - soil interaction, Transportation Research Record, 1541, pp. 76-85.

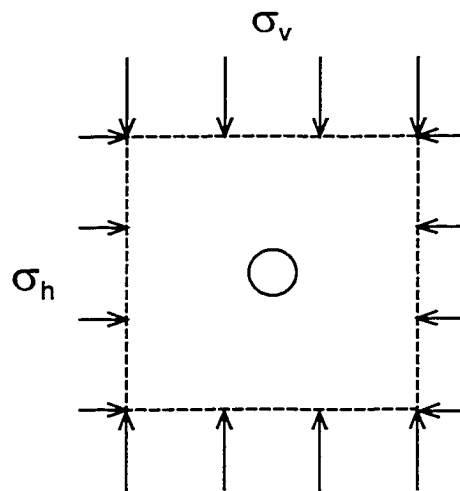
- Selig, E.T., DiFrancesco, L.C., and McGrath, T.J. 1994. Laboratory Test of Buried Pipe in Hoop Compression. Buried Plastic Pipe Technology: 2nd Volume, ASTM STP 1222, pp. 119-132.
- Tognon, A.R.M., Rowe, R.K., and Brachman, R.W.I. (1999) Evaluation of Sidewall Friction for a Buried Pipe Testing Facility. Geotextiles and Geomembranes, 17 (4), (In Press).
- Zanzinger, H. and Gartung, E. 1995. Large-scale Model Tests of Leachate Collection Pipes in Landfills Under Heavy Loads, Advances in Underground Pipeline Engineering, J.K. Jeyapalan and M. Jeyapalan (Eds.), ASCE, pp. 114-125.
- Zanzinger, H. and Gartung, E. 1998. HDPE-Geopipes, Soil-structure interaction, Sixth International Conference on Geosynthetics, Atlanta, GA, USA, pp. 197-200.
- Zhang, C. and Moore, I.D. 1997. Finite element modelling of inelastic deformation of ductile polymers, Geosynthetics International, Vol. 4, No. 2, pp. 137-163.

TABLE 4.1 Calculated pipe deflections at the crown, invert and springline for various levels of side wall friction ϕ_{sw} .

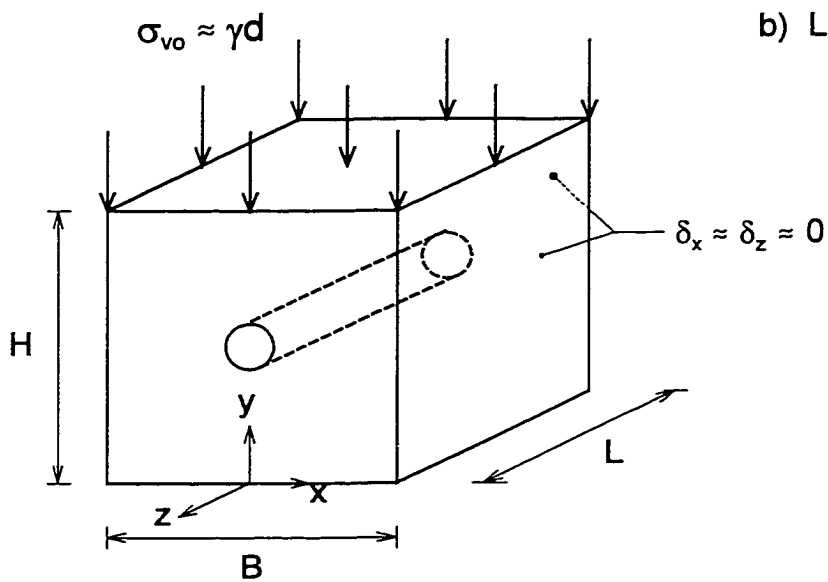
ϕ_{sw}	Pipe Deflection (mm)				
	δ_{cr}	δ_{in}	δ_{sp}	ΔD_V	ΔD_H
0°	-10.9	-5.91	.804	-4.99	1.61
5°	-10.8	-5.78	.818	-5.02	1.64
10°	-10.6	-5.67	.831	-4.93	1.66
24°	-10.2	-5.37	.868	-4.83	1.74
35°	-9.91	-5.13	.907	-4.78	1.84



a) Small diameter pipe under deep burial.



b) Loads acting on soil-pipe system.



c) Laboratory idealization.

FIGURE 4.1 Idealization of loads acting on region of soil around a deeply buried pipe.

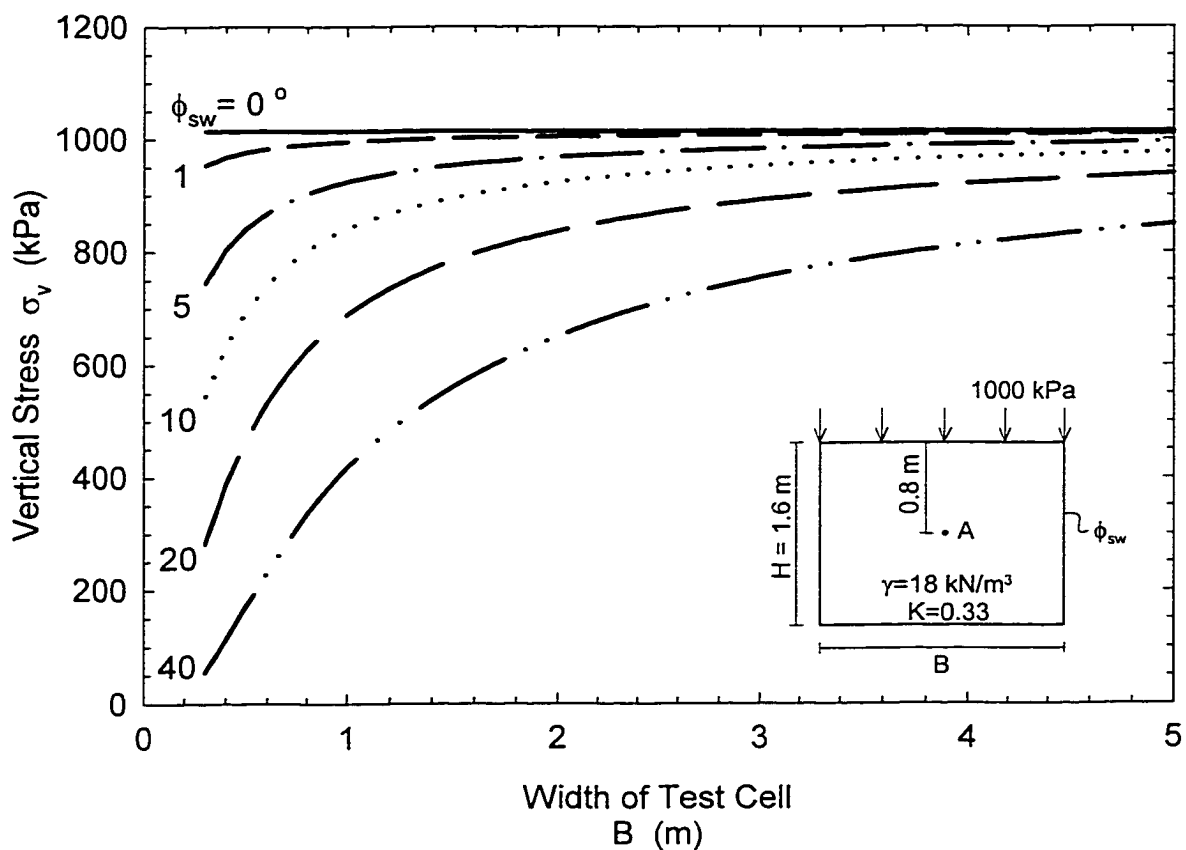


FIGURE 4.2 Estimate of vertical stress at mid-depth (point A) for various levels of side wall friction ϕ_{sw} with increasing width of test cell B when subject to applied vertical pressure of 100 kPa.

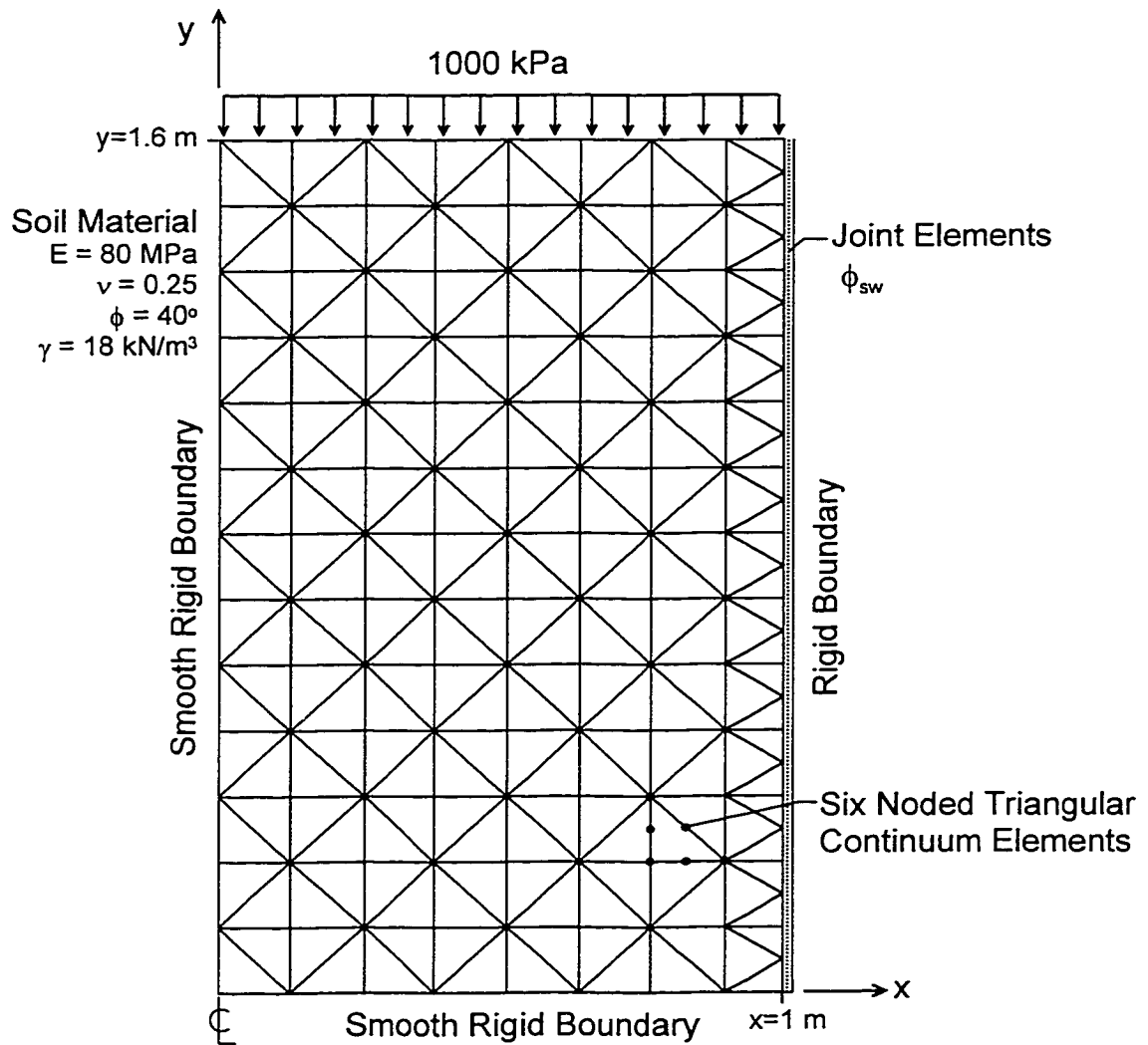


FIGURE 4.3 Finite element mesh used to investigate soil - test cell interaction by considering half of a 2 m wide by 1.6 m high block of soil subject to vertical surcharge with interface friction ϕ_{sw} .

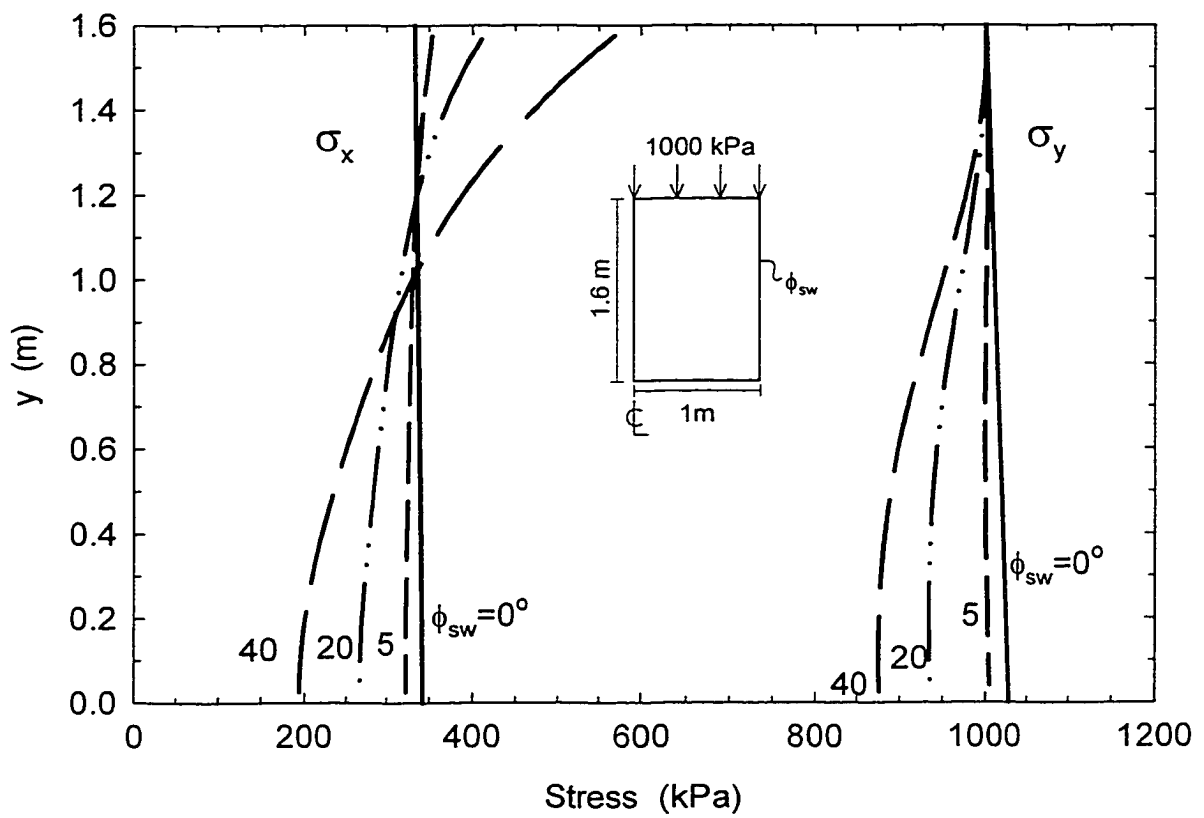


FIGURE 4.4 Vertical σ_y and horizontal σ_x stresses with depth along test cell centreline subject to vertical surcharge of 1000 kPa with different side wall friction ϕ_{sw} values.

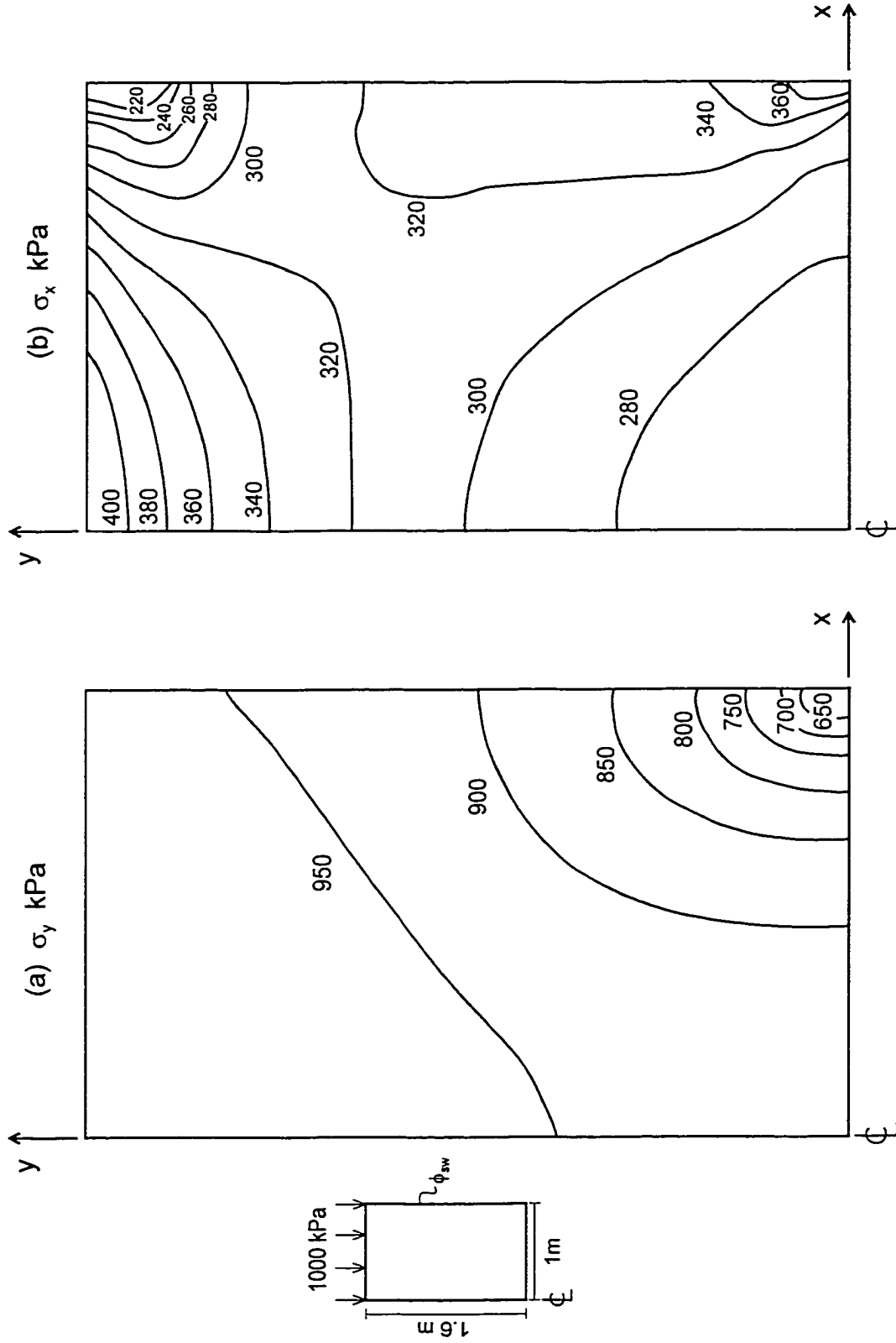


FIGURE 4.5 (a) Vertical and (b) horizontal stresses calculated for half of a 2 m wide by 1.6 m high block of soil subject to a vertical surcharge of 1000 kPa with interface friction ϕ_{sw} of 20° .

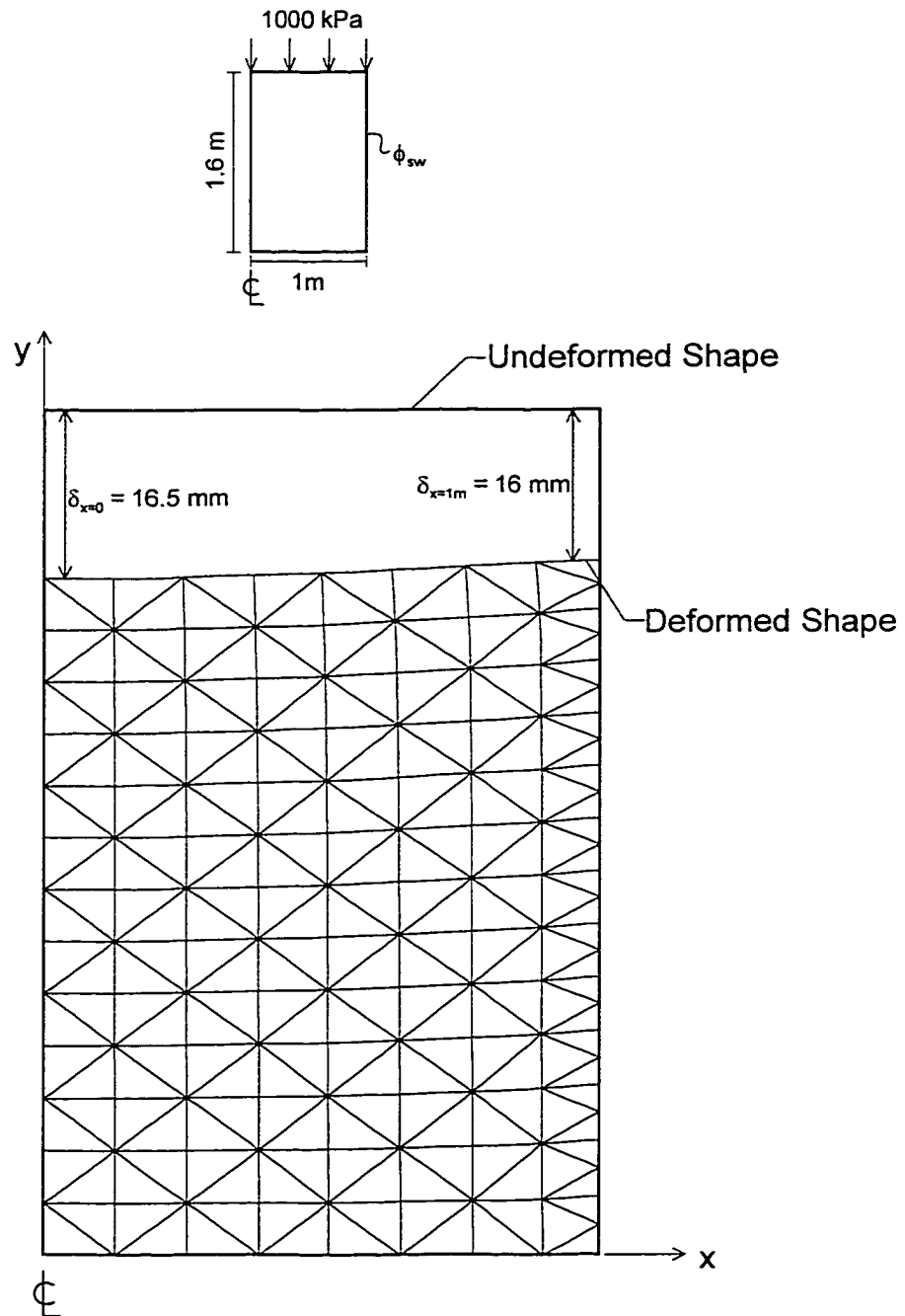


FIGURE 4.6 Deformed shape ($\times 20$) of half of a 2 m wide by 1.6 m high block of soil subject to vertical surcharge of 1000 kPa with interface friction ϕ_{sw} of 20° .

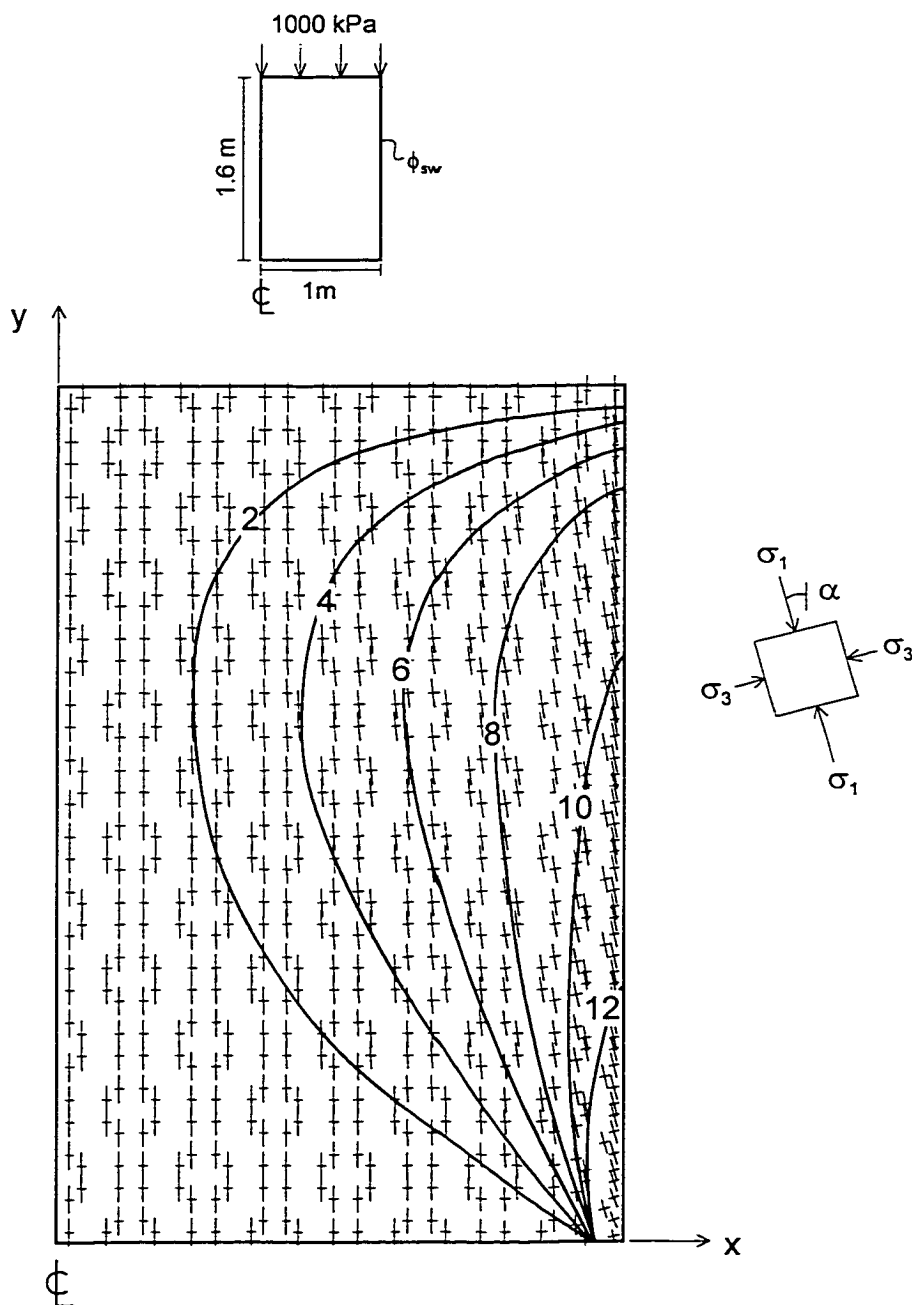


FIGURE 4.7 Vectors of major σ_1 and minor σ_3 principal stress for half of a 2 m wide by 1.6 m high block of soil subject to vertical surcharge of 1000 kPa with interface friction ϕ_{sw} of 20°. Also shown are contours of the rotation of major principal stress from the vertical (α) in degrees.

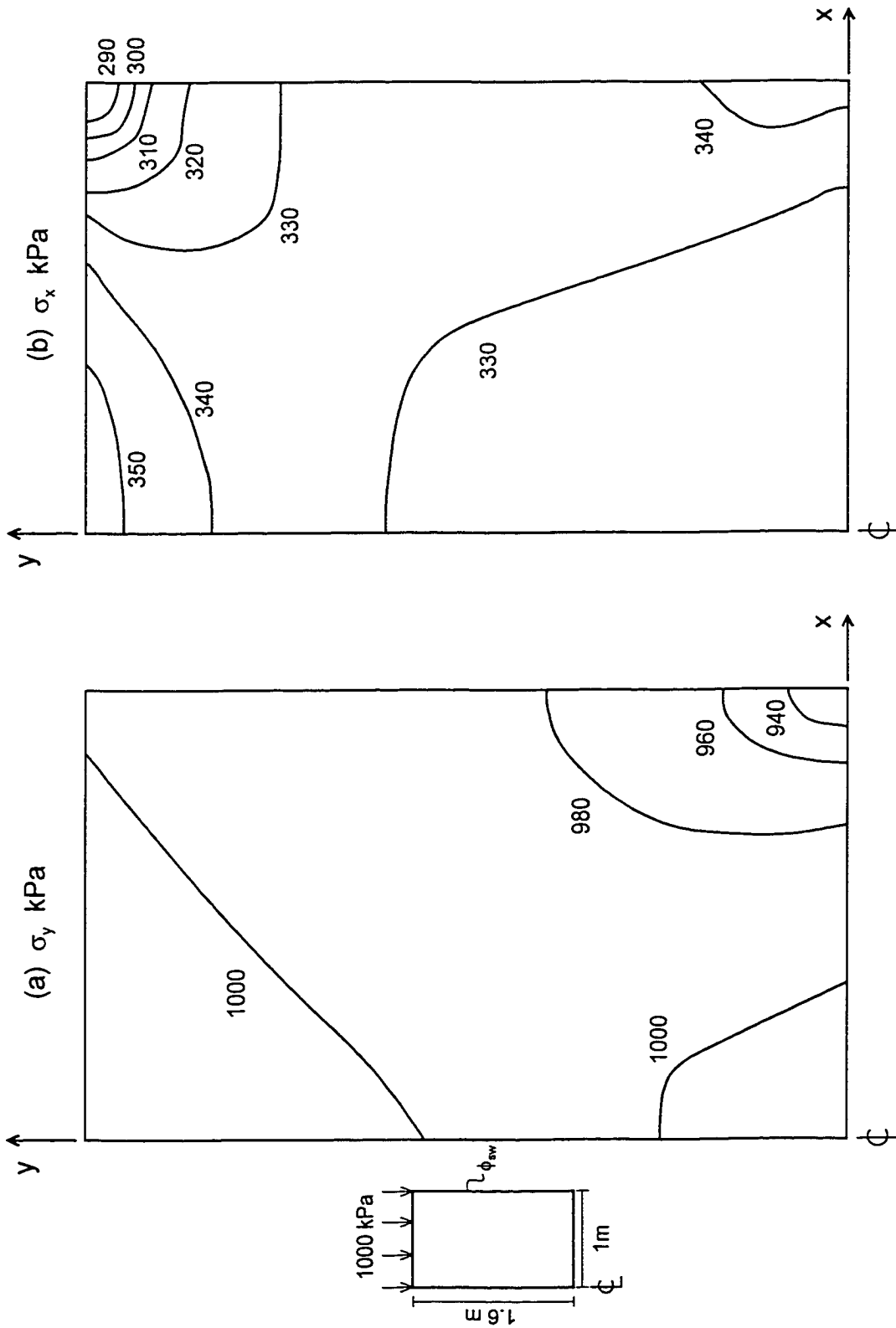


FIGURE 4.8 (a) Vertical and (b) horizontal stresses calculated for half of a 2 m wide by 1.6 m high block of soil subject to a vertical surcharge of 1000 kPa with interface friction ϕ_{sw} of 5°.

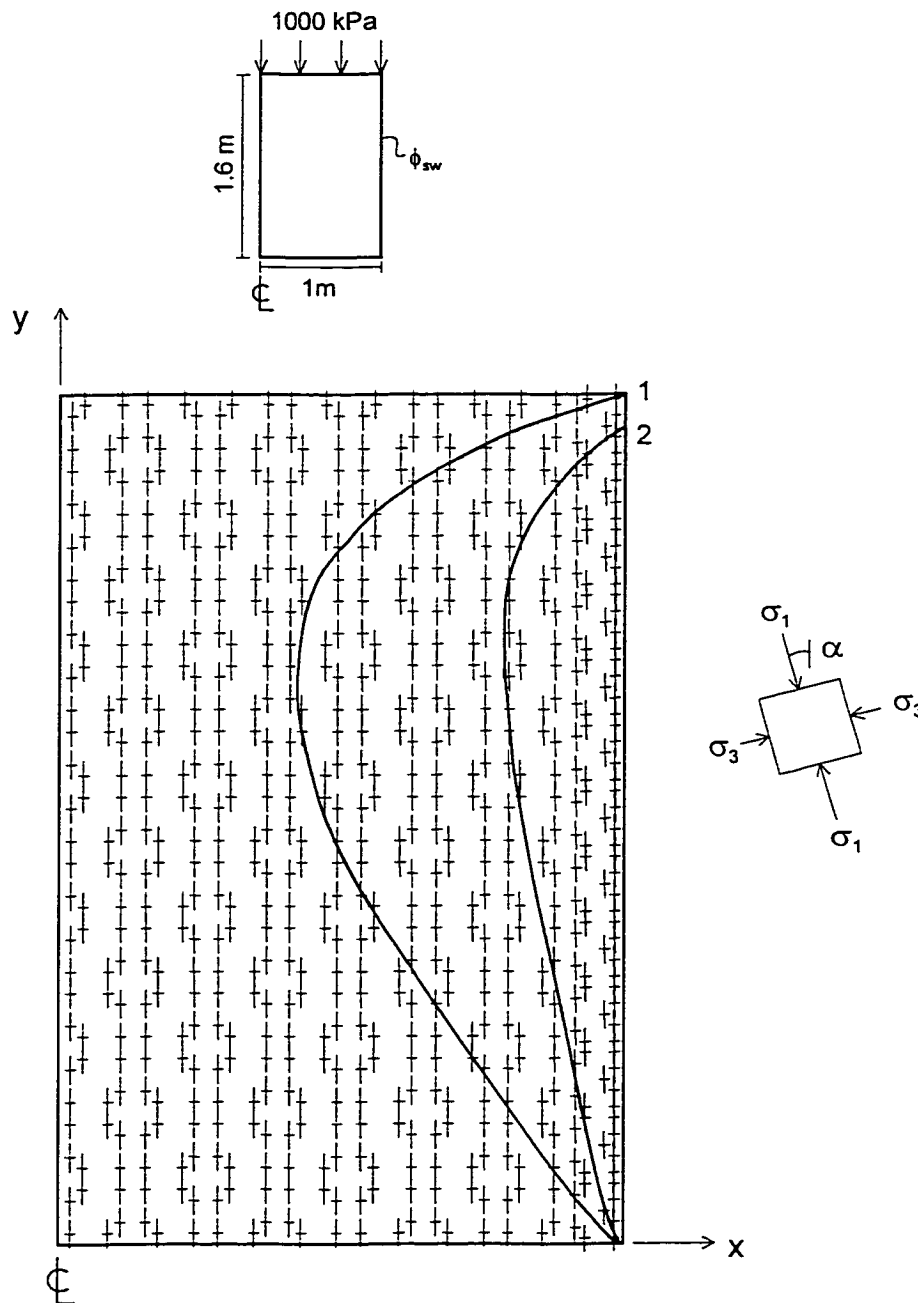


FIGURE 4.9 Vectors of major σ_1 and minor σ_3 principal stress for half of a 2 m wide by 1.6 m high block of soil subject to vertical surcharge of 1000 kPa with interface friction ϕ_{sw} of 5° . Also shown are contours of the rotation of major principal stress from the vertical (α) in degrees.

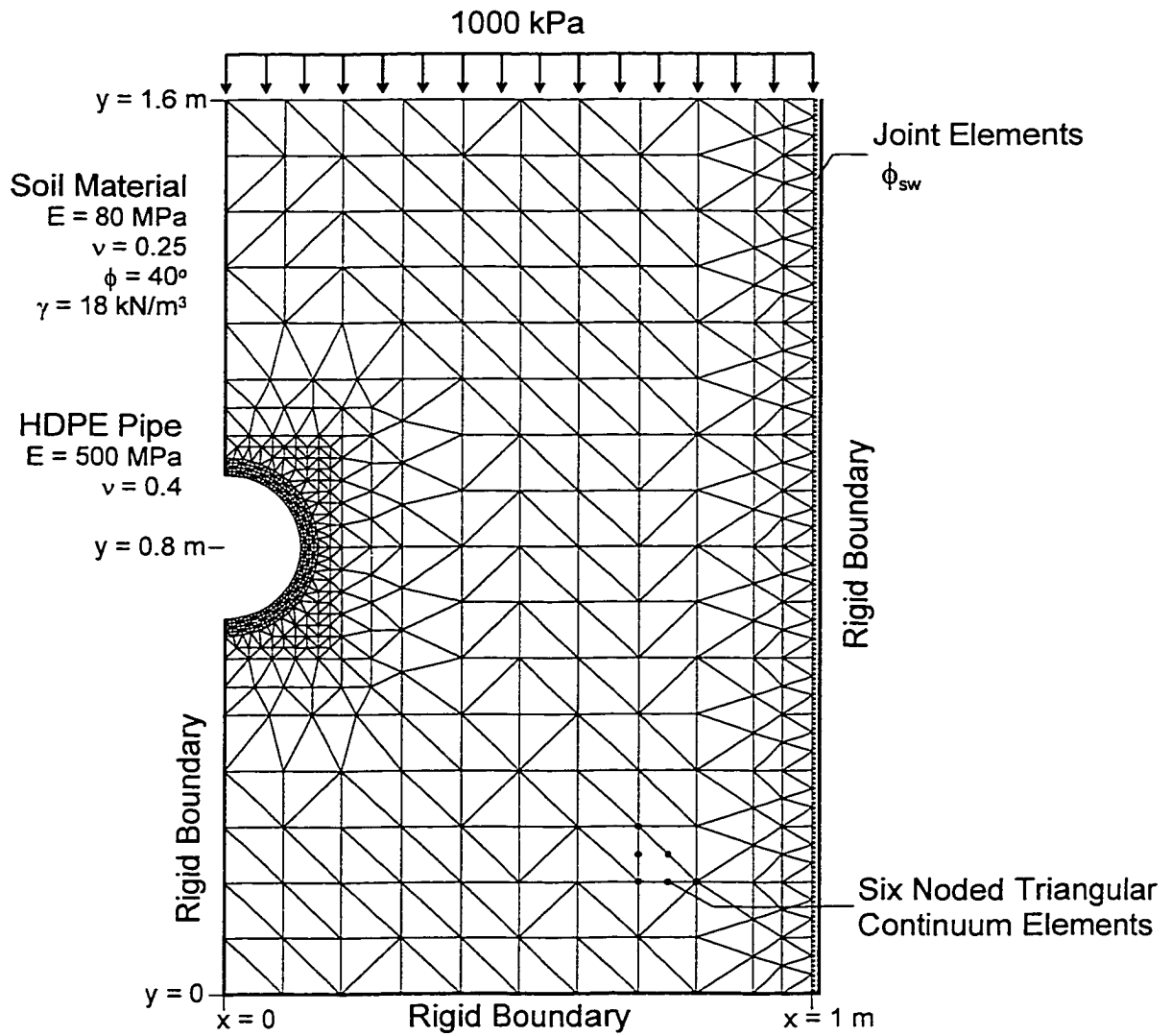


FIGURE 4.10 Finite element mesh used for pipe-soil-cell interaction analysis.

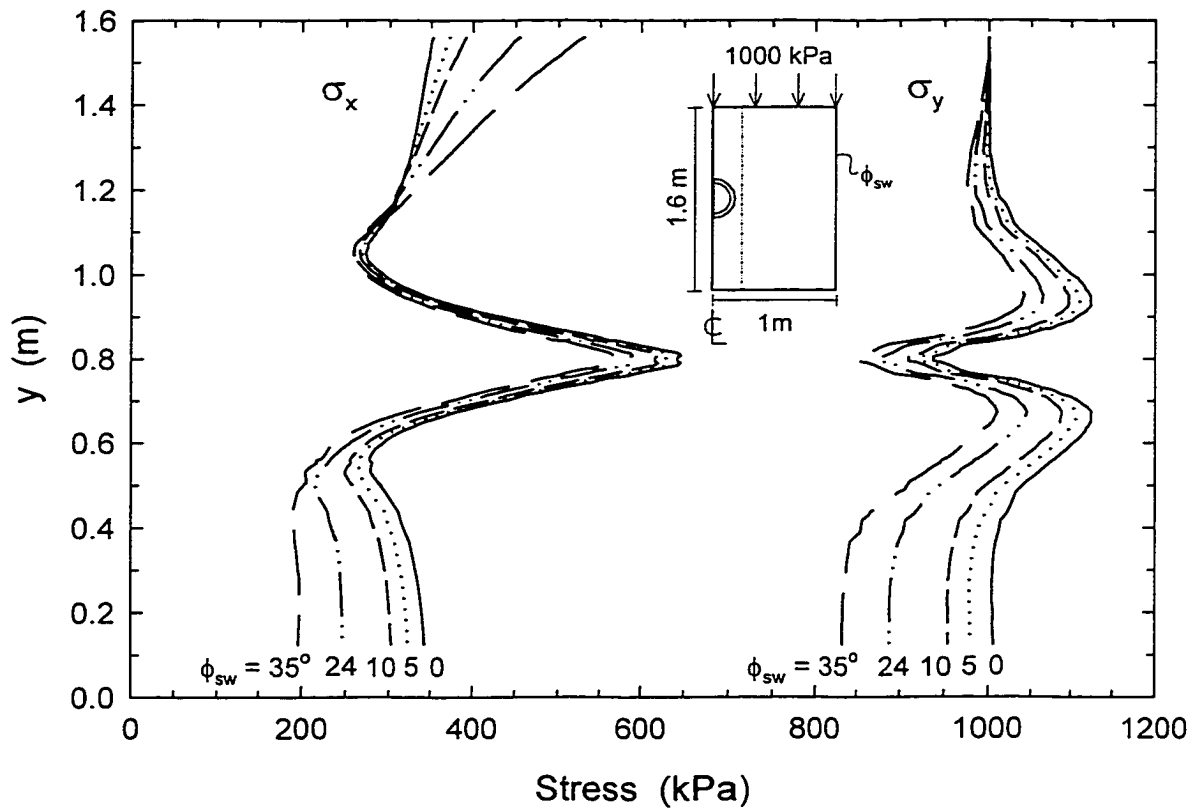


FIGURE 4.11 Calculated vertical σ_y and horizontal σ_x stresses along a vertical section 0.2 m away from the pipe centreline with $\sigma_{vo}=1000$ kPa.

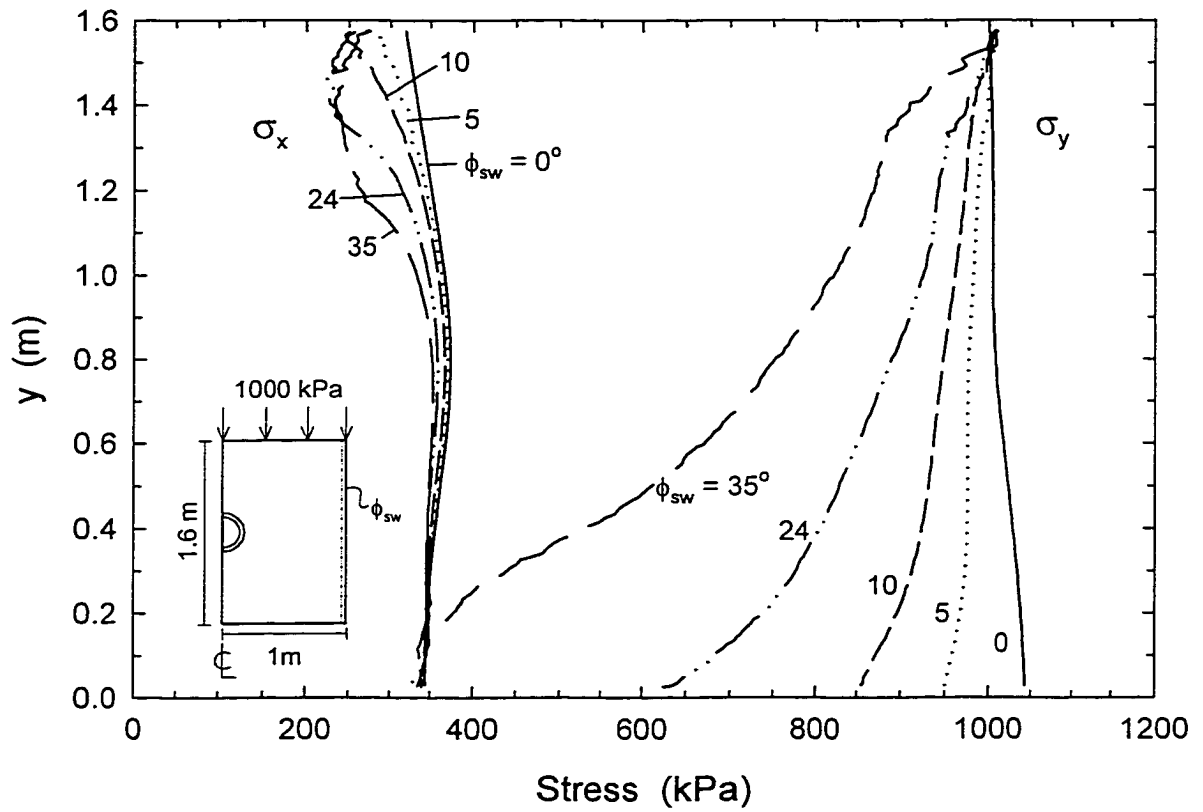


FIGURE 4.12 Calculated vertical σ_y and horizontal σ_x stresses along a vertical section 0.075 m away from the lateral boundary with $\sigma_{vo}=1000$ kPa.

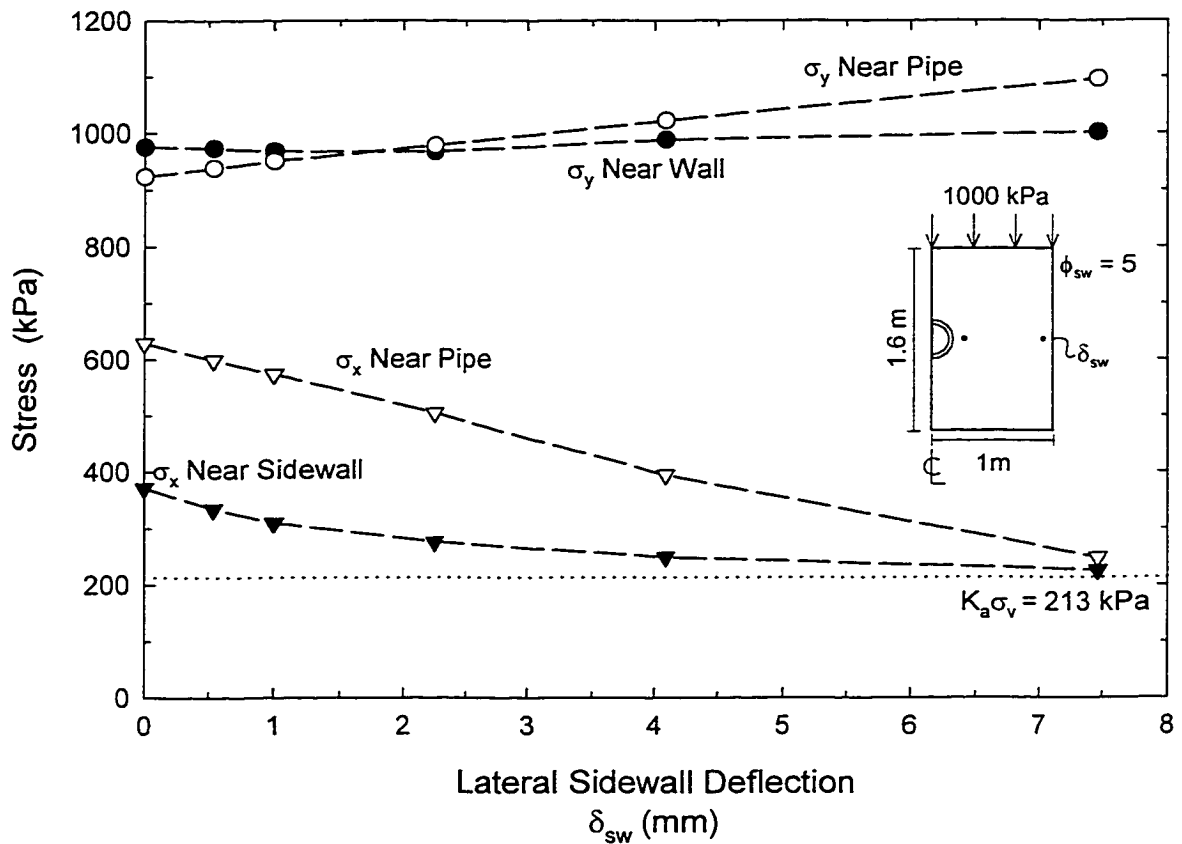


FIGURE 4.14 Vertical and horizontal stresses calculated at mid-depth near the pipe and near the side wall for increasing lateral boundary deformation with $\phi_{sw} = 5^\circ$ and $\sigma_{vo} = 1000$ kPa.

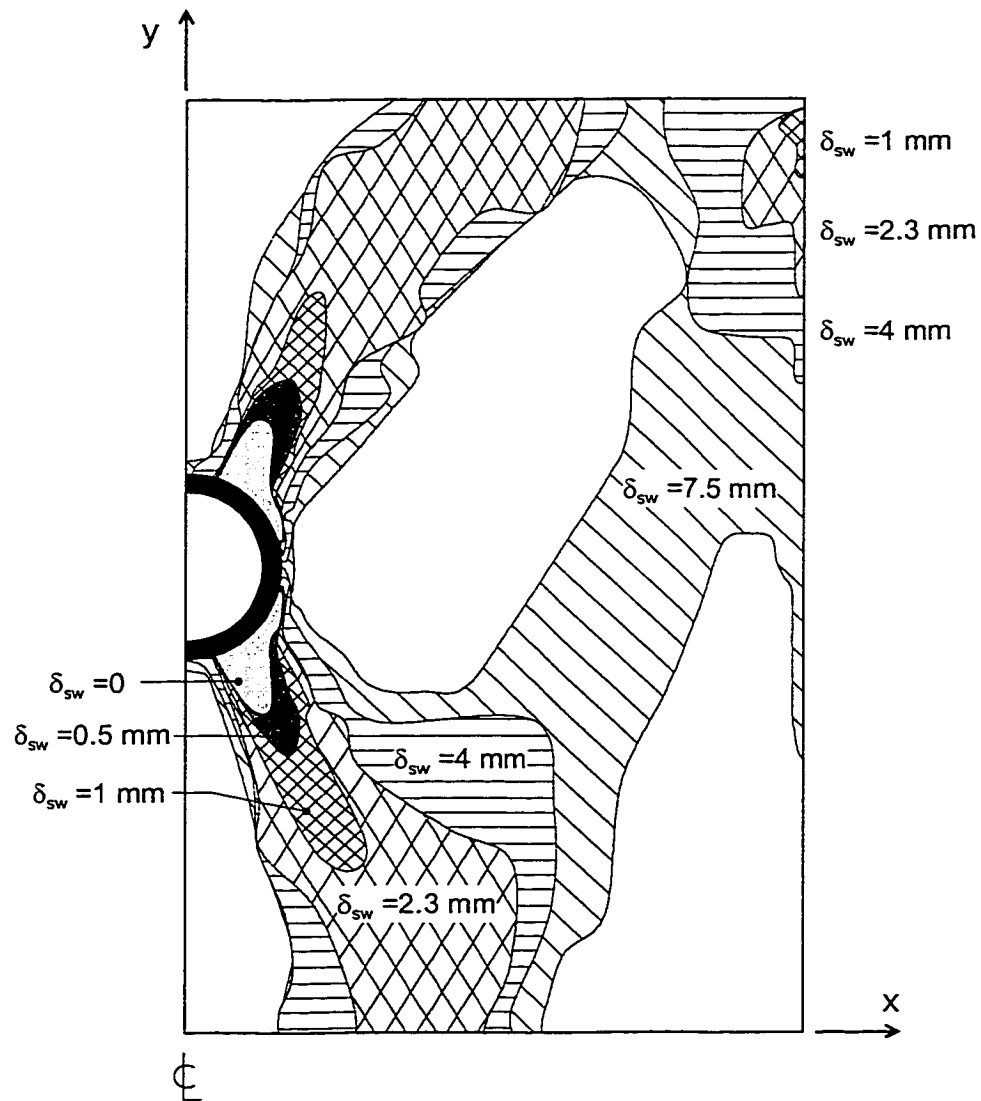


FIGURE 4.15 Calculated zones of shear failure in the soil for various lateral deformations δ_{sw} with $\phi_{sw}=5$ and $\sigma_{vo}=1000$ kPa.

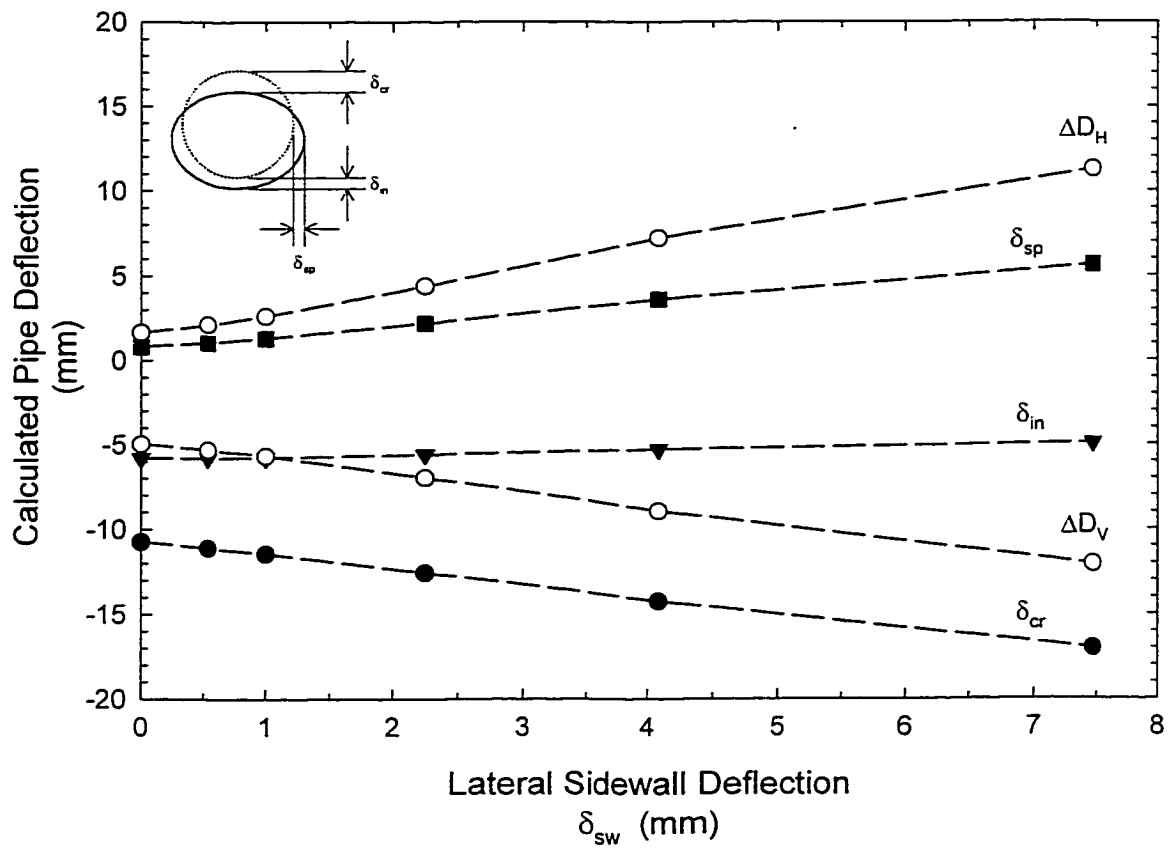


FIGURE 4.16 Calculated pipe deflections at the crown, invert and springline (δ_{cr} , δ_{in} , δ_{sp}) and diameter change (ΔD_V , ΔD_H) for increasing lateral boundary deflection with $\phi_{sw}=5^\circ$ and $\sigma_{vo}=1000$ kPa.

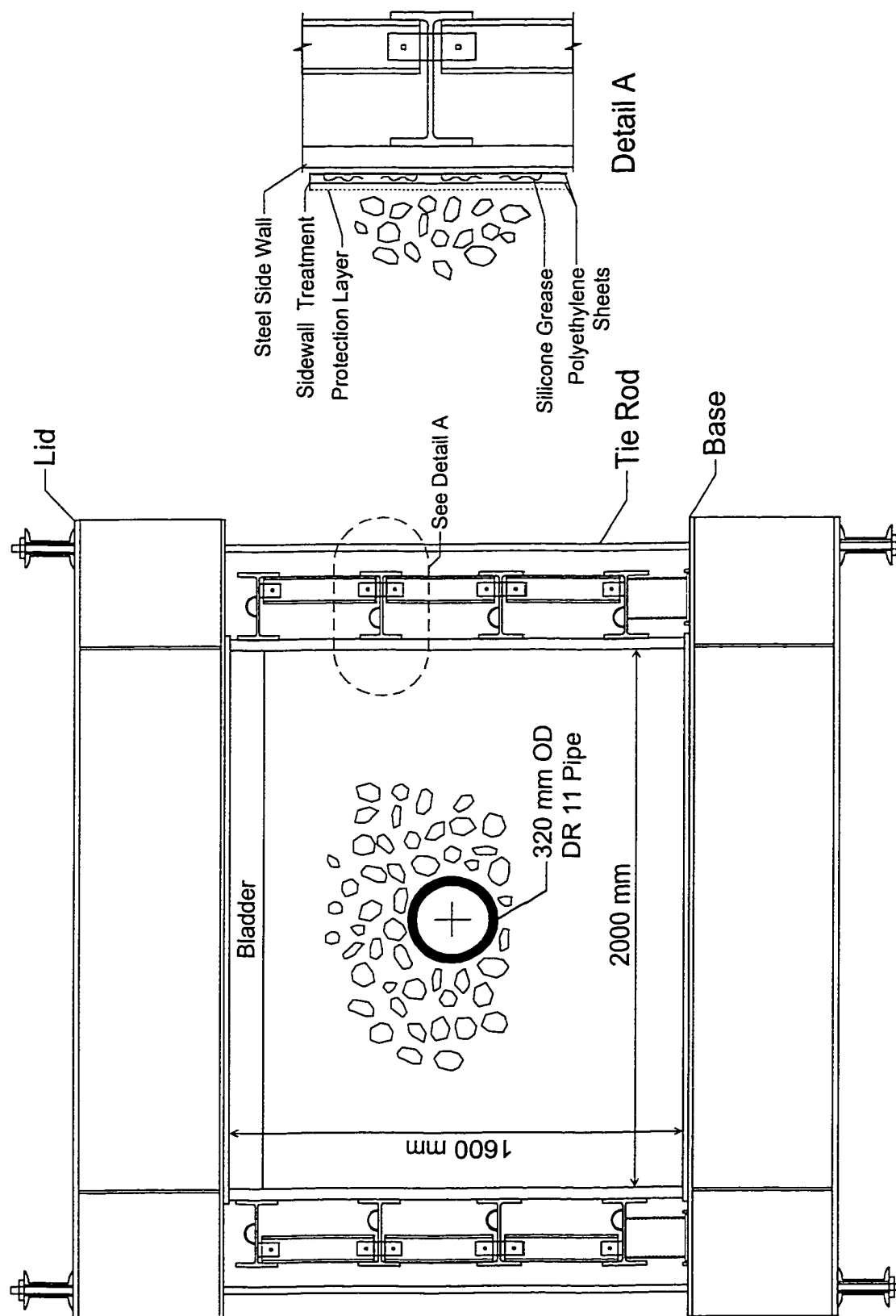


FIGURE 4.17 Transverse section through biaxial compression testing facility.

CHAPTER 5

Performance of a New Laboratory Facility for Testing Small Diameter Pipes Under Simulated Biaxial Earth Pressures

5.1 INTRODUCTION

The design of a new laboratory facility for testing small diameter pipes under simulated field conditions was presented in Chapter 4. This test facility was designed to closely simulate the biaxial earth pressures that act on the vertical and horizontal soil boundaries at some distance from the pipe. Issues such as the selection of dimensions, the simulation of earth pressures and limiting boundary effects from interface roughness and lateral stiffness were discussed.

This chapter reports on the performance of the new laboratory facility. The results of two tests conducted on a small diameter leachate collection pipe are examined to assess the suitability of the laboratory model. The measured response of the soil, pipe and test facility are considered to evaluate how closely the response of the pipe tested in the new facility compares with that expected to occur under field conditions of deep and extensive overburden pressures, and how the measured response compared to the analysis conducted for the design of the test facility. The structural response of a small diameter plastic pipe is then examined for two very different backfill materials. Comparison of these results shows the importance of modelling the biaxial earth pressures in laboratory studies.

5.2 DESCRIPTION OF LABORATORY FACILITY

5.2.1 Laboratory Apparatus

Burial of a pipe under deep and extensive ground materials leads to large vertical and horizontal stresses that act at some distance from the pipe. Idealized in Figure 5.1a are the vertical stresses that arise from the weight of the overburden material and horizontal stresses that develop in the ground from resistance to lateral movement. Since the response of the pipe is a function of both the stiffness of the pipe and the stiffness of the soil, it is important to simulate the response of both of these components in the laboratory model. The new test facility was designed to closely simulate these biaxial earth pressures.

Figures 5.1b and 5.2 show transverse and longitudinal sections of the test cell. The pipe specimen is placed within a prism of soil that is 2.0 m wide \times 2.0 m long \times 1.6 m high. The pipe may be placed at different elevations in the cell depending on the test requirements. The soil is contained within a stiff steel structure. Lid and base units are connected with high-strength tie rods capable of resisting the large vertical forces that develop with the application of large vertical pressures (up to 1000 kPa). The sidewalls consist of 40 mm thick steel plates that are stiffened by four support frames that are welded to the side plates and also have welded moment connections in each corner.

5.2.2 Simulation of Vertical and Horizontal Stresses

5.2.2.1 Vertical Pressures

Vertical load is applied by a pressurized air bladder that provides a uniform vertical pressure across the top boundary. The bladder consists of a large rubber sheet sandwiched between

a square frame, composed of steel angle sections ($127 \times 76 \times 13$ mm) welded together in the corners, and a thin steel plate ($2235 \times 2235 \times 6$ mm), Figure 5.2. The leg of the angle lies inside the sidewalls and provides lateral confinement for the bladder as the lid deflects upwards - otherwise the bladder would be unconfined and fail. The leg of the angle was selected to be larger than the estimated sum of the upward movement of the lid unit (governed by the elongation of the twelve 25 mm diameter tie rods) and the downward movement of the soil. A mechanical seal was obtained by bolting the angle to the 6 mm thick steel plate with 9.5 mm diameter bolts at a spacing of 76 mm. High strength bolts were used to allow tightening to large torques to obtain a good seal. The relatively thin steel plate is supported by the stiff lid unit during testing. The top plate contains an inlet connection and an outlet connection where the bladder pressure can be monitored.

Several rubber materials were evaluated using a cylindrical pressure vessel (400 mm diameter) with a bolted steel lid. Elongation of the rubber was the main criterion for material selection. Reinforced materials provided excellent strength but are undesirable to use to apply a uniform pressure to the soil, since any tensile force mobilized within the membrane reduces the external pressure applied to the soil. Commercially available lifting bags (normally sealed neoprene bags heavily reinforced with either steel or kevlar) were also evaluated and based on this, caution is advised on the use of these bags for simulation of vertical pressures because, as a result of the load transfer to the reinforcement, (a) the pressures applied to the soil are unknown, and (b) the distribution of contact stresses may be highly nonuniform.

Natural gum rubber provided the best performance (even for a relatively thin sample only 1.6 mm thick) however was difficult to seam. Seaming therefore was another important

consideration given that the manufactured width of these materials is less than the width of the test cell. Buna-N rubber (3 mm thick) was selected for use as the bladder material given its good elongation to failure and the success of seaming. The sheets of rubber were joined with a 50 mm-wide chemically-vulcanized lap-seam. Rubber cement (Rema Tip-Top SC2000) was used to chemically vulcanise the seam together. Surface preparation (involving scoring and cleaning) and stitching (pressing the seam together to remove air pockets) were critical factors for obtaining a reliable seam. After seaming, the sharp edges of the lap seam were removed by grinding the rubber to reduce the stress concentrations at the seam. Also, the lap seam was grinded near the location of the mechanical seal in order to provide smooth contact surfaces and to minimize the chance of leakage.

This diaphragm-type arrangement for the bladder was superior to trials of sealed bags composed of various materials. Larger pressures and more uniform loading conditions were obtained with this arrangement. Proper sealing of bag-type bladders often required many layers of additional reinforcement in the corners that resulted in a stiffer bladder, and hence a deviation from uniform pressures applied to the soil.

5.2.2.2 Horizontal Pressures

Horizontal stresses develop in the soil as a result of restraint against lateral movements by the sidewalls. The stiffness of the lateral boundaries was one important consideration during design of the new test facility (Brachman et al. 1999; Chapter 4). Simulation of lateral pressures with pressurized bladders (in a similar manner to the vertical pressures) was contemplated during the conceptual design of the test cell, however, were not adopted given the potential for damage of the bladder from the backfill material (especially when the coarse

gravel material, shown in Figure 5.3, was tested). The method employed in the new laboratory model permits the development of lateral earth pressures appropriate to each material, which is also advantageous when different layers of soil materials are tested (e.g., Fig. 5.3).

5.2.3 Limiting Boundary Friction

The sidewalls of the test cell required treatment to reduce the boundary effects from friction. Figure 5.4 shows the angle of friction ϕ_{sw} mobilized for various treated interfaces considered by Tognon et al. (1999). Limited surface treatment involved a thin polyethylene (PE) sheet (0.1 mm thick) and a nonwoven geotextile GT1 (with mass per unit area of 435 g/m^2), where slip was to occur along this interface. When tested in contact with medium sand, the resulting friction angle was 16° . Tests with the coarse gravel material (crushed stone described in Section 5.3.1.2) yielded a higher interface friction angle of 21° . This increase in ϕ_{sw} relative to the sand backfill results from discontinuous interface contact. Damage to the polyethylene layer was noticed because of the coarse stone particles. This demonstrated a need to protect the friction treatment from impingement of the gravel backfill.

The adopted interface treatment consisted of two polyethylene sheets (0.1 mm thick) lubricated with silicone grease (Dow Corning 44 high temperature bearing grease). This arrangement (illustrated in Fig. 5.3) yielded a friction angle of roughly 5° , as shown in Figure 5.4. Adequate protection of the interface treatment from the possible impingement of the backfill material was obtained with a thinner nonwoven geotextile GT2 (mass per unit area of 120 g/m^2) and a 2 mm-thick geomembrane GM (for specific details see Tognon et al. 1999). The potential for a deleterious interaction between the PE sheets and the silicone was

investigated by conducting direct shear tests on samples of the PE sheets in contact with the lubricant for longer time frames (up to 30 days). No discernable increase in interface friction was found for the Dow Corning 44 grease (Tognon et al. 1999). It was estimated that this level of friction reduces the vertical stresses reaching the pipe by less than 5% and has only a small effect on the pipe response (Brachman et al. 1999; Chapter 4). Since direct measurement of boundary friction would be very difficult (if not impossible) to undertake on the large-scale involved in the pipe tests, an assessment of the friction angle obtained during tests in the new facility and the effect on the pipe are achieved through measurements of the pipe and soil response, as well as from visual observations.

5.3 DESCRIPTION OF LABORATORY TESTS

5.3.1 Soil Materials Tested

5.3.1.1 Test P2a

Two different arrangements were tested. The first involved the small diameter pipe centrally located within the test cell and backfilled with a relatively uniform medium sand (SP). Figures 5.1b and 5.2 show the arrangement of materials used for the first test (P2a).

Sand (poorly-graded medium sand) was selected because it could be consistently placed at a relatively uniform density with moderate compactive effort. The sand was placed in 150 mm lifts (dumped from a constant height) and then compacted by dropping a 9 kg mass a height of 300 mm, with two passes made over each lift. This resulted in a relatively uniform material, with an average dry density of 1760 kg/m^3 and water content of 2%. The

measurements of density compared well with the density obtained by recording the total mass of sand placed in the cell divided by the volume it occupied.

5.3.1.2 Test P2b

The arrangement of materials for the second test (P2b) is shown in Figure 5.3. Three different soil materials were used to attempt to simulate the conditions expected in a municipal solid waste landfill. Here, the pipe was placed within a 600 mm deep layer of uniform coarse gravel (called crushed stone) to simulate the drainage layer. Crushed (40 - 50 mm) dolomitic limestone, similar to that used at the Halton and other Ontario, Canada landfills (Rowe et al. 1993), was used as the backfill material. This material is a poorly-graded coarse gravel (GP) and consists of large angular particles with 70% finer than 51 mm sieve size and only 8% finer than 38 mm. The use of this coarse gravel is desirable to minimize the biological clogging of leachate collection systems in municipal solid waste landfills (Rowe et al. 1995). The crushed stone was placed uncompacted at an average bulk density of 1520 kg/m³. The pipe was placed with approximately 100 to 120 mm of coarse gravel material between the pipe invert and the clay layer.

The drainage layer was underlain by a 200 mm thick clay layer that was included to simulate the effect of a more compressible layer beneath the coarse gravel and pipe. Finite element analysis of this arrangement was used to select the thickness of the clay layer. It was found that there was little difference in pipe response once the thickness of the clay was such that the pipe was at least one pipe-diameter away from the stiff steel base. This silty-clay till of low plasticity (liquid limit of 24% and plastic limit of 14%) was placed at a water content near the plastic limit (corresponding to 2 to 4% wet-of-optimum, which is standard

practice for placing a compacted clay liner; e.g., see Rowe et al. 1995) and an average bulk density of 2100 kg/m³. This till was from the Halton landfill site and its use as a liner has been described by Rowe et al. (1993).

The poorly-graded medium sand (SP) used in the first test was used to fill the remainder of the test cell. A needle-punched nonwoven geotextile (GT1), with mass per unit area of 435 g/m² and equivalent opening size of 75 to 150 µm, was used to separate the sand and coarse gravel materials.

The arrangement shown in Figure 5.3 was also used for four additional tests conducted on two other pipe samples of the same diameter but containing perforations. Some results from tests P3c and P4 are reported in this chapter. Details of these tests can be found in Chapter 6.

5.3.2 Details of Pipe Specimens

The tests were conducted on a thick-wall small-diameter high-density-polyethylene pipe. This pipe was made with a polyethylene material with classification PE 345434C in accordance with ASTM D3350, and Class PE 3408 according to the Plastic Pipe Institute. These pipes are often used as drainage pipes in the leachate collection systems for municipal solid waste landfills, where they would normally be perforated to allow the collection of the leachate. The tests reported in this chapter were conducted on pipes without perforations. Tests conducted on perforated leachate collection pipes are reported in Chapter 6.

The pipe sample had an average outside diameter of 220 mm and an average wall thickness of 25 mm (nominal pipe size of 220 mm OD SDR 9, where SDR is the ratio of outside diameter to the minimum wall thickness). The two metre long specimen contained

two butt-fusion joints, each located 250 mm from the centre of the pipe. This was required to facilitate the application of strain gauges on the interior surface of the pipe. It was also used to test the effect of the seam on the pipe performance. Seaming was conducted in accordance with ASTM D-2657.

5.3.3 Pipe End Conditions

Careful consideration was given to the boundary condition at the ends of the pipe specimen. If plane strain conditions prevailed in the axial direction for both the soil and the pipe, axial strains corresponding to the axial elongation of the pipe would be zero. Such conditions are normally assumed to occur under deep burial, when conditions of long and prismatic geometry exist along the pipe axis. However, some situations may arise where the pipe can experience axial elongation, for example at an expansion joint or where the pipe enters a manhole. In this case, axial extension of the pipe will lead to tensile axial strains, and larger pipe deflections relative to axial plane strain conditions. Tensile axial strains may lead to tensile axial stresses in the pipe depending on the magnitude of the hoop strains that also occur. Since tensile stresses may be more critical for polyethylene pipes (related to long term potential for stress cracking), consideration of non-zero axial strains is important for the performance of the pipe.

Axial strains due to the axial elongation of the pipe can occur when subjected to overburden stresses if the pipe is not fully restrained in the axial direction, or if the soil surrounding the pipe is allowed to deflect in the axial direction relative to the pipe - thereby producing axial strains from the transfer of shear stresses between the soil and the pipe. In such cases these components of axial strain would be tensile. The stiff steel walls of the test

cell were used to limit the outward deflection of the soil, and hence the axial strains that are induced in the pipe from the relative movement of the soil and pipe.

Two alternatives were considered for the restraint imposed at the end of the pipe during testing. The first attempted to provide axial restraint for the pipe. This involved the development of an adjustable end plate, located on either end of the pipe, that could be tightened up against the pipe before testing. The axial strains of the pipe were monitored during this process to impose small compressive axial strains (approximately -0.005%). While this method did limit the axial elongation of the pipe, very small axial deformations still led to tensile axial strains. For example, axial elongation of the pipe of 0.1 mm at each end produces tensile axial strains of 0.01%. Also, despite the fact that measures were taken to limit the friction between the ends of the pipe and the steel plate, some end effects were noticed when measurements of pipe deflection were compared at various locations along the pipe (these tests are not reported here).

The second option was to provide no axial restraint for the pipe. This was achieved by providing a gap (approximately 10 mm wide) on both ends of the pipe (see Fig. 5.2). Measures were taken to ensure that the backfill soil materials were not permitted to fill the space between the ends of the pipe and the lateral boundaries. As confirmed by observations during testing, this arrangement successfully prevented the pipe from jamming up against the sidewalls.

The hoop response of the pipe should not be substantially affected, regardless of the axial conditions imposed for the pipe. This assertion was verified based on numerical modelling of a buried pipe subject to radial loads with varying deflection at the ends of the pipe specimen. Results from preliminary tests, conducted with the pipe restrained and

unrestrained at its ends, also support the fact that the hoop response of the pipe was not sensitive to the end conditions for the pipe. Therefore tests with no end restraint provided to the pipe are reported here.

5.3.4 Instrumentation

5.3.4.1 Pipe Strains

Strains were measured at many locations on the interior and exterior surfaces of the pipe as shown in Figure 5.5. Measurements were made using electrical foil strain gauges (2 mm gauge length) in stacked biaxial arrangements. A central section C was instrumented with eight gauges each on the interior and exterior surfaces, located at the: springlines ($\theta = 0$ and 180°), shoulders ($\theta = 45$ and 135°), crown ($\theta = 90^\circ$), haunches ($\theta = 225$ and 315°) and invert ($\theta = 270^\circ$). The notation used to identify these measurements, for example, has the strain measured at Section C on the exterior pipe surface and located at the crown represented by the abbreviation CE90.

Sections B and D, each located 75 mm from the centre of the pipe, had strain gauges on the interior and exterior locations of the pipe at the crown, invert and springline ($\theta = 180^\circ$). The other sections shown in Figure 5.5 were selected to measure the variation of strain along the pipe as one means of assessing the influence of the test cell boundaries on the pipe response.

Strains were monitored and recorded using a data acquisition system. The error associated with the strain measurements (gauge sensitivity, lead wire effects and data recording) was estimated to be ± 50 microstrain (Tognon 1999).

5.3.4.2 Pipe Deflections

Measurements of vertical and horizontal diameter change were made using potentiometers at three locations along the pipe (corresponding to Sections B, C and D). The tolerance associated with the deflection readings was ± 0.01 mm. The spacing of the deflection measurements at Sections B, C and D are relatively close (75 mm spacing along the pipe axis). Measurements of pipe deformation made at Sections B, C and D for a particular test are not independent quantities - but are likely to be interrelated with one another because of the scale of the problem. This arrangement was selected to be consistent with the next series of tests conducted to measure the deformations at sections containing perforations (see Chapter 6).

5.3.4.3 Earth Pressure Cells

Earth pressure cells with vibrating wire pressure transducers were used to obtain estimates of the stresses acting on the boundaries of the soil. The location of the earth pressure cells for test P2a are shown in Figures 5.1b and 5.2. Three pressure cells (P1, P2 and P3) were located across the top surface to measure the vertical pressures just below the bladder. Pressure cells P5 and P6 were placed against the base. Measurements of lateral stress were made by cells P7 and P8 located against the west wall, and P9 and P10 located against the east wall. One additional earth pressure cell (P11) was placed on the north wall to measure the axial stresses at the boundary. Lubricated polyethylene sheets (an arrangement similar to that described in reference to Fig. 5.4) were placed behind the pressures cells that rested against the lateral boundaries to reduce effects from interface friction. A similar arrangement

of earth pressure cells was used for test P2b, however with no measurements in the coarse gravel layer (see Fig. 5.3).

5.3.4.4 Settlement Plates

The vertical displacement of the sand was measured using settlement plates at seven locations during test P2a. Each settlement plate was comprised of a 100 mm square steel plate (6 mm thick) connected to a 6 mm diameter stainless steel shaft. The shaft extended through the base of the test cell where the vertical movement was measured with a displacement transducer. The rubber bladder across the top surface precluded the settlement plates from extended through to the top of the cell. The shafts were protected from the sand backfill with a stainless steel casing (9 mm outside diameter, 2 mm thick). Grease was used to limit the friction between the shaft and the casing. A special sleeve was attached to the underside of the plate to permit the vertical movement of the plate without jamming up against the casing. This stainless steel sleeve (outside diameter of 16 mm, 3 mm thick) was sharpened to a point at the end to reduce effects of bearing into the sand.

The seven casings were installed prior to placement of the sand backfill. Care was taken during sand placement and compaction so that each casing remained vertical. The top of the lubricated casings were capped to prevent sand getting into the casing. The sand was filled and compacted to an elevation just above the final location of the settlement plate. Then, the shaft was carefully exposed by hand, with a gap for the sleeve made around the shaft. Next, the cap was removed and some additional grease was pumped down the casing. The settlement plate was installed and then covered with sand.

5.4 RESULTS FOR TEST P2a

5.4.1 Measured Surface Strains for Test P2a

Results of measured surface strains of the pipe are presented to study the structural response of the pipe when tested in the new laboratory facility. The strains measured on the interior surface of the pipe during test P2a are plotted versus the applied bladder in Figure 5.6. Circumferential (or hoop) strains ϵ_θ (Fig. 5.6a) and axial strains ϵ_z (Fig. 5.6b) are plotted for the eight locations around the pipe circumference at Section C.

Strains are plotted in the dimensionless units of microstrain ($\mu\epsilon$), where 1000 $\mu\epsilon$ equals 0.1% strain. Compressive strains are shown as negative values; tensile strains are plotted as positive values. The reported values of strain versus applied bladder pressure represent the strain averaged over the last 30 seconds of each 40 minute load increment. Each load step involved the rapid application of an incremental bladder pressure of 50 kPa, which was then held constant for the duration of the load step.

5.4.1.1 Hoop Strains at Section C

Figure 5.6a shows that compressive hoop strains (negative values) occur at the springlines ($\theta = 0$ and 180°) when the pipe is subject to the biaxial earth loading. The average hoop strain measured at the springlines is $-5800 \mu\epsilon$ at an applied vertical surcharge of 600 kPa. The two values recorded at the interior springlines are practically identical (only 2% difference between CI0 and CI180 at 600 kPa), reflecting the close to symmetric response (about the vertical axis of the pipe) expected with uniform vertical and horizontal loading acting on the soil boundaries and good soil support provided to the pipe by the sand backfill.

Tensile hoop strains occur at the crown and invert ($\theta = 90$ and 270°) on the interior surface of the pipe, Figure 5.6a. Larger tensile strains occur at the invert ($2000 \mu\epsilon$) than at the crown ($1400 \mu\epsilon$) at 600 kPa surcharge, resulting from larger circumferential bending at the invert.

Strains at the quarter points (shoulders $\theta = 45$ and 135° , and haunches $\theta = 225$ and 315°) are compressive and smaller in magnitude than those measured at the springline. The magnitude of these strains is of interest, since it is at these locations that perforations (holes to permit collection of fluid) are typically located. These measurements do not show the symmetry observed at the springlines. These differences may arise from local variations in density of the sand material, especially at the haunch location where it is difficult to compact the soil where a 40% difference was measured between CI225 and CI315 at 600 kPa.

Strains measured on the exterior surface (not presented here) of the pipe at these locations show the effect of circumferential bending, since the strains at the crown and invert are compressive and the strains at the springlines are tensile. Of all the measurements made, the maximum compressive strains occurred at the interior springline and the maximum tensile strains occurred at the interior invert.

5.4.1.2 Axial Strains at Section C

The measured axial strains at Section C are plotted in Figure 5.6b. These axial strains are all tensile. Five readings agree quite well (CI0, CI45, CI90, CI135 and CI225) with an average value of $570 \mu\epsilon$ and a 6% coefficient of variation (mean divided by standard deviation). Readings at CI270, CI315 and CI180 are larger than those measured at the other locations. Including all of the readings, the mean is $650 \mu\epsilon$, with a coefficient of variation

of 20%. Overall these values are small, corresponding to less than one millimetre of axial elongation at each end of the pipe.

5.4.1.3 Variation of Strains Along Pipe

The strain gauges shown in Figure 5.5 were located to assess the variation in strains along the pipe. This allows an assessment of the effect of the test cell boundary conditions on the pipe. Figure 5.7 plots the hoop strains measured at the interior crown location ($\theta = 90^\circ$) at various positions along the pipe. Excellent agreement was found for the three readings near the centre of the pipe (Sections B, C and D) with a mean of $1350 \mu\epsilon$, and a coefficient of variation of less than 1%, at an applied vertical pressure of 600 kPa.

There is some reduction in hoop strains closer to the ends of the pipe, as the measured values of hoop strain at Sections A and E are 80% of the values recorded near the middle of the pipe. Axial strains measured at these locations were tensile and larger towards the ends of the pipe. The increase in axial strains and decrease in hoop strains near the ends of the pipe are a result of the end conditions for the pipe and not the test cell. Hoop stresses (computed from both hoop and axial strains) showed little difference between points C and E, as the hoop stress at Section C is only 3% larger than that at E (using Poisson's ratio of 0.46 for the polyethylene pipe). Axial stresses were almost 15% larger near the end of the pipe than at the centre. These calculations show that the hoop stress at the interior crown is similar along the length of the pipe and largely independent of the axial end conditions of the pipe. No substantial effects from boundary friction or axial end conditions are discernable from these calculated values of stress, especially towards the centre of the cell where the main instrumented sections are located.

The hoop strains measured at the interior springline ($\theta = 180^\circ$) along the pipe are shown in Figure 5.8. Again, excellent agreement between values measured near the centre was found. At a vertical pressure of 600 kPa, a mean of $-6000 \mu\epsilon$ and a coefficient of variation of less than 0.5% was calculated from locations B, G, C and D. The strains measured towards the end of the pipe are slightly larger than those near the centre. However this difference is not large, as the mean of all the readings is $-6200 \mu\epsilon$ with a coefficient of variation of only 5%. Axial strains are tensile and are larger towards the ends of the pipe than at the centre. As found for the interior crown, this results in essentially uniform hoop stresses along the pipe and greater axial stresses near the ends of the pipe.

The strain measured at Section I is larger than at other locations, Figure 5.8. This trend was also observed at the interior crown location (Fig. 5.7), which suggests that the sand may have been placed at a lower density near location I, resulting in slightly larger strains.

Similar observations of relatively uniform strain along the pipe were made for measurements on the pipe exterior. Overall, the strain response does not greatly vary along the pipe suggesting only small effects from the boundary conditions imposed in the new laboratory facility. Very good agreement was obtained between results near the centre indicating that differences observed in subsequent tests with coarse gravel or perforations are due to the coarse gravel or perforations and not the test cell.

5.4.2 Pipe Deflections for Test P2a

Vertical (ΔD_v) and horizontal (ΔD_h) diameter changes of the pipe measured during test P2a are plotted in Figure 5.9 (hollow symbols) versus the applied bladder pressure. Figure 5.9

shows a decrease in vertical diameter and an increase in horizontal diameter of the pipe when subject to the biaxial earth pressures.

At an applied vertical pressure of 600 kPa the measured vertical diameter change was -3.0 mm at Sections B and D (in this case an instrumentation problem occurred at Section C). Excellent agreement was also observed for the horizontal diameter change as increases in diameter of 1.8 mm were recorded at Sections B and C. The uniform response near the centre of the pipe is similar to the results observed for the measured strains. This is also consistent with the premise that, when uniformly compacted, sand essentially provides continuous backfill support to the pipe. The latter observation provides a useful benchmark for comparison of pipe response when surrounded by materials that may provide discontinuous support for the pipe (e.g., coarse gravel shown in Fig. 5.3 and used in Test P2b to be discussed in Section 5.6).

5.5 ASSESSMENT OF BOUNDARY CONDITIONS

Although the free end pipe boundary condition did locally influence the strains near the ends of the pipe (but not the hoop stresses), an evaluation of the available data indicates no significant effect of the test cell boundary conditions on the central portion of the pipe response. Thus it appears that the new facility is performing in accordance with the design expectation. Results from additional instrumentation placed to assess the boundary conditions, as well as visual observations made following the tests are now considered to

further demonstrate the effectiveness of the new facility in closely simulating pipe response under biaxial earth pressures.

5.5.1 Soil Deformations

The vertical displacements of the sand measured with the settlement plates are plotted in Figure 5.10. Measurements at S1, S2, and S3 (all 345 mm from the base) showed very similar results. The average of these measurements was 4.1 mm at an applied vertical pressure of 600 kPa. The coefficient of variation was less than 1% for these readings. No effect from the boundaries is evident from these measurements even though they correspond to very different locations with respect to the soil boundaries (see Fig 5.1b).

Settlement plates at S4, S5, S6 and S7 were all located at the same elevation as the invert of the pipe. The average of these four readings was 7.9 mm at 600 kPa vertical surcharge. The coefficient of variation of 9% is larger than that calculated from the measurements at the lower elevation. Soil deformations near the north wall (S6 and S7) are larger than those measured at S4 and S5. This difference may be a result of the soil being less dense around these settlement plates, as it may have been more difficult to compact the sand around locations P6 and P7 given the close proximity to the north wall. These results do not show any detrimental effect arising from the lateral boundary. If substantial shear stresses were mobilized along vertical walls, the settlement at S4 would be expected to be less than the value at S5, and S6 would be less than both S5 and S7; however this is clearly not the case. The similarity of these values confirms that the relatively low friction angles measured from direct shear tests were mobilized during the tests and that the walls are sufficiently smooth.

Measurements of soil deformation provide a method of inferring the modulus of the sand. Simple estimates of soil modulus between 45 to 50 MPa were made from calculations using isotropic Hooke's Law for the limiting cases of plane strain and plane stress in both orthogonal directions.

The deformations of the top boundary (ie. just below the bladder) were observed after each test and showed essentially uniform deflection of the soil surface. Some small local variations, likely arising from small variations in the sand density, were noticed. Overall, these observations provided visual evidence that the bladder applies a relatively uniform pressure across the top surface, and that the methods of boundary friction appear to be reducing the mobilization of shear stresses to acceptable levels.

5.5.2 Boundary Stress Measurements

Difficulties with measurements of earth pressures arise since the earth pressure cells (hollow steel discs filled with fluid) typically have a different stiffness to that of the surrounding soil. Additional problems arise with the placement of backfill soils around the earth pressure cells at the same density as the soil away from the instrument. Dunnicliff (1988) comments that it is usually impossible to measure the total stresses in the soil with great accuracy.

Many earth pressure cells were placed around the cell in an attempt to infer the stresses acting at the boundaries of the test facility. Typical results are given in Figure 5.11 for the backfill conditions used in tests P2b and P4 (those shown in Figure 3.3). Variations of earth pressures in the order of 20% were found. Also some nonsensical measurements were obtained. Earth pressure cells were therefore not relied upon to provide precise

measurements, but rather were useful in making more qualitative observations regarding the boundary stresses.

The earth pressure cells placed near the top surface of the soil (P1, P2 and P3) showed that the vertical stress measured at these locations was essentially the same and equal to the pressure applied by the bladder. These measurements affirm that the simulation of a uniform vertical overburden pressure is successfully attained with the flexible air bladder.

The measurements of lateral earth pressure along the side walls of the facility indicated that the pressures acting on the vertical boundaries parallel to the axis of the pipe were similar and were near to horizontal stresses expected if conditions of zero lateral strain prevailed. A coefficient of lateral earth pressure of 0.3 was found for the sand backfill.

Measurements of vertical stress at the base of the cell were made with attempts to estimate the proportion of vertical stress reaching the base as another method of assessing the boundary friction acting on the side walls. Vertical stresses measured at P5 and P6 were generally less than those located close to the surface, but were consistent with reductions expected because of boundary friction of 5° (as measured from the direct shear tests on the interface treatment).

5.5.3 Test Cell Deflections

Outward deflections of the lateral boundaries of the test cell will reduce the lateral stresses that develop in the ground. These deflections were monitored on all four sides of the test cell during each test to assess the magnitude of these boundary movements. Dial gauges (0.002 mm and 0.01 mm resolution), mounted to stiff columns independent of the test cell, were used to record the test cell deflections. Measurements were made at the centre of the beams

and at the plates at mid-span between the beams. The location of these measurement are shown in Figures 5.1 and 5.2.

The deformation of the steel boundaries is comprised of four components. The first is local plate deformation that occurs between the steel frame supports. Thick (40 mm) steel plates were used to limit this deformation. The second component arises from the bending of the side wall unit (composite plate and frame). The third component occurs because of the axial elongation of the adjacent walls joining it with the opposite side (ie. elongation of north and south walls from pressures acting on the east and west walls, and vice-versa). The fourth component are deflections that result from small distortions of the box-like structure in the horizontal plane.

The deflections measured during test P2a are plotted in Figure 5.12. Boundary deflections were measured at a few more locations during test P3c. These results are shown in Figure 5.13. It is apparent that structure does not deflect in an symmetric manner about the centre of the test cell as opposite walls do not deflect the same amount. Deflections of the west wall are larger compared to the east wall, for the boundary parallel to the axis of the pipe; the deflections of the south wall are larger than the north wall, for the boundaries perpendicular to the pipe axis. This was a consistent observation for the other tests conducted.

For test P2a, the deflection of the east wall measured at the plate in between the second and third rings from the top (EPL2-3) was 0.24 mm, while the deflection on the opposite wall at this location was 1.18 mm (WPL2-3), both at an applied bladder pressure of 600 kPa (Figs. 5.12a and 5.12b, respectively). Despite this difference in boundary deflections the response of the pipe was nearly the same at the east and west springlines

(refer back to Fig. 5.6a). Measurements of earth pressures at locations P7 and P9 (made near the measurement of test cell deflections) were similar which implies that the ground pressures are similar along these boundaries. Despite the large difference in test cell deflections, the evidence that the pressures are nearly equal along these walls suggests that the soil is not greatly affected by the different boundary movements.

The average of EPL2-3 and WPL2-3 yield a value of 0.7 mm at 600 kPa vertical surcharge (denoted as EWPL2-3 in Figure 5.12c). This is quite similar to the average boundary deformation found at this location during test P3c, Figure 5.13c. At 900 kPa the average outward displacement of the plates is roughly 1 mm.

Deflections measured at the north wall are very small (roughly 0.1 mm at NPL2-3). In fact during test P3c, the north wall actually deflected inward (ie. towards the centre of the test cell) accompanied with the larger deflections measured at the south face. The average of the north and south boundary deformations are less than 0.8 mm at 900 kPa. Similar results were obtained for the other tests that were conducted.

Measurements of strain in the steel frames (not reported here) indicate relatively uniform response around the perimeter of the test cell. This suggests that the difference in deflections between the east and west walls, and the north and south walls arises from a very small distortion of the test cell in a horizontal plane.

The measured deflections were slightly larger than anticipated compared with design calculations as full composite action between the beams and plates was not likely mobilized (especially for the axial elongation of the wall which comprises the majority of the deflection and may lead to distortion of the structure). It was shown in Chapter 4 that boundary deformations of 1 mm at 900 kPa do induce stresses that deviate from the boundary stresses

as idealized in Figure 5.1a. However, the new facility was designed to ensure that these differences are small. Reexamining the analysis of Brachman et al. (1999) [Chapter 4], it was estimated that lateral stresses are reduced by roughly 10% as a result of these boundary deformations. Lateral pressures smaller than those for zero lateral strain conditions would result in larger pipe deflections. It was estimated that the vertical diameter decrease would be 10% larger in the test cell relative to that expected for perfectly rigid walls. Horizontal diameter changes would be impacted to a greater degree (1.3 times larger) since their absolute value is smaller than the vertical diameter change. The larger deformations lead to greater bending stresses in the pipe. The pipe response in the new laboratory model is therefore more severe than the behaviour than expected under deep and extensive overburden pressures (ie. the measured pipe deflections and stresses are larger than would be expected under conditions of zero lateral strains).

5.6 RESULTS FOR TEST P2b

Strains and deflections recorded during test P2b (corresponding to the simulated landfill conditions shown in Fig. 5.3) are now examined and compared to those obtained from test P2a (with sand backfill) to study the difference in pipe response between the these two backfill conditions. The two different backfill materials directly around the pipe represent different loading conditions for the pipe. The support provided by the sand backfill will tend to be more uniform (the small sand particles provide almost continuous support around the pipe circumference), whereas the coarse (40 - 50 mm) gravel will provide nonuniform

support (discontinuous support from fewer contact points that are randomly distributed around the circumference).

5.6.1 Measured Surface Strains for Test P2b

The strain versus pressure response is substantially different when tested in the coarse gravel backfill compared to the sand results. The strains tend to fluctuate during the test (Fig. 5.14a), compared to the essentially steady increases in strain found from the sand backfill tests (Fig. 5.6). These fluctuations are attributed to the rearrangement of the coarse gravel particles. Sounds of stones moving were audible during the testing. Some particle breakage of the crushed stone was also evident when the materials were excavated after the test.

5.6.1.1 Hoop Strains at Section C - P2b

The hoop strains measured at Section C around the interior of the pipe are plotted in Figure 5.14a. The hoop strains measured at the springlines ($\theta = 0$ and 180°) are quite different. The hoop strain measured at CI0 of $-11900 \mu\epsilon$ is much smaller than $-16300 \mu\epsilon$ recorded at CI180, both at a vertical pressure of 900 kPa. This differs from the response observed when tested with sand backfill, where these two measurement were nearly identical, Figure 5.6a. The 37% difference between the readings at the springlines for test P2b appears to be a direct result of the coarse gravel backfill.

Also, there is a greater difference between the hoop strains at the shoulders and the haunches compared with the sand results of Figure 5.6a. The strains at the shoulders ($\theta = 45$ and 135°) are nearly zero, while the hoop strains at the haunches ($\theta = 225$ and 315°) are larger compressive values.

The strains measured with the coarse gravel backfill are likely to be highly variable. Consequently, four additional tests were conducted on two different pipe samples to better quantify the effects from the coarse gravel backfill. This work is the subject of Chapter 6. The observations made from the limited number of measurements from test P2a are consistent with the additional tests that were conducted.

5.6.1.2 Axial Strains at Section C - P2b

Figure 5.14b plots the axial strains measured at Section C. These axial strains arise from the axial elongation of the pipe and local bending effects induced from the discontinuous nature of the backfill support provided by the coarse gravel backfill. Larger magnitudes and greater variations in axial strains occur because of the coarse gravel backfill, relative to the axial strain recorded with sand backfill (Fig. 5.6b). The largest axial strain was recorded at CI225 with a magnitude of nearly $5400 \mu\epsilon$, at 900 kPa. The strains at the other locations vary from $3000 \mu\epsilon$ (CI315) to $600 \mu\epsilon$ (CI90), a 400% difference at an applied vertical pressure of 900 kPa.

5.6.1.3 Comparison of Measured Strains Between Tests P2a and P2b

Figure 5.15 plots the hoop strains for tests P2a and P2b measured at Section C for both the interior (Fig. 5.15a) and the exterior (Fig. 5.15b) surfaces of the pipe at an applied bladder pressure of 600 kPa (limit of test P2a). Also shown are the maximum and minimum values recorded at the five central sections of test P2b (B, G, C, H and D) to provide a measure of the influence of the coarse gravel on the strains within the pipe.

These polar plots illustrate the variation of hoop strain around the pipe, with again, compression negative. On the interior surface (Fig. 5.15a), strains are compressive except at the crown and invert where tensile strains were measured. Strains on the exterior surface are predominantly compressive, except for tensile strains that occurred at the springlines. For both the interior and exterior surfaces of the pipe, strains measured at the quarter points (shoulders $\theta = 45$ and 135° , and haunches $\theta = 225$ and 315°) are in between the values measured at the crown, springlines and invert locations, and are generally small compressive or sometimes small tensile strains (e.g., exterior at $\theta = 315^\circ$ for test P2b).

The hoop strains at the crown, springline and invert locations of the pipe are larger when tested with coarse gravel backfill compared to the sand backfill. This is because of the lower lateral confinement provided by the gravel in a state of biaxial compressive pressures, as it has a lower coefficient of lateral earth pressure K compared with the sand. This leads to greater circumferential bending, and hence larger hoop stresses at the locations where bending stresses are the greatest. Also, the variations are much larger when tested in the coarse gravel material than in sand, particularly at the interior invert location where a 160% difference occurred between the maximum and minimum values. These large variations in strain are a result of local bending effects caused by the coarse gravel backfill.

5.6.2 Pipe Deflections for Test P2b

Diameter changes measured during test P2b are plotted in Figure 5.9 (solid symbols). The magnitudes of the vertical and horizontal diameter change are larger for test P2b than for P2a. The vertical diameter change ranged from -4.2 to -6.2 mm for test P2b (compared with

-3 mm for test P2a), at 600 kPa. Horizontal diameter changes are roughly twice as large for test P2b than for P2a.

Pipe deflections can be interpreted as the sum of two components (Moore 1993): one represented by the average of the diameter changes,

$$2w_o = \frac{1}{2} (\Delta D_v + \Delta D_h) \quad (5.1)$$

and the other, by one-half of the difference between the diameter changes,

$$2w_2 = \frac{1}{2} (\Delta D_h - \Delta D_v). \quad (5.2)$$

In such a case, the parameters w_o and w_2 take on a physical representation of radial deflections when subject to mean and deviatoric components of distant boundary stresses, Figure 5.16a. The mean component of deflection (w_o) corresponds to the axisymmetric, radially inward deflection of the pipe when the soil is subject to a radially compressive distant boundary stress field σ_m , which is the mean of the distant boundary stresses (ie. $\sigma_m = \frac{1}{2} [\sigma_v + \sigma_h]$, Figure 5.16a). The deviator component of deflection (w_2) arises from one-half of the difference in the distant boundary stresses (ie. $\sigma_d = \frac{1}{2} [\sigma_v - \sigma_h]$) and varies in the circumferential direction around the pipe as a function of $\cos 2\theta$, Figure 5.16a.

The mean and deviator components of pipe deflections recorded for test P2a and several tests conducted with the simulated landfill conditions (P2b and P3c) are plotted in Figure 5.16b. The mean diameter change ($2w_o$) for the sand test (hollow circles) tends to lie within the scatter of measured values from the tests with coarse gravel backfill (solid symbols). This observation is also valid at 250 kPa where there are a larger number of measurements from two additional tests conducted for the simulated landfill conditions. On average, the mean component of deflection is slightly smaller for the coarse gravel results than for the sand results. This suggests that the stiffness of the coarse gravel for radially

compressive stress conditions (ie. hoop compression) is slightly stiffer than that of the sand. This statement is supported by the results obtained from the tests conducted under hoop compression loading (Chapter 3) where the response of the pipe was slightly stiffer when tested with gravel relative to sand.

The deviatoric diameter change ($2w_2$) for the simulated landfill tests also shows significant variations because of the coarse gravel. However, the sand test shows a deviatoric component smaller than those for the simulated landfill conditions. This difference is also apparent at 250 kPa where additional test results are available. It appears that the coarse gravel backfill produces a similar mean response but different deviatoric response, compared with sand backfill. If the mean component is similar, but the deviatoric component is larger for coarse gravel backfill than that for sand backfill, this would result in larger changes in both vertical and horizontal diameters. This is consistent with the data plotted in Figure 5.9.

One major reason leading to the larger pipe deflections for the coarse gravel backfill is the difference in the response of the materials under biaxially compressive stresses. Such observations would be consistent with two materials having different lateral earth pressure coefficients K . It appears that K for the medium-dense sand is 0.3, while it is 0.2 for the coarse gravel. This is discussed further in Chapter 6. The large difference in response between the sand and gravel backfills highlights the necessity to study the performance of these leachate collection pipes under biaxially compressive earth pressures, since the difference in magnitude of the pipe deflections on average was not detected with the hoop compression tests of Chapter 3. The mechanical response of these landfill pipes when subjected to biaxial earth pressures is studied further in Chapter 6.

5.7 SUMMARY AND CONCLUSIONS

The performance of a new laboratory facility for testing small diameter (less than 300 mm diameter) buried pipes subject to the biaxially compressive earth pressures expected to prevail under deep and extensive overburden was examined. The new facility consists of a prism of soil 2.0 m wide \times 2.0 m long \times 1.6 m high contained within a stiff steel structure. Overburden pressures are simulated with a pressurised air bladder. Lateral earth pressures are developed by limiting the lateral soil strains.

Measurements of pipe and soil response, in addition to visual observations after testing, indicate that the boundary conditions imposed during testing in the new facility closely simulate those expected to prevail under deep and extensive burial. The bladder design adopted consists of a flexible rubber membrane with a mechanical seal around the perimeter, and was found to provide a uniformly distributed pressure across the top surface of the soil. Effects of boundary friction were limited to minimal levels by using lubricated polyethylene sheets that had adequate protection from damage caused by the backfill soil. The stiffness of the lateral boundary was sufficiently large to induce lateral stresses close to those for zero lateral strain conditions. Overall, the effects on the pipe arising from the idealizations involved in the laboratory model are small. The deviations from those expected to occur if plane strain conditions were realized in the field involve slightly larger pipe deflections (10% larger for the vertical diameter change and 30% larger for the horizontal diameter change) and consequently, somewhat larger bending stresses in the pipe.

No major effects on the pipe response were discernable from the boundary conditions for the particular conditions tested. Greater effects may occur for significantly larger

diameter pipes or much stiffer soil materials. In such cases monitoring of the pipe and structure and careful consideration of the measured results guided by finite element analysis, like that conducted by Brachman et al. (1999) [Chapter 4], are warranted.

The application of the new test cell was illustrated by using it to assess the response of a small diameter landfill leachate collection pipe under two different backfill conditions. This comparison showed that the mechanical response of the pipe is significantly impacted by the coarse gravel backfill used in landfill drainage layers. Maximum surface strains and pipe deflections were nearly twice as large when tested in the coarse gravel compared with the sand backfill. Much greater variations of strain and deflection were measured with the coarse gravel when compared with the sand backfill due to local bending effects from the coarse gravel. Further study of these variations and the practical implications for a perforated leachate collection pipe are presented in Chapter 6. Pipe deflections were larger when backfilled with coarse gravel and tested under biaxial earth pressures compared to tests with radially symmetric pressures. This demonstrated the importance of simulating the biaxial earth pressures that are expected to occur in the field.

5.8 REFERENCES

- Brachman, R.W.I., Moore, I.D., and Rowe, R.K. (1999) "The Design of a Laboratory Facility for Evaluating the Structural Performance of Small Diameter Buried Pipes". *Canadian Geotechnical Journal*, (Accepted 25/01/99).

- Dunnicliff, J. (1988) *Geotechnical Instrumentation for Monitoring Field Performance*, John Wiley & Sons, New York.
- Moore, I.D. (1993) "HDPE Pipe for Burial Under Landfill", Proceedings, Sardinia 93, 4th International Landfill Symposium, Cagliari, Italy, Oct. 1993, pp. 1473-1482.
- Rowe, R. K., Quigley, R.M., and Booker, J.R. (1995) *Clayey Barrier Systems for Waste Disposal Facilities*, E & FN Spon (Chapman & Hall), London.
- Rowe, R.K., Caers, C.J., and Chan, C. (1993) "Evaluation of a Compacted Till Liner Pad Constructed Over a Granular Subliner Contingency Layer". *Canadian Geotechnical Journal*, Vol. 37, No. 4, pp. 241-689.
- Tognon, A.R.M., Rowe, R.K., and Brachman, R.W.I. (1999) "Evaluation of Sidewall Friction for a Buried Pipe Testing Facility". *Geotextiles and Geomembranes*, 17 (4), (In Press).
- Tognon, A.R.M. (1999) Laboratory Testing of Barrier System Components. MEng. Thesis, The University of Western Ontario, London, Canada.

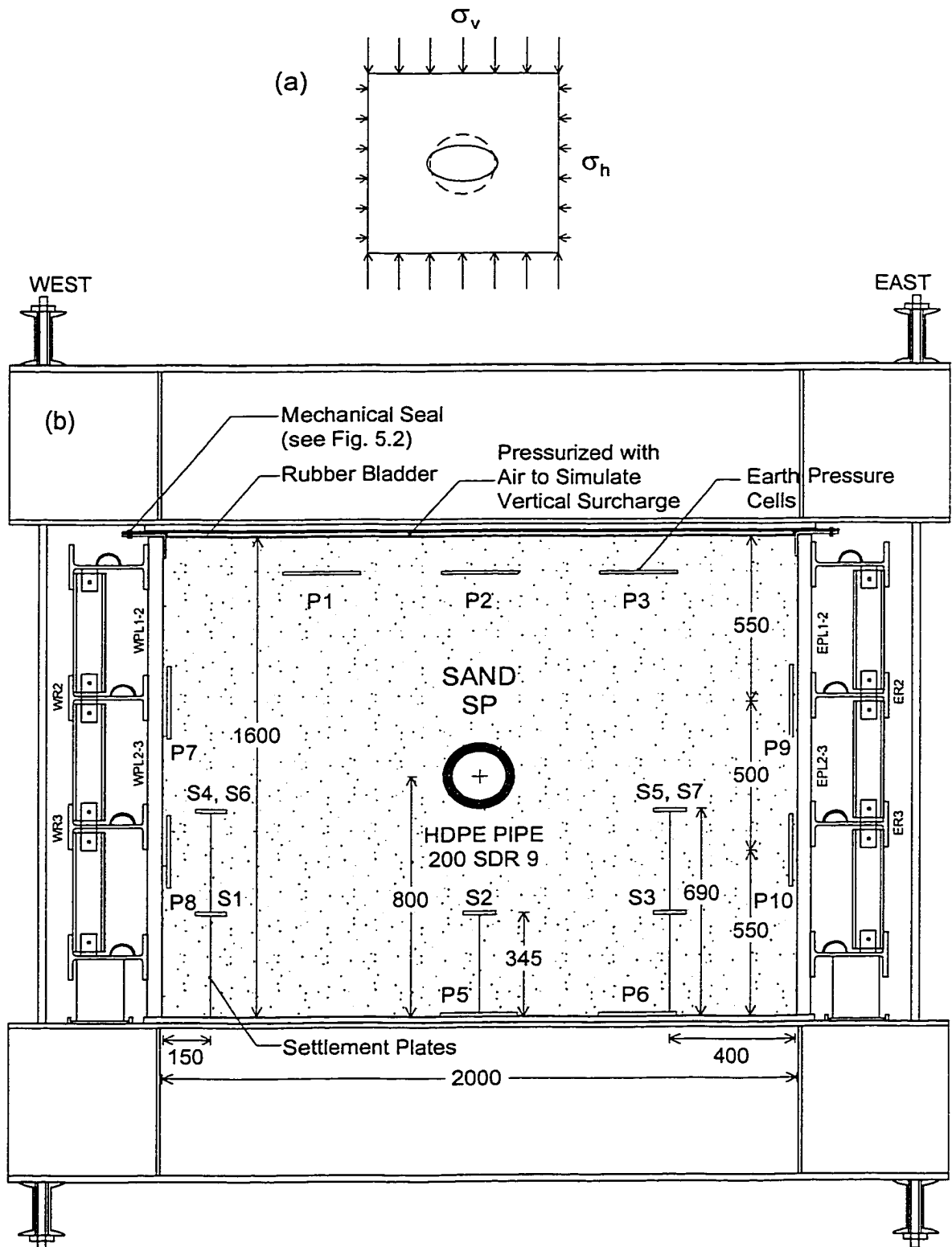


FIGURE 5.1 (a) Idealized earth pressures acting on a deeply buried pipe. (b) Transverse section through pipe test facility designed to closely simulate deep burial conditions. The soil, pipe and instrumentation used for test P2a are also shown. (Dimensions in mm).

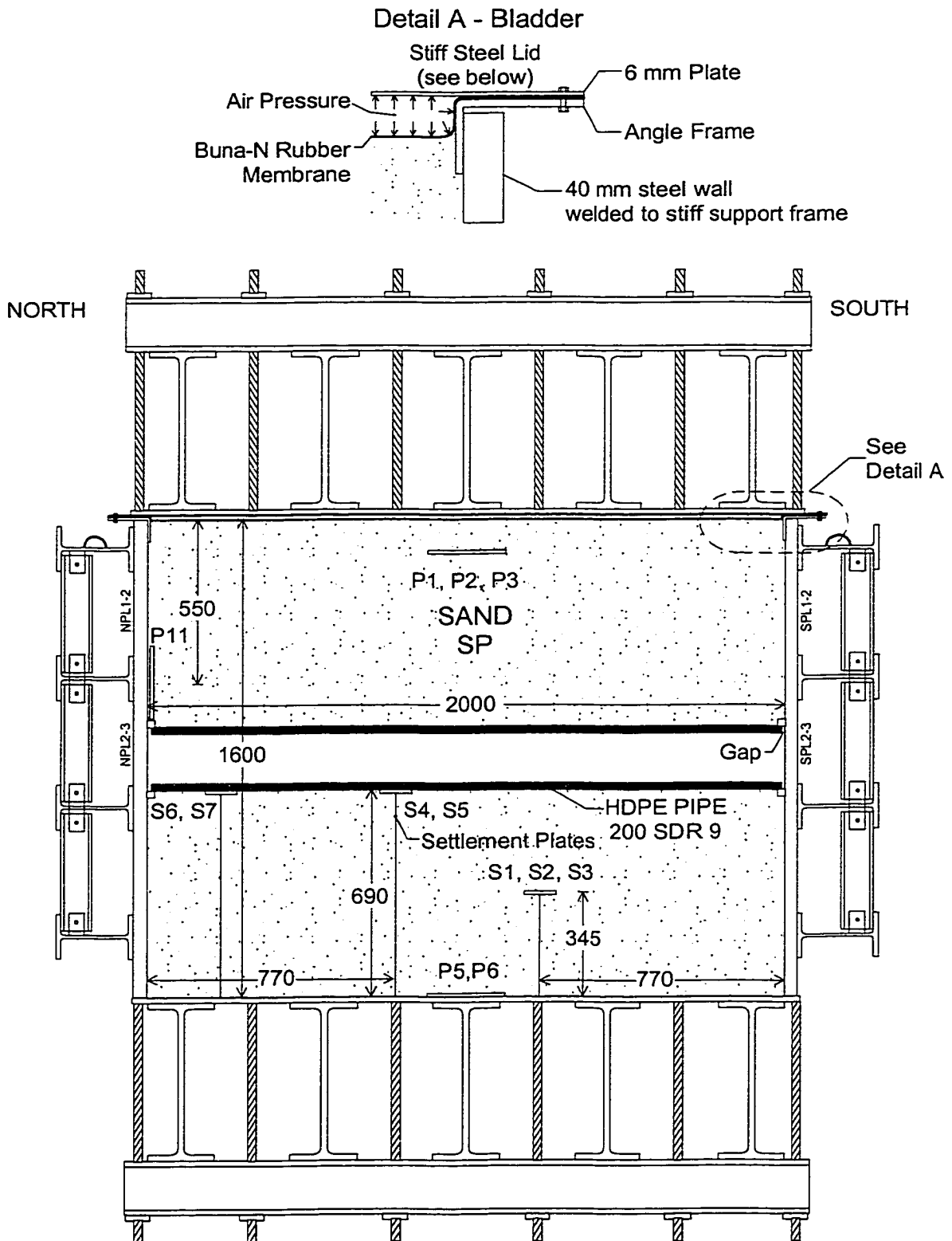


FIGURE 5.2 Longitudinal section through pipe test facility showing the soil, pipe and instrumentation used for test P2a. (Dimensions in mm).

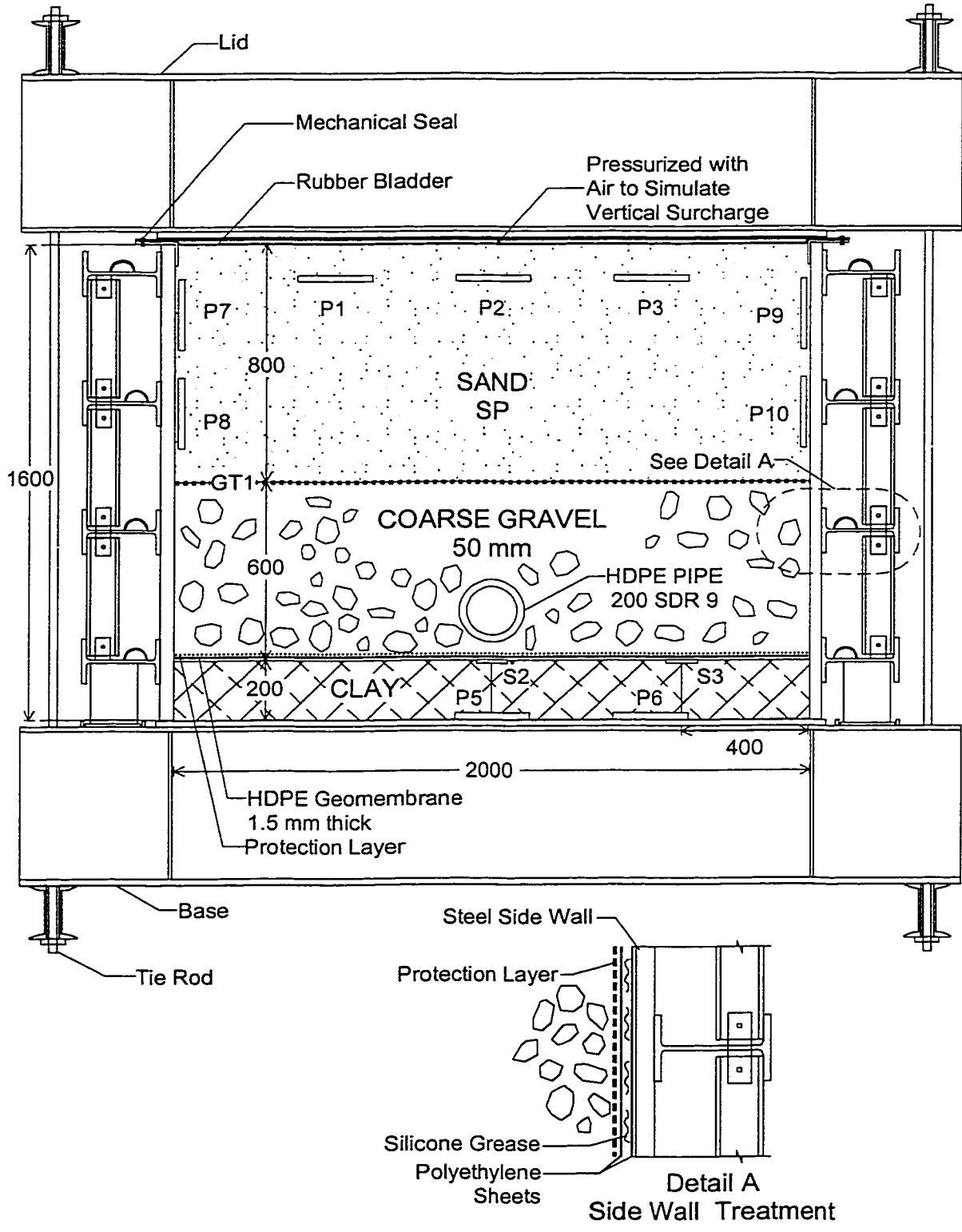


FIGURE 5.3 Transverse section through biaxial compression testing facility showing the soil materials, pipe and instrumentation for tests conducted with simulated landfill conditions. (Dimensions in mm).

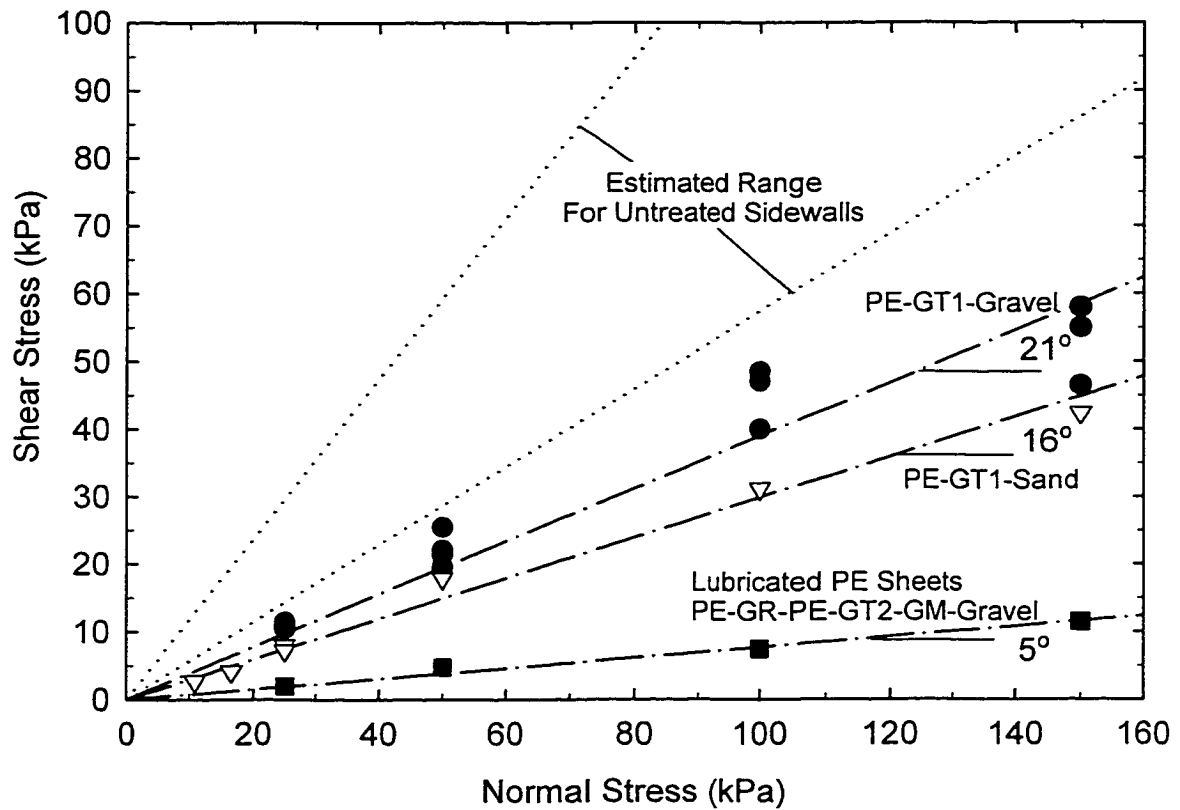


FIGURE 5.4 Angle of friction ϕ_{sw} mobilized for various treated and untreated interfaces. Data obtained from direct shear testing reported by Tognon et al. (1999). NOTE: PE - 0.1 mm thick polyethylene sheet, GT1 - nonwoven geotextile (435 g/m^2), GT2 - nonwoven geotextile (120 g/m^2), GR - silicon grease, GM - 2 mm thick geomembrane.

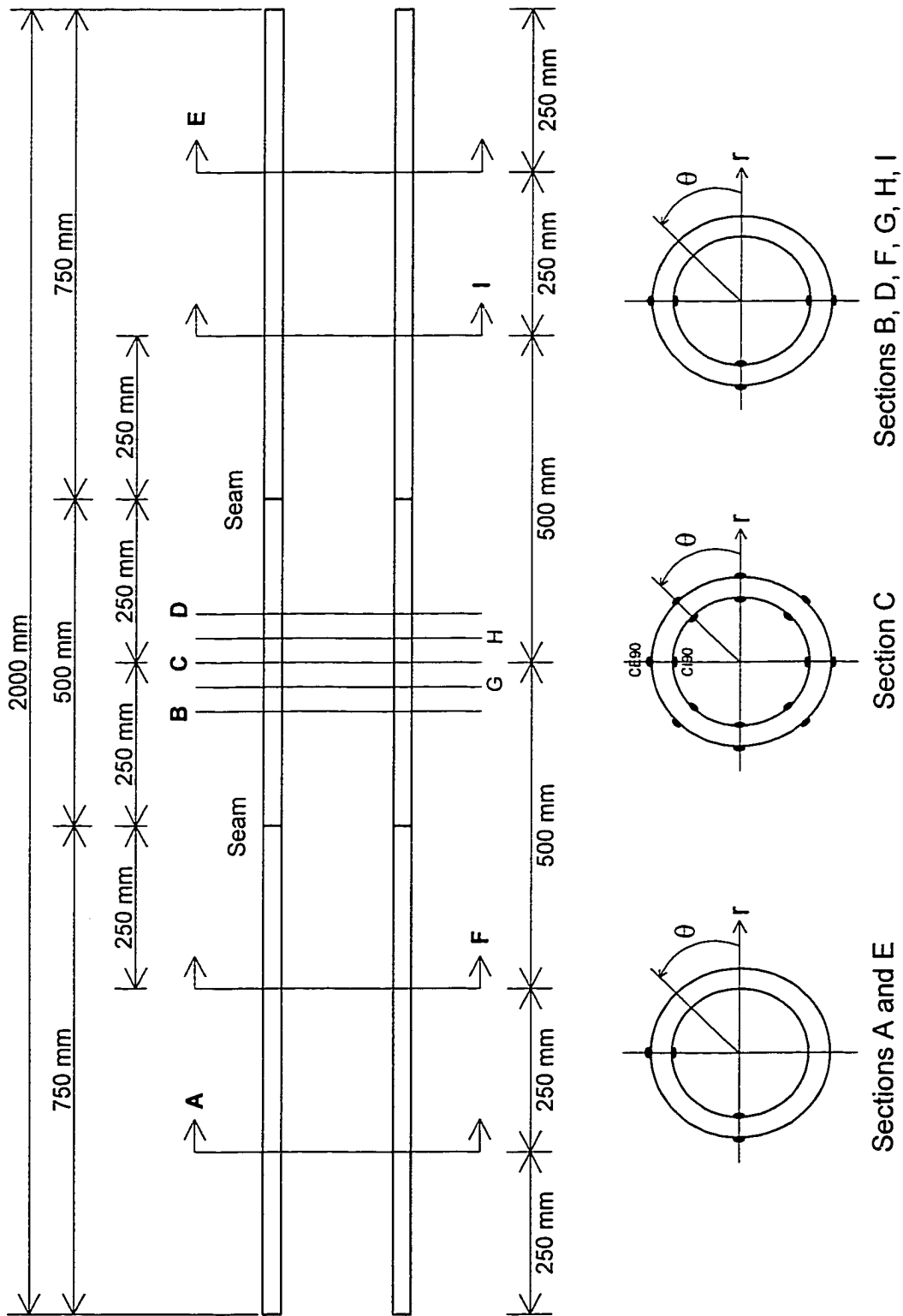


FIGURE 5.5 Location of strain gauges for pipe specimen P2. Pipe deflections recorded at Sections B, C and D.

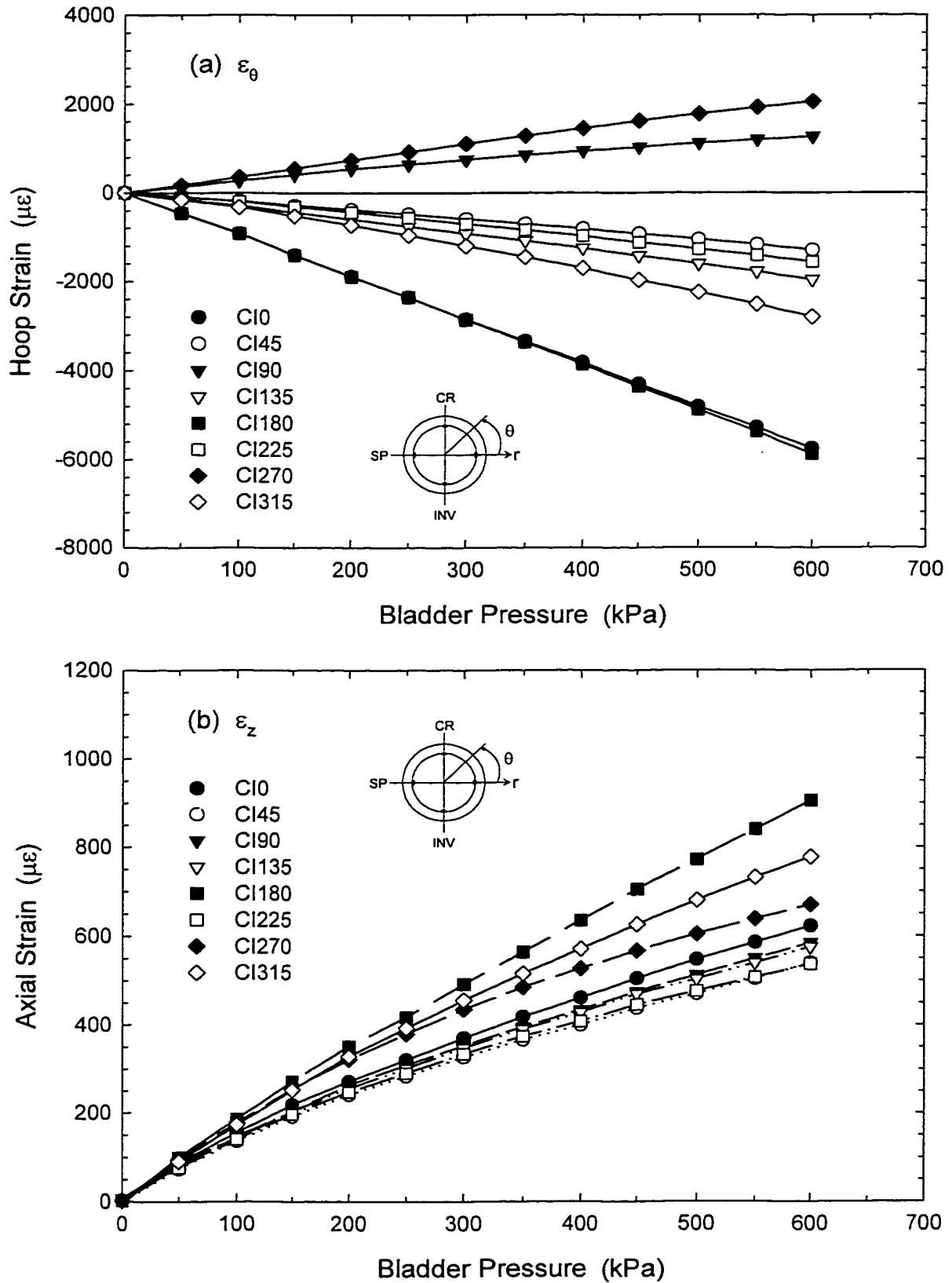


FIGURE 5.6 Measured (a) hoop ϵ_{θ} and (b) axial ϵ_z strains on the interior surface of the pipe at Section C during test P2a - sand backfill (compression negative).

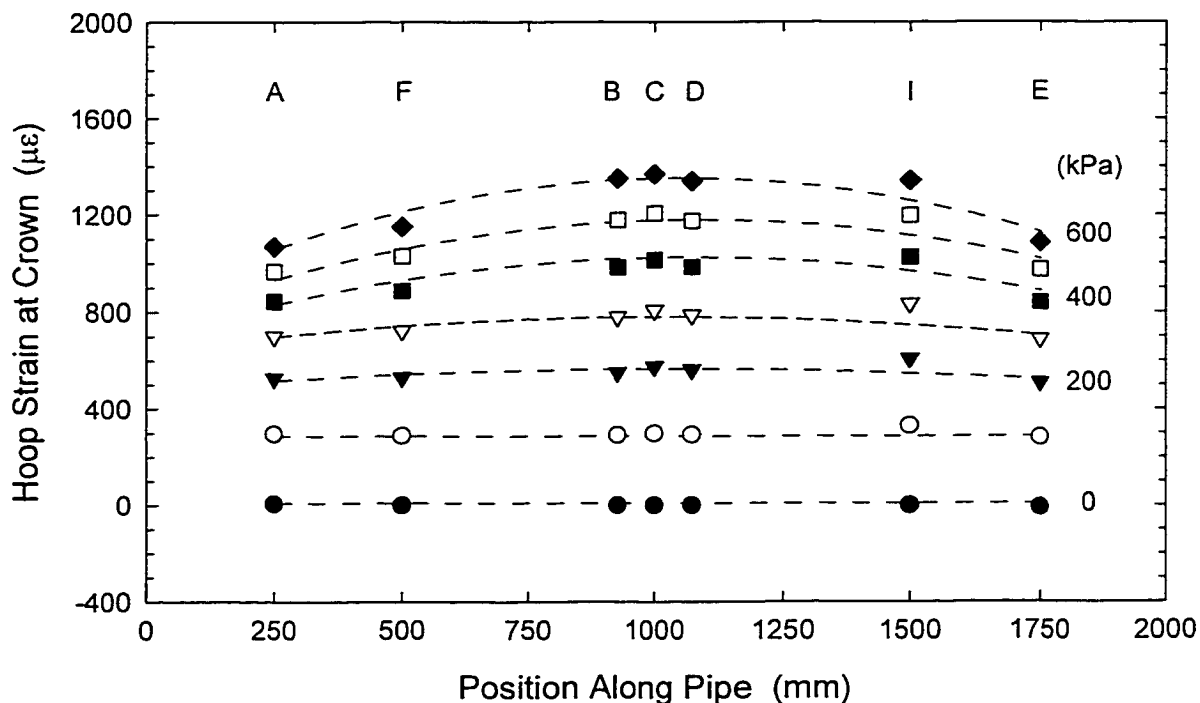


FIGURE 5.7 Variation of hoop strain measured at the interior crown location along the pipe during test P2a.

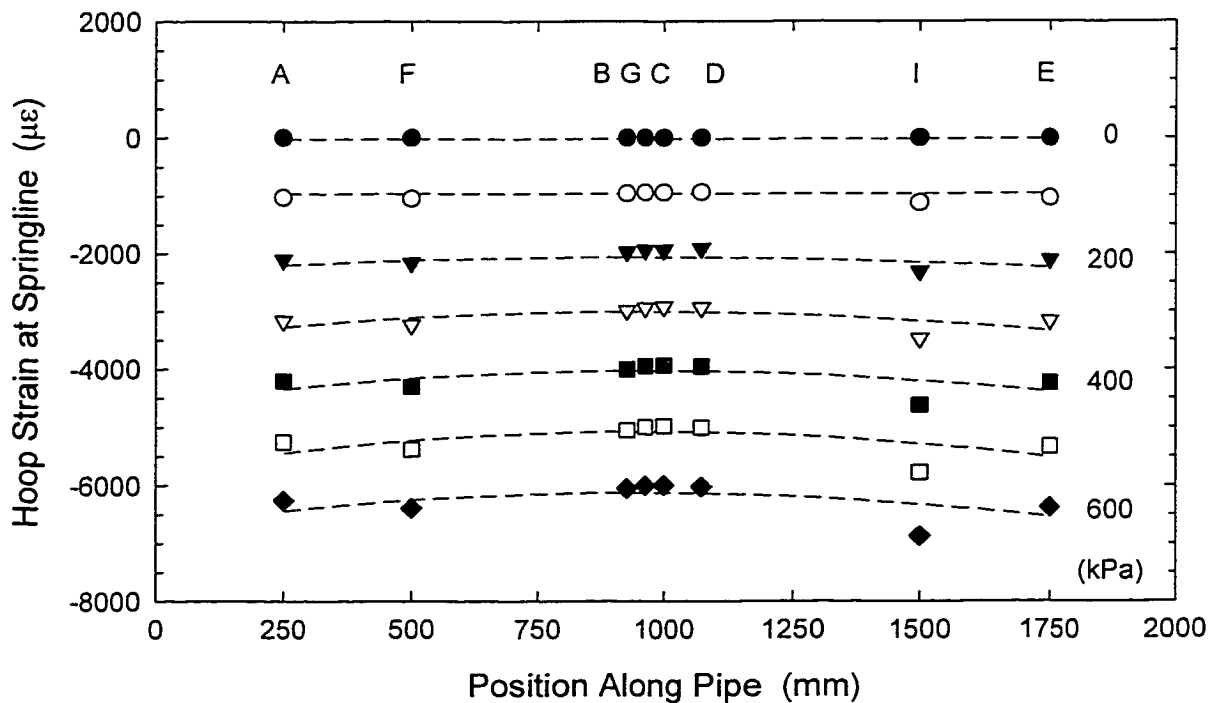


FIGURE 5.8 Variation of hoop strain measured at the interior springline location along the pipe during test P2a.

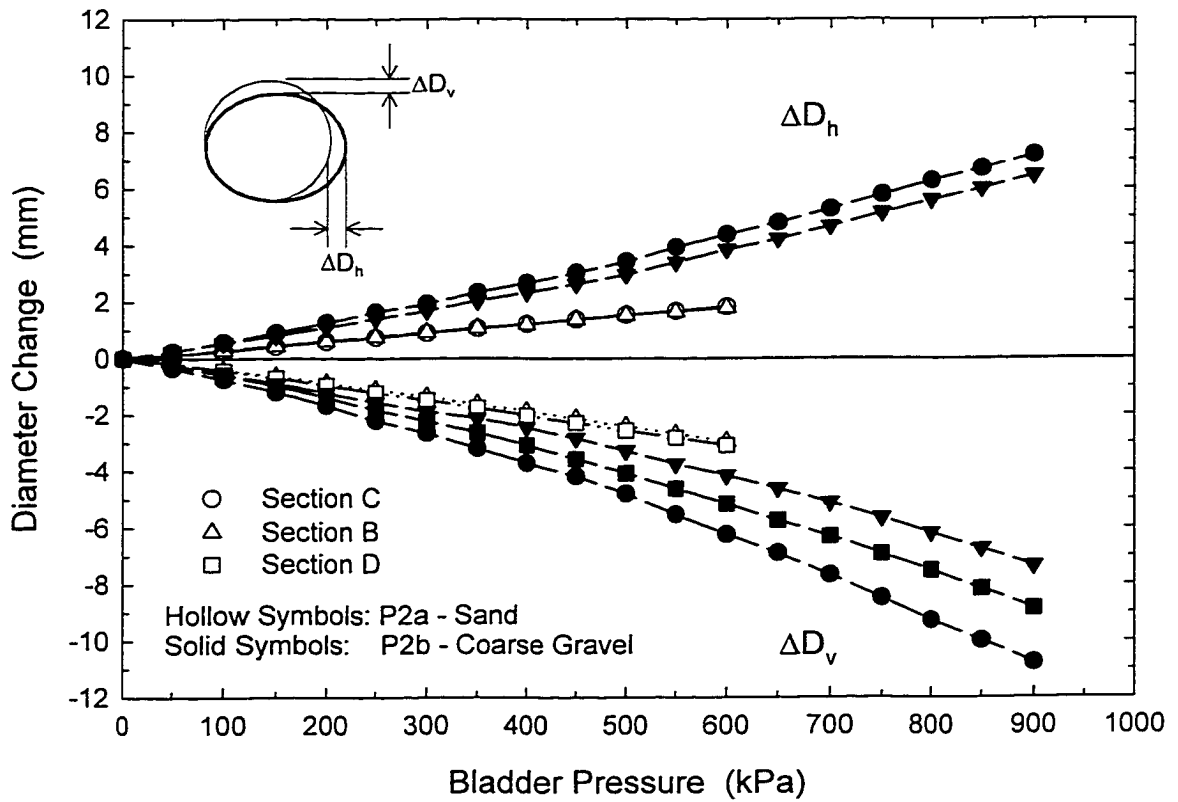


FIGURE 5.9 Vertical ΔD_v and horizontal ΔD_h diameter changes of the pipe measured during tests P2a and P2b.

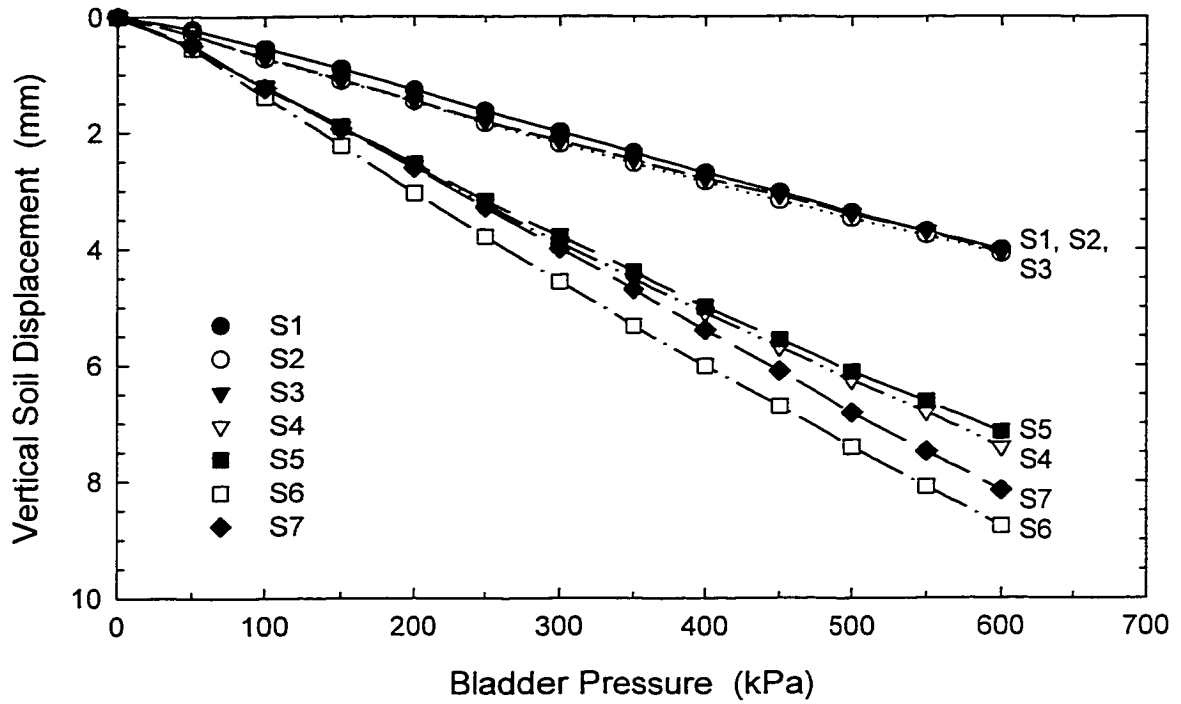


FIGURE 5.10 Vertical displacement of the soil measured at various locations during test P2a.

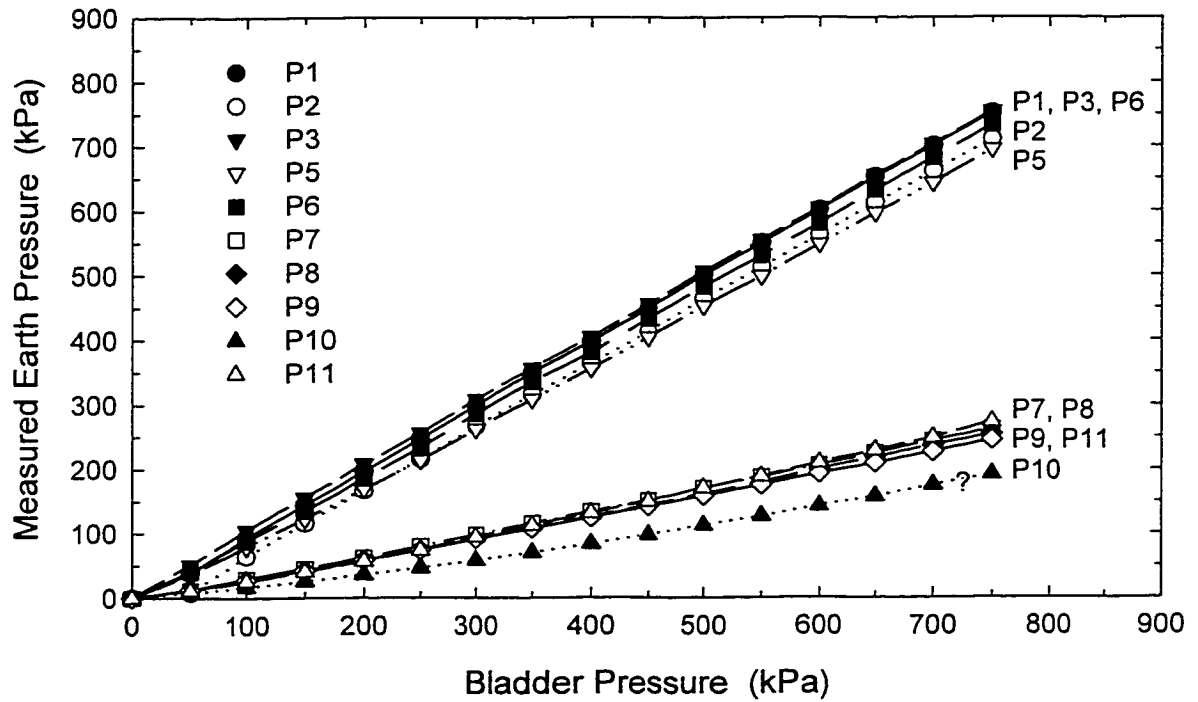


FIGURE 5.11 Measurements of earth pressure made at various locations around the test cell boundaries during test P4.

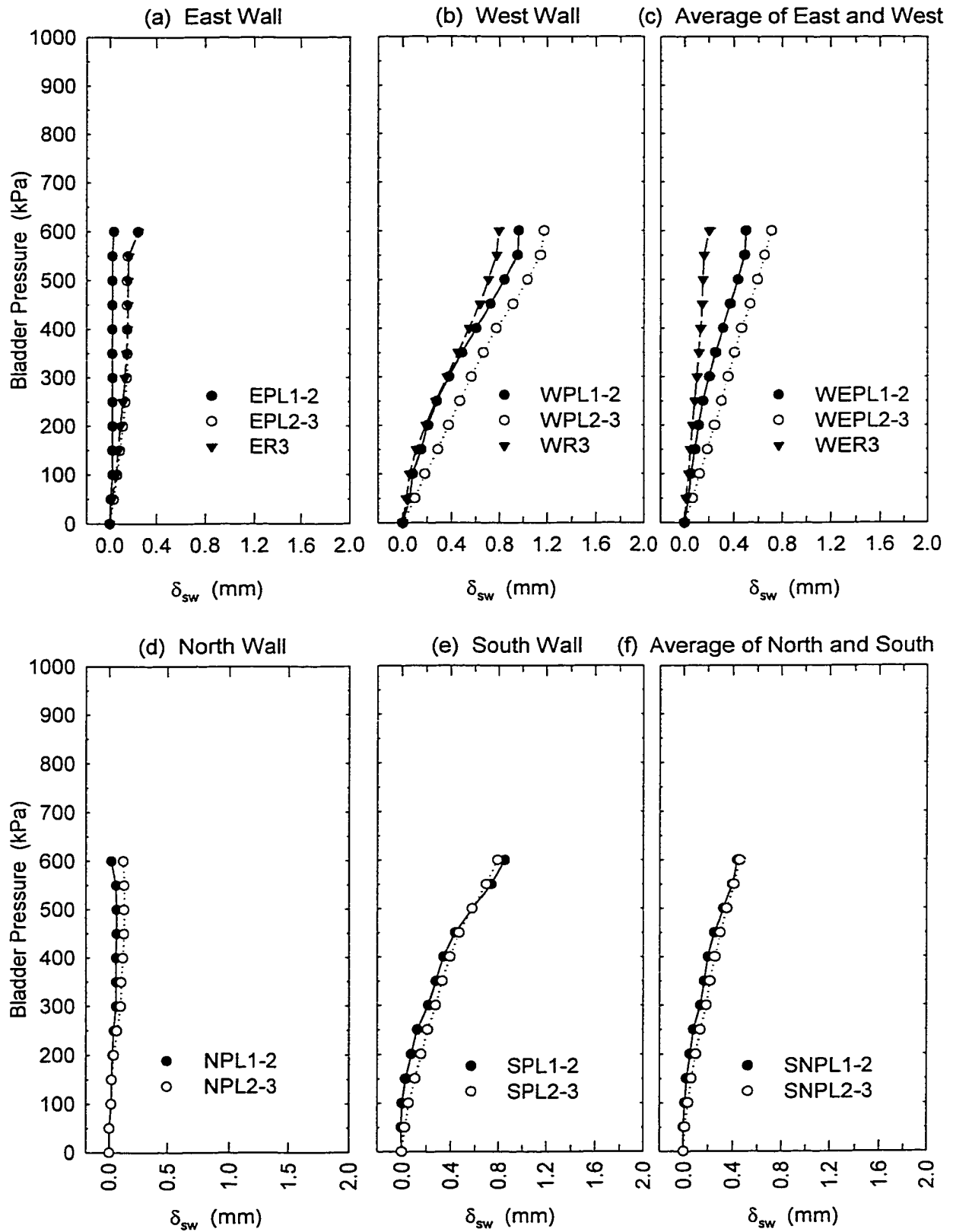


FIGURE 5.12 Lateral deflections of the exterior walls of the test cell measured during test P2a. See Figures 5.1 and 5.2 for location of measurements.

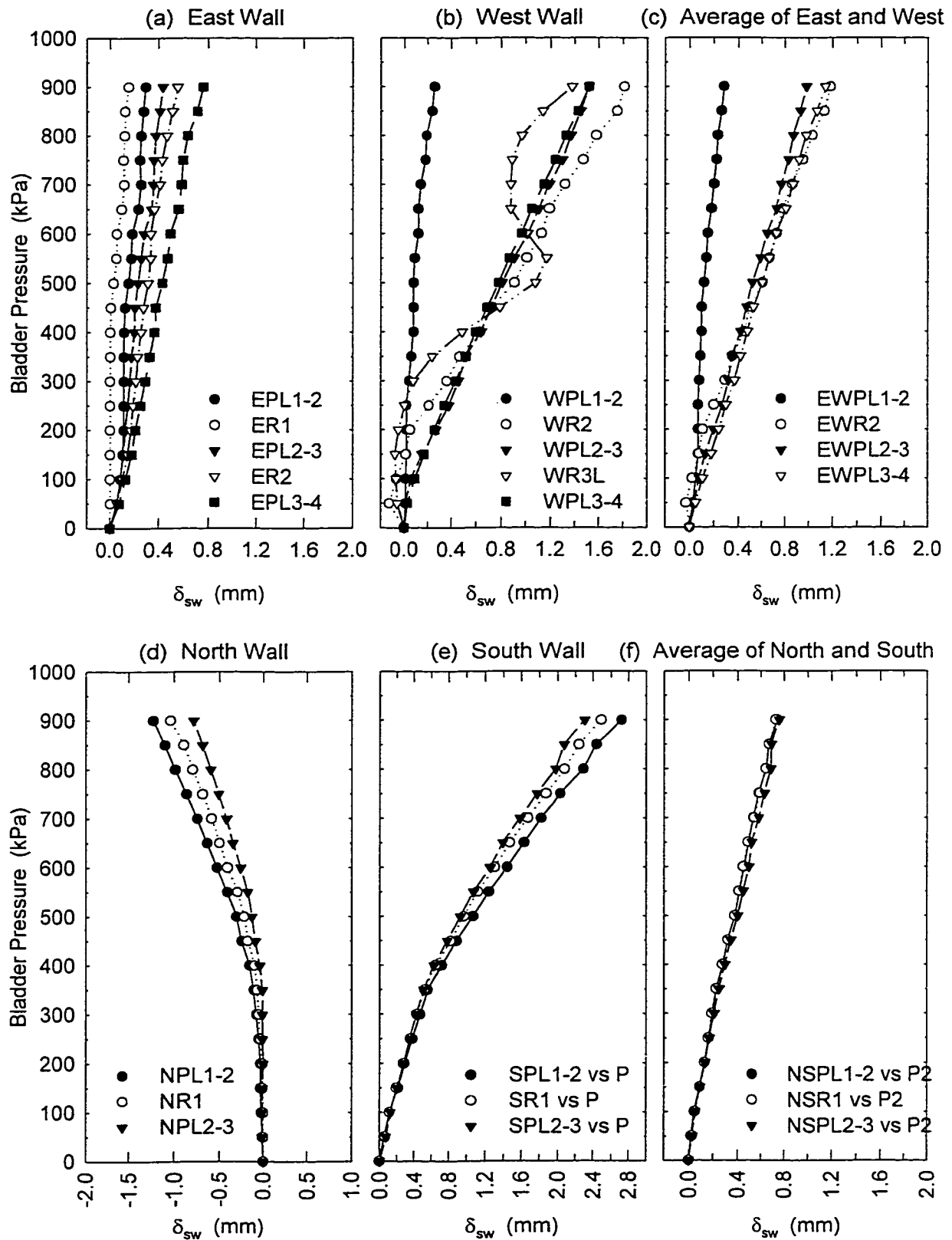


FIGURE 5.13 Lateral deflections of the exterior walls of the test cell measured during test P3c. See Figures 5.1 and 5.2 for location of measurements.

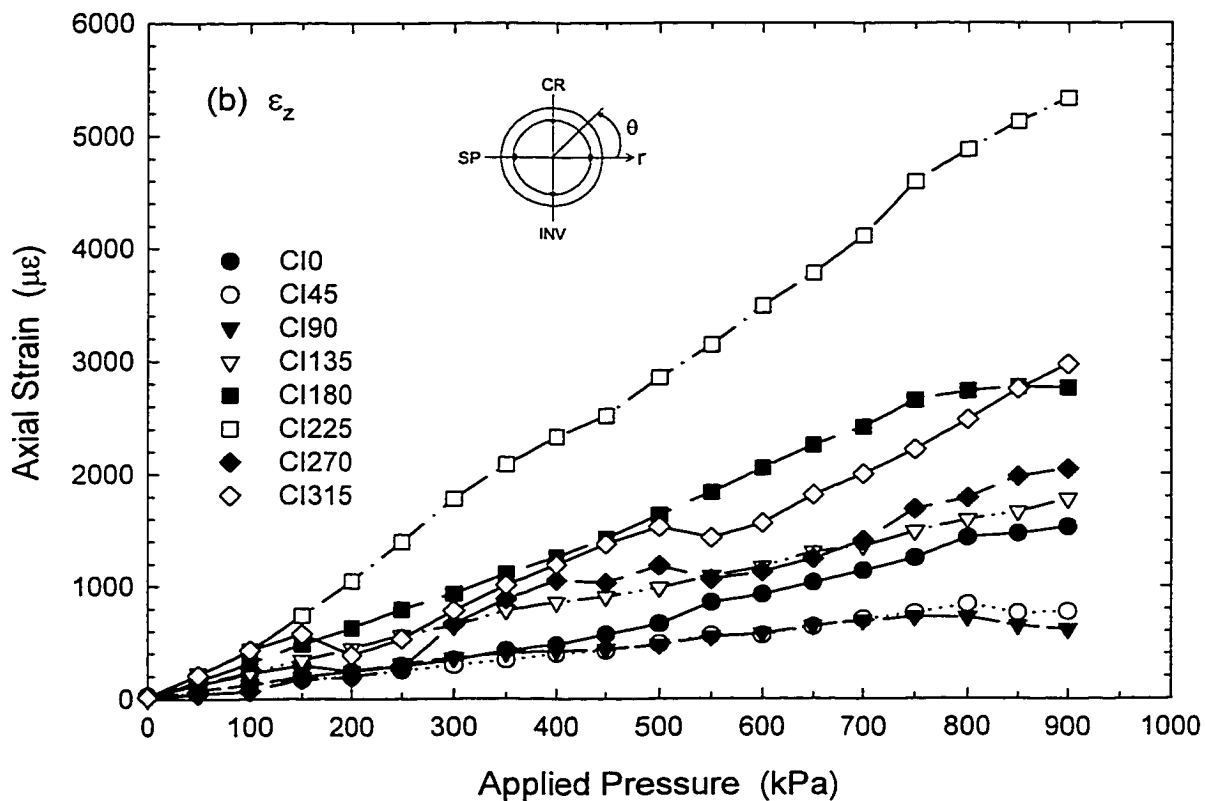
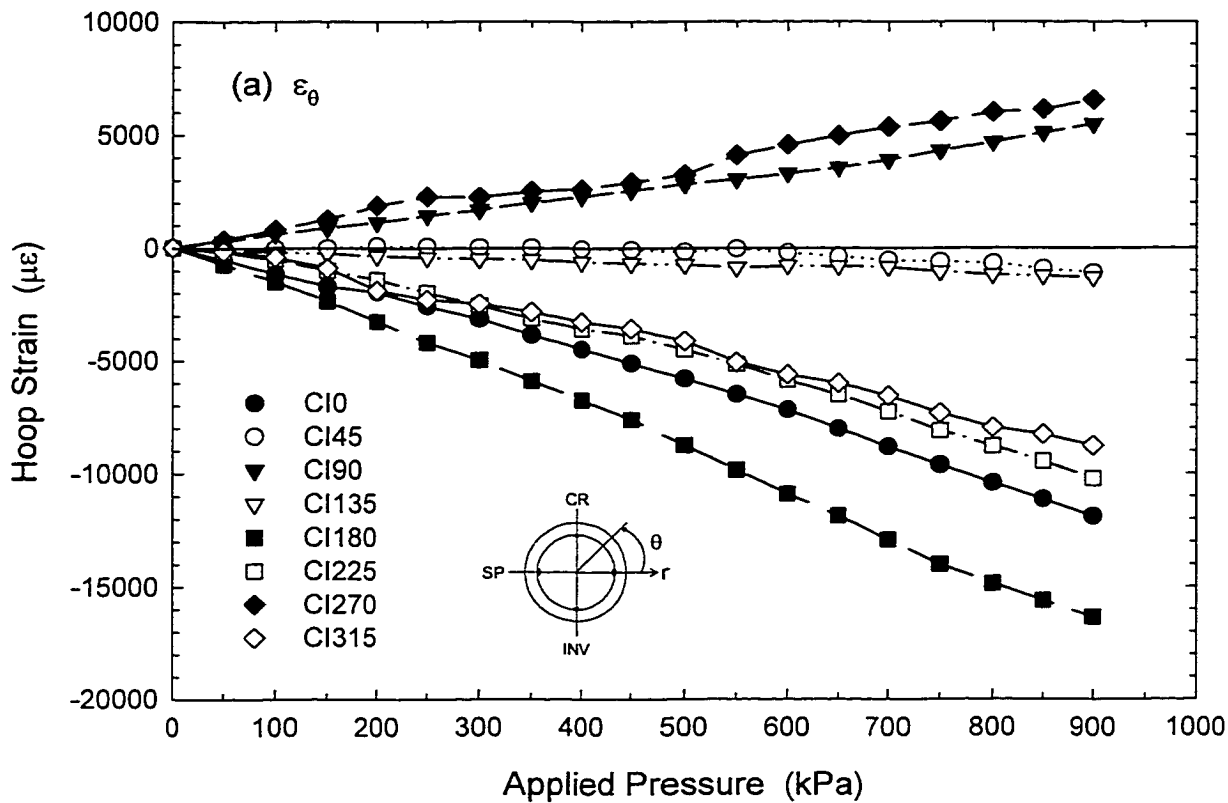


FIGURE 5.14 Measured (a) hoop ϵ_{θ} and (b) axial ϵ_z surface strains on the interior surface of the pipe at Section C during test P2b.

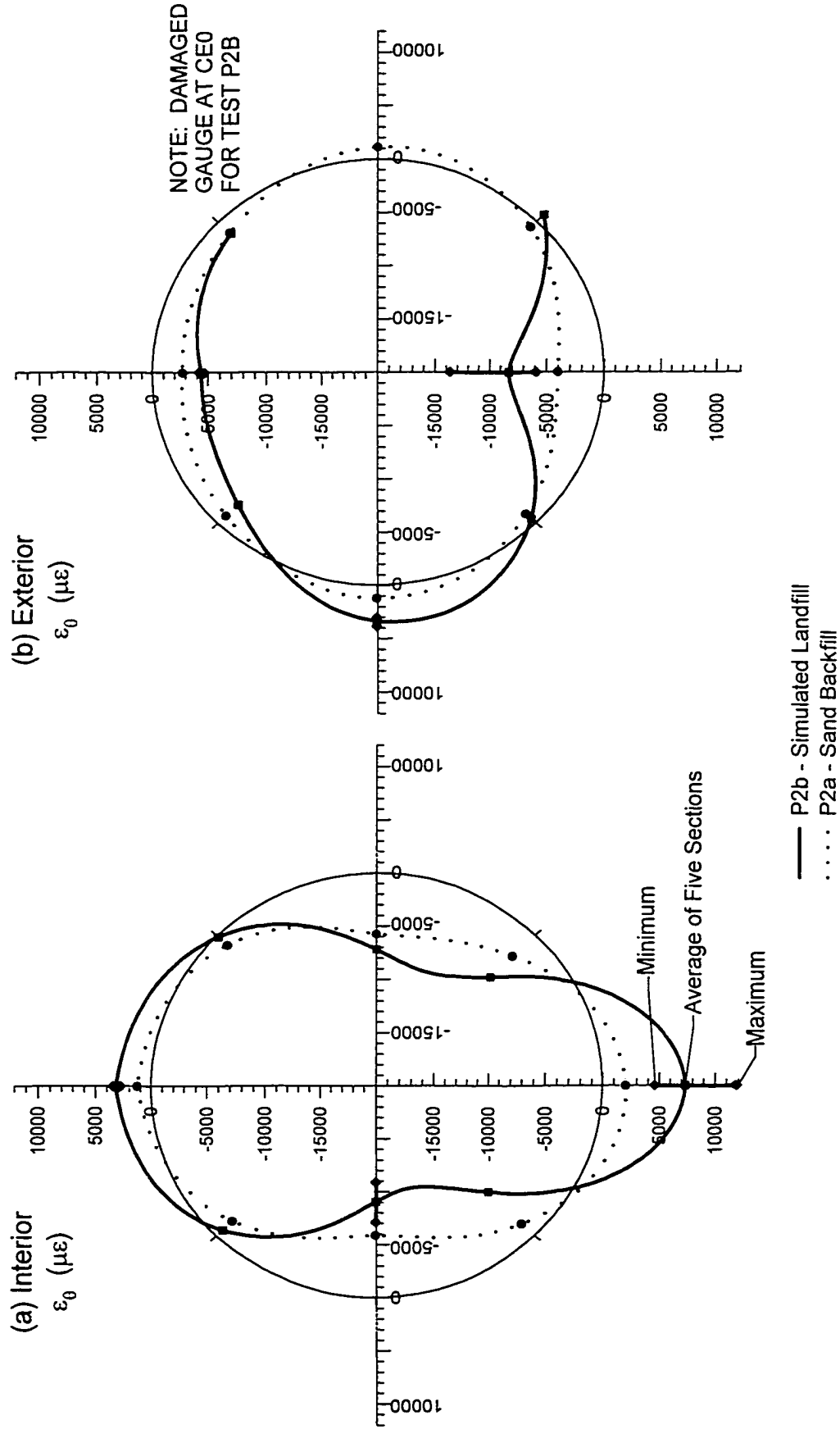


FIGURE 5.15 Hoop strain measured on (a) interior and (b) exterior surfaces of the pipe for tests P2a and P2b at an applied vertical surcharge of 600 kPa.

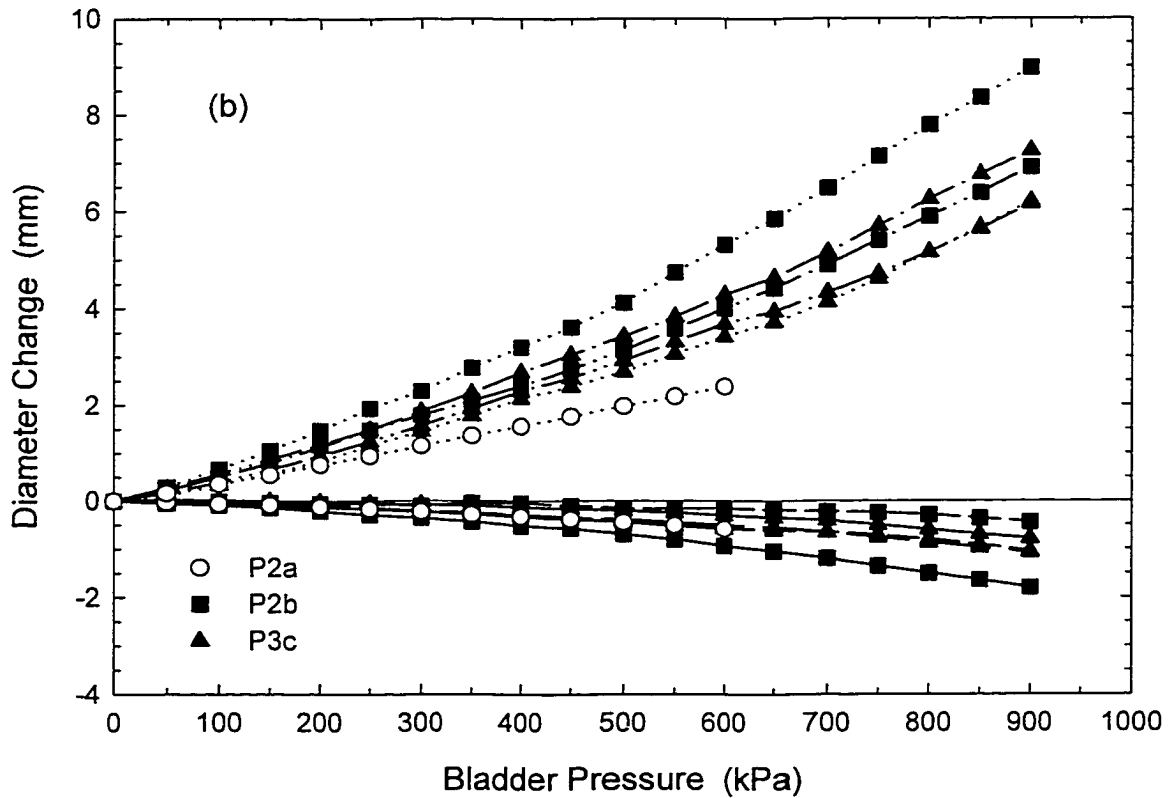
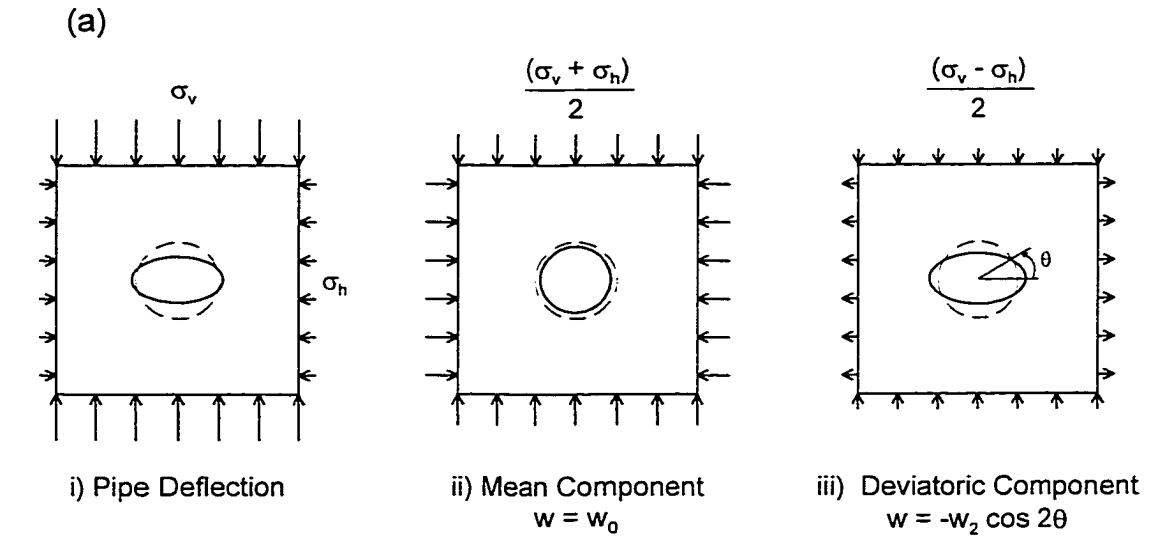


FIGURE 5.16 (a) Illustration of mean $2w_0$ and deviatoric $2w_2$ components of pipe diameter change. (b) Measured components of pipe deflection for tests P2a, P2b and P3c.

CHAPTER 6

Laboratory Investigation of the Effect of Coarse Gravel Backfill on the Mechanical Performance of Perforated Leachate Collection Pipe

6.1 INTRODUCTION

Leachate collection systems are intended to control the hydraulic head acting on the barrier and therefore are an important component of modern waste disposal facilities. It is known that both geosynthetic and geologic materials of leachate collection systems (e.g., geotextiles, pipes and gravel shown in Figure 6.1a) can experience clogging because of particulate, chemical and biological effects (see Rowe et al. 1995). Clogging reduces the effectiveness of leachate collection and may lead to an increase in hydraulic head acting on the landfill liner system.

Design measures intended to minimize the potential of clogging of the leachate collection system can lead to adverse service conditions for the pipe that are not experienced in typical buried pipe applications. For example, uniformly-graded gravel (e.g., crushed stone) with relatively large particle sizes is now commonly specified as the drainage material to minimize clogging (40 - 50 mm gravel is common). The relatively large open void space and small surface area per unit volume provided by coarse gravel help to minimize biologically induced clogging. However, there is a paucity of data that can be used to assess whether coarse gravel has a detrimental effect on the mechanical performance of the pipe. Because the gravel particles are relatively large with respect to the pipe, individual gravel

particles load the pipe at discrete points around its outside surface rather than providing the more continuous load and support of other, traditional backfill materials (e.g., sand, well-graded gravel). The magnitude of the stress variations arising from the coarse gravel backfill, and their effect on the performance of the drainage pipes is presently unknown. The global response of the pipe (ie. pipe deflections and stresses) when tested with coarse gravel is also currently unknown. Thicker polyethylene pipes are typically specified for use in landfill applications as a result of these uncertainties.

The mechanical response of these pipes is further complicated by stress concentrations that arise from the presence of perforations. These holes in the walls of the pipe, which are essential for the purpose of leachate collection, weaken the pipe compared to nonperforated pipe. These holes should be sufficiently large to minimize the potential for clogging themselves and maximize the effectiveness of cleaning efforts (e.g., by hydraulic flushing). Observations from a field exhumation of a landfill leachate collection system suggest that the perforation size currently used in practice clogs too rapidly as Fleming et al. (1999) found that 10 mm diameter holes were mostly blocked by clog material after 1 to 5 years of leachate exposure. Larger perforations are therefore required for landfill collection pipes. However, at the same time, the perforations should not be so large and so numerous that they compromise the structural integrity of the pipe. The magnitude of the stress concentrations and local bending stresses from perforations and coarse gravel backfill, and their effect on the mechanical performance of the drainage pipes are presently unknown. Laboratory testing of thick perforated leachate collection pipes is needed to assess the effects of coarse gravel backfill and perforations on the mechanical performance of these pipes when buried below significant amounts of waste in a landfill.

Test results for three samples of high density polyethylene pipe with an average outside diameter (OD) of 220 mm and wall thickness of 25 mm (SDR = 9, where SDR is the ratio of outside diameter to minimum wall thickness for the pipe) conducted under simulated field conditions are reported in this chapter to examine the effect of coarse drainage gravel and perforations on the structural response of leachate collection pipes. The nature of the loading applied to the pipe and the testing facility are briefly discussed. Vertical and horizontal diameter changes of the pipe are presented to examine the response of the pipe when subject to simulated biaxial earth pressures. Measured values of surface strain at locations around the pipe circumference are used to examine the response of the pipe and to investigate the effects of the coarse gravel backfill. Estimates of stresses in the pipe based on measured values of strain are compared with the short-term strength of the pipe. Factors important to the long-term performance of these pipes are considered. Measured deflections are also compared with estimates obtained using available procedures to assess the ability of design methods that were developed for sand and other fine grained backfills to calculate pipe deflections when used with coarse gravel backfill.

6.2 REVIEW OF PREVIOUS WORK

Previous testing conducted by various researchers has shown that plastic pipes can sustain large applied pressures. For example, Watkins (1987), Sargand (1993) and Zanzinger and Gartung (1995, 1998) have tested thick, small diameter plastic pipe for use in landfills. These tests did not involve the coarse drainage gravel that is desirable to minimize clogging

(gravel passing the 19 mm sieve, 25 mm crushed stone, and 8 to 16 mm gravel, respectively, were tested). Also, the loading conditions imposed by Watkins differ from those expected to prevail under field conditions. Further, Brachman et al. (1996) demonstrated that the boundary conditions of the test reported by Sargand were complex and had a significant effect on the pipe response. Little inference regarding the field behaviour of landfill pipes can be made from the tests of Sargand (1993).

Laboratory tests reported in Chapter 3 that were conducted under axisymmetric loading conditions showed that 40 to 50 mm coarse gravel had an effect on the structural performance of 320 mm outside diameter (32 mm wall thickness) polyethylene pipes (SDR = 11). Nonuniform pipe deformations and large variations in both circumferential and axial strains were measured when backfilled with 40 to 50 mm (nominal size) coarse gravel. The results of two tests reported in Chapter 5 demonstrated the importance of testing these pipes under biaxial earth pressures. Therefore, additional testing of thick perforated leachate collection pipes under simulated landfill conditions is required to assess the effects of coarse gravel backfill and perforations on the mechanical performance of these pipes when buried below significant amounts of waste in a landfill.

6.3 DESCRIPTION OF LABORATORY TESTS

6.3.1 Laboratory Apparatus

Deep burial leads to large vertical and horizontal stresses in the drainage layer containing the pipe, Figure 6.1b. These conditions are simulated in the laboratory using the test facility

described in Chapters 4 and 5. A transverse section of the test cell is shown in Figure 6.2. The pipe specimen is placed within a prism of soil that is 2.0 m wide \times 2.0 m long \times 1.6 m high. The soil is contained within a stiff steel structure. Lid and base units are connected with tie rods capable of resisting large forces arising from the application of large vertical pressures (up to 1000 kPa). The side walls consist of thick steel plates that are stiffened by four support frames. Vertical load is applied by a pressurized air bladder, providing a uniform vertical pressure across the top surface. Horizontal stresses develop in the soil by limiting the deflection of the side walls.

The side walls of the test cell were treated to reduce the boundary effects from friction. The interface consisted of two polyethylene sheets (0.1 mm thick) lubricated with silicone grease. This arrangement yielded a friction angle of approximately 5° , calculated from direct shear tests (Tognon et al. 1999). It is estimated that this level of friction reduces the vertical stresses reaching the pipe by less than 5% and has only a small effect on the pipe response (Brachman et al. 1999; see also Chapters 4 and 5).

6.3.2 Soil Materials Tested

Figure 6.2 also shows the arrangement of materials used for the tests intended to simulate the conditions expected in a municipal solid waste landfill. The pipe was placed within a 600 mm deep layer of coarse gravel to simulate the drainage layer. Crushed dolomitic limestone was used as the backfill material. This material is a poorly-graded coarse gravel (GP) and consists of large angular particles with 70% finer than 51 mm sieve size and only 8% finer than 38 mm. For convenience of description this will be referred to herein as “50 mm coarse gravel” or often simply as “gravel”. The coarse gravel was placed uncompacted

at an average bulk density of 1520 kg/m^3 . The pipe was placed with approximately 100 to 120 mm of gravel material between the pipe invert and the clay layer.

The drainage layer was underlain by a 200 mm thick clay layer, included to simulate the effect of a more compressible layer beneath the gravel and pipe. Finite element analysis of this arrangement was used to select the thickness of the clay layer. It was found that there was little difference in pipe response once the thickness of the clay was such that the pipe was at least one pipe-diameter away from the stiff steel base. This silty-clay till of low plasticity (liquid limit of 24% and plastic limit of 14%) was placed at a water content near the plastic limit (corresponding to 2 - 4% wet-of-optimum, which is standard practice for placing a compacted clay liner; e.g., see Rowe et al. 1995) and an average bulk density of 2100 kg/m^3 . This material was selected as it has been well characterized for use as a liner in previous studies (Rowe et al. 1993).

Since it is common practice to place select waste material for the first several metres above the engineered barrier system, vertical pressures in a landfill are expected to be relatively uniform from the overlying waste. Therefore, poorly-graded medium sand (SP) was used to fill the remainder of the test cell. Sand was selected because it could be consistently placed at a relatively uniform density with moderate compactive effort. The sand was placed in 150 mm lifts (dumped from a constant height) and then compacted by dropping a 9 kg mass a height of 300 mm with two passes made over each lift. This resulted in a relatively uniform material, with an average bulk density of 1800 kg/m^3 (measured by nuclear density and sand cone methods) and water content of 2%. The measurements of density compared well with the density obtained by recording the total mass of sand placed in the cell divided by the volume it occupied. A needle-punched nonwoven geotextile (GT),

with mass per unit area of 430 g/m^2 and equivalent opening size 75 to $150 \text{ }\mu\text{m}$, was used to separate the sand from the coarse gravel.

6.3.3 Details of Pipe Specimens

The tests reported here were conducted on three specimens of high density polyethylene pipe (cell classification PE 345434C in accordance with ASTM D3350, Class PE 3408 according to the Plastic Pipe Institute). Each sample had the same average outside diameter of 220 mm and average wall thickness of 25 mm (220 mm OD, SDR 9 nominal pipe size). The two metre long specimen contained two butt-fusion joints, each located 250 mm from the centre, to facilitate application of strain gauges on the interior surface of the pipe. Seaming was conducted in accordance with ASTM D-2657. Each of the three pipe specimens featured a different perforation geometry. The first specimen, denoted as pipe P2, was a plane pipe without perforations (for details see Chapter 5, Fig. 5.5). Pipes P3 (shown in Figure 6.3) and P4 contained four perforations located at the shoulders and haunches ($\theta = 45, 135, 225$ and 315°) at a centre-to-centre spacing of 150 mm along the pipe. The diameter of the perforation for pipe P3 was 25 mm (ie. $D_p = t$, where t is the average pipe thickness), while the perforation diameter was 37.5 mm for pipe P4 (ie. $D_p = 1.5t$). These holes are much larger than those used in current practice (approximately 10 mm diameter) which have been observed to clog rapidly when in a landfill (Fleming et al. 1999).

6.3.4 Instrumentation

The pipe response was measured with electrical foil strain gauges of 2 mm gauge length with both stacked rosette and biaxial arrangements. Strains were measured at many locations on the interior and exterior surfaces of the pipe. Figure 6.3 shows the location of strain gauges for pipe P3. Sample P4 had a similar arrangement, but with fewer gauges located around the perforations. For each pipe, a central section C was instrumented with eight gauges each on the interior and exterior surfaces located at the springlines ($\theta = 0$ and 180°), shoulders ($\theta = 45$ and 135°), crown ($\theta = 90^\circ$), haunches ($\theta = 225$ and 315°) and invert ($\theta = 270^\circ$). The strain measured at Section C, on the exterior pipe surface, and located at the crown, for example, is represented by the abbreviation CE90.

Sections B and D are each located 75 mm from the centre of the pipe. For pipes P3 and P4, these sections contained instrumented perforations. Gauges at the springlines, crown and invert were located on the interior and exterior surfaces at these sections for all three pipe specimens.

Strains were monitored and recorded using a data acquisition system. Error associated with the strain measurements (gauge sensitivity, lead wire effects and data recording) were estimated to be ± 50 microstrain (for details see Tognon 1999).

Measurements of vertical and horizontal diameter change were made at three locations along the pipe (corresponding to Section B, C and D) using potentiometers. The tolerance associated with the deflection readings is ± 0.01 mm.

6.3.5 The Calibration of Electrical Foil Strain Gauges on Polyethylene

The potential for a strain gauge affixed to a relatively soft material (like polyethylene) to locally perturb the strain value (Beatty and Chewing 1979) is acknowledged. This issue arises because the stiffness of the gauge is similar to that of the polyethylene. To quantify and account for this effect, a comparison between measured strains (from the strain gauges) and true strain (obtained by some other method) was needed. A testing arrangement was devised where an instrumented pipe specimen (pipe P2) was loaded with a uniformly distributed internal radial pressure. The ends of the pipe were sealed to prevent pressure leaks. A specially fabricated end cap permitted the passage of electrical signals from instrumentation inside the pipe to the data acquisition system while providing a proper seal (brass terminals with o-ring seals were used). Strains measured by the electrical foil gauges were compared with strains computed from measured deflections.

For axisymmetric loading conditions (ie. $\partial / \partial \theta = 0$), the strains on the inside surface of the pipe can be expressed as $\varepsilon_{\theta} = \Delta D / D_i$, where D_i is the inside diameter of the pipe and ΔD is the diameter change of the pipe measured by the potentiometers. It was found that the strain gauges consistently measured lower strains than those calculated from the measured deflections. Values of surface strain measured with these electrical foils strain gauges should be multiplied by a gauge correction factor GCF to obtain the true strain of the pipe (ie. $\varepsilon_t = \text{GCF} \times \varepsilon$, where ε_t is the true or actual strain and ε is the measured or uncorrected strain value). The gauge correction factor was not a constant value but varied with strain. For example, for strains corresponding to an internal pressure of 250 kPa the correction factor was 1.4 (similar to that found in Chapter 3), and was estimated to be equal to 2 at 900 kPa. Measured (or uncorrected) strain values are reported in this chapter to assess the variation

in response due to the coarse gravel backfill (the statistical variation is not influenced by the gauge effect since each gauge is equally impacted). Calculations of stresses based on measured strain values for comparison with allowable stresses are corrected for the gauge stiffening effect.

6.3.6 Testing Details

Pressure in the bladder was rapidly increased by 50 kPa every 40 minutes and held constant until the next increment was applied. The maximum applied pressure varied for each test. Tests P2b and P3c were conducted up to 900 kPa. Tests P3a and P3b were performed up to 250 kPa, and P4 was conducted up to 750 kPa. Table 6.1 summarises the details of the six tests reported in this chapter. Note that vertical pressure of 900 kPa in the field corresponds to roughly 70 to 90 metres of waste, assuming that the unit weight of waste is between 13 to 10 kN/m³.

6.4 MEASURED PIPE DEFLECTIONS

Vertical (ΔD_v) and horizontal (ΔD_h) diameter changes of the pipe for the six tests are plotted in Figure 6.4 versus the applied bladder pressure. Figure 6.4 shows a decrease in vertical diameter and an increase in horizontal diameter of the pipe when subject to the simulated earth pressures. The difference in pipe response when tested with sand backfill versus simulated landfill conditions is described first. The effects of the gravel backfill on the pipe deflections are then examined in greater detail.

6.4.1 Sand Backfill Versus Simulated Landfill Conditions

A comparison of tests P2a and P2b provides a direct measure of the effect of the simulated landfill conditions on the pipe response. These tests involve the same pipe (P2) but were conducted with different backfill conditions; P2a was tested with the pipe centrally located in the test cell with only sand backfill, while P2b was tested under the simulated landfill conditions shown in Figure 6.2. The two different backfill materials directly around the pipe provide different loading conditions for the pipe. The support provided by the sand backfill will tend to be more uniform (the small sand particles provide almost continuous support around the pipe circumference), whereas the coarse gravel will provide nonuniform support (discontinuous support from a finite number of contact points randomly distributed around the circumference). Also, the presence of a clay layer beneath the gravel will also potentially influence the results in Test P2b. Observed differences between the results from P2a and P2b can therefore be attributed to the simulated landfill conditions (ie. gravel backfill and clay layer).

Several observations can be made from the results plotted in Figure 6.4 for tests P2a (solid circle symbols) and P2b (solid square symbols). First, it is apparent that the magnitude of the vertical diameter change for test P2b is larger than that for P2a. The vertical diameter change is roughly -3 mm for test P2a (based on two measurements) compared with deflections ranging from -4.2 to -6.2 mm for test P2b, at a vertical surcharge of 600 kPa. A summary of these measured values is provided in Table 6.2 at an applied pressure of 600 kPa (the limit of Test P2a). Horizontal diameter changes also have a larger magnitude for test P2b than those measured for P2a, by a factor of 2.3 at 600 kPa vertical surcharge. The difference in magnitude implies that, on average, the stiffness of the gravel is less than that

of the sand compacted at this particular density when tested under biaxial earth pressures. This appears to conflict with the hoop compression laboratory data from Chapter 3 where the stiffness of the gravel was found to be slightly larger than that of the sand (for similar dry density tested here) when tested under the uniform and radially compressive pressures. This discrepancy between hoop and biaxial testing results from the difference in stiffness of the coarse gravel between mean and deviator response, as explained in Chapter 5. This reinforced the need to test the pipes subject to biaxial earth pressures.

Second, the deflections vary much more when the pipe is tested in gravel than when tested with sand backfill. When tested in sand, the deflections measured at two different locations along the pipe show very similar results. For example, at 600 kPa the measured vertical diameter change was -3.0 mm and -3.1 mm at Sections B and D, respectively (in this case an instrumentation problem occurred at Section C). In contrast, when tested in gravel there were significant differences between the measured vertical diameter changes of -4.2, -6.2 and -5.1 mm at Sections B, C and D for the same applied pressure. Similar comparisons made for the horizontal diameter change from the data in Figure 6.4 and Table 6.2 show that two measured values for the test with sand backfill are quite similar, while definite variations can be noticed for the gravel test. This is consistent with the premise that sand provides continuous backfill support to the pipe. These variations are also consistent with the nonuniform deformations reported in Chapter 3. This comparison shows that the coarse gravel backfill does influence the deformation behaviour of the pipe - which is not surprising given the large particle size of the gravel relative to the pipe diameter.

Third, the nature of the load versus deflection behaviour differs between sand and gravel backfill (Figure 6.4). When tested in sand the results are essentially linear up to the

limit of the test (600kPa). However, the deflection response obtained under simulated landfill conditions shows a nonlinear response with increases in bladder pressure. This nonlinearity is evident at lower pressures and becomes prominent for applied bladder pressures larger than 450 kPa. The observed softening response is attributed to the constitutive response of the coarse gravel backfill. The hypothesis that the observed softening is due to nonlinear polyethylene response can be rejected as this response was not observed for test P2a. The observed softening is likely associated with the volumetric response of the coarse gravel material although the possibility that the soft clay beneath the pipe also produces larger deflections can not be excluded. Sounds of gravel particles moving were audible during the testing and evidence of some particle breakage of the coarse gravel was found while excavating the materials after the test, both suggesting volumetric change of the coarse gravel during the test.

6.4.2 Measured Deflections for Pipe P3

Pipe sample P3 was tested three different times to better quantify the response of the pipe when backfilled with coarse gravel. The measured pipe deflections from tests P3a, P3b and P3c are isolated in Figure 6.5 and deflections at 250 kPa are summarized in Table 6.3. Tests P3a and P3b were limited to a maximum vertical pressure of 250 kPa to limit strains of the polyethylene to permit retesting. An applied bladder pressure of 250 kPa roughly corresponds to 20 to 25 metres of waste, representing a medium-size landfill.

Figure 6.5 shows that the average magnitude of the diameter changes measured during test P3a is larger than those for P3b, which are in turn, slightly larger than those for

P3c. It appears that the coarse gravel backfill produces a mechanical response that is sufficiently variable to yield the measured scatter.

Tests P3a, P3b and P3c all involved the same pipe sample (P3), tested with the same backfill geometry (shown in Figure 6.2). The possibility that the pipe response is different after being previously tested was excluded on the basis of: (1) negligible permanent strain was measured on unloading after tests P3a and P3b; and (2) the response of pipe P2 subject to uniform internal radial pressure (to measure the stiffening effect) did not differ when loading was repeated. The potential that the clay response is different between these three tests was also rejected since no significant change in water content was recorded for the clay layer after these three tests, therefore the stiffness of the clay should be similar between the tests. The only difference between these three tests was that the geomembrane protection layer used for test P3c differed from that used for tests P3a and P3b. Since there was no difference in protection layer used in test P3a and P3b, the difference in results between these tests cannot be explained by a difference in protection layer. It is also very likely, that a thin layer of geomembrane protection (thin relative to the distance from the pipe) has little effect of the pipe response. It therefore appears that the gravel backfill produces a response sufficiently variable to account for the observed scatter plotted in Figure 6.5. This allows statistical comparisons to be made from deflections measured from the different tests to better quantify the response of the pipe when backfilled with coarse gravel.

6.4.3 Influence of Perforations on Pipe Deflection

Location of the deflection readings were selected to measure the diameter change of the pipe at two perforated sections and one nonperforated section. Sections B and D both contain

four perforations with $D_p = t$ (as previously described with reference to Figure 6.3), while section C is located half-way between the two perforated sections. Comparison of the diameter changes from the three tests on Pipe P3 (from the data in Table 6.3) provides a measure of the effect of perforations on the local pipe response. No apparent correlation between the diameter change and location of the perforations is evident, since for each test conducted on pipe P3 the maximum vertical diameter change was recorded at a different location (ie. maximum ΔD_v at C for P3a, B for P3b and D for P3c). A similar observation can be made for the horizontal diameter changes for these tests.

Measured deflections from tests P2b (nonperforated pipe) and P4 (perforated pipe with larger holes $D_p = 1.5 t$) are now included in this comparison to better assess the effect of perforations on pipe deflections. In this case, the maximum vertical diameter change was still recorded during test P3a at Section C, while the smallest was recorded during test P3c - both for the perforated pipe with $D_p = t$. Vertical diameter changes for the pipe with the larger size holes (P4) lie between the measured results of tests P3b and P3a. The variation of results for the nonperforated pipe (P2b) shows agreement with the range of deflections measured for the perforated pipes. Based on the data summarized in Table 6.3, it appears that the deflections are not greatly influenced by the presence of the perforations (for the hole sizes and pattern examined). This is not to say that perforations cannot affect the diameter change of the pipe but rather that for the given hole sizes and pattern tested, this effect is small in relation to the dominant effect of the coarse gravel. This conclusion will be discussed further with regard to the measured strains.

6.4.4 Variation of Pipe Deflections

6.4.4.1 Diameter Changes at 250 kPa Vertical Surcharge

The spacing of the deflection measurements at Sections B, C and D are relatively close (75 mm spacing along the pipe axis) when compared with the size of the backfill material (50 mm gravel) which is exacerbated by the random nature of the contact locations on the pipe. Therefore, measurements of pipe deflection made at Sections B, C and D for a particular test are not independent quantities - but are likely to be interrelated because of the scale of the problem. To facilitate comparison of independent quantities (required for descriptive statistical analysis), the measurements at one particular section can be compared between the different tests to gauge the effect of the gravel.

Table 6.4 summarizes the mean vertical and horizontal diameter changes at each section (B, C and D) for the five different tests (P2b, P3a, P3b, P3c, and P4) at an applied bladder pressure of 250 kPa. The validity of this comparison is contingent on the assumption that the deflections are not greatly influenced by the presence of perforations as suggested in the previous section. Table 6.4 also presents the standard deviation, coefficient of variation, and 95% confidence levels on the mean for each section. The coefficient of variation (sample standard deviation divided by the sample mean) provides a measure of the variation of the measured values. Confidence intervals were calculated based on the conventional *t*-distribution for small samples with unknown population variance.

For the five different tests, the mean vertical diameter change at Sections C and D were nearly identical (-1.9 mm) and a bit smaller at Section B (-1.7 mm). The coefficient of variation at Section C (28%) is larger than the values at Section B and D (17% each) - this is reflected by the larger 95% confidence interval for Section C. Based on the 95%

confidence limits for the values measured at C, the average vertical diameter change for all the tests at 250 kPa may be described as $-2.5 \text{ mm} \leq \Delta D_v \leq -1.2 \text{ mm}$. This range also bounds the maximum and minimum observed values. These deflections correspond to 0.9 to 1% decrease in vertical diameter (diameter change normalized by the mean diameter $\Delta D_v / D_m$, where D_m is the average of the internal and external pipe diameter) at a vertical surcharge of 250 kPa.

Based on data from the five tests, the mean horizontal diameter changes were roughly 1.4 mm for Section B and D, and 1.5 mm for Section C. The standard deviation (and hence also the coefficient of variation and confidence limits) is larger at Section D since this calculation is based on three observations rather than the five samples available for Section C. A range of $1.1 \text{ mm} \leq \Delta D_h \leq 1.8 \text{ mm}$ describes the average measured horizontal diameter change at 250 kPa, using the lower confidence limit from Section B and the upper limit from Section C. Increases in horizontal diameter of roughly 0.7 to 0.8% of the mean pipe diameter were measured at a vertical surcharge of 250 kPa.

6.4.4.2 Diameter Changes at Larger Vertical Surcharges

Diameter changes of the pipe were found to increase at a greater rate for larger applied pressures than at lower pressures. This softening response results in further increases in diameter change. At an applied pressure of 900 kPa, the vertical diameter changes vary from -7.0 mm (P3c - Sec. C) to -10.8 mm (P2b - Sec. C), Figure 6.4. On average, the pipe experienced a vertical diameter decrease of 4 to 5% of the mean pipe diameter. These values are smaller than empirical limits for changes in geometry of the pipe section generally

specified in North American codes of practice to be 7.5% (CAN / CSA-b182.7-87; ASTM F 894 - 93b) and 6% based on German practice (ATV).

Changes in horizontal diameter are slightly smaller than the vertical deflections, varying from 5.0 mm (P3c - Sec. B) to 7.2 mm (P2b - Sec. C) when subject to 900 kPa vertical surcharge. On average, there is an increase in horizontal diameter of 3% of the mean pipe diameter. Since the magnitude of the horizontal diameter change is less than the vertical diameter change, often the vertical diameter change alone is considered for pipe design. The circumferential shortening of the pipe (leading to $|\Delta D_v| > |\Delta D_h|$) is not as prominent for this thick-walled polyethylene pipe as for thinner plane pipes or even profiled pipes made of polyethylene (Moore 1993).

The ratio of vertical to horizontal diameter change is not constant during the test. Considering the data from tests P2b and P3c (to permit comparisons up to 900 kPa) the ratio of vertical to horizontal diameter change increases as the applied pressures increase. Also, the coefficient of variation decreases as the load increases. This latter observation tends to suggest that results become more uniform at higher pressures as the movements of the individual gravel particles is less when compared with lower confining pressures.

6.4.5 Summary of Deflection Measurements

The pipe deflections measured during the six tests indicate that the coarse gravel backfill has a significant influence on the mechanical response of the pipe. Pipe deflections were found to be nearly twice as large when tested in the gravel as compared with medium-dense sand, indicating that the stiffness of the gravel when subject to biaxial earth pressures is less stiff than the sand backfill. Much larger variations in deflections were measured with gravel than

with sand arising from the discontinuous support provided by the relatively large gravel particles. The coefficient of variation for vertical diameter change ranged from 17 to 28%, while varying from 14 to 22% for the horizontal diameter change at a vertical surcharge of 250 kPa. Despite the large variations and the softer response measured for the gravel (both relative to the sand) the magnitudes of deflection are less than allowable limits, even up to applied vertical pressures of 900 kPa. Thus based on consideration of deformations only (other factors will be discussed later) the pipes tested in the coarse gravel with perforations up to 1.5t in diameter (37.5 mm) performed adequately under short term vertical pressures of up to 900 kPa.

6.5 MEASURED SURFACE STRAINS FOR PIPE P3

Results from measured surface strains of the pipe are now presented to further study the effect of coarse gravel on the mechanical response of the pipe. The strains measured on the interior and exterior surfaces of the pipe during test P3c are plotted versus the applied bladder pressure in Figures 6.6 and 6.7 respectively. Circumferential (or hoop) strains ϵ_θ (Figures 6.6a and 6.7a) and axial strains ϵ_z (Figures 6.6b and 6.7b) are plotted at crown, springline and invert locations for Sections B, C and D.

Strains are plotted with dimensionless units of microstrain ($\mu\epsilon$), where 1000 $\mu\epsilon$ equals 0.1% strain. Compressive strains are shown as negative values; tensile strains are plotted as positive values. The reported values of strain versus applied bladder pressure represent the strain averaged over the last 30 seconds of each 40 minute load increment.

6.5.1 Strain Response During Test

Strains show nonlinear increases in magnitude as the bladder pressure increases, consistent with similar observation for pipe deflections. Measured values do not increase at a constant rate but appear to vary during the test with numerous and varied changes during the test. Such variations were observed for the measured diameter change, but local strain measurements appear to be more sensitive to the nature of the discontinuous support provided by the gravel (since the strains are measured over a much smaller region of the pipe relative to the deflections). These fluctuations during the test are attributed to the nature of the gravel backfill since the strain response when tested with sand backfill did not show this varied response (e.g., see Figure 5.6 from Chapter 5).

Some apparent anomalies with the measured strain values can be examined by considering the behaviour of the orthogonal strain measurement at the same location, and also comparing with the values of strain measured on the opposite surface of the pipe. For example, the relatively large tensile hoop strain measured at DI270 (Fig. 6.6a) is consistent with the large compressive value observed at the exterior surface at this location DE270 (Fig. 6.7a). This appears to arise from a local effect of the gravel (not an instrumentation error) and is corroborated by the large compressive axial strain on the inside DI270 (Fig. 6.6b) and tensile axial strain on the exterior DE270 (Fig. 6.7b) measured at this location.

The interior strain measured at the invert of Section B (BI270 in Fig. 6.6a) shows a relatively steady increase up to 600 kPa, followed by a slight decrease and then by a rapid increase. This strange response is also observed for the exterior strain at this location (BE270 in Fig. 6.7a), again with a deviation from the other results at an applied pressure of 600 kPa. Both interior and exterior axial strains at this location show marked changes past

600 kPa, as BI270 decreases while BE270 increases, Figures 6b and 7b, respectively. Also, large jumps in the tensile axial strains measured at the invert of Section C occurred after 600 kPa (CI270 in Fig. 6.6b), while it decreases on the exterior surface (CE270 in Fig. 6.7b). These responses are attributed to local rearrangements of gravel particles near the pipe and lead to larger variations in the measured data.

These three examples of strain fluctuations during the test all occurred at the invert of the pipe. It is not surprising that the response near the invert is particularly sensitive to the gravel backfill given that the contacts with the backfill are likely to be more varied at the invert than at other locations around the pipe. The bedding material below the pipe invert was prepared as level as possible with the 50 mm gravel, and the pipe was then placed on top. The gravel material placed around the pipe has a greater potential to rearrange itself with respect to the pipe during construction than the material that is already placed at the invert.

6.5.2 Interior Pipe Strains

Figure 6.6a shows the circumferential response of the pipe to increases in load at the crown, invert and springlines. Compressive hoop strains (negative values) occur at the springlines ($\theta = 0$ and 180°) and tensile hoop strains develop at the crown and invert ($\theta = 90$ and 270°) on the interior surface of the pipe. These are the locations of the maximum compressive and tensile strains. Strains at the quarter points (shoulders and haunches) are much smaller in magnitude, and generally compressive.

6.5.2.1 Interior Springlines

At a vertical surcharge of 900 kPa the mean hoop strain recorded at the springlines ($\theta = 0$ and 180°) of Section C was $-20000 \mu\epsilon$. Values recorded at Sections B and D are smaller with -14500 and $-17000 \mu\epsilon$, respectively, recorded on average at 900 kPa. The significance of the magnitude of these strains as well as the magnitude of the pipe stresses are examined later in Section 6.7.2. Strains at Section C were also found to be larger on average than those at B and D during tests P3a and P3b. The perforations and the gravel are both likely to influence the measured responses at these locations. Therefore, it is worthwhile to examine the statistical significance of this difference and the degree to which it is due to the perforations or the random nature of the gravel contacts.

The measured strains at the interior springlines from the three tests conducted on the same pipe sample (tests P3a, P3b and P3c) are summarized in Table 6.5 at an applied bladder pressure of 250 kPa. The maximum hoop strain at the springline occurred at Section C for all three tests - at CI0 for test P3a, and CI180 for tests P3b and P3c. A comparison of strains at perforated (B and D) and nonperforated (C) sections can be made at 250 kPa. Averaging the strains recorded at Section C for the three tests yields a mean hoop strain of $-4700 \mu\epsilon$ ($\pm 900 \mu\epsilon$), with a coefficient of variation of 19%. The value in the bracket following the reported mean provides the 95% confidence intervals on the mean. Averaging the values measured at the perforated sections (B and D) gives a mean hoop strain of $-3700 \mu\epsilon$ ($\pm 500 \mu\epsilon$) with a 21% variation about the mean. On average, the strains measured at the interior springlines of Section C are 1.3 times those measured at Sections B and D.

To test whether this difference between perforated and nonperforated sections is statistically significant requires the formulation of a null hypothesis (H_0) that the results from

C are the same as those for B and D combined, and an alternate hypothesis (H_2) that the results from C differ from those at B and D (i.e., $H_0: X_C - X_{BD} = 0$; $H_2: X_C - X_{BD} \neq 0$, where X are the sample means). The null hypothesis can then either be accepted or rejected at a stated significance level based on statistical hypothesis testing. Rejection of the null hypothesis implies that the alternative hypothesis is true; acceptance of the null hypothesis merely implies that it is tenable based on the given data.

A two sample t -test statistic was used for testing the difference between the two sample means where variances in the normal parent populations may not necessarily be equal (Snedecor and Cochran 1989). This analysis was conducted with the assumption that the difference in measured strains at both perforated sections B and D is solely attributed to the gravel contacts (hence they can be averaged and compared to values at C to assess the effect of perforations on the strains at the springlines). Further, it was assumed that the strains measured at each location are independent observations.

The null hypothesis that the interior springline hoop strains are the same at Section C and Sections B and D can be rejected at the 5% significance level ($P = 4\%$). The stated probability (P) refers to the chance that a false hypotheses is accepted or that a true hypothesis is rejected. The null hypothesis is rejected if the significance level is greater than P . Therefore the difference in hoop strains measured at the interior springline at Section C and those at Sections B and D is statistically significant at the 95% confidence level.

This difference in interior hoop strains at the springlines is likely due to the presence of the perforation. Local deformation of the pipe material around the hole would lead to less compression at the perforated section and greater compression half-way between the perforations at a location that is 2.5 perforation diameters away from the edge of the hole (ie.

the distance along the mid-surface of the pipe between the perforation and springline). This was found by modelling a hole in an elastic medium, with dimensions corresponding to one-eighth of the pipe circumference, subject to prescribed boundary displacements distant from the hole. Results from this simplistic analysis are consistent with the measured data at the interior springline.

Axial strains also vary widely for the three sections plotted in Figure 6.6b for test P3c. These values are typically tensile, except for the large compressive values measured at the invert DI270 of Section D. Comparison of the interior axial strains for three different tests on pipe P3 can also be made from the data in Table 6.5. On average, the axial strains at Section C are roughly twice those recorded at the perforated sections. This difference is also statistically significant at the 95% confidence level ($P < 1\%$) and occurs because of local deformations of the perforation.

6.5.2.1 Interior Crown and Invert

Tensile hoop strains occur on the interior surfaces of the pipe at the crown ($\theta = 90^\circ$, solid symbols) and invert ($\theta = 270^\circ$, hollow symbols), as shown in Figure 6.6a. One large measurement of tensile strain was made at DI270, approaching $15000 \mu\epsilon$ at a pressure of 900 kPa. The other measurements at the invert were $6000 \mu\epsilon$ (at CI270) and $8000 \mu\epsilon$ (at BI270) at 900 kPa. Hoop strains at the interior of the crown are smaller than those measured at the invert, varying from 3000 to $5000 \mu\epsilon$, at 900 kPa.

Measured data at the interior crown and invert locations are summarized in Table 6.6 for the three tests (P3a, P3b and P3c) at an applied pressure of 250 kPa. The average of the three measurements (from test P3a, P3b and P3c) at the interior crown yields a mean hoop

strain of $1400 \mu\epsilon$ ($\pm 400 \mu\epsilon$) at Section C, compared to a mean of $1800 \mu\epsilon$ ($\pm 700 \mu\epsilon$) at Section B and D (at a pressure of 250 kPa). Here, the average of the strains at the perforated section is roughly 1.3 times larger than the average at the nonperforated section. This difference is also consistent with the previously described simple analysis of a hole in an elastic medium. This difference however is not statistically significant at the 95% confidence level ($P = 22\%$), given the large variances in the measured samples (due to the gravel) and the small number of observations. This result does not prove that the null hypothesis ($H_0: X_C - X_{BD} = 0$) is true, but rather suggests that it is tenable based on the measured observations. The data does not give adequate grounds for rejecting the null hypothesis. Thus any affect that the perforation may have on the hoop strains at the crown is concealed by the dominant influence of the gravel.

At the interior invert location, the mean hoop strain at Section C is $2000 \mu\epsilon$ ($\pm 4500 \mu\epsilon$) and the mean hoop strain for Sections B and D is $3000 \mu\epsilon$ ($\pm 1200 \mu\epsilon$). These differences are also not statistically significant at the 95% level ($P = 47\%$). The coefficient of variation of the three readings made at the interior invert at Section C is 90%, while it is 40% for the six readings at Sections B and D for tests P3a, P3b and P3c. These large variations illustrate the prominence of local bending effects on the pipe response at the invert. Since tensile stresses are a maximum at the interior invert, it is important to know how the local gravel affects the tensile stresses in the pipe. This is discussed in greater detail later in this chapter.

The values measured at the invert and crown locations show two important points. First, the magnitude of hoop strains is larger at the invert than for strains measured at the crown which suggests that the pipe response at the invert may govern the maximum load the

pipe can sustain. Second, there appears to be greater variations in measured strains at the invert and crown, compared to the variations recorded at the springlines. Both of these issues will be further examined later in this chapter.

6.5.3 Exterior Pipe Strains

The circumferential bending of the pipe when subject to biaxial earth pressures is evident by comparing the strains measured on the interior surface to those on the exterior of the pipe. Figure 6.7a shows compressive strains at the crown and invert locations, and tensile strains at the pipe springlines, the opposite of that measured at the pipe interior.

For this test (P3c), the maximum compressive hoop strain of roughly $-12000 \mu\epsilon$ was recorded at the invert of Section D (DE270) while the maximum tensile hoop strain of $7000 \mu\epsilon$ was measured at CEO, both at vertical surcharge of 900 kPa . These strains however, are less than the maximum strains measured on the interior surface. Thus, limiting strain (or stress) of the pipe during design will be governed by the hoop response at the interior springline and invert for the specific conditions tested. Study of the exterior strains is still worthwhile to better characterise the mechanical response of the pipe and the influence of coarse gravel backfill.

6.5.3.1 Exterior Springlines

Exterior strains for tests P3a, P3b and P3c measured at the springline for an applied pressure of 250 kPa are summarized in Table 6.7 to permit a further examination of perforations on the measured pipe strain. The average at Section C for the three tests is $1400 \mu\epsilon (\pm 150 \mu\epsilon)$. The average of twelve measurements at the perforated sections is $1400 \mu\epsilon (\pm 200 \mu\epsilon)$. There

appears to be no substantial difference between the response at the exterior springlines because of the presence of the perforations based on the averages of the measured data. The null hypothesis that the exterior strains at the springlines are not effected by the presence of the perforations cannot be rejected based on the measured data at the 5% level ($P = 68\%$). This differs to the observation made for the interior springlines.

The perforations still likely have some (albeit small) influence on the response of the pipe. The fact that the gravel is in contact with the pipe on the exterior surface may be one possible reason why no difference from the perforation was noticed. Greater number of measurements would therefore be required to discern the effect at the pipe exterior.

6.5.3.2 Exterior Crown and Invert

The perforations also have no apparent effect on the exterior strains measured at the crown and invert. Table 6.8 summarizes the hoop and axial strains measured on the exterior of the pipe at the crown and invert. The measurements made at CE90 have an average of $-2100 \mu\epsilon$ ($\pm 900 \mu\epsilon$), which is quite similar to the average measured at BE90 and DE90 of $-2200 \mu\epsilon$ ($\pm 300 \mu\epsilon$). This difference is not significant at the 5% level ($P = 90\%$).

Likewise at the invert, an average hoop strain of $-2500 \mu\epsilon$ ($\pm 2900 \mu\epsilon$) for the CE270 measurements is similar to those for BE270 and DE270 with a mean of $-2500 \mu\epsilon$ ($\pm 1000 \mu\epsilon$). The relatively large confidence level on the mean for the values at Section C result from a large standard deviation ($1180 \mu\epsilon$) based on a small sample size of three observations. These means are also not statistically different at the 5% level ($P = 98\%$). The implications of the statistical testing is discussed in the next section.

The coefficient of variation of the hoop strains at the exterior invert is nearly 40% - much larger than the variation at the exterior crown of roughly 15%. Also, no significant difference was noticed between axial strains at the perforated sections and the nonperforated section.

6.5.4 Interpretation of Statistical Testing

The results from the three tests conducted on pipe P3 indicate no statistically significant difference between the strains measured at sections having perforations at the quarter-points (B and D) and a nonperforated (C) section, except at the interior springlines. There is likely to be a difference between perforated and nonperforated sections because of the influence of deformation of the hole on the response away from the hole. This effect is estimated to be a 20% increase in compressive hoop strain at the interior springline at a nonperforated section. Tensile strains at the crown and invert may also be slightly larger at the perforated section from the effect of the hole. However to discern this effect at other locations around the pipe based on data from laboratory testing would require a lot of measurements given the large variations induced by the gravel. Both the mean and standard deviation (used for the statistical hypothesis testing) depend on the size of the sample. The cost associated with the gathering of additional data must be weighed against the risk of accepting a false hypothesis (or rejecting a true hypothesis).

Based on the measured data it appears that the difference at the crown, invert and springline locations between perforated sections and nonperforated sections is small relative to the influence of the gravel. Thus the principal effect that the perforation has on the mechanical performance of the pipe is a local perturbation in the strain field and the

influence is concentrated around the hole. The design implications of these local effects near the hole need to be considered and are discussed later in the chapter. Variations produced by the gravel are sufficiently large such that they dominate the mechanical response of the pipe. This conclusion is important since strains measured at both perforated and nonperforated sections can be considered together to better characterize the effect of the gravel on the mechanical performance of the pipe.

6.6 VARIATION OF MEASURED SURFACE STRAINS FOR ALL TESTS

6.6.1 Measured Hoop Strains at 250 kPa Vertical Surcharge

The strains during all the tests are now examined to further assess the variation in pipe response arising from the coarse gravel backfill. This includes results from three pipe samples - two perforated (P3 and P4) and one nonperforated (P2) - to better describe the variations in the measured populations. Results at a vertical surcharge of 250 kPa are examined first given the large number of readings during the five different tests. The magnitude and variations of strains at larger vertical pressures are examined in Section 6.6.3.

Figure 6.8 plots the average hoop strains for the five tests measured on the interior (Fig. 6.8a) and the exterior (Fig. 6.8b) surfaces of the pipe, at vertical surcharge of 250 kPa. Also shown are the maximum and minimum values. These polar plots illustrate the variation of hoop strain around the pipe, with again, compression negative. The mean, 95% confidence levels, standard deviation and coefficient of variation for all of the measured data

are reported in Table 6.9. Also included in Table 6.9 is the ratio of maximum observed strain to the average strain which may be useful for the design of these landfill pipes.

Overall, consistent trends were observed for the five different tests. On the interior surface, compressive strains were measured at the springlines and tensile strains at the crown and invert (Fig. 6.8a), while on the exterior surface tensile strains occurred at the springlines and compressive strains at the crown and invert. For both the interior and exterior surfaces of the pipe, strains measured at the quarter points (shoulders $\theta = 45$ and 135° , and haunches $\theta = 225$ and 315°) are in between the values measured at the crown, springlines and invert locations, and are generally small compressive or sometimes small tensile strains.

The maximum and minimum strain values plotted in Figure 6.8 provide a measure of the variation in pipe response because of the gravel. This assumes that variations in strain because of perforations are small relative to those caused by the gravel, as argued in the previous section. It is also assumed that the strain measurements made at Sections B, C and D for the same test are independent observations. The latter assumption was not tenable for deflections measured at Sections B, C and D, as it was argued that the location of the displacement measurements was close relative to the spacing of the gravel contacts. This was supported by the data plotted in Figure 6.5. However, it is likely that the local measurements of strain (over the 2 mm gauge length) made at the three sections are to a lesser degree dependent upon one another than the measurements of diameter change. No apparent dependence was observed for the measured strains. Also, the strain gauges detected local strain variations, as discussed earlier in reference to Figures 6.6 and 6.7, that were attributed to the movement of individual gravel particles. While the strain measurements at

B, C and D for a particular test may not provide truly independent observations, the data suggests that the measurements of strain are strongly influenced by the gravel contacts.

6.6.1.1 Springlines

The average of the twenty-seven measurements of hoop strain made at the interior springlines during the five tests is $-3900 \mu\epsilon$ ($\pm 400 \mu\epsilon$), again where the number in parentheses is the 95% confidence level of the mean. These values include measurements at both interior springlines (ie. $\theta = 0$ and 180°) for Sections B, C and D, for tests P2b, P3a, P3b, P3c and P4. Of these measurements, the largest compressive strain of $-6100 \mu\epsilon$ was recorded at CI0 during test P3a, while the smallest occurred at CI0 during test P2b and DI0 during test P3b with a value of $-2600 \mu\epsilon$. There is a 60% difference between the maximum and minimum values recorded (ie. $[\max - \min] / \max$). The coefficient of variation of 23% provides an indication of the spread of the measured data from the mean. The maximum hoop strain at the interior springline is roughly 1.6 times the average at this location. Therefore, multiplying the average strain by the ratio of maximum to average strain (obtained from Table 6.9) provides a rational means to account for the coarse gravel backfill during pipe design. For example, an analytical solution like that of Höeg (1968) could be used to calculate the response at the springline pipe based on the average stiffness of the gravel (estimated, say, from the measured deflections) and then multiplied by a factor to account for variations due to the gravel. This maximum compressive stress could then be compared with the allowable stress for polyethylene. This will be discussed later with regard to pipe stresses following study of the statistical variation at the other locations around the pipe.

The hoop strains measured at the exterior springline averaged $1400 \mu\epsilon (\pm 100 \mu\epsilon)$ based on twenty-nine measurements from the five separate tests. Of these measurements at the exterior crown, maximum and minimum measured tensile strains of $2150 \mu\epsilon$ (P4 at BE0) and $900 \mu\epsilon$ (P3b - DE0), respectively, were recorded - a 60% difference between these values. A coefficient of variation 21% was found for the exterior springline data. These variations are quite similar to those observed at the interior springlines.

6.6.1.2 Crown

The average tensile hoop strain at the interior crown was $1600 \mu\epsilon (\pm 400 \mu\epsilon)$ based on fifteen measurements from the five different tests. The coefficient of variation of 27% is a bit larger than that observed at the springlines. The maximum tensile hoop strain was $2750 \mu\epsilon$ (P3a - BI90) and the minimum was $900 \mu\epsilon$ (P3c - DI90) - a 66% difference between these values.

On the exterior surface, the hoop strains at the crown averaged $-2100 \mu\epsilon (\pm 200 \mu\epsilon)$. Here the strains varied between the maximum of $-2850 \mu\epsilon$ (P4 - CE90) and the minimum of $-1750 \mu\epsilon$ (P3b - CE90). The variation between the extreme values is smaller than the interior crown with a 38% difference between the largest and smallest observation. The coefficient of variation is smaller than at the interior with 15% variation about the mean.

6.6.1.3 Invert

The strains measured at the invert are larger in magnitude and have a larger variation when compared with the values measured at the crown. The average of the strains measured at the interior invert location for the five tests was $2600 \mu\epsilon (\pm 800 \mu\epsilon)$, with a coefficient of

variation of 49% about the mean. There is a 87% difference between the maximum value of 4900 $\mu\epsilon$ (P2b - DI270) and the minimum of 650 $\mu\epsilon$ (P3c - CI270).

On the exterior surface at the invert, the average of the strains for the five tests was -2800 $\mu\epsilon$ ($\pm 900 \mu\epsilon$), with a coefficient of variation of 47% about the mean. A 78% difference between the maximum value of -6700 $\mu\epsilon$ (P2b - DI270) and the minimum of -1500 $\mu\epsilon$ (P3b - BI270) was recorded at this location. The variations at the invert are quite similar between the interior and exterior locations.

Limiting the tensile strain (or stress) is another important design issue for leachate collection pipes. The maximum tensile strain occurs at the interior invert location. Multiplying the average strain at the invert by a factor of two would account for the variations induced by the gravel at this location.

6.6.1.4 Shoulders and Haunches

Strains at the quarter-points (shoulders and haunches) are much smaller in magnitude than those at the invert and springlines, and are generally compressive or small tensile values. Although they are small, these strains are of interest because perforations are typically located at the quarter-point locations around the pipe. Based on the measured results, it appears to be good practice to place the perforations at the quarter-points, since the strains (and hence stresses) at these locations are small.

The variations of the measured strains at the quarter-points are much larger than at other locations around the pipe. The coefficients of variations range from nearly 40% at the exterior shoulder to 360% at the exterior haunch locations and are larger than at other

locations given the small magnitudes of strains measured at these locations. These values are also summarized in Table 6.9.

6.6.2 Measured Axial Strains at 250 kPa Vertical Surcharge

The average axial strains for the five tests measured on the interior and the exterior surfaces of the pipe are plotted in Figure 6.9 at an applied bladder pressure of 250 kPa. Also shown are the maximum and minimum observations. The mean, 95% confidence levels, standard deviation and coefficient of variation for all of the measured data are also summarized in Table 6.9.

Axial strains arise from the axial elongation of the pipe and local bending effects from the gravel contacts. If plane strain conditions prevailed in the axial direction, the axial strain corresponding to the axial elongation of the pipe would be zero. Such conditions could exist in a landfill with long and prismatic geometry along the pipe axis. However, situations arise where the pipe may experience axial elongation (e.g., at thermal expansion joints or where the pipe enters a manhole) leading to tensile axial strains.

Non-zero axial extension conditions for the pipe are therefore likely to result in worse conditions for the pipe relative to axial plane strain conditions as tensile axial strains tend to increase tensile hoop stresses and decrease compressive hoop stresses within the pipe. Since tensile stresses may be more critical (due to long term concerns regarding stress cracking), consideration of non-zero axial strains are important for assessing the potential performance of the pipe. As discussed in Chapter 5, the ends of the pipe were not restrained during testing to permit the pipe to extend axially.

The measured axial strains were predominately tensile, with local axial bending producing compressive strains at the interior crown and invert (Fig. 6.9a). However, these compressive strains are small (less than $-600 \mu\epsilon$). Of greater importance, are the effects of local axial bending on the tensile strains, since tensile strains are likely to have more impact on the pipe performance.

The maximum axial tensile strain was recorded at the interior springline with a value of $1900 \mu\epsilon$ (P3a - CI0). At this location the mean axial strain was $800 \mu\epsilon (\pm 200 \mu\epsilon)$. The average axial strain at the interior invert was $300 \mu\epsilon (\pm 500 \mu\epsilon)$ with measurements varying between the maximum $1800 \mu\epsilon$ (P4 - BI270) and minimum $-550 \mu\epsilon$ (P2b - BI270) values.

At the exterior springline, the average axial strain was $400 \mu\epsilon (\pm 100 \mu\epsilon)$, varying between the largest observation of $950 \mu\epsilon$ (P3a - CE0) and the smallest value of $-300 \mu\epsilon$ (P3b - DE180). Large variations again occurred at the exterior invert ranging between $1300 \mu\epsilon$ (P2b - DE270) and the smallest value of $-450 \mu\epsilon$ (P4 - DE270), with a mean of $700 \mu\epsilon (\pm 400 \mu\epsilon)$.

Axial strains vary more than the hoop strains. The coefficient of variation for the axial strains is roughly 50% (at interior springlines and haunches) and much larger at other locations around the pipe (e.g., greater than 200% at the interior invert) see Table 6.9. Large variations in axial strain were expected since the pipe is less stiff in the axial direction than the hoop direction. This is consistent with the observations from the test results of Chapter 3.

A measure of the effect that the gravel backfill has on the axial strains can be obtained from a comparison with the axial strains recorded during the test with only sand backfill (P2a) which are also shown in Figure 6.9. The details of test P2a were reported in

Chapter 5 (see Fig. 5.1). Similar boundary deformations were measured between the sand and gravel tests. The axial strains recorded during the sand tests were also tensile, but with a smaller magnitude (between 300 and 400 $\mu\epsilon$) on the inside of the pipe, and had much less variation around the pipe circumference. The axial strains recorded on the exterior surface during test P2a were, on average, similar to the gravel results, except at the pipe haunches. The lack of gravel support in the haunch region (it is difficult to place coarse gravel in good contact with the pipe in this region) may produce greater axial bending, accounting for the larger tensile strains recorded at the interior at 225° and smaller tensile, and even compressive, axial strains at 315° on the exterior surface of the pipe. The importance of axial strains will be highlighted when pipe stresses are estimated based on the measured strains.

6.6.3 Measured Strains at Larger Vertical Surcharges

The statistical analysis of the laboratory data at an applied pressure of 250 kPa provides a good measure of the distribution of strains around the pipe circumference and the variation of strains because of the gravel contacts with the pipe. For larger applied vertical surcharges, it is also desirable to know the variations in the strains arising from the gravel backfill. However, there is only limited data at higher pressures, with three tests conducted up to 750 kPa, and two conducted up to 900 kPa. One approach to resolve this issue is to compare the variation of data for tests P2b, P3c and P4 at 250 kPa and 750 kPa to assess whether the variations become larger or smaller as the applied vertical surcharge increases.

No appreciable increase in the calculated variation (considering both the coefficient of variation and ratio of maximum to mean values) between the hoop strains measured at 250

kPa and 750 kPa was found, for both the interior and exterior surfaces of the pipe. In most cases (interior crown and invert, and exterior springline and crown), variations actually decrease as the pressure increases. This observation was also made for the measured diameter changes, suggesting that the response may become more stable for applied loads up to 900 kPa. Possibly, there are a greater number of contacts between the gravel and the pipe at larger pressures resulting in less local bending. Thus the descriptive statistics for the data at a vertical surcharge of 250 kPa are not only applicable for medium-size landfills, but also characterize the variations at larger pressures (up to 750 kPa). Additional measurements are required at vertical pressures exceeding 750 kPa to confirm the results at these large pressures.

6.7 CALCULATED PIPE STRESSES BASED ON MEASURED STRAINS

The magnitude of stresses that exist in the pipe are of practical interest. An estimate of the pipe stresses can be obtained based on the measured surface strains. One approach is to use classical Hooke's Law for plane stress in the radial direction (ie. $\sigma_r = 0$) to express the desired quantities of hoop and axial stress in terms of the measured hoop and axial strains viz:

$$\begin{bmatrix} \sigma_{\theta} \\ \sigma_z \end{bmatrix} = \text{GCF} \frac{E_p}{1 - \nu_p^2} \begin{bmatrix} 1 & \nu \\ \nu & 1 \end{bmatrix} \begin{bmatrix} \varepsilon_{\theta} \\ \varepsilon_z \end{bmatrix} \quad (6.1)$$

where:

σ_{θ} , σ_z = calculated hoop and axial stresses,

GCF = correction factor to account for strain gauge stiffening,

E_p = Young's modulus for polyethylene,

ν_p = Poisson's ratio for polyethylene, and

ϵ_{θ} , ϵ_z = measured hoop and axial strains.

The assumption of zero radial stresses on the surface of the pipe is applicable for the interior surface of a pipe which is not subject to an internal pressure (e.g., a leachate collection pipe). This expression is also valid for exterior surface locations that are not directly beneath a gravel contact. For other backfill materials, this simple expression can be modified to include the effect of non-zero radial stresses, provided that the radial stresses are known.

An important consideration in estimating the pipe stresses based on measured strains is the selection of appropriate constitutive parameters for polyethylene. In general, the mechanical response of polyethylene is highly nonlinear and time dependent. Various models are available to estimate the modulus of polyethylene (e.g., Chau 1986; Moore and Hu 1996; Zhang and Moore 1997). The viscoplastic constitutive model of Zhang and Moore (1997) - that was developed using specimens taken from pipe of the same material as the ones tested here - was used to estimate Young's modulus for the appropriate strain levels and time.

6.7.1 Calculated Pipe Stresses at 250 kPa Vertical Surcharge

Calculated stresses based on the average strains (values from Table 6.9) are reported in Table 6.10 for the interior and exterior surfaces of the pipe (tensile stresses positive) at an applied bladder pressure of 250 kPa. A secant modulus of 420 MPa was used for an estimate of E_p , along with Poisson's ratio of 0.46 and a strain gauge correction factor of 1.4.

The variation of stress around the pipe circumference is similar to the variation of strain around the pipe plotted in Figures 6.8 and 6.9. The largest compressive hoop strain recorded at the interior springline gives rise to the maximum compressive hoop stress of -2.6 MPa. The largest tensile stress of 2.0 MPa occurs at the interior invert. The stress at the interior crown is also tensile and has a magnitude of 1.3 MPa. Smaller compressive stresses occur at the quarter-points and are also given in Table 6.10.

Hoop stresses on the exterior surface of the pipe are predominately compressive, with the maximum occurring at the exterior invert ($\sigma_\theta = -1.9$ MPa), except for tensile stresses at the exterior springlines ($\sigma_\theta = 1.2$ MPa).

Axial stresses are tensile, except at locations where large compressive hoop strains occur (at the interior springline and the exterior crown and invert positions). The largest axial stress occurs at the interior invert, with a value of 1.1 MPa.

Since the maximum strain was found to be roughly twice the average value (Table 6.9), the maximum tensile stresses can be estimated to be 4 MPa, found by multiplying the calculated stresses by a factor of two to account for variations caused by the coarse gravel. All of these stresses are less than the short term strength of the pipe material discussed in Section 6.7.3.

6.7.2 Calculated Pipe Stresses at 900 kPa Vertical Surcharge

The calculated hoop and axial stresses in the pipe at an applied vertical surcharge of 900 kPa are plotted in Figures 6.10 and 6.11, respectively. These stresses were calculated from the average of the measured strains from tests P2b and P3c using E_p of 310 MPa (also obtained from the constitutive model of Zhang and Moore (1997) for the appropriate strain rate), ν_p of 0.46 and a strain gauge correction factor of 2.0. Also shown in these figures are the maximum and minimum calculated stresses based on strain readings from tests P2b and P3c.

Figure 6.10 shows compressive hoop stresses at the interior springlines and the exterior crown and invert locations. Hoop stresses at the crown and invert on the interior surface are tensile, as well as at the exterior springlines. Maximum compressive hoop stresses of roughly -15 MPa were calculated at the interior springline location (Fig. 6.10a).

The maximum tensile stress occurs at the interior invert given the larger tensile hoop and axial strains measured at this location. Tensile stresses up to 10 MPa were calculated at the interior invert.

The axial stresses plotted in Figure 6.11 show similar distributions around the pipe as observed for the hoop stresses. The maximum compressive axial stress of roughly -5 MPa was calculated at the interior springlines and exterior invert. The largest tensile axial stress of roughly 6 MPa occurred at the interior invert location. The magnitude of these stresses are next compared with the short-term strength of the polyethylene material.

6.7.3 Implications for Pipe Performance

6.7.3.1 Comparison With Short-Term Strength

One criterion to ensure the adequate structural performance of the pipe may be to limit the hoop stress or strain to some value. For this approach, either tensile stresses are kept below

the tensile yield stress, and compressive stresses are maintained below the compressive yield stress or alternatively, tensile strains are kept below the tensile yield strain, and compressive strains are maintained below the compressive yield strain. Selection of appropriate values of either yield stress or strain is complicated by the stress-strain response for polyethylene, since there is no distinguishable yield stress for this material (if one defines the yield stress as the onset of plastic deformation) as plastic deformations occur even at small strains (Zhang and Moore 1997).

Strength is sometimes characterised by the ultimate stress, which often occurs at very large strains. Zhang and Moore (1997) conducted uniaxial compression tests on the polyethylene material used for these pipes at constant strain rates varying from 10^{-1} to 10^{-5} sec^{-1} , and found that the stress-strain response is highly dependent on the strain rate. Estimates of the short-term strength of polyethylene can be made using the viscoplastic constitutive model of Zhang and Moore (1997). To permit such a calculation, extrapolation to a much slower strain is required (average strain rate for tests P2b and P3c is approximately 10^{-7} sec^{-1}).

A rectangular block was modelled with the maximum corrected tensile hoop strain at 900 kPa (P3c - DI270) and the corresponding axial strain prescribed on the boundaries to estimate both the stress corresponding to the largest tensile hoop strain, and the ultimate stress for the average strain rate (ie. total strain / total time) for test P3c. This analysis provided a tensile hoop stress of approximately 8 MPa (at 3% strain) at location DI270, which is less than the ultimate tensile stress of roughly 15 MPa (at greater than 8% strain) for this particular strain rate (Figure 6.12a). Similar analysis conducted for the maximum

measured compressive strain (P3c - CI180) yielded a maximum compressive hoop stress of 11.8 MPa, which is also less than the estimated short-term strength shown in Figure 6.12b.

Thus, the maximum tensile and compressive stresses calculated at the interior invert and springline are less than the short-term strength of the material, even up to 900 kPa vertical surcharge for the particular strain rate and conditions tested.

6.7.3.2 Long-Term Performance

Consideration of the long-term response of these pipes is complicated by very slow strain rates in the field. Also, after construction is completed the pipe will experience stress relaxation. It is difficult to infer the long-term response of these pipes from relatively short-term tests.

Pipe failure from stress cracking is an important consideration for the long-term performance of these polymer structures. Stress cracking is a brittle failure mechanism that occurs at tensile stresses well below the ultimate stress and is a common concern for pressurised plastic pipes. The necessary elements for stress cracking are tensile stresses and a small defect or crack for initiation of the rupture.

Conditions conducive to stress cracking exist for leachate collection pipes. Axial cracking of the pipe at locations distant from butt fusion joints, and circumferential cracking at the butt fusion joints are the likely modes of failure for leachate collection pipes. This assertion is based on the work of Parmar and Bowman (1989), who reported on the brittle failure of polyethylene pipes with butt-fusion joints subject to internal pressure. Tensile hoop stresses may lead to axial cracking, with the crack often initiating at a local defect in

the material. The fusion process involved in joining sections of pipe together may induce circumferential cracks that could propagate under tensile axial stresses.

The hydrostatic design basis (HDB) is often used to limit the long-term tensile stresses in pressurized thermoplastic pipes. The HDB value is found by testing the pipe subject to uniform (i.e. hydrostatic) internal pressure for various times-to-failure. The hoop stress extrapolated to 10^5 hours on a logarithmic plot of stress versus time-to-failure is defined as the HDB stress (see ASTM Test Standard D 2837 for details). The pipes tested in this work have a HDB equal to 8.6 MPa. It is common practice to limit the working stresses to one-half of the HDB, giving a hydrostatic design stress (HDS) of 4.3 MPa.

The consequences of stress cracking may be quite different for pressurized pipes and gravity-flow drainage pipes. Stress cracking in pressure pipes ultimately leads to failure of the pipe involving the development of leaks and loss of pressure. The HDB is a well accepted and generally successful basis for pressure rating thermoplastic pipe (Mruk 1990). However, the implications of stress cracking in a leachate collection pipe may not be as severe as for pressurized pipes. Provided that the pipe does not collapse, it could still perform its intended design function (that is to provide a pathway for liquid drainage) if cracks develop.

The extent to which a crack can propagate also differs between pressurised pipes and gravity flow pipes subject to earth pressures. For a pipe under internal pressure, the hoop stresses in the pipe wall are generally tensile (depending on the internal pressure relative to the external pressures). Once a crack is initiated, the stress conditions are conducive to propagation of the crack through the entire thickness of the pipe, ultimately leading to failure of the pressurised pipe. However, when subject to external, biaxially compressive earth

pressures (ie. in a landfill), at no point around the pipe circumference do tensile hoop stresses exist on both the interior and exterior surfaces of the pipe, recall Figure 6.10. The only exception may be at the pipe haunches where local effects from the gravel backfill lead to tensile stresses - but these tensile stresses are well below the HDS even in the short term prior to stress relaxation. Conceivably, a crack could initiate and propagate at the location of maximum tensile hoop stress (ie. interior invert), but then crack growth may be retarded when it reaches compressive stresses that prevail at the exterior surface at this location. The effect on the pipe response if an axial crack develops at the interior invert is uncertain. It is possible that progressive failure of the pipe could result. Since stresses are redistributed with cracks in a bending situation, propagation of a crack through the wall may or may not be possible. This issue requires additional research.

Stress conditions in landfill pipes are also conducive to propagation of circumferential cracks induced by the butt fusion seaming. Again, tensile stresses do not prevail through the entire wall thickness, which may limit the extent to which a crack can propagate. Parmar and Bowman (1989) indicated that removal of the internal weld bead (heated polyethylene material that “rolls-into” the pipe under pressure and subsequently cools - where cracks may initiate) relocated the failure away from the butt fusion joint and increased the fatigue life of the pipe. For critical applications, one may wish to undertake the potentially expensive removal of the interior weld beads to reduce the potential for circumferential cracking - provided that during the process of bead removal additional cracks or defects are not induced.

The maximum tensile stress estimated from the short-term laboratory tests of 8 MPa at an applied surcharge of 900 kPa is less than the hydrostatic design basis of 8.6 MPa, but

larger than the hydrostatic design stress (which includes a factor of safety of two). The use of design criteria for pressurised pipes (ie. limiting tensile stresses to 4.3 MPa) may be overly conservative for nonpressurised applications since the implications and extent of stress cracking may be less critical for leachate collection pipes. Given that the pipe stresses for a real landfill situation are likely to be smaller than those estimated from these tests (because of stress relaxation), and that the short-term deflections are less than empirical design limits, adequate structural performance of the pipe (for the specific gravel material, and perforation size and pattern tested) could be expected up to vertical pressures of 900 kPa, if a reduced factor of safety for leachate collection pipes (relative to pressurised pipes) is accepted. For critical applications, it may be prudent to limit the long-term tensile stresses to the hydrostatic design stress.

Further research is warranted to study the long term performance of these buried structures. Resolution of issues such as the degree to which the stresses in the pipe decrease over time and the propagation of cracks in a pipe subject to biaxially compressive earth loading would be useful for the design of these buried pipes. Any such work is complicated by the extremely long time frames involved and the complexity of the constitutive response of high density polyethylene.

6.8 COMPARISON OF PIPE DEFLECTIONS WITH DESIGN PROCEDURES

Limiting the change in geometry of the pipe section is one structural performance criterion often considered when specifying leachate collection pipes. Various methods are available

to estimate the pipe deflection for a proposed design. Calculations of deflections are now presented for the pipe tested (220 mm OD, SDR 9) backfilled with uncompacted, coarse gravel, subject to an overburden pressure of 250 kPa. These calculations are intended to provide a comparison of diameter changes between design values and those measured in the laboratory tests. Deflections are calculated using semi-empirical and theoretically based procedures. For all cases, key parameters related to the stiffness of the soil are obtained from recommended values published in the literature. Calculations were performed with the AASHTO (1996) values for polyethylene pipe modulus of 758 MPa (short term) and 152 MPa (long term). Calculations are also included using a better estimate of polyethylene modulus of 420 MPa corresponding to an average strain rate for strains up to 250 kPa, made from the constitutive model of Zhang and Moore (1997). The results are summarized in Table 6.11.

6.8.1 Modified Iowa Equation

One commonly used method to estimate pipe deflections is the Modified Iowa equation (e.g., see Howard 1977). This semi-empirical equation was originally developed to predict the horizontal diameter change of flexible metal pipes. Estimates of pipe deflection are a function of: soil support (characterised by the modulus of soil reaction, E'), pipe stiffness, and empirical deflection lag (D) and bedding constant (k) parameters. Calculated deflections are largely dependent on the empirical parameter E' , which is a function of soil modulus, pipe size, type of material, and ratio of horizontal to vertical stresses (Gumbel 1983). Koerner (1998), Oweis and Khera (1998) and USEPA (1983) recommend the use of this method, along with the E' values of Howard to calculate the pipe deflection for landfill pipes.

Diameter changes calculated using the Modified Iowa equation are presented in Table 6.11 for a range of E' values that Howard (1977) recommends for use with crushed rock material (7 MPa for uncompacted, to 20 MPa for compacted conditions). The diameter change calculated with the lower E' value (to represent material dumped in place) and the short term pipe modulus, is larger than the measured vertical diameter change by a factor of two. The Modified Iowa equation assumes that the full prism load acts on the pipe. This neglects the redistribution of stresses (ie. arching) which may occur because of the difference in stiffness between the pipe and the backfill material.

Also, the Modified Iowa equation is generally used under the assumption that vertical and horizontal diameter changes are of equal magnitude and opposite sign. For polyethylene pipes this is not necessarily the case, as the pipe experiences some circumferential shortening. As a result, the estimate of ΔD_h using the Iowa equation ($E_p=758$ MPa, $E'=7$ MPa) is nearly three times the measured value.

Increasing E' from 7 MPa to 20 MPa (with $E_p=758$ MPa) decreases the calculated pipe deflections, however they are still larger than the measured values. Using the long term polyethylene modulus yields larger deflections, particularly for the case with the lower value of E' . Conceivably, a better estimate of E' for use in the Modified Iowa equation could be made based on the measured deflections, or even from empirical relationships with the elastic soil modulus (Selig 1990). However, care is required because of the empirical nature of the Modified Iowa equation. Values of E' equal to 43 and 56 MPa were back-calculated from the measured values at Section C.

6.8.2 Elastic Continuum Approach - Thin Tube Theory

Calculations of pipe deflection based on the theoretical solution of Höeg (1968) are also included in Table 6.11. This solution considers the plane strain response of a thin, elastic, circular tube buried within an elastic, isotropic, homogeneous medium subject to biaxial stresses applied distant from the pipe. This approach explicitly considers the stiffness of the soil (Young's modulus E_s and Poisson's ratio ν_s) and the pipe (E_p and ν_p) as well as the loading conditions similar to those under deep burial in a landfill.

Estimates of elastic soil modulus can be made from the data of Selig (1990). For appropriate levels of confining stress, E_s may vary between 20 to 40 MPa, for 85% and 95% of maximum dry density compaction levels (ASTM D698 test). Values are also shown for E_s equal to 25 MPa and 30 MPa.

Calculations using the AASHTO short term pipe modulus and $E_s=20$ MPa are slightly larger than the measured results. The calculated vertical diameter changes are larger than the calculated horizontal diameter changes by factors ranging from 1.2 to 1.4 (for $E_p=758$ MPa), depending on the soil modulus. This is consistent with the measured laboratory results, where ΔD_v is 1.3 times larger than ΔD_h . The elastic continuum approach estimates the mode of deformation similar to that measured in the laboratory tests.

The sensitivity of calculated values to changes in soil and pipe modulus are also shown in Table 6.11. Decreasing the polyethylene modulus to the AASHTO long term value of 152 MPa results in larger values of vertical diameter change, where as the horizontal diameter calculated may be smaller depending on the soil stiffness relative to that of the pipe.

Thin ring theory, as assumed by Höeg, is typically satisfactory for pipes with an SDR greater than 50. However leachate collection pipes typically are much thicker than this limit.

Although thin tube theory assumes no radial variation of hoop stresses through the pipe wall and negligible radial stresses compared to the hoop stresses, the assumption of thin pipe response for use with thick leachate collection pipes was sufficiently close to deformations obtained using the thick elastic tube theory of Moore (1990).

There is good agreement between calculations using E_p equal to 420 MPa (appropriate for the strain rate and time of the laboratory results at 250 kPa) and E_s of 25 MPa and the measured values in the laboratory. The use of the thin elastic solution is recommended to estimate the deformation of leachate collection pipes. This method of analysis also allows calculation of stresses within the pipe.

6.9 SUMMARY AND CONCLUSIONS

High density polyethylene drainage pipes are extensively used in landfill leachate collection systems because of their excellent resistance to chemical degradation, relative ease of construction and overall good performance. However, certain design issues that are intended to minimize the extent of biologically induced clogging of the leachate collection system (e.g., the use of coarse drainage gravel and large perforations) give rise to conditions not typically experienced by pipes in more conventional gravity-flow-sewer applications. Large scale laboratory tests were conducted to assess the influence of coarse gravel backfill and large perforations on the structural response of leachate collection pipes.

The testing conditions were selected to simulate the conditions expected to prevail in a landfill. Three different pipe sections, instrumented with displacement transducers and

electrical foil strain gauges, were tested subject to large vertical surcharges (up to 900 kPa) applied over relatively short time periods (relative to real conditions). The principal objective of these tests was to measure the effect of coarse drainage gravel on the mechanical response of these perforated pipes.

The magnitude of pipe deflections were larger when tested with coarse gravel backfill than recorded with sand backfill. Overall, the stiffness of the coarse gravel was found to be less than that of the compact sand material. Volumetric effects resulting from the rearrangement of gravel particles during the test is a likely contributing factor to the softer response observed for the coarse gravel.

For the 220 mm OD, SDR 9 HDPE pipes tested with coarse gravel backfill, the average vertical and horizontal diameter changes were approximately -1% and 0.8%, of the mean diameter at an applied pressure of 250 kPa (representative stresses for a medium size landfill with 20 to 25 metres of waste). When subject to a vertical pressure of 900 kPa, the changes in vertical and horizontal diameter were roughly -5% and 3% of the mean pipe diameter. These measured changes in geometry are less than empirical limits generally specified in codes of practice. Thus based on consideration of deformations, the pipes tested in the coarse gravel with perforations up to 1.5t in diameter (37.5 mm) performed adequately under short term vertical pressures of up to 900 kPa.

Greater variations in deflections were observed for the coarse gravel material relative to the sand backfill. The support provided by the sand backfill tended to be relatively uniform (the small sand particles provide essentially continuous support around the pipe circumference), whereas the coarse gravel will provide nonuniform support (discontinuous support from discrete contact points randomly distributed around the circumference). The

deflections varied between 30 to 50% (at a vertical surcharge of 250 kPa) when tested in the simulated landfill conditions.

Maximum compressive hoop strains were measured at the interior springline; maximum tensile hoop strains were recorded at the interior invert. Tensile axial strains, also a maximum at the interior invert, were measured for the pipe as a result of local bending effects from the gravel and the end conditions imposed during the tests, resulting in larger tensile stresses relative to axial plane strain conditions. Both hoop and axial strains were heavily influenced by local bending effects caused by the coarse gravel backfill.

Measured values of surface strain also showed considerable variations when tested in the simulated landfill conditions. The variations, largely imposed by the gravel, were studied at a vertical pressure of 250 kPa. It was found that maximum strains of roughly twice the average value occur because of the coarse gravel backfill. Similar variations were found when the pipe was subjected to larger vertical pressures.

No discernable effect from the perforations was noticed on either the pipe deformations or surface strains. This appears to be reasonable given that the cross-sectional area of the pipe (per unit length) is reduced by only 3%, even with these relatively large perforations, because of the thickness of the pipe. Local effects around the perforation may be important considerations for the performance of the pipe and will be the subject of future work.

Estimates of the stresses in the pipe (based on the measured strains) indicate that these structures should perform well when subject to 250 kPa of vertical surcharge, since the maximum short-term tensile stresses are below the allowable long-term hydrostatic design stress for this material.

Stress conditions conducive to stress cracking do prevail for leachate collection pipes and are worsened when backfilled in coarse gravel from local bending induced by the discrete gravel contacts. Cracks are most likely to propagate in the axial direction from tensile hoop stresses, and at butt fusion joints in the circumferential direction from tensile axial stresses. Stress conditions are not as severe for stress cracking as for pressure pipes, as tensile stresses do not exist through the entire thickness of the pipe wall when subject to biaxially compressive earth pressures. While the implications of cracking on the structural response of the pipe are unknown, conceivably the landfill drainage pipe could still perform its intended function if cracks propagated to a limited extent, retarded by compressive stresses on the opposite fibre of the pipe wall.

Estimates of pipe stresses at higher pressures (up to 900 kPa) are below the short-term strength calculated using a viscoplastic constitutive model for this material. These short-term stresses are roughly equal to the hydrostatic design basis, which is the unfactored long-term tensile strength used in the design of pressurised pipes. Acceptance of a lower factor of safety applied to the hydrostatic design basis than that used for pressurised pipes suggests that the 220 mm OD, SDR 9 pipe tested (for the given backfill materials, loading conditions and perforation details) the pipe could be expected to perform its intended function when subject to vertical pressures up to 900 kPa. For critical applications, it may be prudent to limit the long-term tensile stresses to levels below the hydrostatic design stress. Further work is required to confirm the long-term performance of these pipes.

The use of the Modified Iowa equation is not recommended to calculate the vertical deflection of the pipe. It was found that using published values of modulus of soil reaction (E') for use in the Modified Iowa equation yielded much larger values of pipe diameter

change. Also, this method neglects the soil-structure interaction between the soil and the pipe, and predicts the wrong mode of deformation. Analysis based on thin elastic tube theory and elastic continuum theory for the surrounding backfill provided good estimates of pipe deflection when compared with measured laboratory results.

Although coarse gravel backfill does impose adverse support conditions relative to sand backfill, the measured variations of deflection and strain do not, however, preclude the use of coarse 50 mm gravel in direct contact with leachate collection pipes. In fact, the 220 mm OD, SDR 9 pipe would be expected to perform well in a medium-size landfill (vertical pressures up to 250 kPa) for the given gravel and perforation size and pattern tested.

6.10 REFERENCES

AASHTO (1996) *Standard Specifications for Highway Bridges*, 16th Edition, American Association of State Highway and Transportation Officials, Washington, DC, USA.

ASTM (1993) Standard Specification for Polyethylene (PE) Large Diameter Profile Wall Sewer and Drain Pipe, Designation F-17F 894 - 93b, American Society for Testing and Materials, Philadelphia, PA, USA.

ATV (1984) Guidelines for Static Calculation of Drainage Conduits and Pipelines, The German Wastewater Association, (Gesellschaft zur Forerung der Abwassertechnik, E.V.)

- Beatty, M.F., and Chewning, S.W. 1979. "Numerical analysis of the reinforcement effect of a strain gauge applied to a soft material", *International Journal of Engineering Science*, Vol. 17, pp. 907 - 915.
- Brachman, R.W.I. (1997) "Hoop Compression Testing of HDPE leachate Collection Pipe", *Geosynthetics '97*, IFAI, Long Beach, CA, USA, pp. 337 - 350.
- Brachman, R.W.I., Moore, I.D., and Rowe, R.K. (1996) "Interpretation of a Buried Pipe Test: Small Diameter Pipe in the Ohio University Facility", *Transportation Research Record*, 1541, pp. 64 - 70.
- Brachman, R.W.I., Moore, I.D., and Rowe, R.K. (1999) "The Design of a Laboratory Facility for Evaluating the Structural Performance of Small Diameter Buried Pipes", *Canadian Geotechnical Journal*, (Accepted 25/01/99).
- CSA (1987) CAN / CSA-b182.7-87 Plastic Drain and Sewer Pipe and Fittings, fourth edition, December 1987. Canadian Standards Association.
- Chau, K.M. (1986) *Time-dependent interaction of soil and flexible pipe*, Ph.D. Thesis, Texas A & M University, USA.
- Fleming, I.R., Rowe, R.K., and Cullimore, D.R. (1999) "Field Observations of Clogging in a Landfill Leachate Collection System", *Canadian Geotechnical Journal*, (accepted).
- Gumbel, J.E. (1983) *Analysis and Design of Buried Flexible Pipes*, Ph.D. Thesis, Department of Civil Engineering, The University of Surrey, United Kingdom.
- Höeg, K. (1968) "Stresses Against Underground Structural Cylinders", *Journal of the Soil Mechanics and Foundations Division*, Proceedings of the American Society of Civil Engineers, SM4, pp. 833-858.

- Howard, A.K. (1977) "Modulus of Soil Reaction Values for Buried Flexible Pipe", *Journal of the Geotechnical Engineering Division*, Proceedings of the American Society of Civil Engineers, Vol. 103, GT 1, pp. 33-43.
- Koerner, R.M. (1998) *Designing With Geosynthetics*, 4th Edition, Prentice Hall.
- Moore, I.D., and Hu., F. (1996) "Linear viscoelastic modelling of profiled high density polyethylene pipe" *Canadian Journal of Civil Engineering*, Vol. 23, No. 2, pp. 395-407.
- Moore, I.D. (1990) "Three Dimensional Response of Elastic Buried Tubes", *International Journal of Solids and Structures*, Vol. 26, No. 4, pp. 391 - 400.
- Moore, I.D. (1993) "Structural design of profiled polyethylene pipe - Part I - Deep burial", Geotechnical Research Centre Report GEOT-8-93, The University of Western Ontario, London, Canada.
- Oweis, I.S., and Khera, R.P. (1998) *Geotechnology of Waste Management*, 2nd Edition, PWS publishing Company, Boston, USA.
- Parmar, R., and Bowman, J. (1989) "Crack Initiation and Propagation Paths for Brittle Failures in Aligned and Misaligned Pipe Butt Fusion Joints", *Polymer Engineering and Science*, Vol. 29, No. 19, pp. 1396-1405.
- Rowe, R. K., Quigley, R.M., and Booker, J.R. (1995) *Clayey Barrier Systems for Waste Disposal Facilities*, E & FN Spon (Chapman & Hall), London.
- Rowe, R.K., Caers, C.J., and Chan, C. (1993) "Evaluation of a Compacted Till Liner Pad Constructed Over a Granular Subliner Contingency Layer", *Canadian Geotechnical Journal*, Vol. 37, No. 4, pp. 241-689.
- Sargand, S.M. (1993) "Structural Performance of an HDPE Leachate Collection Pipe", *31st Annual International Solid Waste Exposition*, San Jose, CA, USA, pp. 381 - 402.

- Selig, E.T. (1990) "Soil Properties for Plastic Pipe Installations", *Buried Plastic Pipe Technology*, ASTM STP 1093, G.S. Buczala and M.J. Cassady (Eds.), ASCE, pp. 141 - 158.
- Snedecor, G.W., and Cochran, W.G. (1989) *Statistical Methods*, Iowa State University Press, Ames, Iowa.
- Tognon, A.R.M., Rowe, R.K., and Brachman, R.W.I. (1999) "Evaluation of Sidewall Friction for a Buried Pipe Testing Facility". *Geotextiles and Geomembranes*, 17 (4), (In Press).
- Tognon, A.R.M. (1999) Laboratory Investigation of Barrier System Components, M.E.Sc. Thesis, The University of Western Ontario, London, Canada.
- USEPA (1983) *Lining of Waste Impoundment and Disposal Facilities*, SW-870, Environmental Protection Agency, Cincinnati, OH, USA.
- Watkins, R.K. (1987) *Structural Performance of Perforated and Slotted High-Density Polyethylene Pipes Under High Soil Cover*, Report Submitted to King County Solid Waste, Seattle, WA, USA, 13 p.
- Zanzinger, H., and Gartung, E. (1995) "Large-scale Model Tests of Leachate Collection Pipes in Landfills Under Heavy Loads", *Advances in Underground Pipeline Engineering*, J.K. Jeyapalan and M. Jeyapalan (Eds.), ASCE, pp. 114 - 125.
- Zanzinger, H., and Gartung, E. (1998) "HDPE-Geopipes, Soil-Structure Interaction", *Sixth International Conference on Geosynthetics*, IFAI, Atlanta, GA, USA, pp. 197-200.
- Zhang, C., and Moore, I.D. (1997) "Nonlinear Mechanical Response of High Density Polyethylene. Part I: Experimental Investigation and Model Evaluation", *Polymer Engineering and Science*, Vol. 37, No. 2, pp. 404-413.

Table 6.1 Summary of Tests

Test	Pipe	Perforation Details	Maximum Pressure (kPa)	Description
P2a	P2	None	600	Test plain pipe under idealized conditions with sand backfill only.
P2b	P2	None	900	Test plain pipe response under simulated landfill conditions.
P3a	P3	$D_p = t$ ¹	250	Test perforated pipe at lower applied pressure to limit permanent deformation.
P3b	P3	$D_p = t$	250	Test perforated pipe at lower applied pressure to limit permanent deformation.
P3c	P3	$D_p = t$	900	Test perforated pipe up to large applied pressure.
P4	P4	$D_p = 1.5t$	750	Test larger perforation size.

¹ D_p is the diameter of the perforation; t is the average thickness of the pipe ($t = 25$ mm).

Table 6.2 Comparison of diameter changes ΔD for tests P2a and P2b at an applied bladder pressure of 600 kPa (deflections in mm). Note that ΔD_v is the vertical diameter change and ΔD_h is the horizontal diameter change.

Test		Section		
		B	C	D
P2a	ΔD_v (mm)	-3.0	-	-3.1
	ΔD_h (mm)	1.8	1.8	-
P2b	ΔD_v (mm)	-4.2	-6.2	-5.1
	ΔD_h (mm)	3.9	4.4	-

Table 6.3 Comparison of diameter changes ΔD for tests P2b, P3a, P3b, P3c and P4 reported at Sections B, C and D at an applied bladder pressure of 250 kPa.

Test	Vertical Diameter Change ΔD_v (mm)			Horizontal Diameter Change ΔD_h (mm)		
	B	C	D	B	C	D
P2b	-1.6	-2.2	-1.8	1.4	1.6	-
P3a	-2.2	-2.5	-2.3	-	1.8	1.8
P3b	-1.7	-1.5	-1.6	1.5	1.3	1.2
P3c	-1.4	-1.2	-1.6	1.1	1.1	1.3
P4	-1.9	-2.0	-2.1	1.5	1.6	-

Table 6.4 Summary of descriptive statistical parameters for vertical and horizontal diameter changes measured at Sections B, C and D for tests P2b, P3a, P3b, P3c, and P4 at 250 kPa.

Statistic	Vertical Diameter Change ΔD_v (mm)			Horizontal Diameter Change ΔD_h (mm)		
	B	C	D	B	C	D
Mean	-1.7	-1.9	-1.9	1.4	1.5	1.4
Standard Deviation	0.3	0.5	0.3	0.2	0.3	0.3
Coefficient of Variation	17%	28%	17%	14%	19%	22%
95% Confidence Level	± 0.4	± 0.7	± 0.4	± 0.3	± 0.4	± 0.8

Table 6.5 Comparison of hoop and axial strains at the interior springlines for tests P3a, P3b, and P3c at an applied bladder pressure of 250 kPa.

	P3a		P3b		P3c		P3a, P3b and P3c		
	ϵ_{θ} ($\mu\epsilon$)	ϵ_z ($\mu\epsilon$)	ϵ_{θ} ($\mu\epsilon$)	ϵ_z ($\mu\epsilon$)	ϵ_{θ} ($\mu\epsilon$)	ϵ_z ($\mu\epsilon$)	ϵ_{θ} ($\mu\epsilon$)	ϵ_z ($\mu\epsilon$)	
CI0	-6150	1900	-3600	1000	-4100	1300			
CI180	-5000	1300	-4900	1200	-4500	900			
							Mean	-4700	1300
							Standard Deviation	900	300
							Coefficient of Variation	19%	26%
BI0	-4400	600	-2800	500	-3100	600			
BI180	-4500	850	-3550	700	-3450	500			
DI0	-4800	700	-2550	900	-3450	200			
DI180	-3900	400	-	800	-	700			
							Mean	-3650	600
							Standard Deviation	800	200
							Coefficient of Variation	21%	33%

Table 6.6 Comparison of hoop and axial strains at the interior crown and invert for tests P3a, P3b, and P3c at an applied bladder pressure of 250 kPa.

Location		P3a		P3b		P3c	
		ϵ_{θ} ($\mu\epsilon$)	ϵ_z ($\mu\epsilon$)	ϵ_{θ} ($\mu\epsilon$)	ϵ_z ($\mu\epsilon$)	ϵ_{θ} ($\mu\epsilon$)	ϵ_z ($\mu\epsilon$)
Crown	CI90	1400	1150	1500	200	1200	400
	BI90	2750	-300	2200	200	1650	-150
	DI90	1500	100	900	300	1450	-0
Invert	CI270	4100	300	1300	1050	650	550
	BI270	2700	-200	3100	-450	1300	1100
	DI270	4800	500	3300	100	3050	-700

Table 6.7 Comparison of hoop and axial strains at the exterior springlines for tests P3a, P3b, and P3c at an applied bladder pressure of 250 kPa.

	P3a		P3b		P3c		P3a, P3b and P3c		
	ϵ_{θ} ($\mu\epsilon$)	ϵ_z ($\mu\epsilon$)	ϵ_{θ} ($\mu\epsilon$)	ϵ_z ($\mu\epsilon$)	ϵ_{θ} ($\mu\epsilon$)	ϵ_z ($\mu\epsilon$)	ϵ_{θ} ($\mu\epsilon$)	ϵ_z ($\mu\epsilon$)	
CE0	1500	950	1200	300	1300	0			
CE180	1450	750	1600	650	1450	500			
							Mean	1400	500
							Standard Deviation	150	300
							Coefficient of Variation	10%	60%
BE0	1550	350	1100	350	1000	0			
BE180	1800	-	1800	550	1400	50			
DE0	1900	700	900	0	1400	500			
DE180	1150	500	1550	-300	1000	400			
							Mean	1400	300
							Standard Deviation	350	300
							Coefficient of Variation	26%	109%

Table 6.8 Comparison of hoop and axial strains at the exterior crown and invert for tests P3a, P3b, and P3c at an applied bladder pressure of 250 kPa.

Location		P3a		P3b		P3c	
		ϵ_{θ} ($\mu\epsilon$)	ϵ_z ($\mu\epsilon$)	ϵ_{θ} ($\mu\epsilon$)	ϵ_z ($\mu\epsilon$)	ϵ_{θ} ($\mu\epsilon$)	ϵ_z ($\mu\epsilon$)
Crown	CE90	-2400	300	-1750	950	-2200	550
	BE90	-2600	850	-2100	150	-2200	1000
	DE90	-2100	850	-1800	750	-2100	350
Invert	CE270	-3850	100	-2050	1150	-1650	1400
	BE270	-2000	850	-1900	900	-1500	700
	DE270	-4000	100	-3150	1150	-2650	100

Table 6.9 Summary of measured strains for tests P2b, P3a, P3b, P3c, and P4 at an applied bladder pressure of 250 kPa.

Location		Mean ($\mu\epsilon$)	95% Confidence ($\mu\epsilon$)	Standard Deviation ($\mu\epsilon$)	Coefficient of Variation	Max ϵ ÷ Mean	Number of Data Points
Interior Springline	ϵ_{θ}	-3900	± 400	900	23%	1.6	27
	ϵ_z	800	± 160	400	47%	2.4	30
Exterior Springline	ϵ_{θ}	1400	± 100	300	21%	1.5	29
	ϵ_z	400	± 100	300	77%	2.4	28
Interior Crown	ϵ_{θ}	1600	± 300	400	27%	1.7	15
	ϵ_z	300	± 300	400	137%	4	15
Exterior Crown	ϵ_{θ}	-2100	± 200	300	15%	1.3	15
	ϵ_z	600	± 200	300	45%	1.7	15
Interior Invert	ϵ_{θ}	2600	± 800	1300	49%	1.9	15
	ϵ_z	300	± 500	700	210%	4.7	15
Exterior Invert	ϵ_{θ}	-2800	± 900	1300	47%	2.4	15
	ϵ_z	700	± 400	600	76%	1.9	15
Interior Shoulder	ϵ_{θ}	-600	± 500	500	87%	2.3	10
	ϵ_z	700	± 300	400	57%	2	10
Exterior Shoulder	ϵ_{θ}	-900	± 300	400	39%	1.7	10
	ϵ_z	500	± 200	300	59%	1.9	10
Interior Haunch	ϵ_{θ}	-1100	± 1000	1200	104%	2.2	10
	ϵ_z	900	± 400	400	46%	1.8	10
Exterior Haunch	ϵ_{θ}	-200	± 600	700	360%	-6.4	10
	ϵ_z	400	± 400	500	125%	2.7	10

Table 6.10 Calculated hoop and axial stresses in pipe based on average measured strains at an applied bladder pressure of 250 kPa. (Note: $E_p = 420$ MPa, $\nu_p = 0.46$, GCF = 1.4)

Location	Interior		Exterior	
	σ_θ (MPa)	σ_z (MPa)	σ_θ (MPa)	σ_z (MPa)
Springline	-2.6	-0.7	1.2	0.8
Crown	1.3	0.8	-1.4	-0.3
Invert	2.0	1.1	-1.9	-0.4
Shoulder	-0.2	0.3	-0.5	0.1
Haunch	-0.5	0.3	-0.0	0.2

Table 6.11 Comparison of measured and calculated diameter change for 220 mm OD SDR9 pipe at an applied vertical pressure of 250 kPa.

Method	Pipe Deformation (mm)					
	$E_p=758$ MPa ¹		$E_p=420$ MPa ²		$E_p=152$ MPa ³	
	ΔD_v	ΔD_h	ΔD_v	ΔD_h	ΔD_v	ΔD_h
Measured (Sec. C)						
Mean	-1.9	1.5				
Standard Deviation	0.5	0.3				
Modified Iowa ⁴						
$E'=7$ MPa ⁵	-4.1	4.1	-5.9	5.9	-9.4	9.4
$E'=20$ MPa ⁵	-2.6	2.6	-3.3	3.3	-4.2	4.2
$E'=43$ MPa ⁶	-	-	-1.9	1.9	-	-
$E'=56$ MPa ⁷	-	-	-1.5	1.5	-	-
Elastic Continuum ⁸						
Thin Tube Theory						
$E_s=20$ MPa	-1.8	1.5	-2.3	1.8	-3.3	1.9
$E_s=25$ MPa	-1.6	1.3	-2.0	1.5	-2.8	1.5
$E_s=30$ MPa	-1.4	1.1	-1.8	1.3	-2.4	1.2
$E_s=40$ MPa	-1.2	0.9	-1.5	1.0	-2.0	0.9

Notes: $\nu_p=0.46$; ¹ Short term AASHTO modulus; ² Modulus estimated from Zhang and Moore (1997) for average strain rate; ³ Long term AASHTO modulus; ⁴ $D=1$, $k=.083$; ⁵ E' from Howard (1977); ⁶ E' required to match measured ΔD_v ; ⁷ E' required to match measured ΔD_h ; ⁸ E_s estimated from Selig (1990), $\nu_s=0.25$, $K=0.2$.

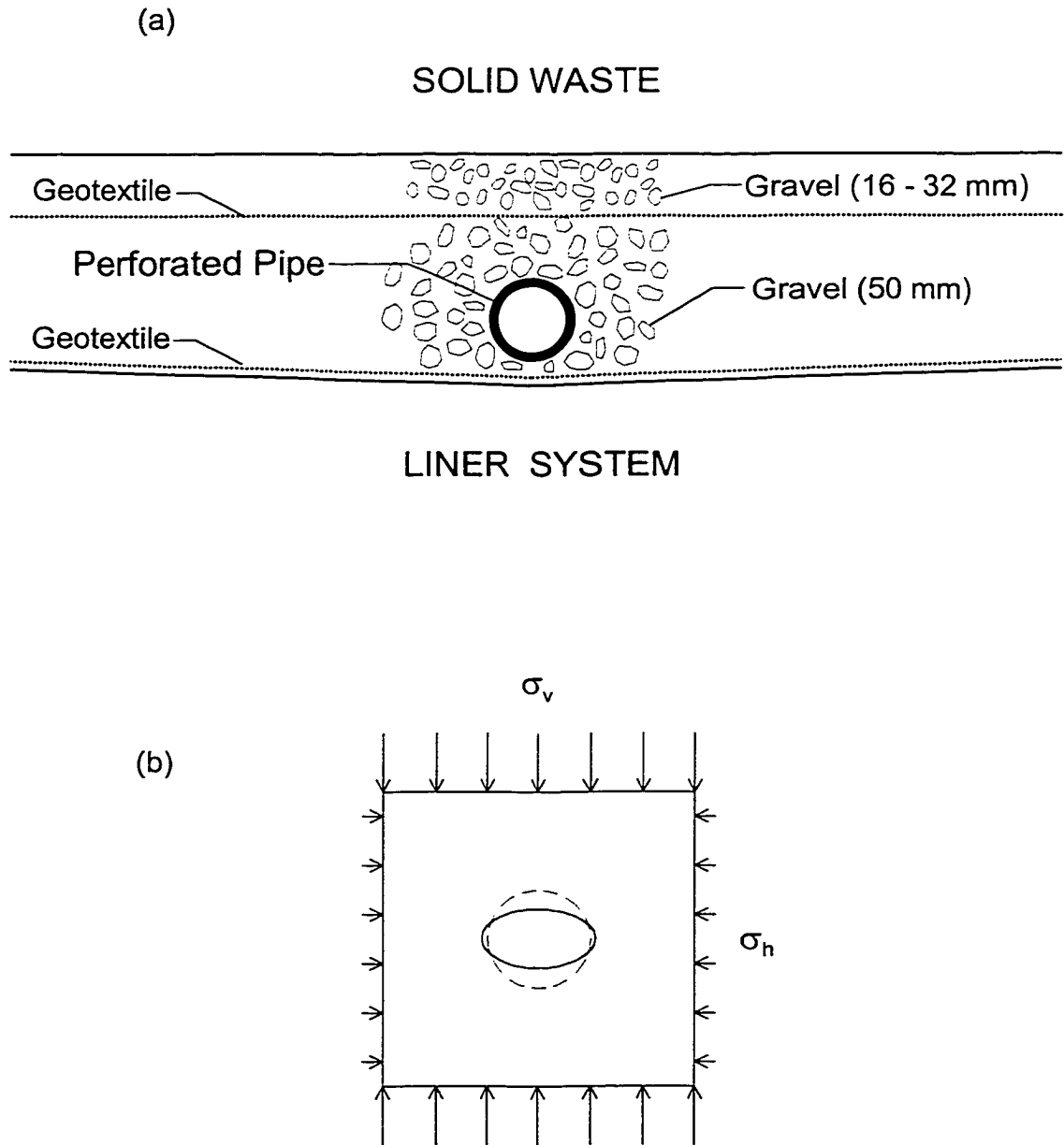


FIGURE 6.1 (a) Cross section through a leachate collection system in a municipal solid waste landfill designed to minimize the extent of biologically induced clogging. (b) Biaxial earth pressures acting distant from the pipe under deep burial.

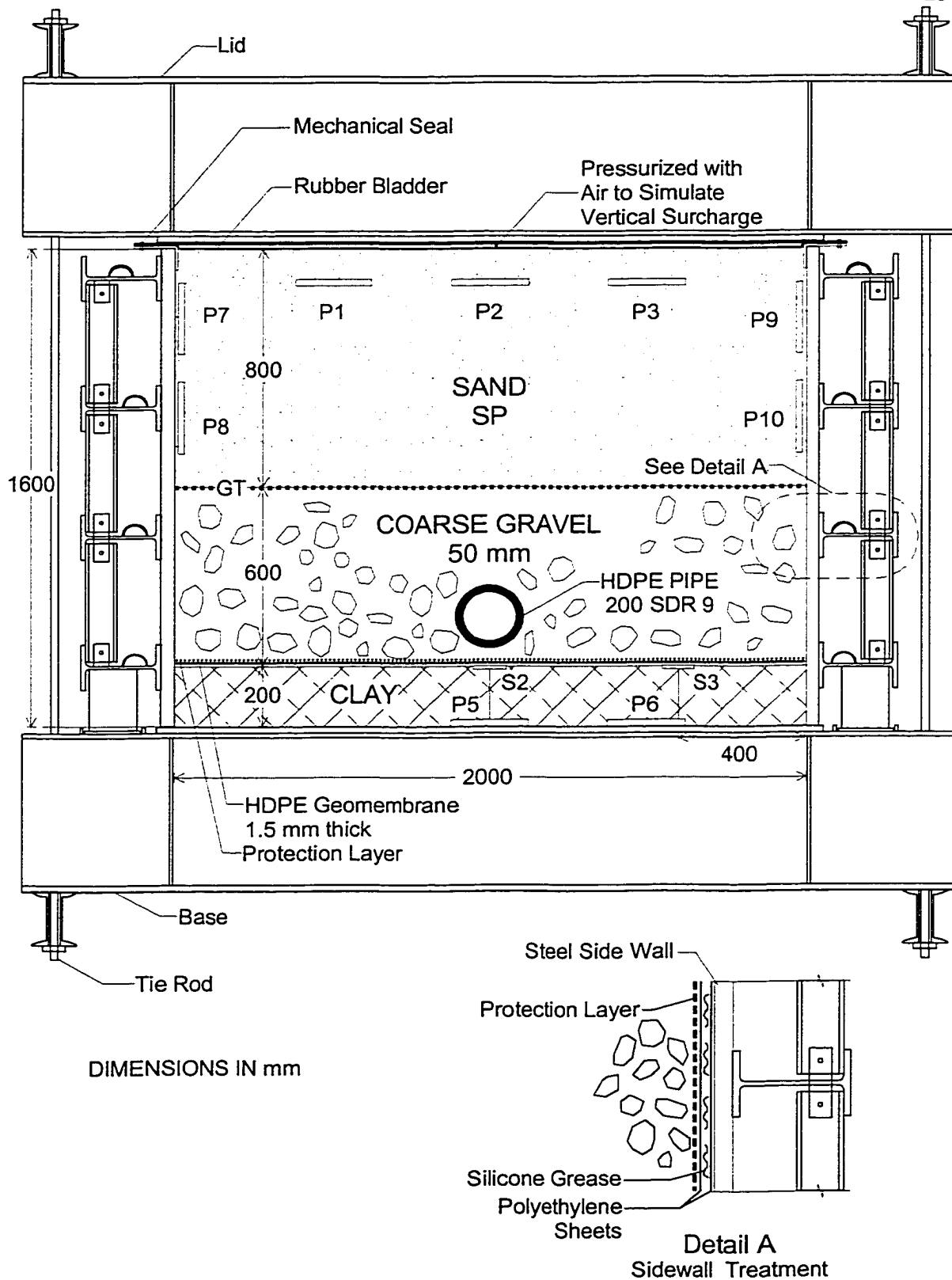


FIGURE 6.2 Transverse section through biaxial compression testing facility.

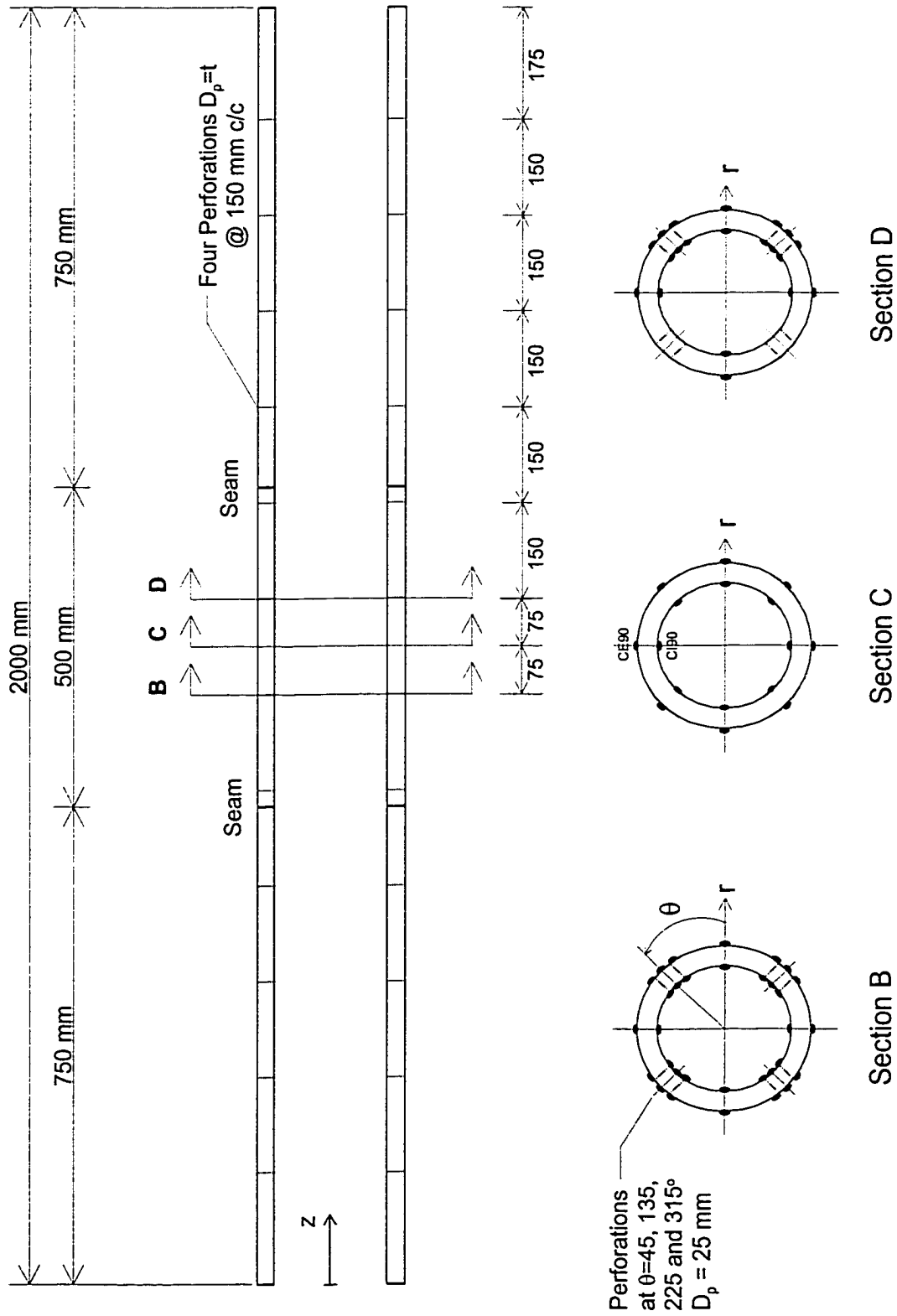


FIGURE 6.3 Location of Strain Gauges for Pipe Specimen 3.

(220 mm OD, SDR9)

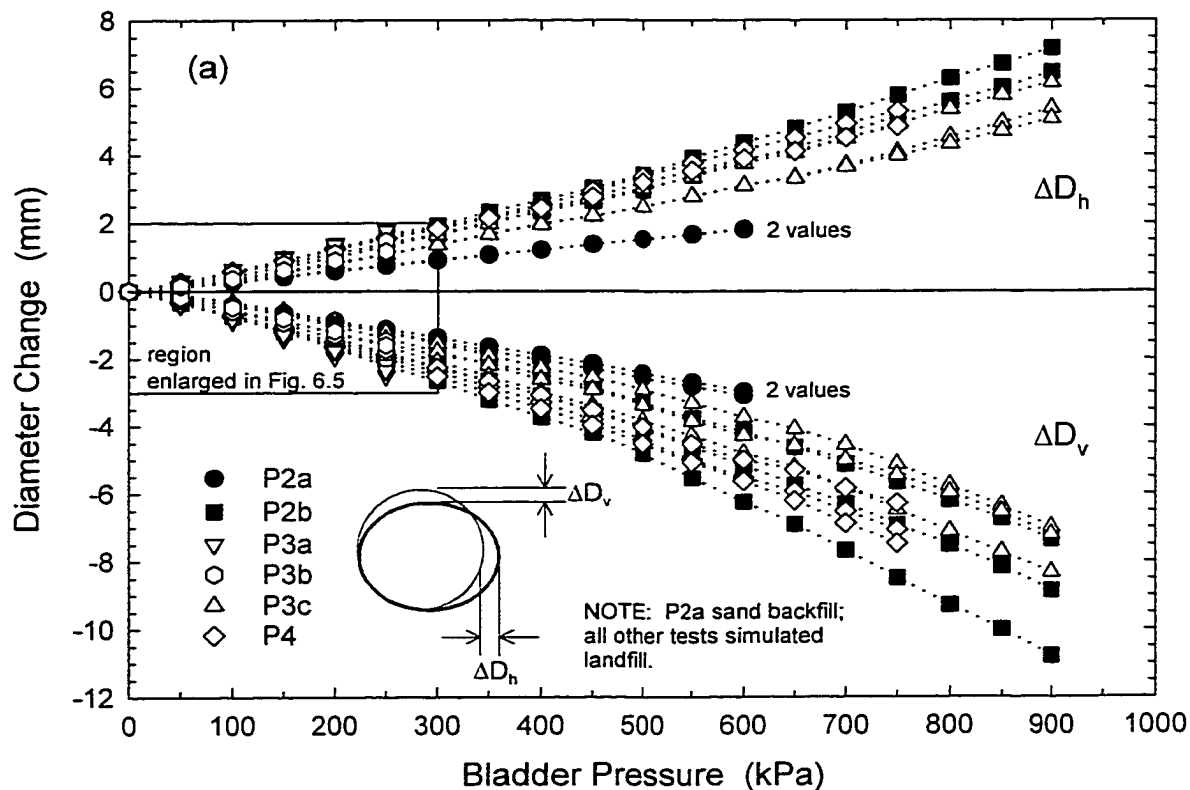


FIGURE 6.4 Measured vertical ΔD_v and horizontal ΔD_h diameter change for all tests.

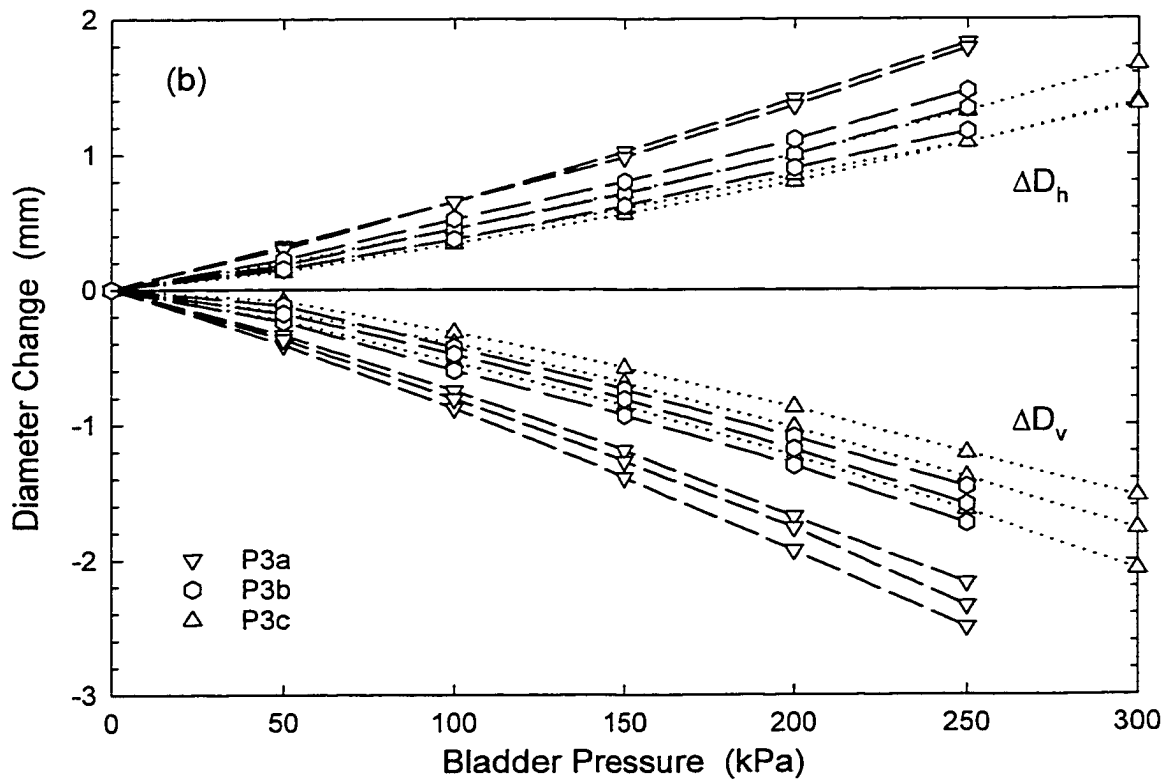


FIGURE 6.5 Vertical ΔD_v and horizontal ΔD_h diameter change for pipe P3 only.

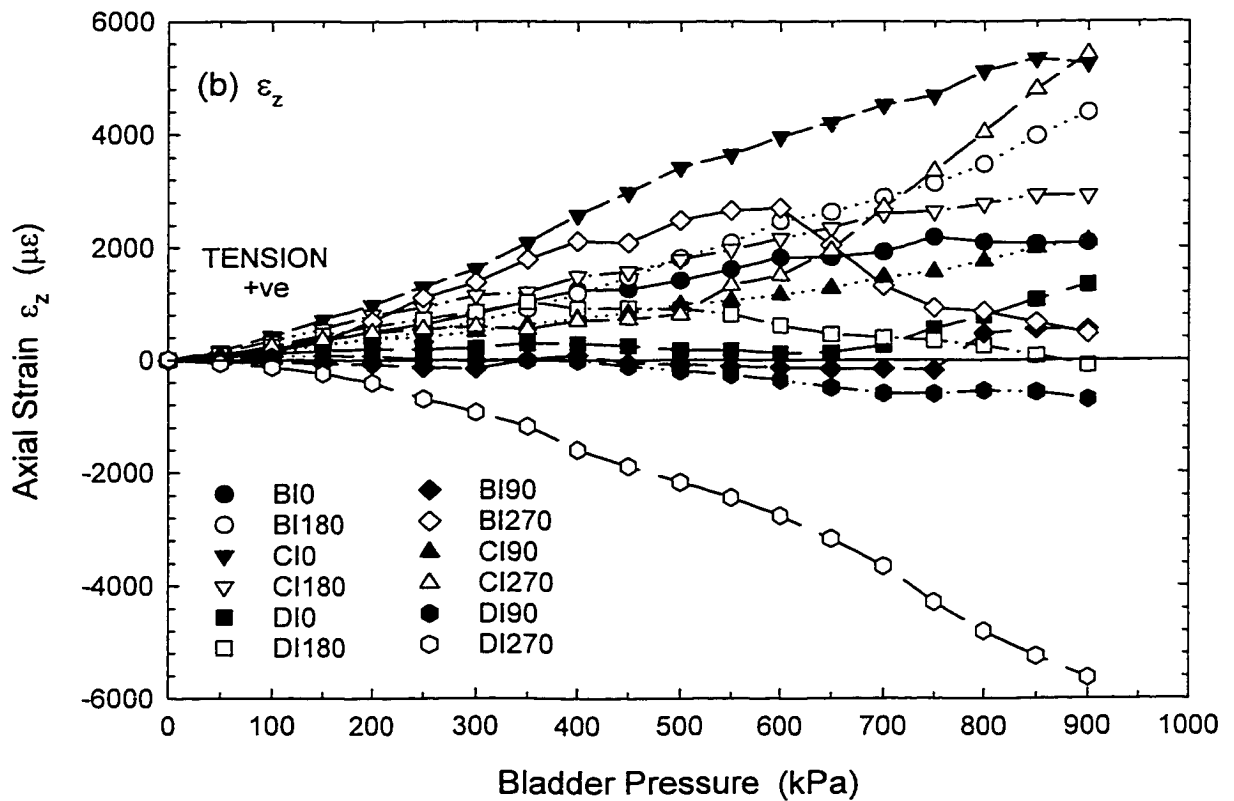
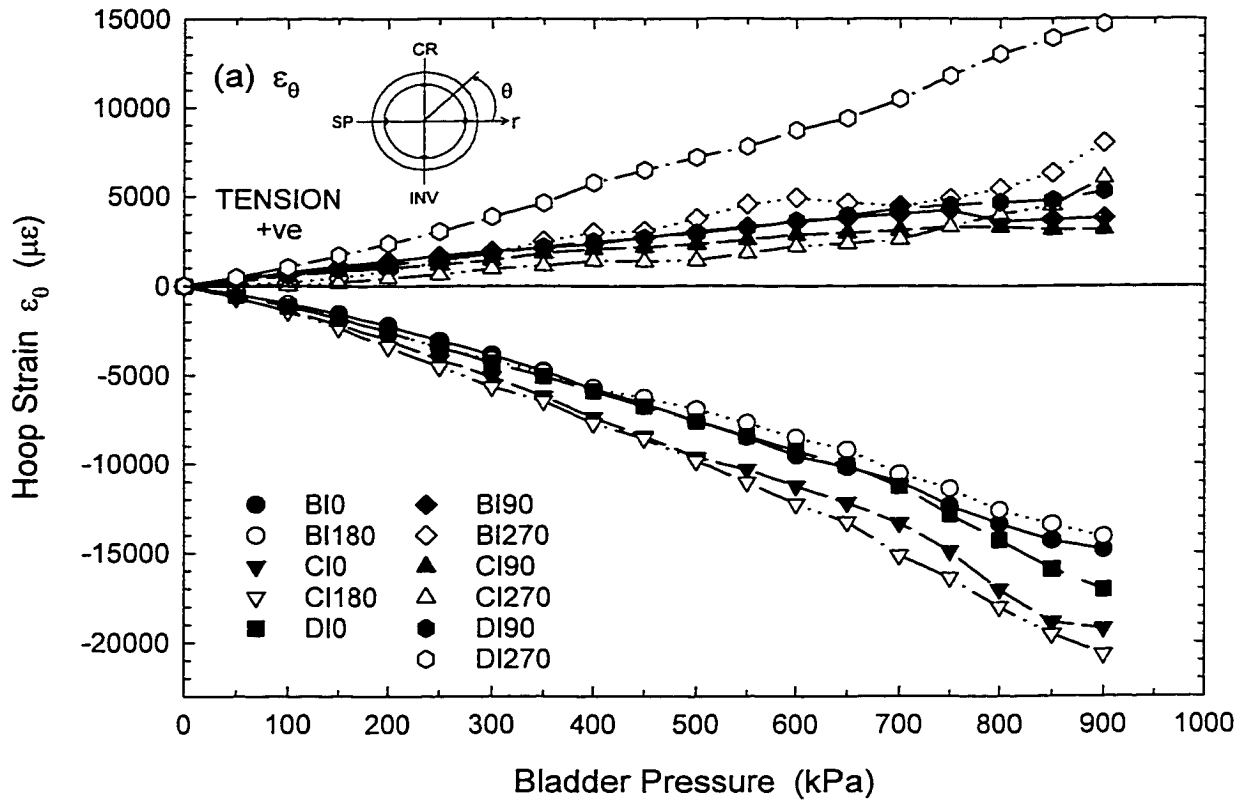


FIGURE 6.6 Interior strains ($\mu\epsilon$) versus applied bladder pressure (kPa) for Test P3c: (a) Hoop strains (ϵ_{θ}), and (b) Axial strains (ϵ_z) measured at Sections B, C and D.

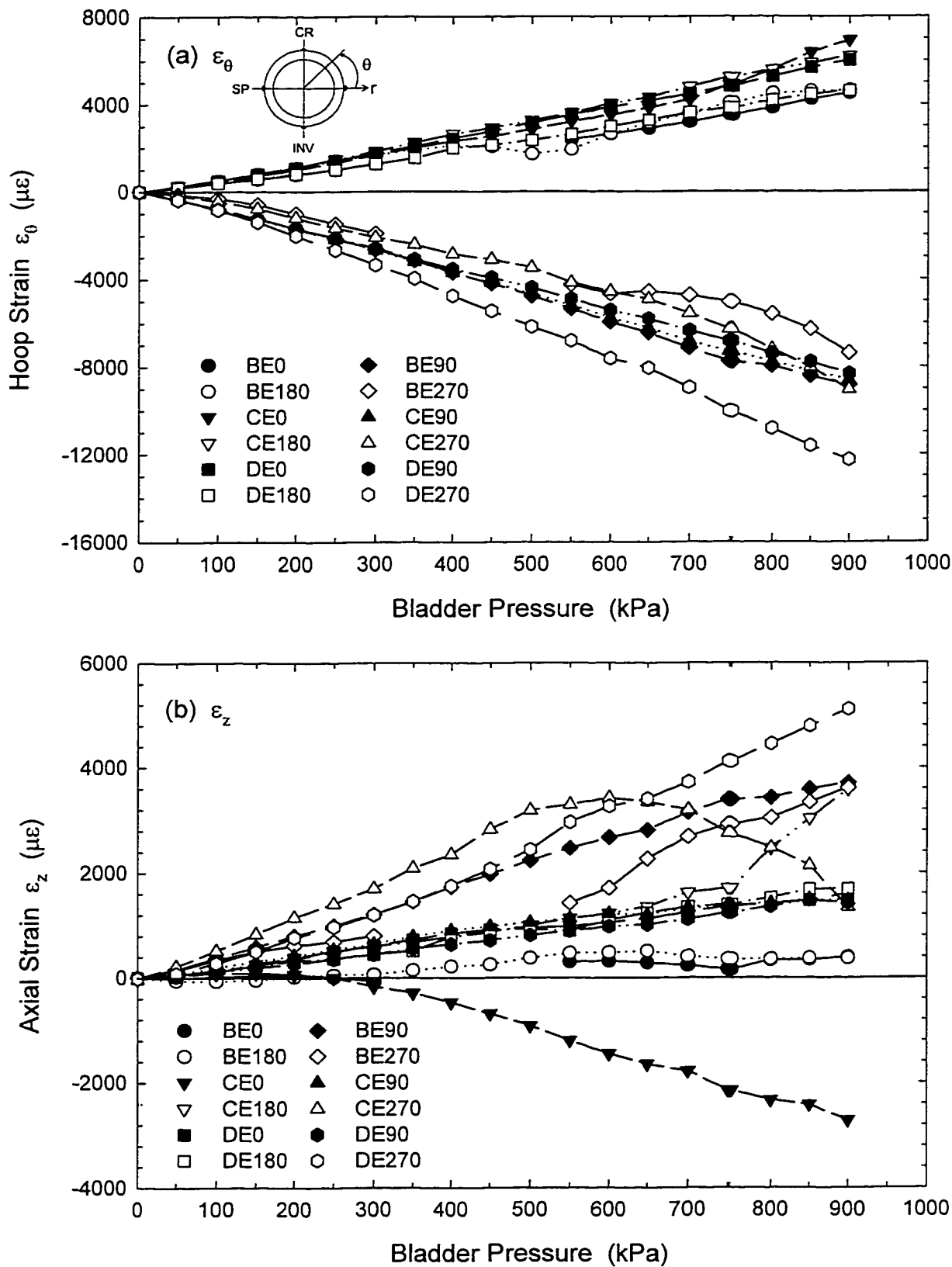


FIGURE 6.7 Exterior strains ($\mu\epsilon$) versus applied bladder pressure (kPa) for Test P3c: (a) Hoop strains (ϵ_{θ}), and (b) Axial strains (ϵ_z) measured at Sections B, C and D.

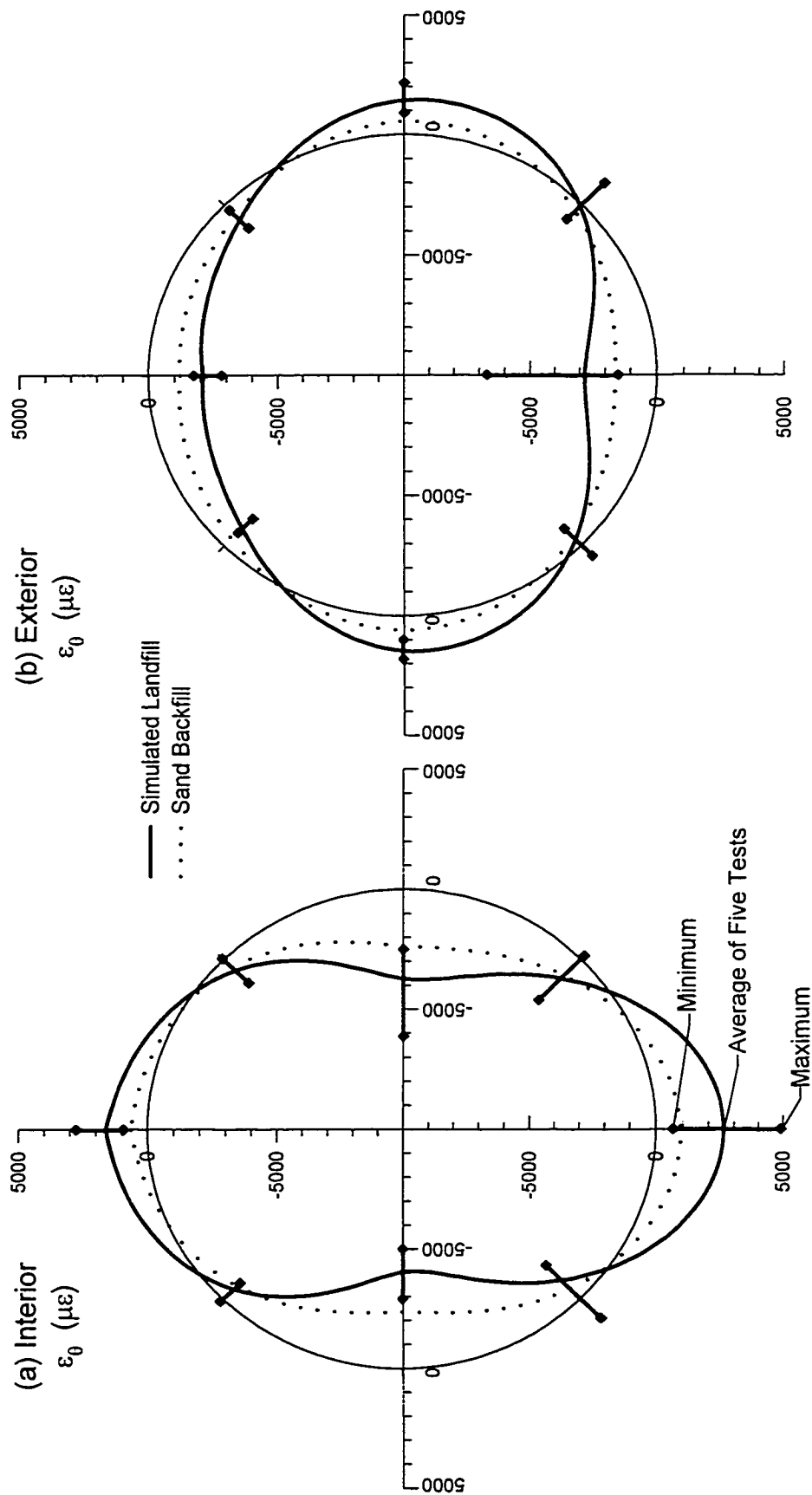


FIGURE 6.8 Hoop strain measured on (a) interior and (b) exterior surfaces of the pipe for tests P2b, P3a, P3b, P3c and P4 at an applied bladder pressure of 250 kPa.

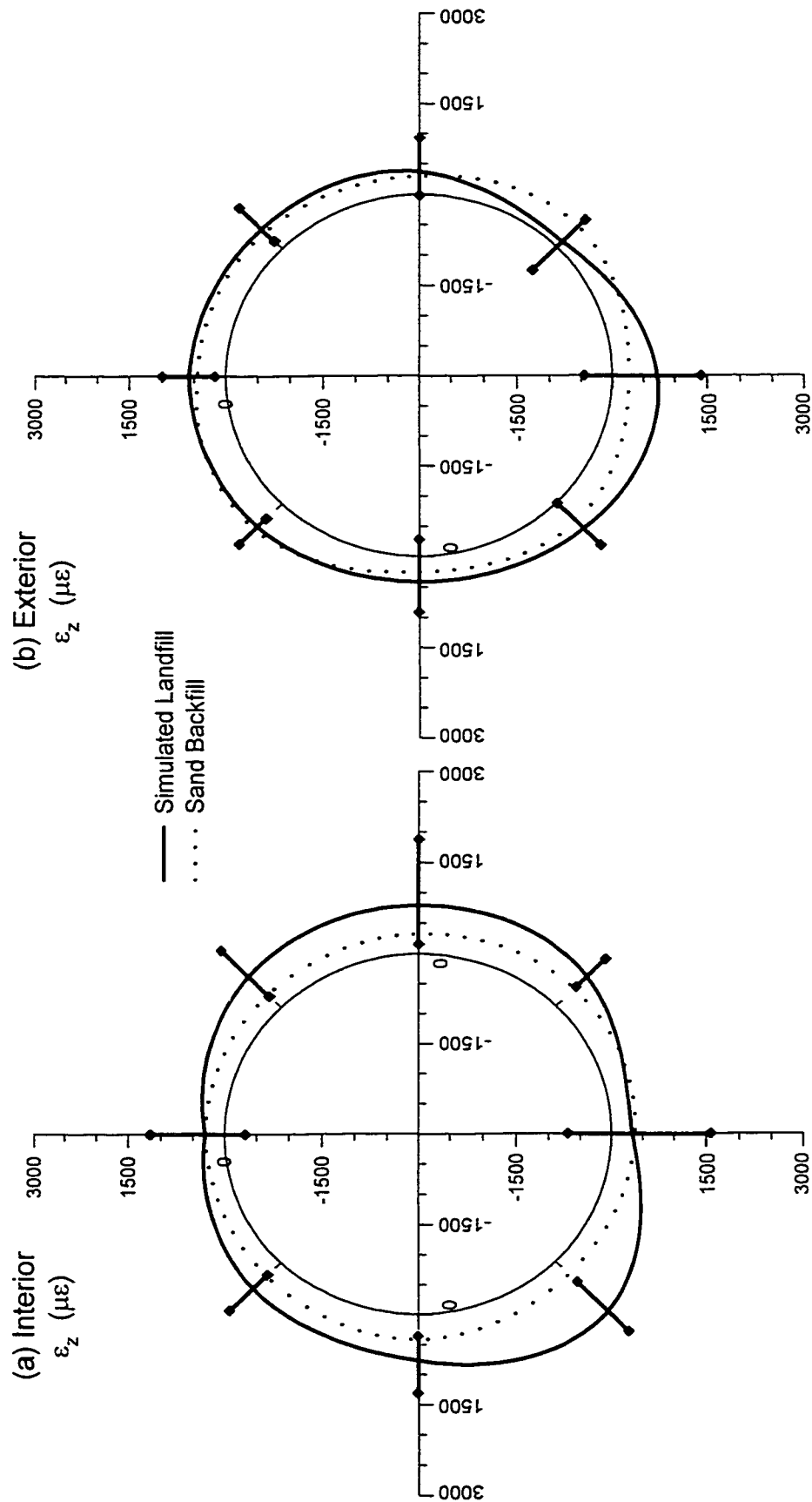


FIGURE 6.9 Axial strain measured on (a) interior and (b) exterior surfaces of the pipe for tests P2b, P3a, P3b, P3c and P4 at an applied bladder pressure of 250 kPa.

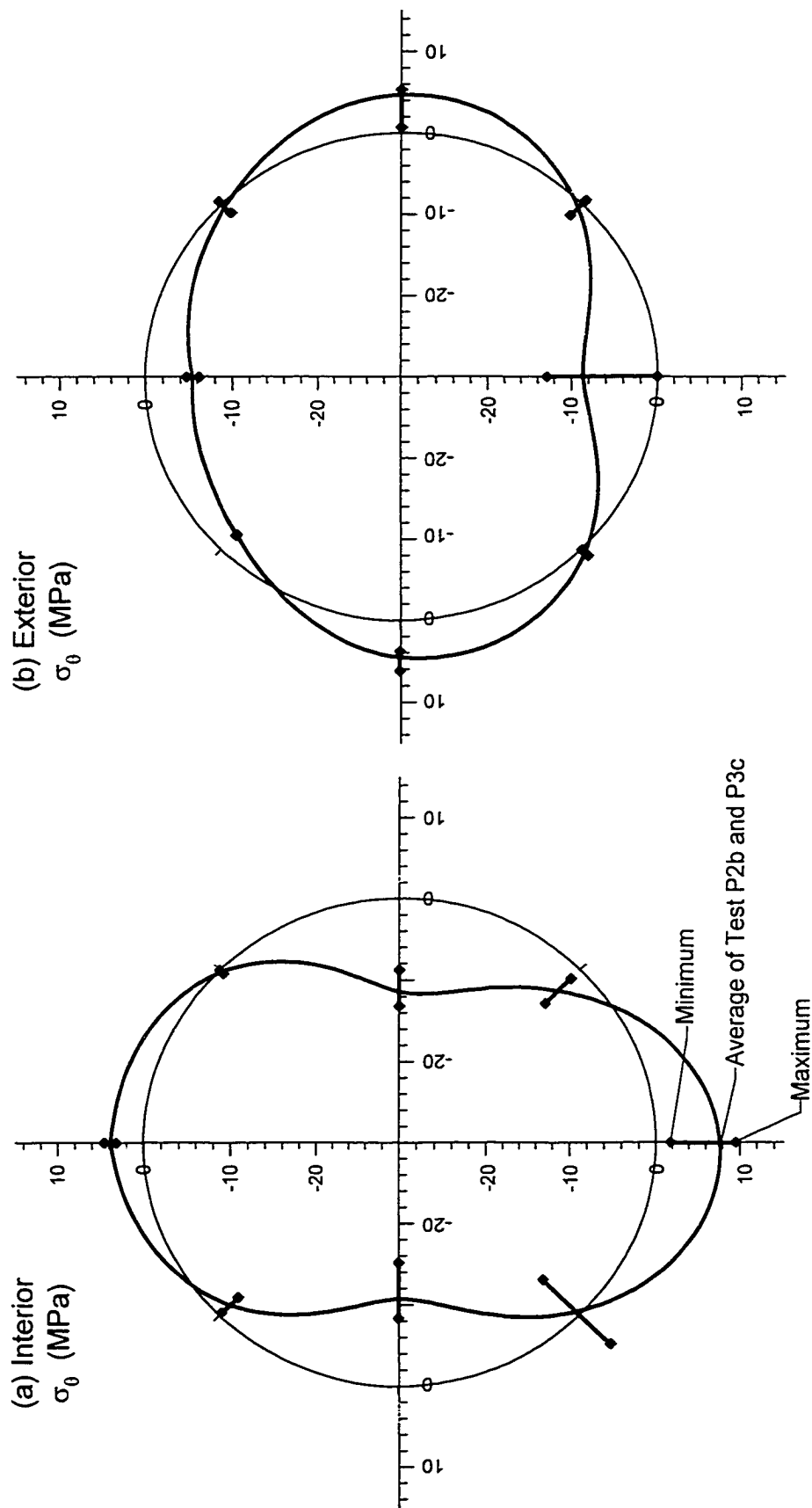


FIGURE 6.10 Hoop stress calculated for (a) interior and (b) exterior surfaces of the pipe for tests P2b and P3c at an applied bladder pressure of 900 kPa. (Note: $E_p = 310$ MPa, $\nu_p = 0.46$ and $GCF = 2$).

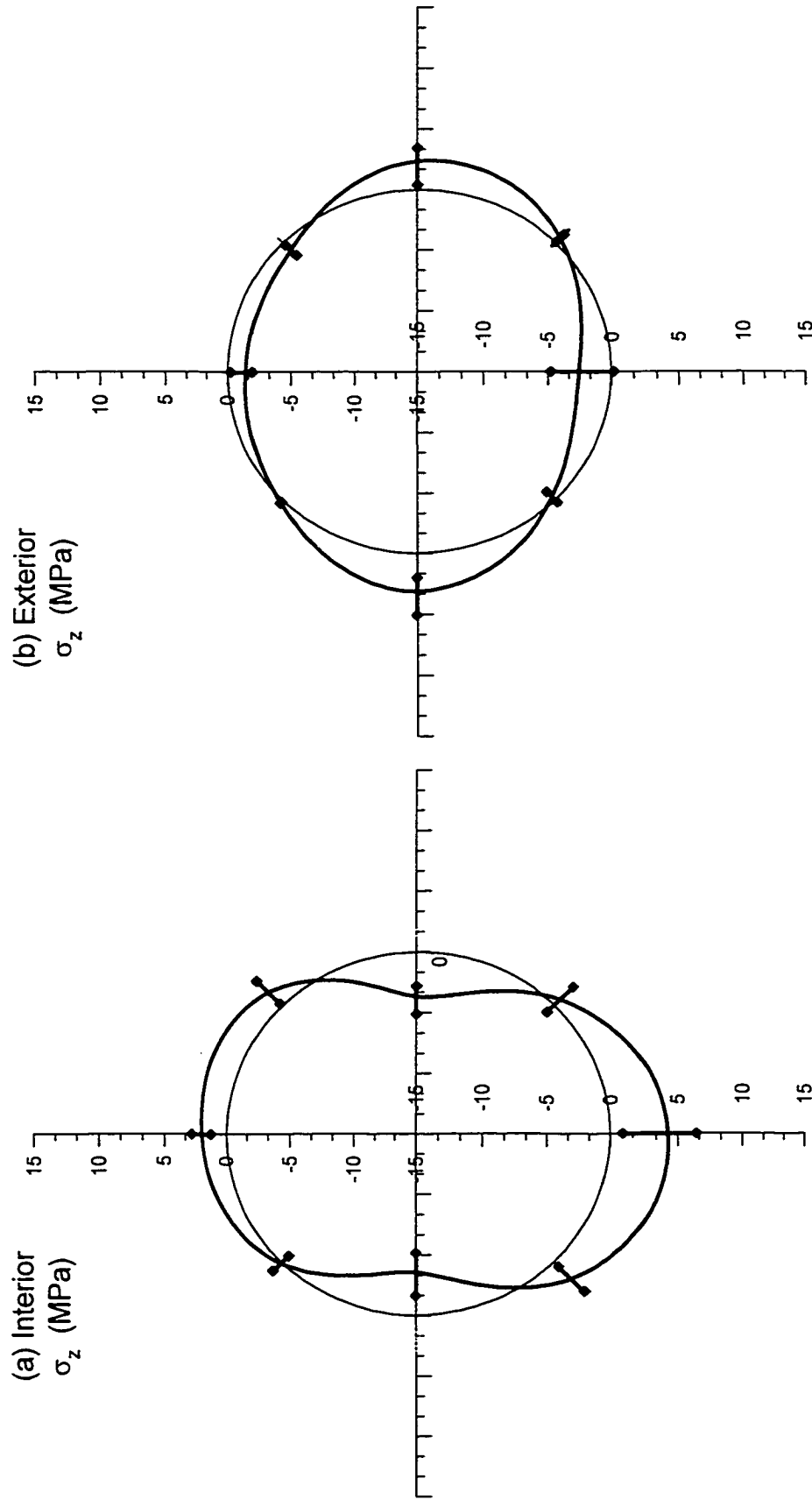


FIGURE 6.11 Axial stress calculated for (a) interior and (b) exterior surfaces of the pipe for tests P2b and P3c at an applied bladder pressure of 900 kPa. (Note: $E_p=310$ MPa, $\nu_p=0.46$ and $GCF=0.4$).

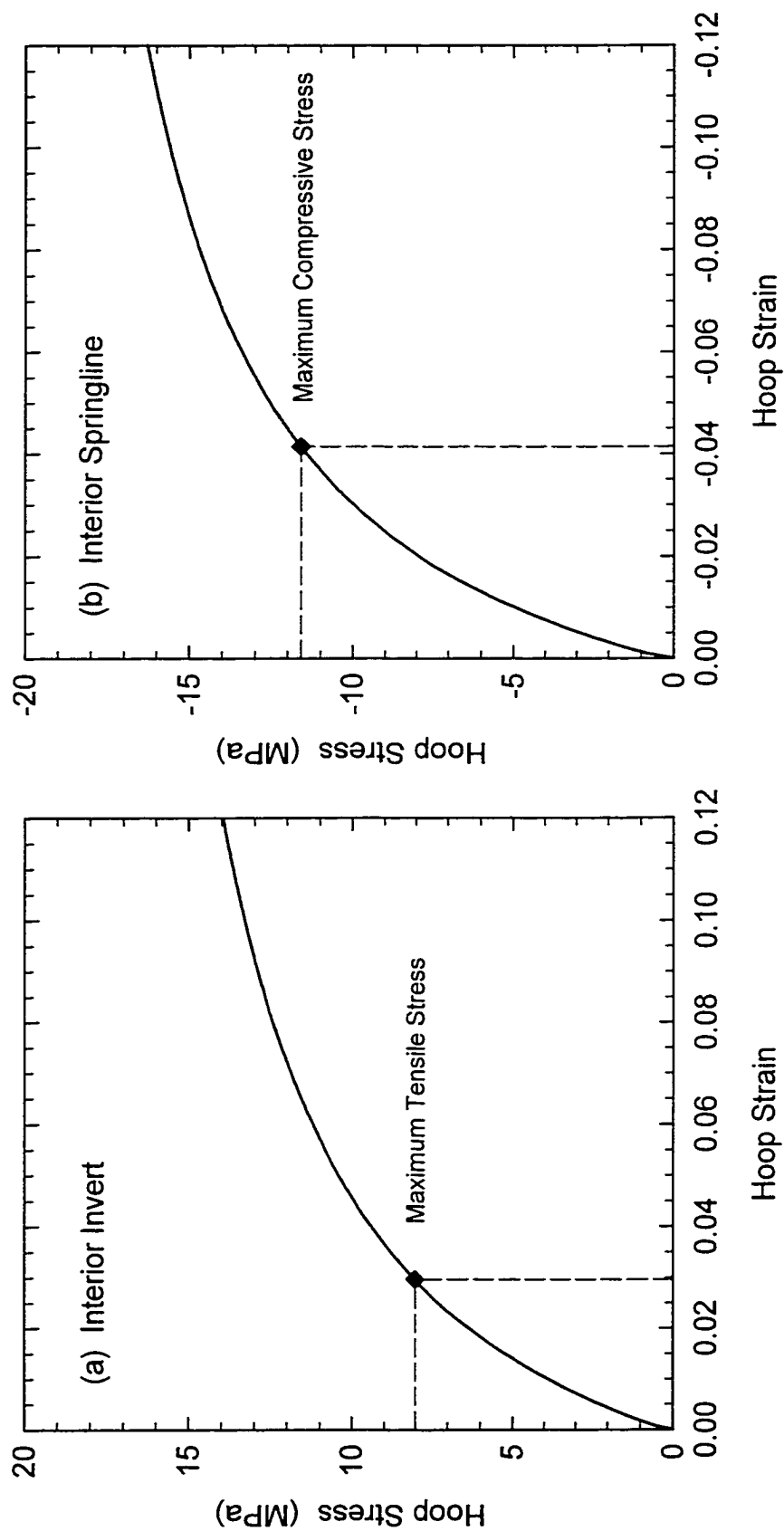


FIGURE 6.12 Stresses calculated at the interior invert and springlines based on the maximum measured strains (with GCF=2) using the viscoplastic constitutive model for polyethylene of Zhang and Moore (1997).

CHAPTER 7

Summary and Conclusions

A study of the mechanical performance of perforated leachate collection pipes for use in municipal solid waste landfills was presented. Concern regarding potentially adverse service conditions for the pipe arising from the use of coarse gravel backfill and large perforations - both required to minimize the degree of biologically induced clogging of the leachate collection system - coupled with uncertainties in the mechanical response of these thick plastic pipes warranted study. A laboratory testing program was therefore conducted to assess the effects of coarse gravel backfill and large perforations on the structural response of high density polyethylene (HDPE) pipes for use in landfills. A new laboratory facility, capable of simulating large earth pressures that act on a deeply buried pipe, was designed and developed to permit the measurement of the response of these pipes under controlled experimental conditions. In this chapter, the principal findings from the different studies conducted for this thesis are summarized. Preliminary recommendations are made for the design of these pipes for use in municipal solid waste landfills. Suggestions for further work are given.

7.1 INTERPRETATION OF LARGE SCALE PIPE TESTING

The results from a large scale test conducted on a small diameter leachate collection pipe at Ohio University (Sargand 1993) were analysed and interpreted. This work of Chapter 2 demonstrated that the boundary conditions of the Ohio facility result in complex stress

conditions with the soil and the pipe tested due to their attempt to simulate vertical overburden pressures by applying vertical force to a stiff rectangular load platform. It was found that the response of the pipe differed substantially to that expected if the pipe was subject to large and extensive overburden pressures. Further it was shown that their interpretation of the test results (Masada et al. 1996) would (unconservatively) overestimate the equivalent vertical surcharge acting on the soil and the pipe. Little inference can be made with respect to the mechanical performance of leachate collection pipes from the Ohio University test since the vertical pressures were applied by a rigid footing that does not simulate field conditions, and because there appears to have been extensive shear failure in the soil that involved the development of a failure mechanism through the underlying and adjacent clayey materials.

7.2 DESIGN AND PERFORMANCE OF A NEW LABORATORY FACILITY FOR TESTING SMALL DIAMETER PIPES UNDER BIAXIAL EARTH PRESSURES

The design and performance of a new laboratory facility for testing small diameter buried pipes subject to the biaxial earth pressures expected to prevail under deep and extensive overburden were discussed in Chapters 4 and 5. The new facility consists of a prism of soil 2.0 m wide \times 2.0 m long \times 1.6 m high contained within a stiff steel structure. Overburden pressures are simulated with a pressurised air bladder. Lateral earth pressures are developed by limiting the lateral soil strains.

Attention was focussed on the potential influence of the boundary conditions of the new facility on the soil and pipe response, and how reasonably the test cell represents the

field conditions for a buried pipe. Issues such as the selection of test cell dimensions, the impact of boundary roughness and the importance of boundary stiffness on the response of the soil and pipe were examined using a finite element analysis.

Measurements of pipe, soil and test cell response during a test with uniform medium-sand backfill indicated that the new laboratory facility closely simulates the conditions expected to prevail under deep and extensive burial. The bladder design consisted of a flexible rubber membrane with a mechanical seal around the perimeter. This design provided a uniformly distributed pressure across the top surface of the soil. The effects of boundary friction were limited to minimal levels by using lubricated polyethylene sheets that had adequate protection from damage by the backfill soil. The stiffness of the lateral boundary was sufficiently large to induce lateral stresses close to those for zero lateral strain conditions. Uniform pipe response was obtained for the middle portion of the pipe indicating only small effects from the boundary conditions in the new laboratory model.

7.3 LABORATORY INVESTIGATION OF THE EFFECT OF COARSE GRAVEL BACKFILL ON THE MECHANICAL PERFORMANCE OF PERFORATED LEACHATE COLLECTION PIPE

Leachate collection pipes were tested under simplified boundary conditions where a uniform radial stress was applied to the soil to impart compressive hoop stresses in the pipe. These tests (Chapter 3) were conducted with both medium sand and coarse gravel backfill materials that represent two different loading conditions for the pipe. The sand backfill essentially provided continuous support for the pipe (relatively small particles in close contact with the

pipe), while the coarse gravel backfill provided discontinuous support for the pipe (large particles randomly distributed around the exterior pipe circumference). Large variation in surface strains resulting from the coarse gravel backfill were measured. This demonstrated local bending effects in the pipe due to the coarse gravel and not because of the applied boundary stresses.

Large scale laboratory tests were also conducted under biaxial earth pressures to assess the influence of coarse gravel backfill and large perforations on the structural response of leachate collection pipes (Chapter 6). Measurements showed that the coarse gravel backfill results in larger pipe deflections and greater variations in deflections than those obtained for a medium-dense sand backfill. For the 220 mm OD, SDR 9 HDPE pipes tested with coarse gravel backfill, the average vertical and horizontal diameter changes were approximately -1% and 0.8%, of the mean diameter at an applied pressure of 250 kPa (representative overburden stresses for a medium size landfill with 20 to 25 metres of waste). When subject to a vertical pressure of 900 kPa, the changes in vertical and horizontal diameter were roughly -5% and 3% of the mean pipe diameter. The coefficient of variation for the vertical diameter change ranged from 17 to 28%, while that for the horizontal diameter change was from 14 to 22% at a vertical surcharge of 250 kPa. Despite the greater magnitudes and larger variations in pipe deflections with the coarse gravel relative to the sand, the deflections are less than allowable limits, even up to applied vertical pressures of 900 kPa.

Maximum compressive hoop strains were measured at the interior springline; maximum tensile hoop strains were recorded at the interior invert. Tensile axial strains, also a maximum at the interior invert, resulted from local bending effects from the gravel and the

zero end restraint provided for the pipe during the tests, and gave larger tensile stresses relative to axial plane strain conditions. Both hoop and axial strains were heavily influenced by local bending effects caused by the coarse gravel backfill. With a coarse gravel backfill the maximum strains were found to be roughly twice the average value. Similar variations were found when the pipe was subjected to larger vertical pressures. Based on these results it appears that the estimates of stress obtained from measured strains be multiplied by factor of two to account for the stress increases due to the coarse gravel. Estimates of the stresses in the pipe (based on the measured strains) indicate that these pipes should perform well when subject to 250 kPa of vertical surcharge, since the maximum short-term tensile stresses are well below the allowable long-term hydrostatic design stress for this material.

The influence of the relatively large perforations (large with respect to those currently used in practice) on the strains measured at the crown, springline or invert was found to be small relative to the dominant influence of the coarse gravel. Thus the principal effect that the perforation has on the mechanical performance of the pipe is a local perturbation in the strain field with its influence concentrated around the hole. Holes of 25 mm diameter (for the 220 mm OD, SDR 9 pipe tested) placed at the quarter-points (ie. shoulders and haunches) at an axial spacing of 150 mm had no significant negative impact on pipe response, likely because the strains and hence stresses are smaller at these locations relative to those at the crown, springline or invert.

The use of the Modified Iowa equation (e.g., Howard 1977; Koerner 1998) for calculating the vertical deflection of the pipe is not recommended given that this method neglects the soil-structure interaction between the soil and the pipe and predicts the wrong mode of deformation. Published values of modulus of soil reaction (E') for use in the

Modified Iowa equation yielded much larger values of pipe diameter change than those measured in the laboratory tests. Analysis based on thin elastic tube theory and elastic continuum theory for the surrounding backfill (Moore 1993) provided good estimates of pipe deflection when compared with measured laboratory results.

Although coarse gravel backfill does impose adverse support conditions relative to sand backfill, the measured variations of deflection and strain do not, however, preclude the use of coarse (40 - 50 mm) gravel in direct contact with leachate collection pipes. In fact, the 220 mm OD, SDR 9 high density polyethylene pipe would be expected to perform well in a medium-size landfill (vertical pressures up to 250 kPa) for the gravel, perforation size and perforation pattern tested.

7.4 SUGGESTIONS FOR FUTURE WORK

Further research is warranted to study the long term performance of these buried polymer pipes. Resolution of issues such as the degree to which the stresses in the pipe decrease over time and the propagation of cracks in a pipe subject to biaxially compressive earth pressures would be useful for the design of these pipes. Further characterization of the constitutive response of HDPE, especially at very slow strain rates, is required. Any such work is complicated by the extremely long time frames involved and the complexity of the constitutive response of high density polyethylene.

7.5 REFERENCES

- Howard, A.K. (1977) "Modulus of Soil Reaction Values for Buried Flexible Pipe", *Journal of the Geotechnical Engineering Division*, ASCE, Vol. 103, GT 1, pp. 33 - 43.
- Koerner, R.M. (1998) *Designing With Geosynthetics*, 4th Edition, Prentice Hall.
- Masada, T., Sargand, S.M. and Hazen, G.A. (1996) Discussion of: Interpretation of a buried pipe test: Small diameter pipe in the Ohio University facility. *Transportation Research Record*, 1541, pp. 71-72.
- Moore, I.D. (1993) "Structural Design of Profiled Polyethylene Pipe - Part I - Deep Burial", Geotechnical Research Centre Report GEOT-8-93, The University of Western Ontario, London, Canada.
- Sargand, S.M. (1993) "Structural Performance of an HDPE Leachate Collection Pipe", *31st Annual International Solid Waste Exposition*, San Jose, CA, USA, pp. 381 - 402.

APPENDIX I

Numerical Integration During Fourier Integral Analysis ¹

AI.1 INTRODUCTION

Various researchers are employing Fourier Integral methods in the analysis of the three dimensional elastic response of long prismatic soil structures (eg., Small and Wong, 1988; Moore and Brachman, 1994; Brachman et al., 1996; Fernando et al., 1996; Fernando and Carter 1998). These procedures use Fourier Integrals to transform the response in the longitudinal direction of the prismatic structure into harmonic form. Solutions are then assembled from harmonics through evaluation of the inverse integrals. This note describes the nature of these integrals and how Gaussian integration can be used in their calculation. Specific examples feature rectangular pressure distributions in the longitudinal direction.

AI.2 FOURIER INTEGRALS

The description, theory and implementation of the three dimensional semi-analytic finite element technique is as discussed by Moore and Brachman (1994). The Fourier integral approach removes the dependence upon the longitudinal spatial coordinate (ie. z) in lieu of a transform variable, α . The Fourier cosine integral of any function $f(\xi)$ is defined as:

¹ A version of this Appendix has been accepted for publication.

Brachman, R.W.I., and Moore, I.D. 1998. Numerical Integration During Fourier Integral Analysis. *International Journal for Numerical and Analytical Methods in Geomechanics*, In Press, Accepted 7/16/98.

$$F_c(\alpha) = \int_0^{\infty} f(\xi) \cos(\alpha\xi) d\xi \quad (\text{AI.1})$$

where: $F_c(\alpha)$ is the Fourier cosine integral of $f(\xi)$,
 α is the transform variable, and
 ξ is the variable being transformed.

For example, vertical applied loads $f_y(z)$, displacements $u_y(z)$ and stresses $s_y(z)$ can be transformed by:

$$F_{yc}(\alpha) = \int_0^{\infty} f_y(z) \cos(\alpha z) dz \quad (\text{AI.2})$$

$$U_{yc}(\alpha) = \int_0^{\infty} u_y(z) \cos(\alpha z) dz \quad (\text{AI.3})$$

$$S_{yc}(\alpha) = \int_0^{\infty} s_y(z) \cos(\alpha z) dz \quad (\text{AI.4})$$

Harmonic finite element analysis can then be performed with a two dimensional mesh (descretized in the x-y plane) to solve for the transformed displacements $U(\alpha)$ and stresses $S(\alpha)$ for specific values of α . Inverse integrals convert the harmonic response back to the Cartesian coordinate system. Inversions of the Fourier integrals to obtain the vertical applied load, displacement and stress quantities as a function of z are given by:

$$f_y(z) = \frac{2}{\pi} \int_0^{\infty} F_{yc}(\alpha) \cos(\alpha z) d\alpha \quad (\text{AI.5})$$

$$u_y(z) = \frac{2}{\pi} \int_0^{\infty} U_{yc}(\alpha) \cos(\alpha z) d\alpha \quad (\text{AI.6})$$

$$s_y(z) = \frac{2}{\pi} \int_0^{\infty} S_{yc}(\alpha) \cos(\alpha z) d\alpha \quad (\text{AI.7})$$

The integrands of Equations AI.5, AI.6 and AI.7 are functions of the transform variable α which can be evaluated for any particular z value of interest.

Elastic solutions for three dimensional problems with long prismatic geometry can therefore be obtained using a two dimensional finite element mesh and Fourier integrals. The successful application of the Fourier Integral approach is contingent on the evaluation of these inverse Fourier integrals.

AI.3 VARIATION OF APPLIED LOADING

Figure AI.1a illustrates the longitudinal variation of applied loading considered by Moore and Brachman (1994). It consists of two uniform patches of pressure of width w separated by a distance $2z_s$ acting on the ground surface. Vehicle loading of buried structures was simulated with w equal to the tire width and $2z_s$ as the axle length. Similar surface pressure distributions were considered by Fernando et al. (1996) in their solution of a similar problem. A single patch of pressure of width $2w$ centred at $z=0$ is modelled when z_s equals zero.

More complex loading functions can also arise. Brachman et al. (1995) have described how the Fourier Integral technique can be used to assess the elastic ground response to load from a rigid rectangular footing. Here, the contact pressure under the footing was subdivided into a series of uniformly loaded patches. Fourier Integral analysis was used to assemble a flexibility relationship between patch pressures and displacements that was used to solve for the contact pressure. This analysis featured narrow patches of pressure characterized by the load variation of Figure AI.1a, with z_s equal to zero and for several patch half-widths (ie. w). The following sections are based on the solution requirements of Brachman et al. (1995), but are largely generic so that similar principles apply to most such Fourier Integral applications.

AI.4 TRANSFORMED LOADING FUNCTION

Of the transformed quantities, only the load variation in the longitudinal direction $f_y(z)$ is known at the outset of the analysis. The Fourier cosine integral of the general load function $f_y(z)$ depicted in Figure AI.1a is given by:

$$F_{yc}(\alpha) = \frac{1}{\alpha} [\sin(z_s \alpha + w \alpha) - \sin(z_s \alpha)] \quad (\text{AI.8})$$

The inversion of the Fourier integral to obtain the original load function would involve performing the integral of Equation AI.5. For a single patch of pressure (ie. $z_s=0$) this integral is equal to:

$$f_y(z) = \frac{2}{\pi} \int_0^{\infty} \frac{\sin(w\alpha) \cos(z\alpha)}{\alpha} d\alpha = \frac{2}{\pi} \int_0^{\infty} g(\alpha) d\alpha \quad (\text{AI.9})$$

Figure AI.1 presents plots of the inverse integrand $g(\alpha)$ of Equation AI.9 for two cases with load half widths (w) equal to 152 and 76 mm (Figs. AI.1b and AI.1c, respectively). In the limit, as α approaches zero, the integrand $g(\alpha)$ equals w ; as α becomes very large (ie. $\alpha \rightarrow \infty$), $g(\alpha)$ approaches zero. Between these limits, the amplitude of $g(\alpha)$ is inversely proportional to α . The latter two points are advantageous as the integral in Equation AI.9 can be truncated at some sufficiently large value to facilitate numerical integration.

The zeros of the inverse integrand of Equation AI.9 are functions of both w and z , and are controlled by the $\sin(w\alpha)$ and $\cos(z\alpha)$ components. Zeros are located at $\alpha = p\pi/w$ ($p=1, 2, 3, \dots$) for $z=0$. Decreasing w results in an increase in the period of $g(\alpha)$. For non-zero z , additional roots arise from the $\cos(z\alpha)$ component and are located at $\alpha = (2p-1)\pi/2z$ ($p=1, 2, 3, \dots$), as shown by the $z=2740$ mm curves. The additional complexity of the integrand for larger z values is significant as greater numerical effort is required to invert the transform.

AI.5 TRANSFORMED DISPLACEMENTS AND STRESSES

Transformed displacements $U(\alpha)$ and stresses $S(\alpha)$ are initially unknown and thus prohibit a direct examination of the inverse integrands as previously performed for the applied load. A simple test case involving a uniformly loaded patch was therefore

analyzed to calculate the transformed displacements and stresses for various harmonic values. Results are shown for the case of a square patch of pressure ($z_s=0$) of dimensions $2w \times 2w$ ($w=152$ mm) acting on an elastic surface ($E=50$ MPa, $\nu=0.3$). The two dimensional (x - y) finite element mesh used for the analysis consisted of fifty two six-noded triangles, Figure AI.2.

AI.5.1 Transformed Stresses

Figure AI.3a shows the stress integrand $S_{yc}(\alpha)\cos(\alpha z)$ for the vertical stress s_y at point A near the surface. This plot is very similar to the integrand $g(\alpha)$ of the applied load previously shown in Figure AI.1b. As expected the vertical stress near the surface is close to the applied surface traction. There is a 30% decrease in amplitude of the function in Figure AI.3a relative to that in Figure AI.1b resulting from slight attenuation with depth. As previously noted, the integrand becomes more complex for larger values of z , indicated by the $z=2740$ mm curve in Figure AI.3a.

Figure AI.3b shows the function to be inverted to obtain the vertical stress at point B (0.9 m below the surface). Significant attenuation with depth occurs in comparison with point A. The magnitude of the stress integrand at point B is roughly one-fifth of that for point A, when α equals zero. More importantly, the magnitude of the stress integrand at point B is essentially zero for α larger than 10. This is in sharp contrast to the periodic function for point A that extends to large values of α .

AI.5.2 Transformed Displacements

The inverse Fourier integral for vertical displacement $U_{yc}(\alpha)\cos(\alpha z)$ at point A is plotted

in Figure AI.3c. This integrand is much simpler than that required to invert the transformed loads. The magnitude of the displacement integrand decreases more rapidly for an increase in α than does the load integral. The displacement integrand shown in Figure AI.3c is nearly zero for α larger than 40.

The integrand for the transformed displacements also displays significant attenuation with depth when evaluated at location B (Figure AI.3d). The integrand of the transformed displacements also becomes less complex with depth.

AI.5.3 Implications For Fourier Integral Analysis

Two major conclusions may be drawn from the comparison of the integrands for evaluation of stresses and displacements. First, the Fourier integral of the original load function is more complex than other quantities like displacement since the surface load features a discontinuity. Therefore the numerical inversion of the transform of surface load is more difficult than other transform quantities. Second, the inversion of stress or displacement quantities at the surface is more difficult than the inversion of those quantities below the surface.

Therefore, the most difficult integrand to integrate numerically would correspond to the inversion of the transform of the original applied load at the surface. This is advantageous as the load variation is known *a priori*. Provided that the numerical inversion is sufficient for this most difficult case, confidence of an accurate solution can be assured for other quantities, both at the surface and at other locations in the ground.

AI.6 NUMERICAL INTEGRATION

Now that the nature of the Fourier integrals has been examined, a discussion of the numerical technique used to perform the inverse integrals is presented. The integration of some function of α between zero and infinity can be performed numerically by first truncating the upper limit of the integrand from infinity to some finite value, and second by evaluating the truncated integral piece wise as a number of sub-integrals, i.e.:

$$\int_0^{\infty} f(\alpha) d\alpha \approx \sum_{i=1}^N \int_{\Delta\alpha(1-i)}^{\Delta\alpha i} f(\alpha) d\alpha \quad (\text{AI.10})$$

where: N = number of sub-integrals, and

$\Delta\alpha$ = width of sub-integral.

Each sub-integral was evaluated using ten point Gaussian integration. Trials were also conducted with two point Gaussian integration which was found to be somewhat less efficient.

The accuracy of the integration is controlled by the number (N) and size ($\Delta\alpha$) of the sub-integrals. The selection of these parameters, which determine the upper limit of the integration ($\Delta\alpha \times N$) and the refinement of each sub-integral, is dictated by the need for a solution to be both accurate and efficient.

AI.6.1 Solution of Test Case - Uniformly Loaded Patch

The trial case involving a uniformly loaded patch ($2w \times 2w$) was also analyzed to investigate the effectiveness of the integration scheme and to verify that correct vertical

displacements at the surface were obtained even for large z values away from the load, as required by the particular problem considered by Brachman et al. (1995).

Since the test problem is symmetric along the lines $x=0$ and $z=0$, the vertical deflections along these lines should be the same. This premise was used to test the inversion scheme by comparing the vertical deflections along the line $z=0$ to those obtained along $x=0$.

Figure AI.4a plots three sets of vertical deflection results for w of 152 mm. The solid curve represents the deflections obtained in the x - y plane (ie. along $z=0$). The other sets are the calculated deflections in the y - z plane (ie. along $x=0$) for two different Gaussian quadrature schemes. The prediction with $N=5$, $\Delta\alpha=15$ provides reasonable results up to z of 1.8 m, and then differs from the solid curve. The deflections here are essentially zero, however this difference illustrates the effect of large z values on the success of the integration scheme. As previously shown in Figure AI.3c, the function to be integrated $U_{yc}(\alpha)\cos(\alpha z)$ becomes more complicated as z increases, consequently a finer sub-integral width is required. Figure AI.4a shows that with $N=5$ and $\Delta\alpha=10$, which involves integration with a smaller upper limit, but with greater refinement compared to $N=5$, $\Delta\alpha=15$, the correct displacements are obtained for z values up to 3 m.

Figure AI.4b presents the calculated vertical deflections for w of 76 mm. The solid curve again shows the vertical deflection along the line $z=0$, against which the values obtained along the z axis will be compared. Curve ii) presents the deflections obtained using the adopted integration scheme for w of 152 mm (ie. $N=5$, $\Delta\alpha=10$). These results provide a reasonable estimate of the vertical deflections, however the value at the centre of the patch is slightly overestimated and there is some slight oscillation of the

predictions for the higher z values. Curve iii) shows the consequences of integrating to larger values of α with a coarse sub-integral size. Poor results are obtained with $N=5$, $\Delta\alpha=20$, especially for z larger than 1.7 m. Extending the integration scheme to the same α value used for curve iii) but with twice the number of sub-integrals (ie. $N=10$, $\Delta\alpha=10$) yields good results up to z of 3 m, shown by curve iv).

These trial cases confirm that the numerical integration techniques may be successfully used to invert Fourier integrals provided that enough Gaussian quadrature intervals, of small enough size are employed.

AI.7 ANALYSIS WITH MULTI-STEP LOADING

Analysis of multi-step loading (eg. the two load patches of width w separated by distance $2z_s$ of Figure AI.1a) is more arduous than that for a single patch of pressure. The Fourier cosine integral for the generalized load distribution of Figure AI.1a was given previously in Equation AI.8. The corresponding equation to invert the transform is:

$$f(z) = \frac{2}{\pi} \int_0^{\infty} \frac{[\sin(z_s\alpha + w\alpha) - \sin(z_s\alpha)] \cos(z\alpha)}{\alpha} d\alpha \quad (\text{AI.11})$$

The integrand of Equation AI.11, $g(\alpha)$, is plotted in Figure AI.5 for cases of $w=152$, and 76 mm (with $z=0$). Values are shown for both z_s equal to zero and a large value of z_s . The increased complexity of the integrand for non-zero values of z_s is illustrated in Figure AI.5. A greater number of zeros result from the $\sin(z_s\alpha)$ components of Equation AI.11

and the amplitude of $g(\alpha)$ is harmonic for non-zero z_s . For locations other than at $z=0$, $g(\alpha)$ may be even more complex. The additional complexity introduced into the integrand by non-zero z_s values means that greater computational effort is needed to invert the transform.

The transform of the load function becomes increasingly complex for the case of large z_s relative to w . When evaluating inverse integrals for large z_s relative to w , it was found to be considerable more efficient to employ superposition to assemble the solution for the multi-step load variation from two simpler solutions with z_s equal to zero. For example, solution efficiency was improved by considering the response to a load with half-width $(z_s + w)$ minus the response to the a load with half-width (z_s) , rather than by direct evaluation of the load case shown in Figure AI.1a.

AI.8 SUMMARY

The nature of the inverse integrals and the numerical integration required to employ Fourier Integral analysis of three dimensional problems has been described. These integrals may be complex functions for the generalized load function considered, particularly for evaluation at non-zero longitudinal positions ($z \neq 0$) and for patches separated by distance z_s .

The Fourier integral of applied load is more complex and thus more difficult to invert than those for stresses and displacements. Since the applied load is known *a priori*, integration schemes can be selected that provide accurate and efficient inversion of

the original load function. This assures correct stresses and displacements throughout the elastic body. The complexity of Fourier integrals of stress and displacement decreases significantly with depth. Accuracy of Fourier integral inversions therefore improves as depth increases below the applied loading.

The use of piece wise Gaussian integration over a truncated region provides good results provided that sufficient number and refinement of sub-integrals is selected. For the case of a simple loaded area, these choices depend on the relative magnitude of load width w and maximum longitudinal coordinate (maximum z value). For multi-step loads integration must be refined to account for the additional complexity of the inverse integrals. For cases with loaded areas separated by large distances (relative to the load width) the use of superposition involving load components with less complex inverse integrals is beneficial.

AI.9 REFERENCES

- Brachman, R.W.I., I.D. Moore, and R.K. Rowe. 1995. Analysis of pipe structures in soil test cells - Ohio University facility, Geotechnical Research Centre Report GEOT-14-95, The University of Western Ontario.
- Brachman, R.W.I., I.D. Moore, and R.K. Rowe. 1996. Interpretation of a buried pipe test: Small diameter pipe in the Ohio University facility. Transportation Research Record, 1541, pp. 64-70.

- Fernando, N.S.M., and Carter, J.P. 1998. Elastic analysis of buried pipes under surface patch loading, *Journal of Geotechnical and Geoenvironmental Engineering*, Vol. 124, No. 8, ASCE, 720-727.
- Fernando, N.S.M., J.C. Small, and J.P. Carter. 1996. Elastic analysis of buried structures subject to three-dimensional surface loading, *International Journal for Numerical and Analytical Methods in Geomechanics*, Vol. 20, 331-349.
- Moore, I.D. and R.W.I. Brachman. 1994. Three dimensional analysis of flexible circular culverts, *Journal of Geotechnical Engineering*, Vol. 120, No. 10, pp. 1829-1844.
- Small, J.C., and W.K. Wong. 1988. The use of integral transforms in solving three dimensional problems in geomechanics, *Computers and Geotechnics*, 6(3), 199-216.

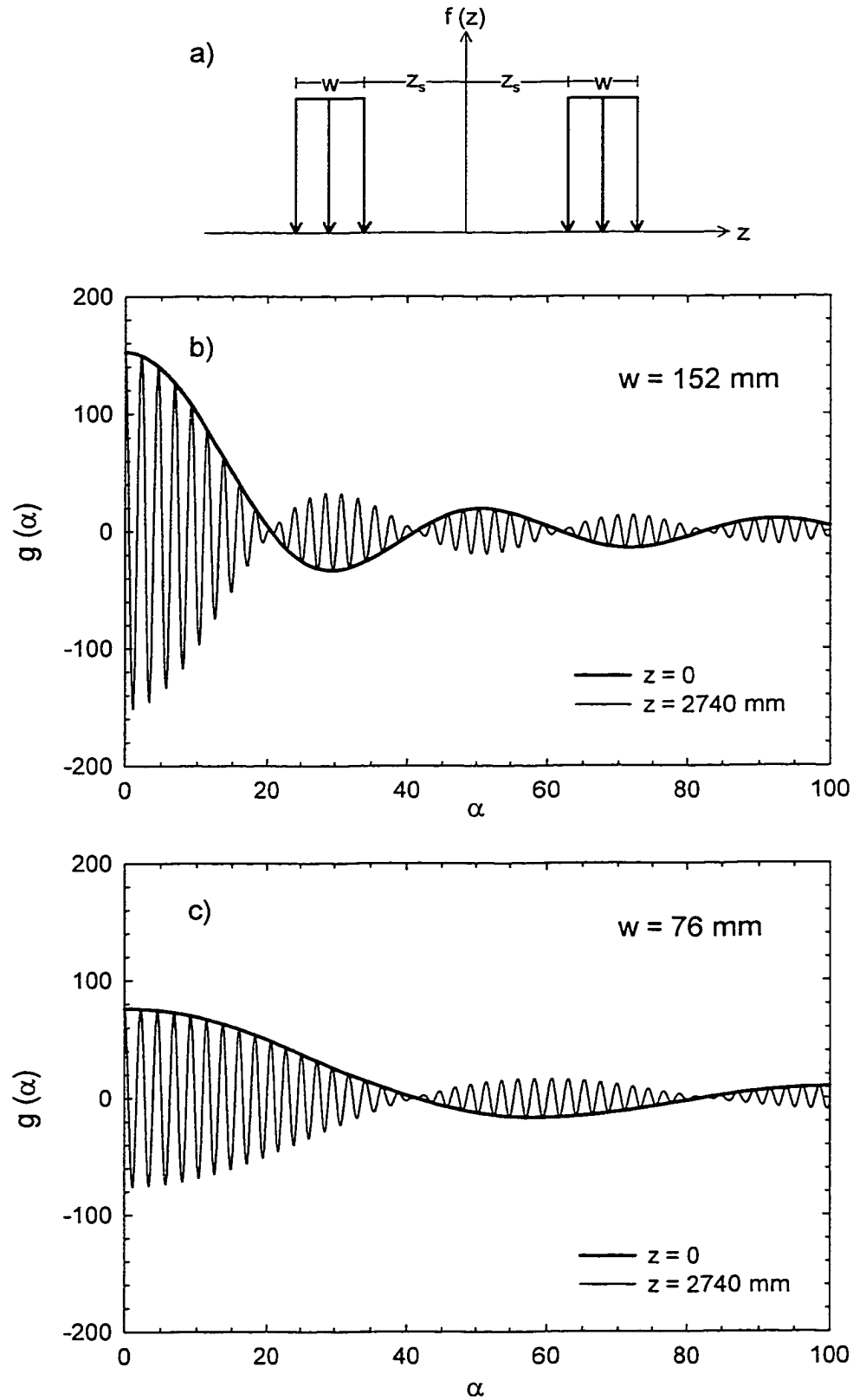


FIGURE AI.1 Inverse Fourier integrals for vertical applied loads. Generalized load function (a). Inverse integral for $z_s=0$ with: $w=152$ mm (b) and $w=76$ mm (c).

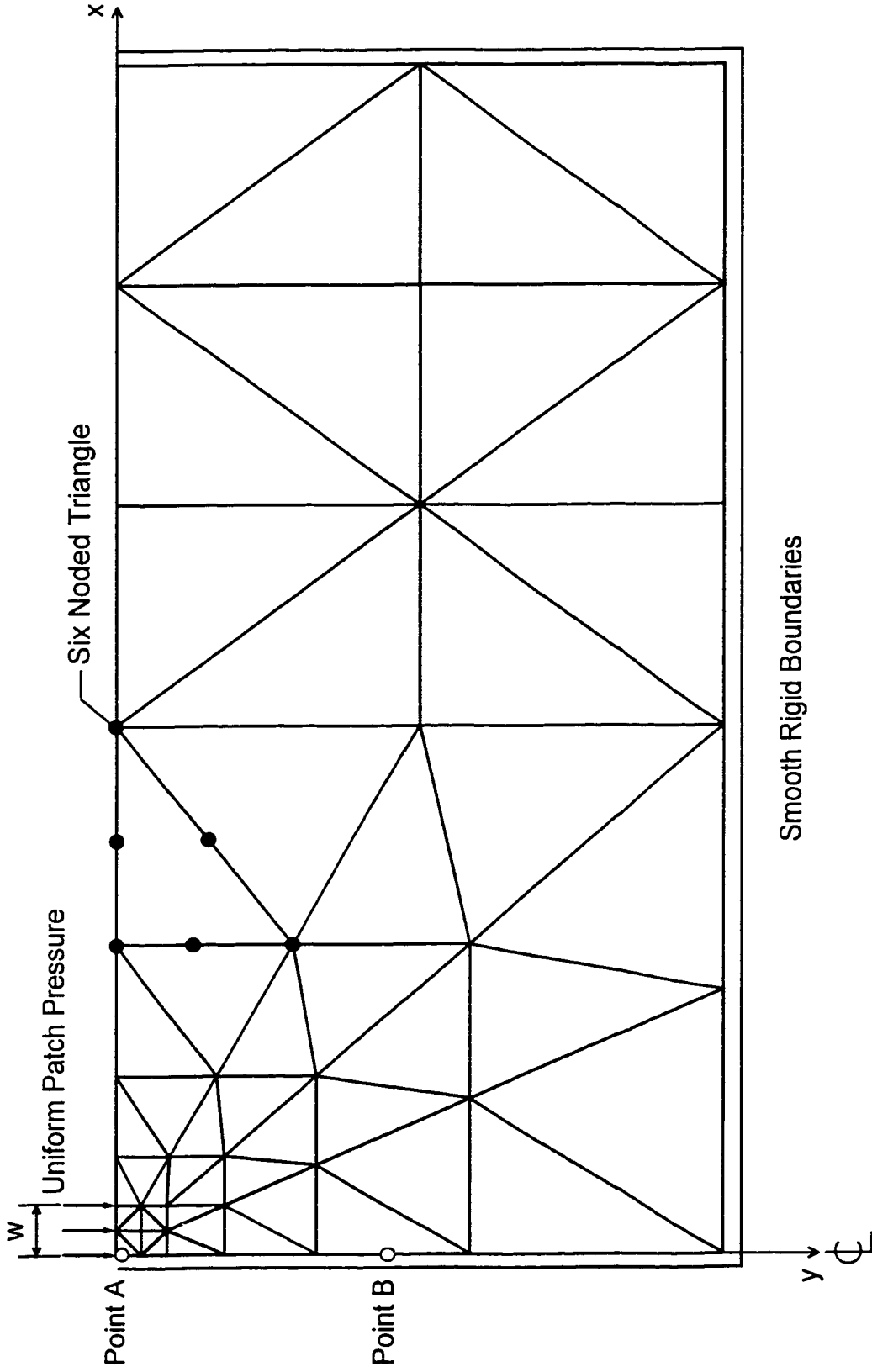


FIGURE A1.2 Two-dimensional finite element mesh used for test case.

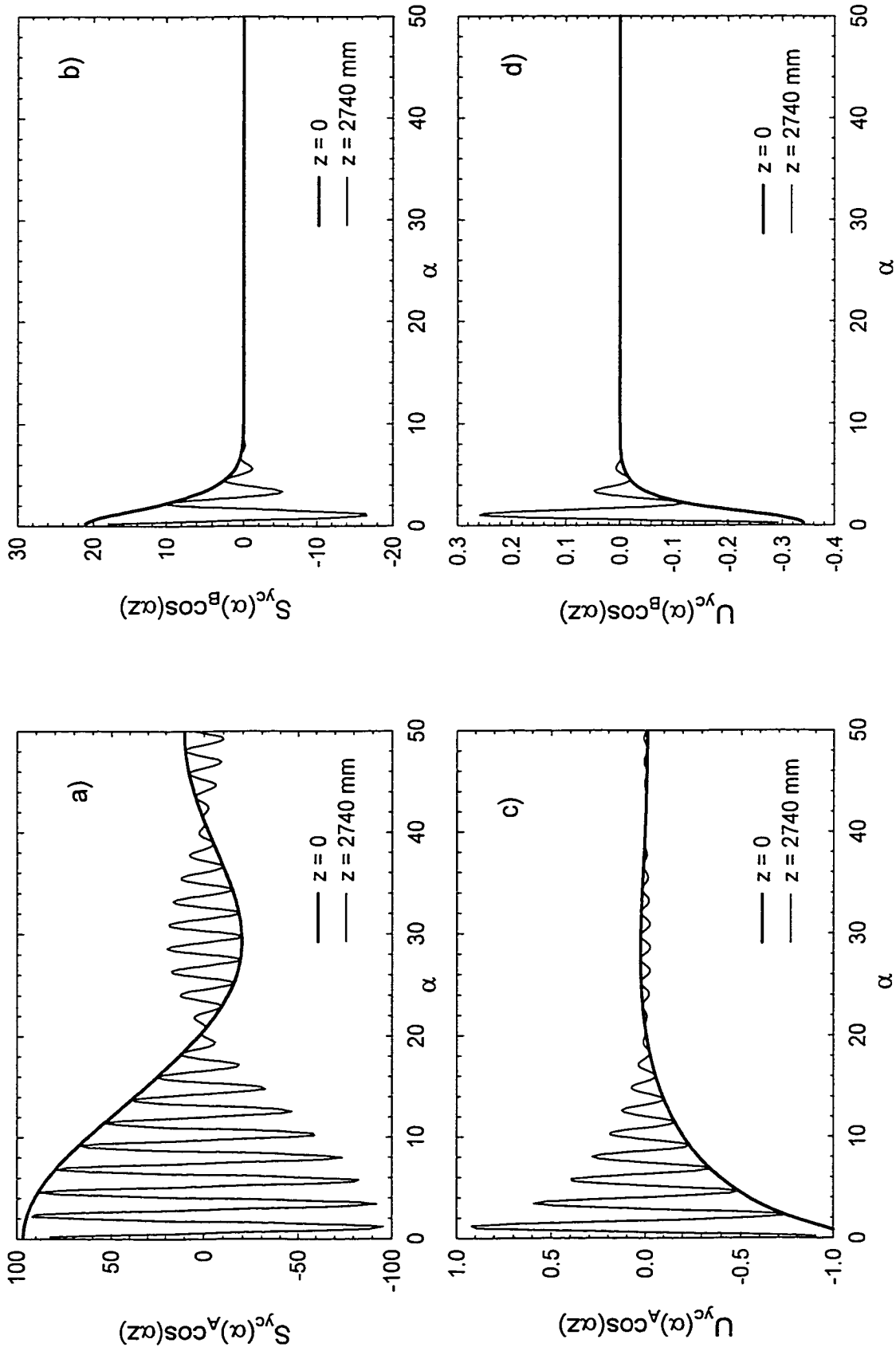


FIGURE A1.3 Inverse Fourier integrals for: (a) vertical stress at point A; (b) vertical stress at point B; (c) vertical displacement at point A; and (d) vertical displacement at point B (all with $w=152$ mm, $z_s=0$).

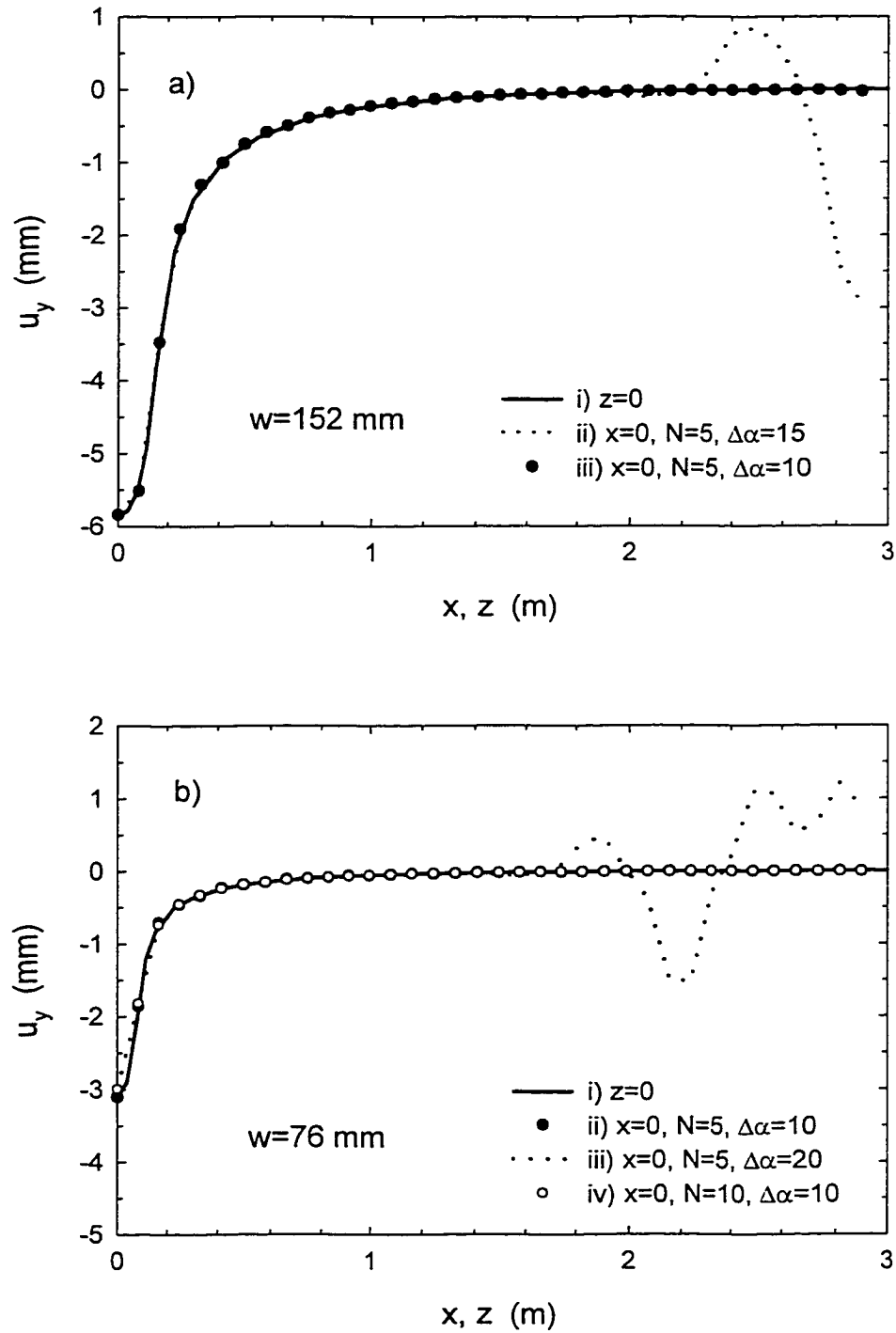


FIGURE AI.4 Vertical deflections (u_y) calculated at the surface using different integration schemes for: (a) $w=152$ mm, and (b) $w=76$ mm.

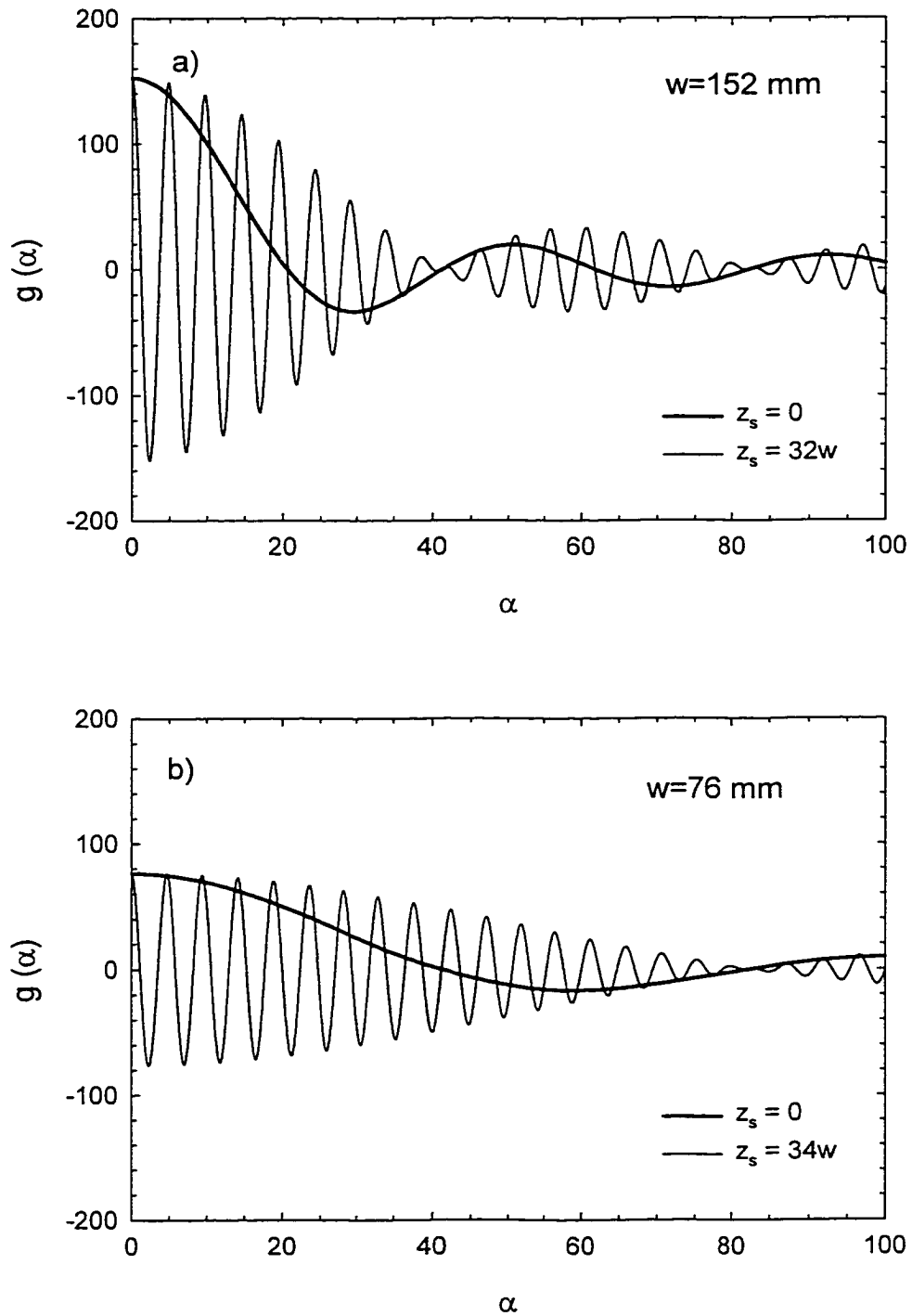


FIGURE AI.5 Inverse Fourier integrals for multi-step load variation showing effect of non-zero z_s (calculated at $z=0$) for: (a) $w=152$ mm, and (b) $w=76$ mm.

APPENDIX II

Constitutive Modelling of Soil Materials for Interpretation of Ohio University Test

AIL.1 INTRODUCTION

This appendix reports the details of a parametric study conducted to assess the significance of key soil and pipe constitutive parameters for the numerical analysis of a leachate collection pipe tested under stiff plate loading in the Ohio University test facility.

The constitutive modelling of the materials tested is of primary importance in the analysis of the load test. It is important to select a suitable constitutive model to represent the material behaviour, and appropriate parameters for use in the constitutive model. Several models were considered for use in the analysis. The features of each model are discussed and the implications for the analysis are clarified. Selection of parameters for use in the model is ideally based on appropriate laboratory or field tests. Unfortunately, Sargand (1993) does not report any strength or stiffness data for the materials used in the test. The approach to resolve this paucity of material parameters is two fold. First a range of expected values is estimated based on published constitutive data. Then a sensitivity analysis is performed over the identified range of values to ascertain the significance of key parameters. This approach permits engineering decisions to be made regarding the selection of material properties.

AII.2 CONSTITUTIVE MODEL

A key choice in the finite element analysis is the selection of a constitutive model to represent the strength and stiffness of the materials considered. It is useful to review the expected behaviour of the materials tested, prior to the selection of a constitutive model, so that the dominant features can be captured with the analysis. The stiffness of the crushed stone and cover soil materials (see Chapter 2, Fig. 2.1) are likely to be influenced by the stress levels within these materials. Shear failure is also expected to occur in this particular test beneath the corners of the rigid load platform, adjacent to the pipe in the crushed stone and both in the recompacted and *in situ* clay materials. The mechanisms leading to this shear failure are examined in Chapter 2. It is important to select a constitutive model with the ability to simulate shear failure of the soil materials.

The constitutive models that were considered for use in the analysis included: linear elastic, linear elasto-plastic and non-linear elasto-plastic models. The linear elastic model, characterized by Young's modulus E and Poisson ratio ν , models stress as linearly proportional to strain at a constant rate (E) for any stress level, and implies that no permanent deformation occurs upon unloading. Linear elasticity often provides a useful first approximation to solving complex problems, and will be useful in subsequent sections to clarify the behaviour observed in the Ohio University test facility.

The linear elasto-plastic model invokes linear elastic behaviour until a stress level is reached where the material yields. The strength of the materials is represented mathematically by the Mohr Coulomb failure criterion, characterized by cohesion c and angle of internal friction ϕ . Once yield occurs, a flow rule is used to characterise the plastic

strains in the material. Both associated and non-associated flow rules (Davis 1969) were considered, the latter featuring angle of dilation ψ less than the angle of internal friction. The non-linear elasto-plastic analysis differs from the linear elasto-plastic analysis by including the potential for non-linear elastic response. It is assumed that the material has a constant Poisson ratio and a variable Young's modulus E_t . The elastic tangent modulus E_t was represented using the Janbu (1963) stress dependent model:

$$E_t = K p_a \left(\frac{\sigma_3}{p_a} \right)^n \quad \text{AII - (1)}$$

where: E_t = elastic tangent Young's modulus,
 K = modulus number,
 n = modulus exponent,
 p_a = atmospheric pressure,
 σ_3 = minor principal stress.

Numerical analysis tools utilizing hyperbolic elasticity models, for example the U.S. Federal Highways Administration program CANDE (Katona et al. 1976; Musser 1989), are widely accepted approaches for analysing buried structures under working loads. Models formulated based on hyperbolic elasticity assume that incremental stress is proportional to incremental strain. This is not the case once soil materials yield, so CANDE cannot be expected to provide reliable solutions for this particular problem because of the widespread

shear failure in the soil for the Ohio University test. The mechanisms leading shear failure in the soil are examined in a later section.

Following the selection of a constitutive model, appropriate parameters are chosen for use in the analysis. The next sections outline the selection of material parameters for the materials featured in the Ohio University test.

AII.3 CRUSHED STONE

The stiffness of the crushed stone material surrounding the pipe (Fig. 2.1) is expected to have a significant effect on the results obtained from the numerical analysis. Typically, the modulus of the backfill material controls the deflections for HDPE pipes (Moore and Hu 1995). Unfortunately, Sargand (1993) does not report any information on the strength, stiffness, or even field density of the crushed stone.

Selig (1990) reports a data base of backfill modulus values for various stress levels. Figure AII.1 shows the dependence of modulus upon stress level for a well graded gravelly sand (SW) that Selig (1990) recommends for use with poorly graded gravel (GP) materials. Values are shown for two levels of compaction and were estimated for various values of major principal stress σ_1 with $\sigma_3 = \sigma_1/2$. Note that SW 95 refers to a well graded sand (Unified Soil Classification System) compacted to 95% of the maximum dry density (ASTM D698).

Modulus data obtained from large diameter triaxial tests on 25 mm crushed limestone railroad ballast (Ho 1980) are also plotted in Figure AII.1, again for two compaction levels. The modulus values of Ho (1980) are not extrapolated to high stress levels as these tests were

conducted at low confining pressures (maximum $\sigma_3=103$ kPa).

The modulus of the stone used in the Ohio University test may be inferred from the values in Figure AII.1. This approach should provide a reasonable range of modulus values both for variations in confining stress and for possible degrees of stone compaction. The stress levels in the stone around the pipe are expected to range from 150 kPa to 300 kPa for the load level investigated (see Figure 2.13). Over this stress range and with the variation in the degree of compaction, the modulus is estimated to vary between 25 MPa and 100 MPa.

The Poisson ratio ν may also be estimated from the data base of Selig (1990). Figure AII.2 shows the variation of ν with stress level and degree of compaction. There is no significant variation in this parameter for the expected stress levels in the Ohio University test facility. Therefore $\nu=0.25$ was selected for the crushed stone.

A sensitivity study was performed to determine the significance of the variation of the stone modulus upon the results of the analysis. Two dimensional elasto-plastic finite element analysis (described earlier) was performed with the material parameters summarized in Table 3. The selection of the cover soil, clay and *in situ* clay parameters will be discussed later. With these other parameters held constant, the modulus of the stone was varied between $E_{\text{stone}}=25$ MPa to 100 MPa. Figure AII.3 summarizes the results of the sensitivity analysis showing the calculated horizontal ΔD_H and vertical ΔD_V diameter change of the pipe for $E_{\text{stone}}=25$ MPa, 50 MPa and 100 MPa. These results are plotted along with the measured diameter changes.

As expected, an increase in the stone modulus results in a decrease in the magnitude of pipe deflection. However it appears that the pipe deflections are not that sensitive to the modulus of the stone. For the load level of $P_T=1400$ kN, doubling E_{stone} from 25 to 50 MPa

results in only a 15% decrease in the magnitude of ΔD_H and a 20% decrease in ΔD_V . A further increase in E_{stone} from 50 to 100 MPa yields only 15% and 8% decreases in the magnitude of ΔD_H and ΔD_V , respectively. Overall, it appears that the results of the analysis are not particularly sensitive to the modulus of the stone for the range of values expected in the test cell. This indicates that there may be some other dominant influence upon the pipe response. It will be shown subsequently that the presence of the rigid load platform leads to shear failure in the stone so that the significance of the stone modulus is reduced. The calculated response of the load platform showed only slight variation for the range of stone modulus values examined.

The sensitivity analysis was also repeated for the more realistic case of a stress dependent modulus for the stone. The parameters of Selig (1990) for SW 85 and SW 95 were again used with the Janbu stress dependent model. The results of these analyses are presented in Figure AII.4. Two cases are shown: $E_{\text{stone}}=6025\sigma_3^{0.6}$ kPa and $E_{\text{stone}}=9054\sigma_3^{0.35}$ kPa, which respectively correspond to values for SW 95 and SW 85 of Selig (Note: σ_3 in kPa). Again the deflections are only slightly smaller when a stiffer modulus is used. Overall, no significant effect is observed upon the calculated pipe response for the variation in modulus. Based upon the insensitivity of the pipe response to modulus selection, and coupled with the large uncertainties in the parameters, the use of a more complex model featuring stress dependent modulus appears to be unwarranted. For the remainder of the study, a stone modulus of $E_{\text{stone}}=50$ MPa is employed.

The influence of the angle of internal friction of the crushed stone ϕ_{stone} on the pipe response must also be considered. It is likely that this parameter is around 48° (explaining the value of $\phi_{\text{stone}}=48^\circ$ used in the previous analyses). The effect of a lower value of ϕ_{stone}

is examined in Figure AII.5 which shows the calculated pipe deflections for $\phi_{\text{stone}}=38^\circ$ and 48° , with all other parameters as listed in Table 3. These values are, again, compared with the measured deflections. The angle of internal friction was found to have only a slight effect upon the pipe deflections at high load levels.

The selection of ϕ_{stone} does have some effect upon the calculated response of the load platform. Figure AII.6 plots the platform deflections versus the total load applied to the platform P_T . Results are shown for the two values of ϕ_{stone} (38° and 48°) along with the values measured by Sargand (1993). The non-linear behaviour leading to an ultimate load exhibited in this plot is indicative of a bearing capacity failure of the ground beneath the rigid load platform. (The substantiation and implications of this issue will be further examined later in the report). A decrease in ϕ_{stone} from 48° to 38° leads to a 6% decrease in ultimate load calculated. Overall, the pipe and platform deflections are not greatly affected by ϕ_{stone} . Therefore the value of $\phi_{\text{stone}}=48^\circ$ was selected for use in the analysis.

The effect of the flow rule adopted for the stone on the calculated results was investigated for both associated $\psi_{\text{stone}}=\phi_{\text{stone}}$ and non-associated $\psi_{\text{stone}}\neq\phi_{\text{stone}}$ flow rules. The pipe and platform deflections calculated with a variation in ψ_{stone} are shown in Figures AII.7 and AII.8, respectively. Again, all other parameters were as specified in Table 3. The values obtained using the associated flow rule over estimate the volume change of the stone material. The softening response observed with $\psi=\frac{1}{2}\phi$ yields greater pipe and platform deflections than that with $\psi=\phi$. The more realistic non-associated flow rule was adopted for use in the analysis.

AII.4 COVER SOIL

The parameters for the cover soil (GP dumped in place) may be estimated in a similar manner as that for the crushed stone. However, it is likely that this parameter does not significantly influence the pipe response. The cover soil is located away from the pipe (greater than 4.5 pipe diameters) as it is placed between the crushed stone and the *in situ* clay material (see Fig. 2.1).

The modulus of the cover soil may be expected to vary within this layer as it is confined in locations beneath the load platform, while the material closer to the *in situ* clay is subjected to lower confining stress. A value of $E_{\text{cover}}=20$ MPa was selected for the analysis. Doubling of the modulus resulted in less than a 14% decrease in ΔD_v . The properties of the cover soil material do not significantly influence the results since, as will be shown subsequently, there is shear failure beneath the corner of the load platform.

AII.5 CLAY

The strength and stiffness of the compacted clay "liner" and *in situ* stiff clay materials (Fig. 2.1) are expected to dominate the response of the load platform for this particular test. The only information Sargand (1993) provides regarding the clay material was that the average *in situ* density was 16.7 kN/m^3 and the average moisture content was 25.3%.

The data base of Selig (1990) was consulted again to estimate the likely range of modulus values for the clayey materials (E_{clay}). For the load level investigated (see Fig. 36)

the stress level is expected to be around 170 kPa to 250 kPa. Using data for CL 85 and CL 95, the modulus is likely to be from 5 MPa to 10 MPa. Figure AII.9 indicates that the selection of E_{clay} has little effect on the diameter change calculated with clay modulus values of 5 and 10 MPa. The slope of the load deflection curve is influenced by the value of clay modulus, Figure AII.10, as a stiffer response is observed for $E_{\text{clay}}=10$ MPa than for $E_{\text{clay}}=5$ MPa.

The presence of the softer clayey material beneath the crushed stone may lead to bending type deformations within the stone layer. The ratio of stone to clay modulus ($E_{\text{stone}}/E_{\text{clay}}$) is therefore an important feature to model in the analysis. Table 4 provides estimates of the ratio of stone modulus to clay modulus for various stress levels. Using SW 85 data that Selig (1990) recommends for use with SW, SP, GW and GP materials and CL 95 (implying a high degree of compaction) to characterise the modulus of the stone and clay, respectively, provides a lower bound estimate of modulus ratio. Likewise using SW 95 and CL 85 provides an upper estimate of modulus ratio. These results demonstrate that the ratio of elastic stone modulus to elastic clay modulus is expected to lie between 2.4 and 20. The selection of $E_{\text{stone}}=50$ MPa with $E_{\text{clay}}=10$ MPa provides a modulus ratio of 5 which appears to be reasonable based on the data in Table AII.2.

The nature of the load-deflection curve for the platform is indicative of bearing capacity failure in the ground below. Consequently, the strength parameters of the clay are expected to control the peak load applied to the platform. An estimate of clay cohesion can be inferred from the ultimate capacity of the load-deflection curve. From Figure AII.11 the ultimate load is estimated to be $P_{\text{ULT}} \approx 2200$ kN. Conventional bearing capacity analysis (Rowe and Soderman 1987) for the clay foundation, treating the granular material as a

surcharge and with a shape factor of 1.1, yields an estimate of clay cohesion (assuming undrained conditions, ie. $\phi_{\text{clay}}=0^\circ$) of 60 kPa (explaining the value adopted for the previous analyses). The effect of varying the clay cohesion on the load platform response is presented in Figure AII.11 for c_{clay} values of 40, 60 and 80 kPa. Doubling the clay cohesion essentially doubles the ultimate load applied to the platform. Clay cohesion, however, has negligible effect on the pipe deflections calculated with the finite element analysis. Therefore the selection of clay cohesion of 60 kPa appears to be reasonable.

The previous analyses assume that the clay material is saturated. Based on the reported density and water content, and assuming a value for the relative density of the solid phase, the degree of saturation for the recompacted clay may be estimated to be around 70%. The shear strength of an unsaturated soil includes a contribution of strength from matrix suction. Traditional shear strength parameters were not reported by Sargand, let alone information on the soil-water characteristic curve required to interpret the shear strength behaviour of a partially saturated soil (Fredlund and Rahardjo 1993). An alternative analysis was performed with a non-zero angle of internal friction for the clay to assess the assumption of ϕ_{clay} equal to zero. For $c_{\text{clay}}=30$ kPa and $\phi_{\text{clay}}=10^\circ$, which yields a similar ultimate load as that for $c_{\text{clay}}=60$ kPa and $\phi_{\text{clay}}=0^\circ$ (Fig. AII.13), a slight influence on pipe deflection was calculated, Figure AII.12. In this light, it appears reasonable to characterise the clay with a cohesion of 60 kPa and a zero friction angle.

AII.6 HDPE PIPE

The HDPE response was characterized with a secant Young's modulus of $E_{HDPE}=470$ MPa and Poisson ratio of $\nu=0.4$. The secant modulus was selected using data reported by Moore and Hu (1994), corresponding to the 2.5 hour time interval of the test. The selection of HDPE modulus will have some influence on thrust and moment predictions. However, pipe deflections are not significantly affected by pipe modulus as shown in Figure AII.14. Increasing E_{HDPE} to 705 MPa (which would be an upper bound estimate) yields a 20% decrease in the calculated pipe deflections at a load level of $P_T=1500$ kN. Therefore a secant modulus of 470 MPa appears to be reasonable.

AII.7 SUMMARY

Linear elastic, linear elasto-plastic and non-linear elasto-plastic constitutive models were evaluated for use in analyzing the results from the Ohio University test. Analysis featuring a constant modulus was shown to give reasonable results. A linear elasto-plastic model with a non-associated flow rule was demonstrated to provide good results. Published data and a parametric study of the effect of uncertainty regarding: E_{stone} , ϕ_{stone} , ψ_{stone} , E_{cover} , c_{clay} , ϕ_{clay} and E_{HDPE} were used to select the material properties for use in the analysis. The constitutive parameters used in the final analysis are summarized in Table AII.1.

AIL.8 REFERENCES

- Davis, E.H. 1969. Theories of Plasticity on the failure of soil masses. *Soil Mechanics Selected Topics*. I.K. Lee (Ed.), London: Butterworth, pp. 341-374.
- Fredlund, D.G., and H. Rahardjo. 1993. *Soil Mechanics for Unsaturated Soils*, Wiley Publications, New York.
- Ho, Deh Chao. 1980. Stress-strain properties of railroad ballast. M.Sc. Project Report, University of Massachusetts at Amherst, March, 1980.
- Janbu, N. 1963. Soil compressibility as determined by oedometer and triaxial test. In *Proceedings of the European Conference on Soil Mechanics and Foundation Engineering*, Weisbaden, Volume 1, pp. 19-25.
- Katona, M.G., J.M. Smith, R.S. Odello, and J.R. Allgood. 1976. CANDE - A modern approach for the structural design and analysis of buried culverts. Federal Highway Administration, Report No. FHWA-RD-77-5, October 1976.
- Moore, I.D. and F. Hu. 1994. Analysis and design of buried high density polyethylene gravity flow pipe, Geotechnical Research Centre Report GEOT-17-94, University of Western Ontario. pages.
- Moore, I.D. and F. Hu. 1995. Significance of time dependent HDPE response. 1995 Annual Conference of the Canadian Society of Civil Engineering, June 1-3, 1995, Ottawa, Ontario, pp. 555-564.
- Musser, S.C. 1989. CANDE-89 User Manual, U.S. Department of Transportation, Federal Highway Administration, Publication No. FHWA-RD-89-169, June 1989, 236 pages.

- Rowe, R.K., and K.L. Soderman. 1987. Stabilization of very soft soils using high strength geosynthetics: the role of finite element analyses, *Geotextiles & Geomembranes*, Vol. 6, pp 53-80.
- Sargand, S.M. 1993. Structural performance of an HDPE leachate collection pipe. *Proceedings of the 31st Annual International Solid Waste Exposition*, August 2-5, 1993, San Jose, CA, pp. 381-402.
- Selig, E.T. 1990. Soil properties for plastic pipe installations. *Buried Plastic Pipe Technology*, ASTM STP-1093, Buczala and Cassady (Eds.), ASTM, Philadelphia, pp. 141-158.

TABLE AII.1 Constitutive Soil Parameters Used in the Study

	Stone	Cover Soil	Clay	<i>In Situ</i> Clay
E (MPa) / ν	50 / 0.25	20 / 0.20	10 / 0.35	10 / 0.35
c (kPa) / ϕ°	0 / 48	0 / 36	60 / 0	60 / 0

TABLE AII.2 Estimates of Elastic Modulus Ratio $E_{\text{stone}}/E_{\text{clay}}$ (modulus data from Selig 1990). Modulus in MPa.

Stress Level (kPa)	Lower Estimate			Upper Estimate		
	E_{stone}	E_{clay}	$E_{\text{stone}}/E_{\text{clay}}$	E_{stone}	E_{clay}	$E_{\text{stone}}/E_{\text{clay}}$
	SW 85	CL 95		SW 95	CL 85	
6.9	9.0	2.8	3.3	11	0.69	16
35	15	5.5	2.6	28	1.7	16
69	18	7.6	2.4	41	2.8	15
140	23	9.0	2.5	59	4.1	14
280	28	9.7	2.9	90	4.8	19
410	32	10	3.1	110	5.5	20

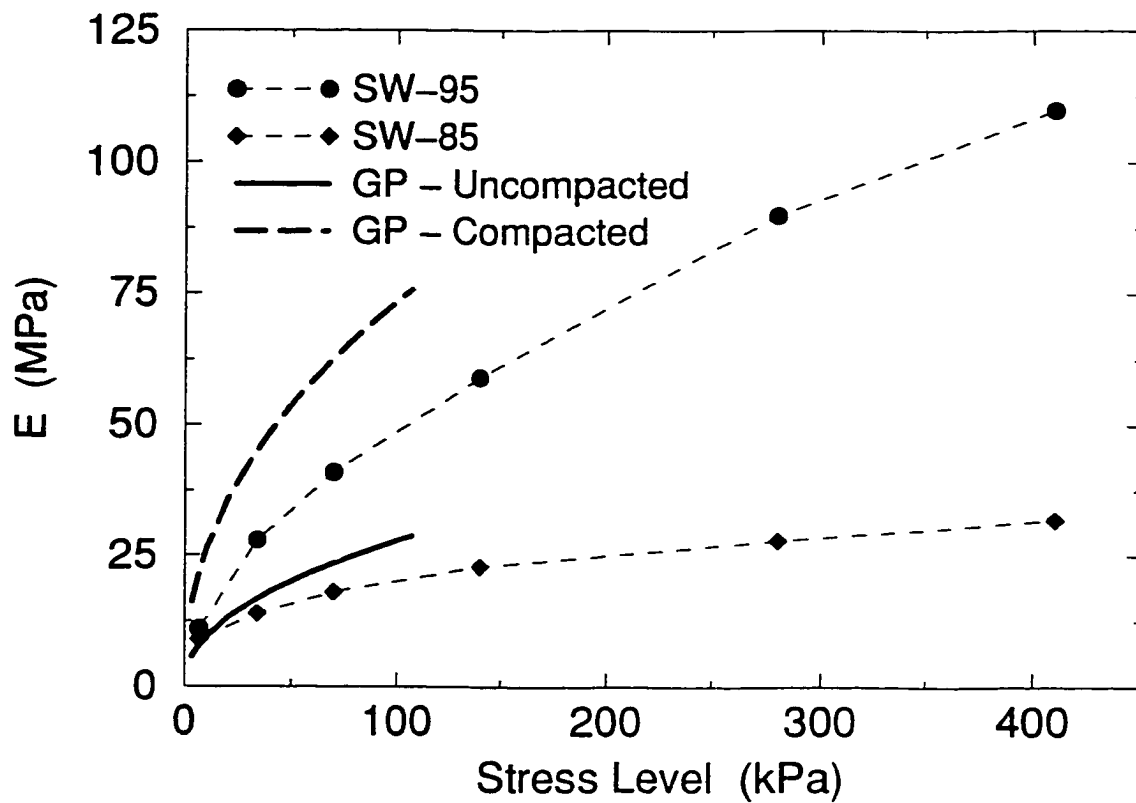


FIGURE AII.1

Elastic modulus (E) as a function of stress level for well graded sand compacted to 85% and 95% maximum dry density (data from Selig, 1990) and for 25 mm crushed limestone (data from Ho, 1980).

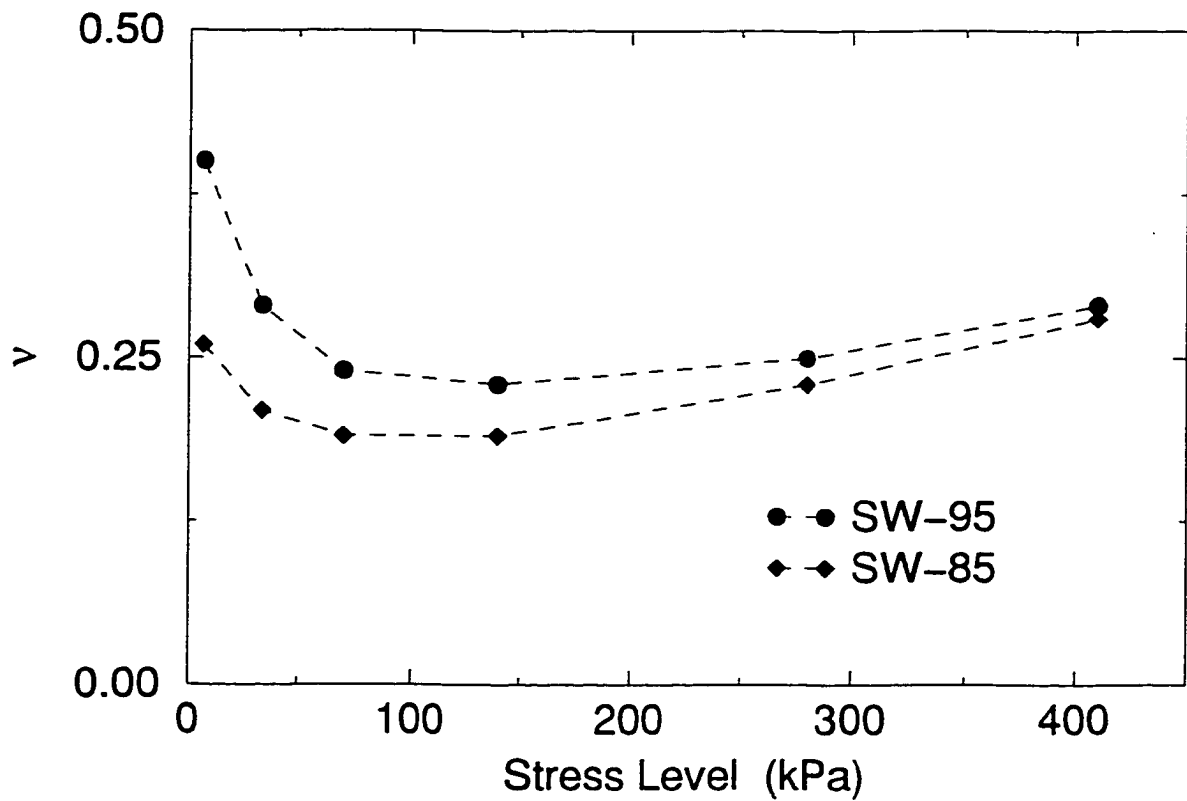


FIGURE AII.2

Poisson ratio (ν) as a function of stress level for well graded sand compacted to 85% and 95% maximum dry density (data from Selig, 1990).

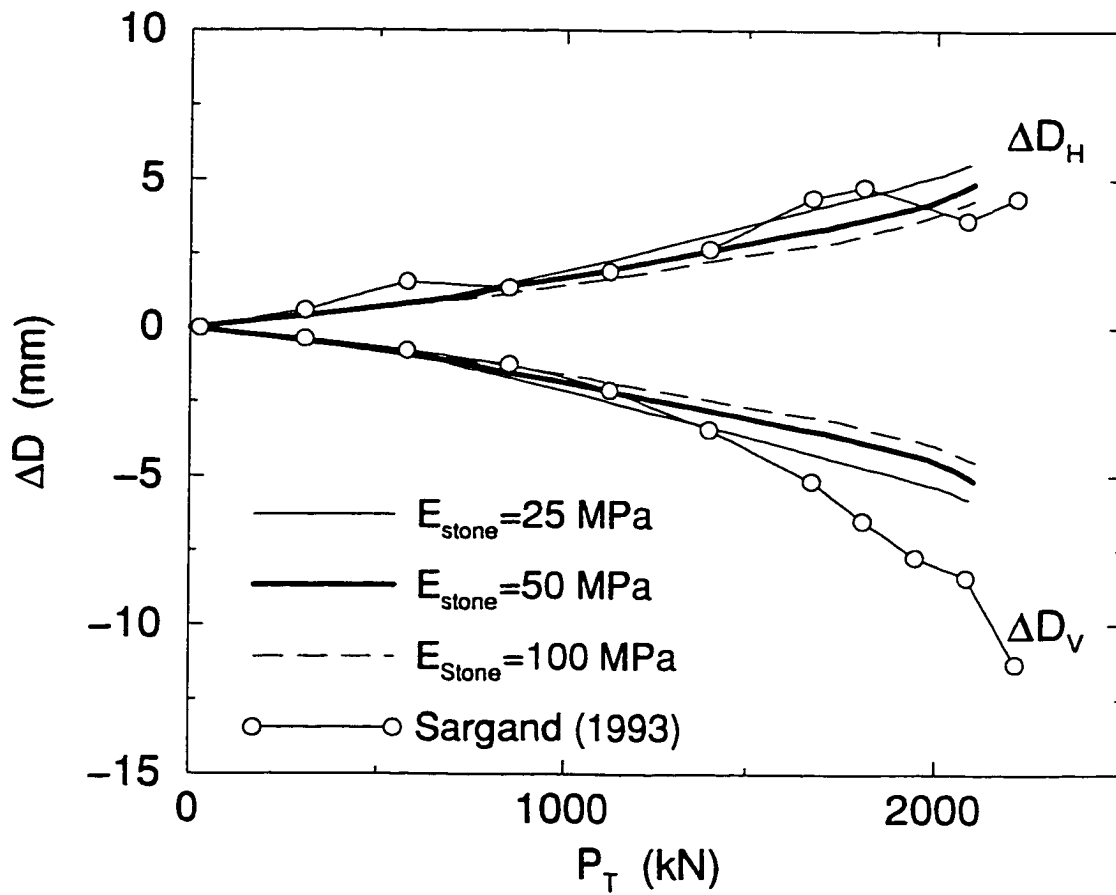


FIGURE AII.3 Effect of constant stone modulus (E_{stone}) on pipe deflections.

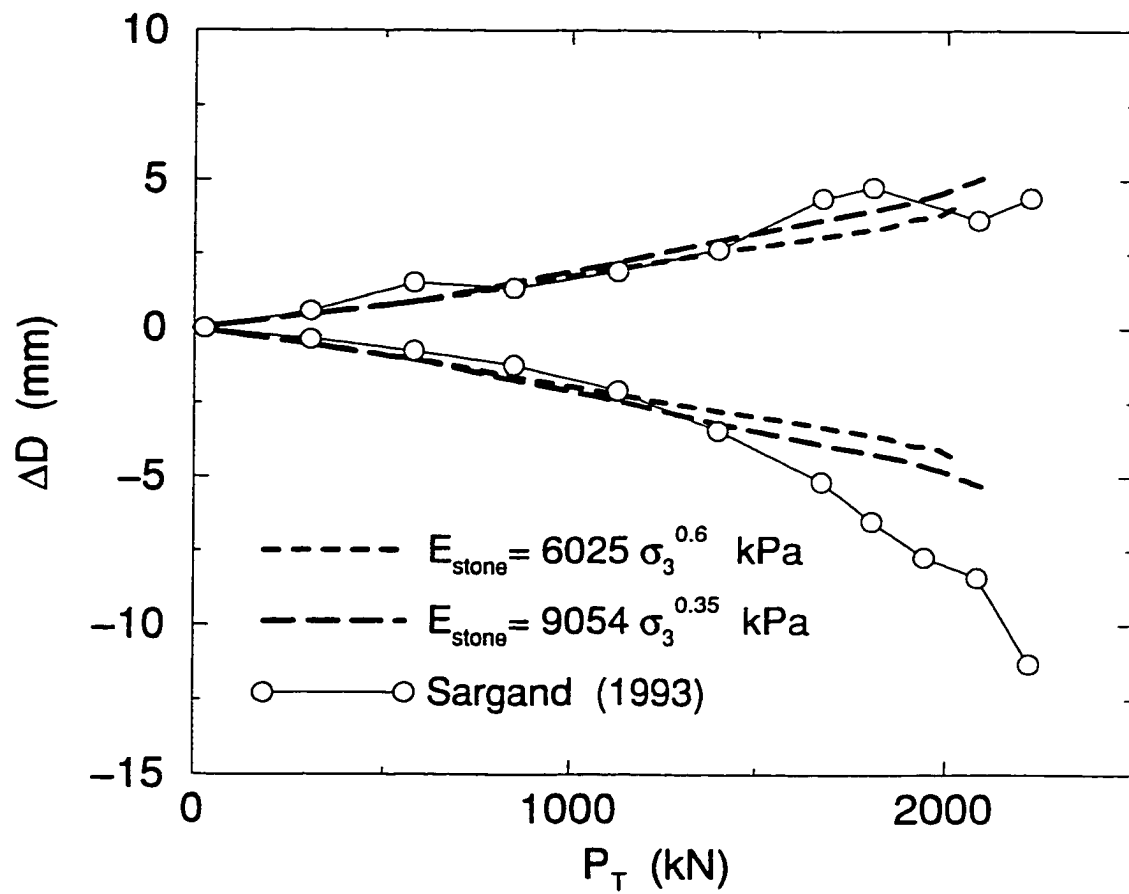


FIGURE AII.4 Effect of stress dependent modulus ($E_{\text{stone}}(\sigma)$) on pipe deflections (NOTE: σ_3 in kPa).

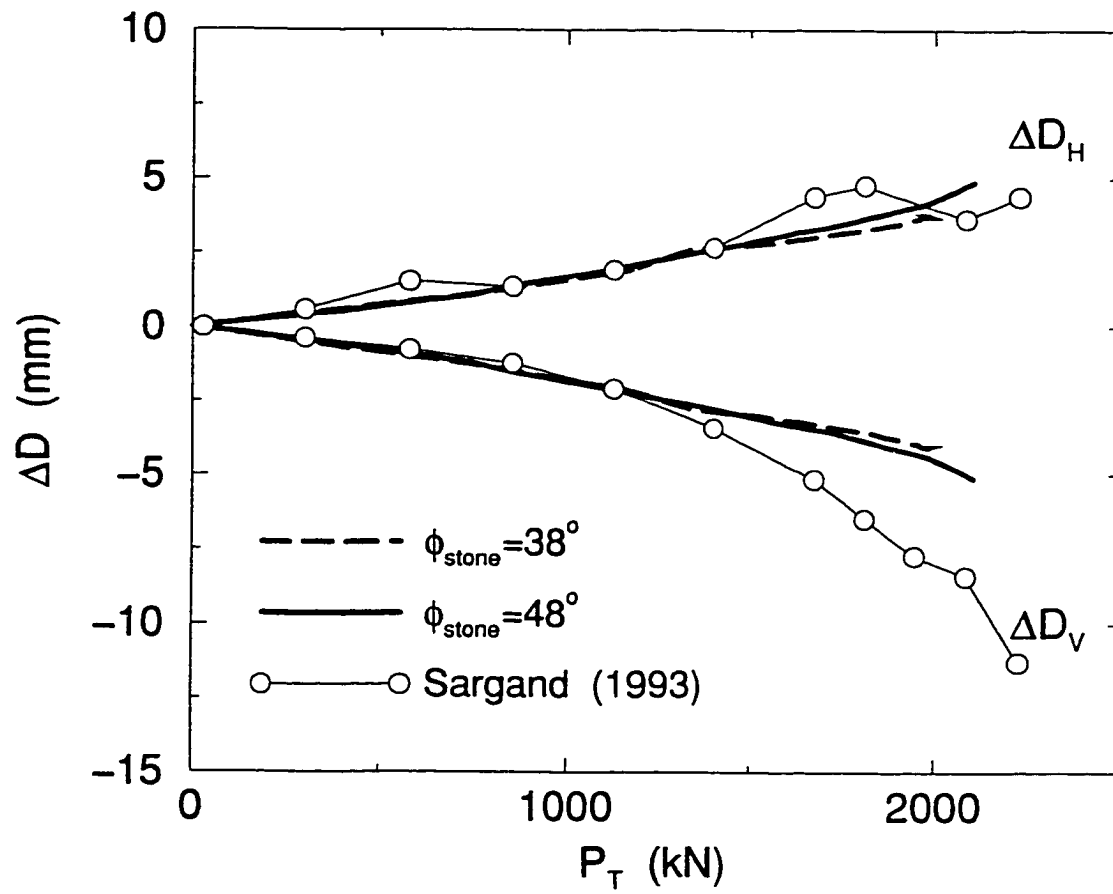


FIGURE AII.5 Effect of the angle of internal friction (ϕ_{stone}) of the stone on pipe deflections.

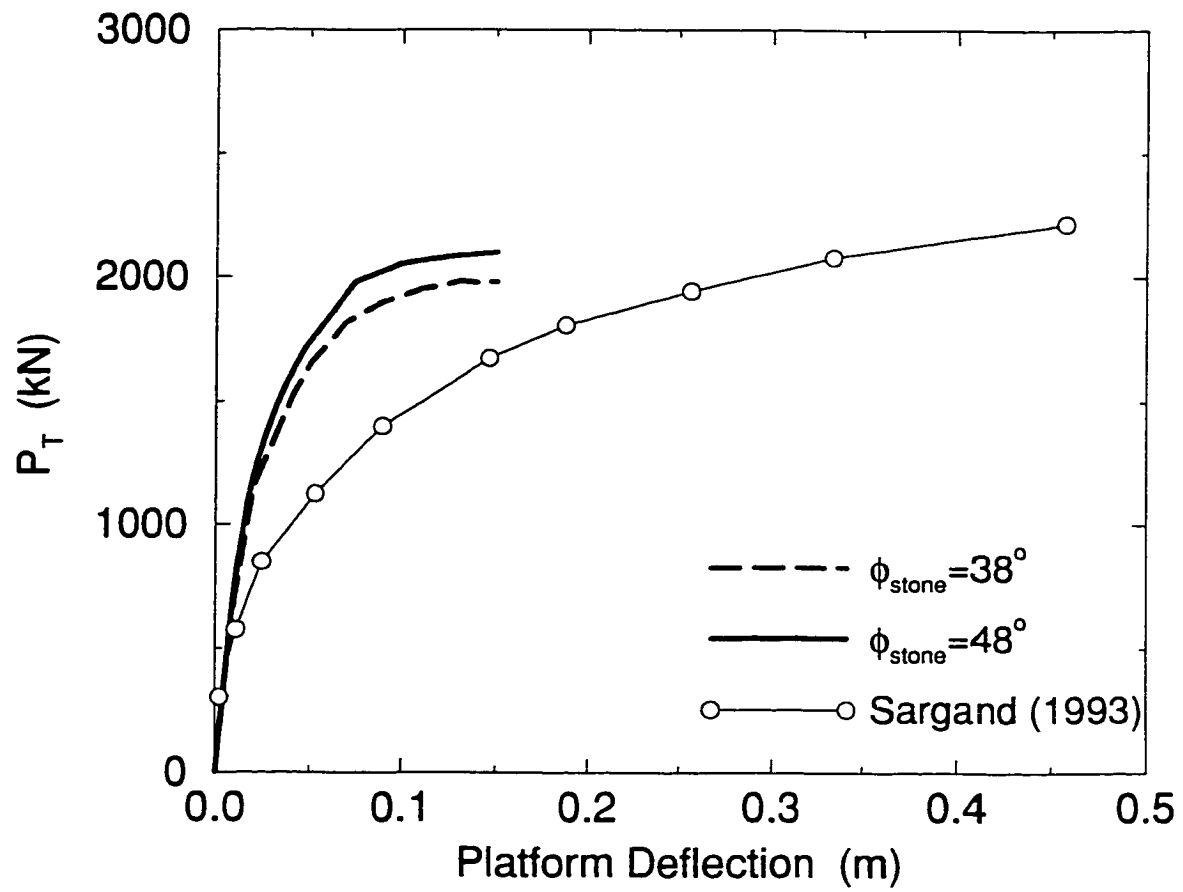


FIGURE AII.6

Effect of the angle of internal friction (ϕ_{stone}) of the stone on load platform deflections.

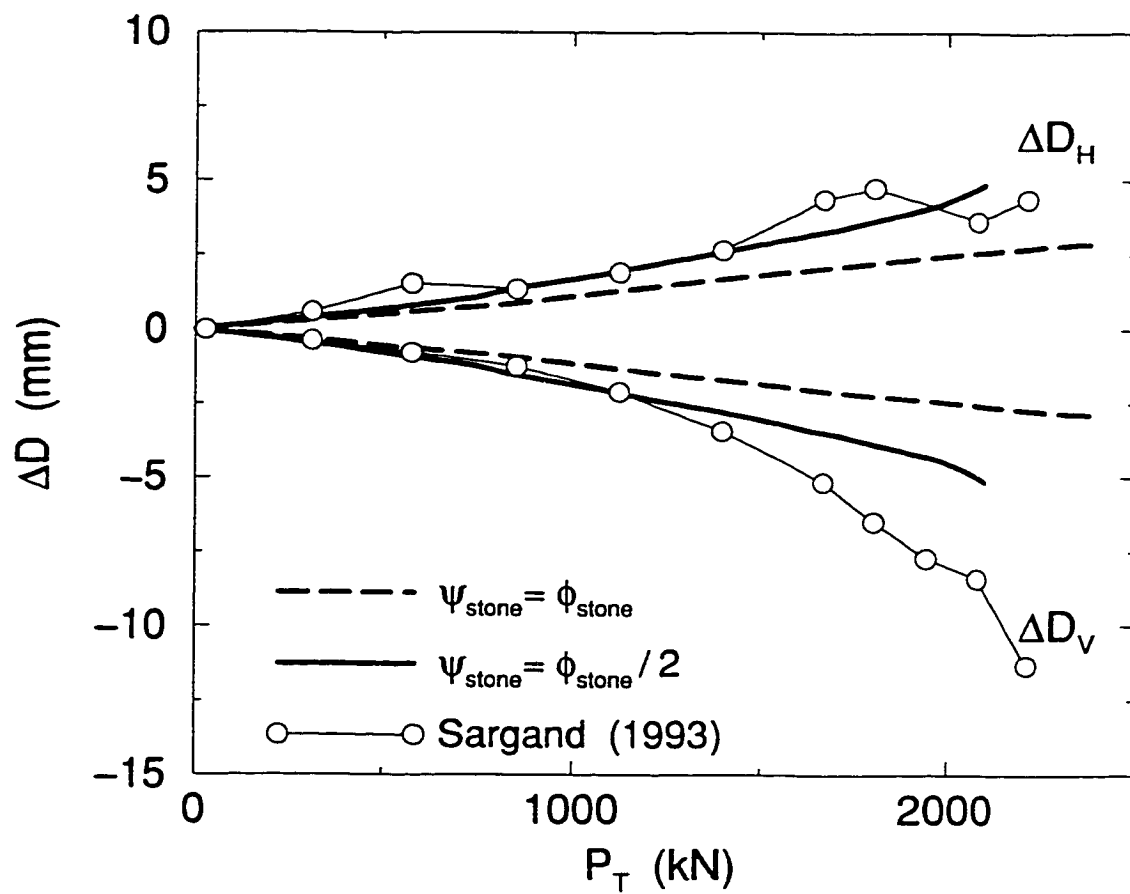


FIGURE AII.7 Effect of flow rule adopted for stone on pipe deflections.

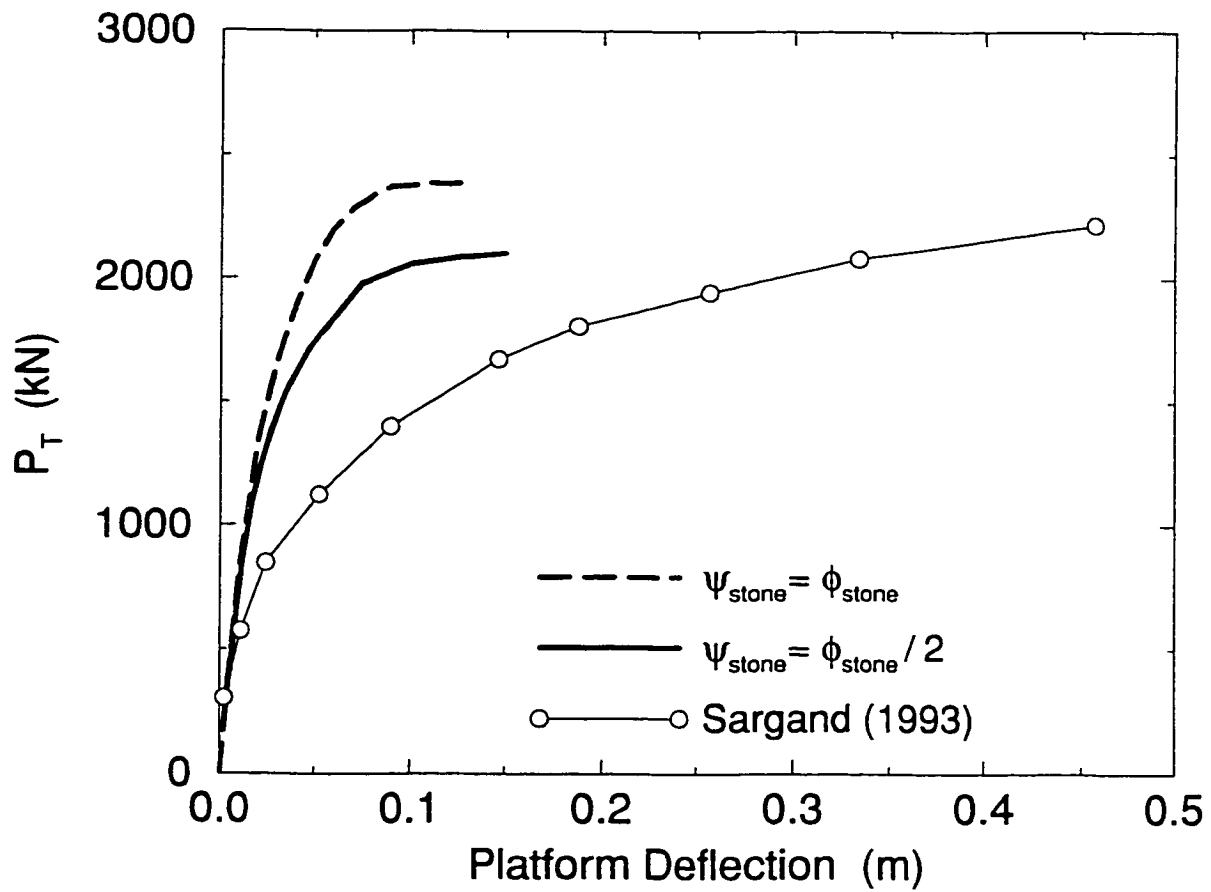


FIGURE AII.8 Effect of flow rule adopted for stone on platform response.

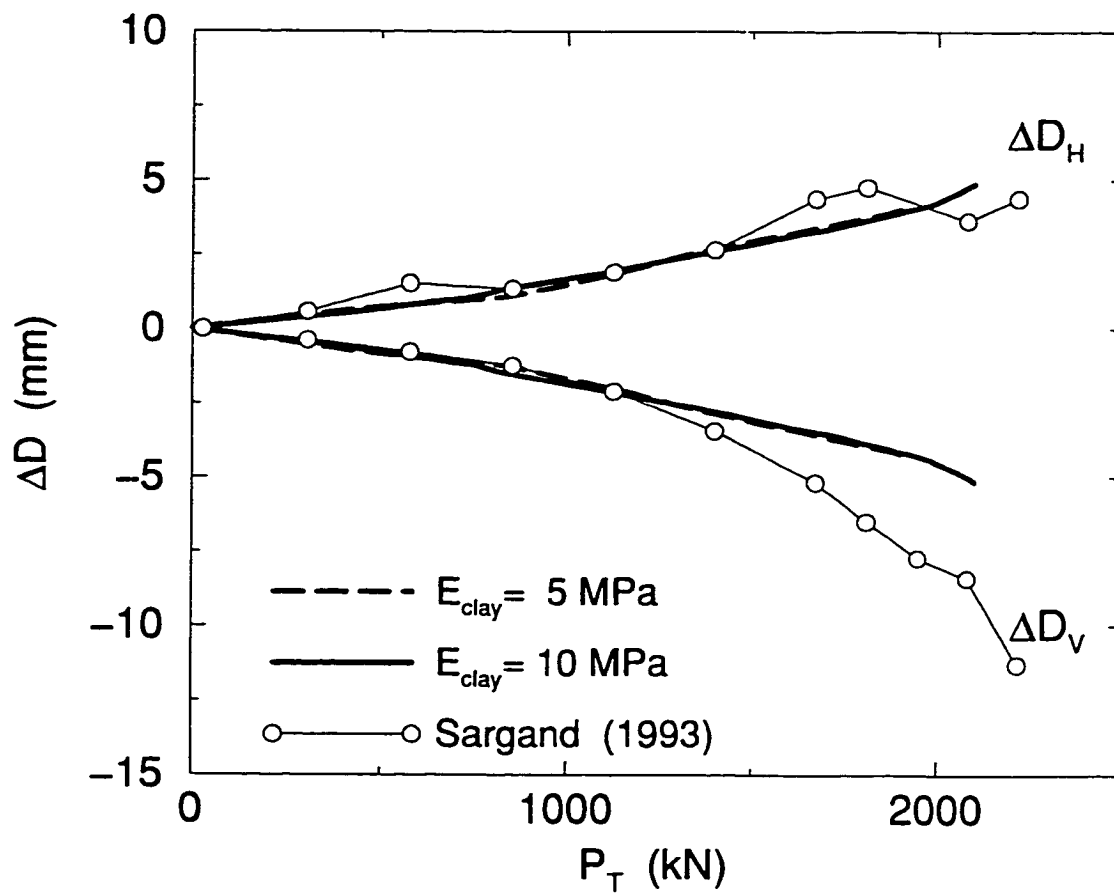


FIGURE AII.9 Effect of clay modulus (E_{clay}) on pipe deflections.

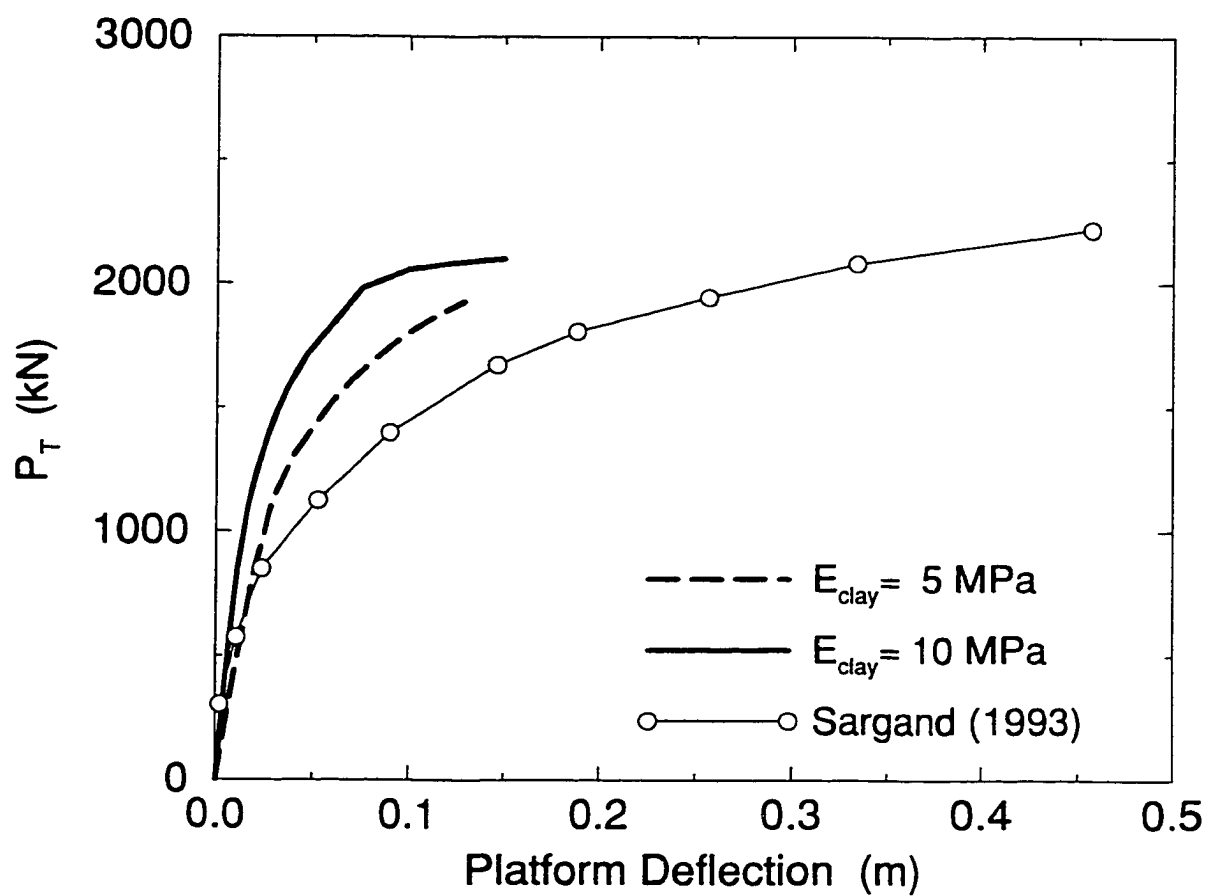


FIGURE AII.10 Effect of clay modulus (E_{clay}) on load platform response.

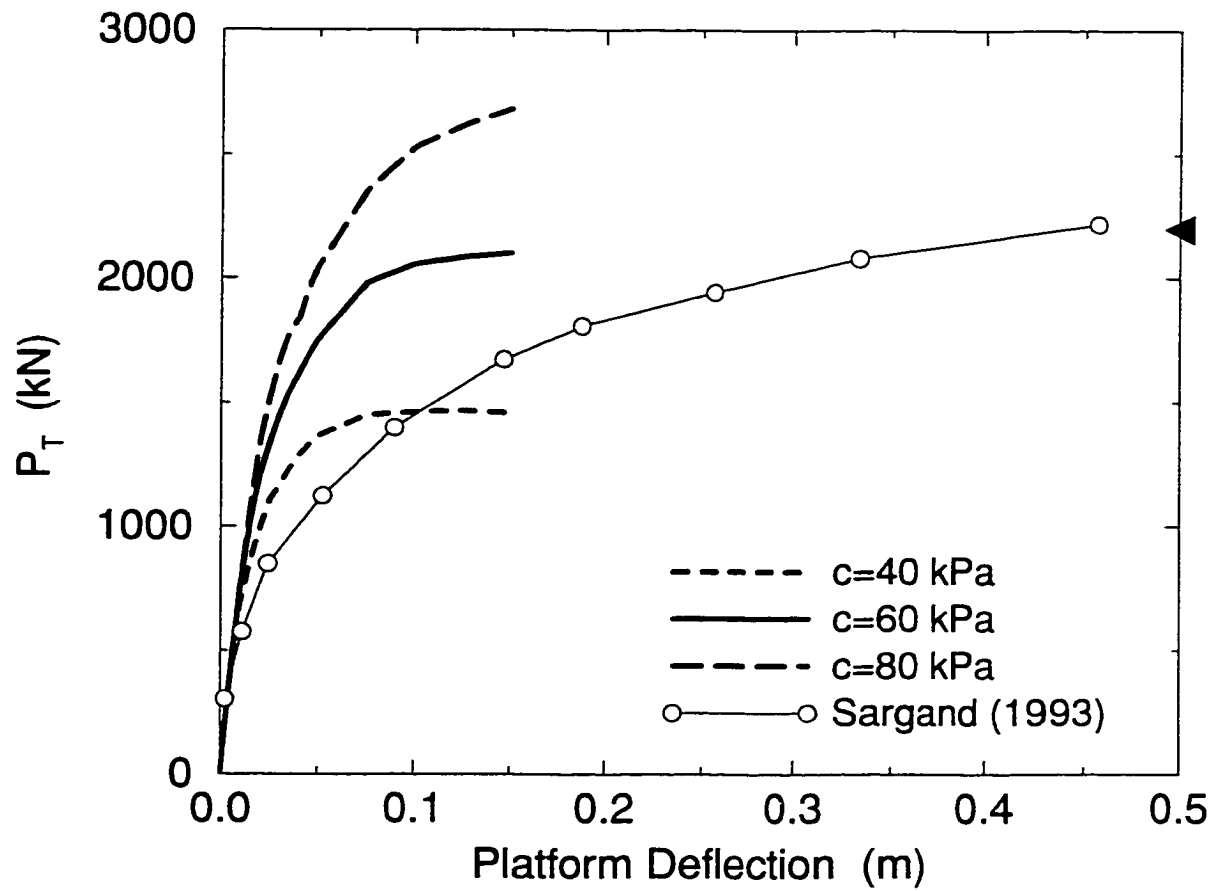


FIGURE AII.11 Effect of clay cohesion (c_{clay}) on load platform response.

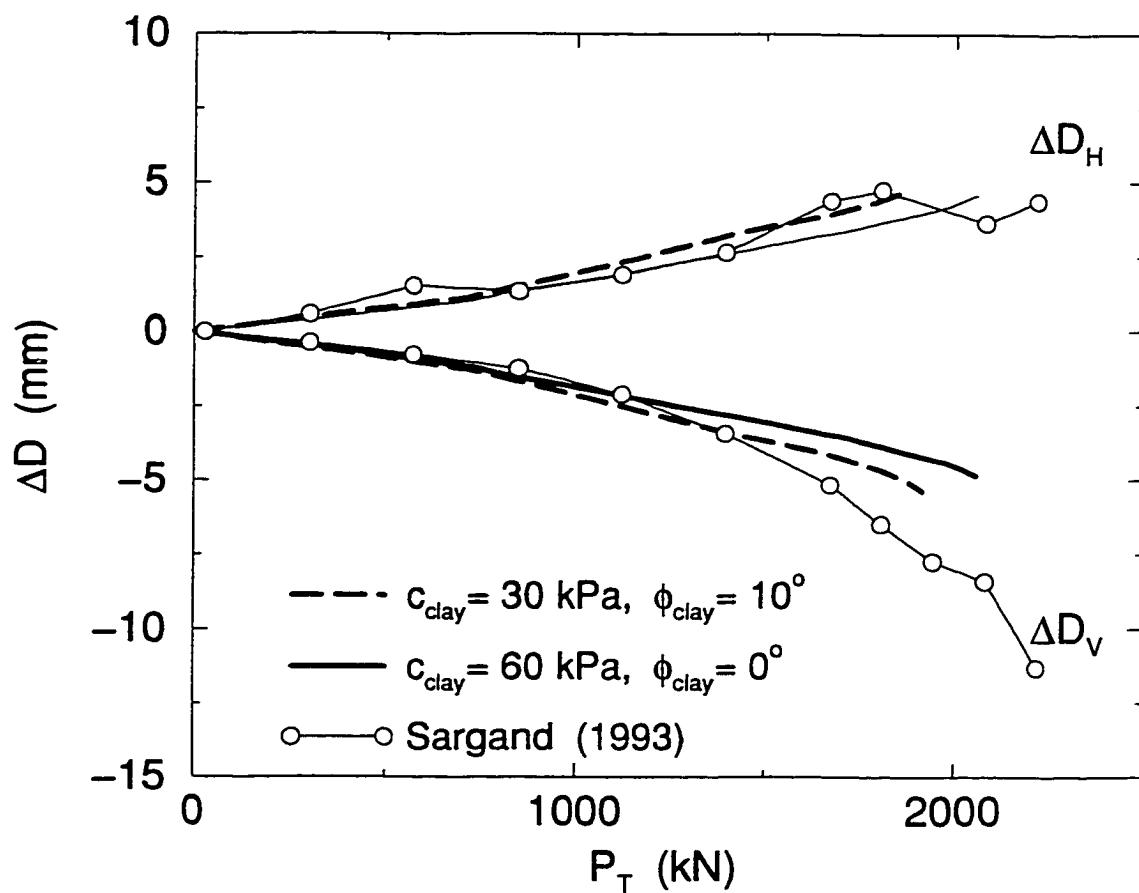


FIGURE AII.12 Effect of clay cohesion and angle of internal friction (c_{clay} , ϕ_{clay}) on pipe deflections.

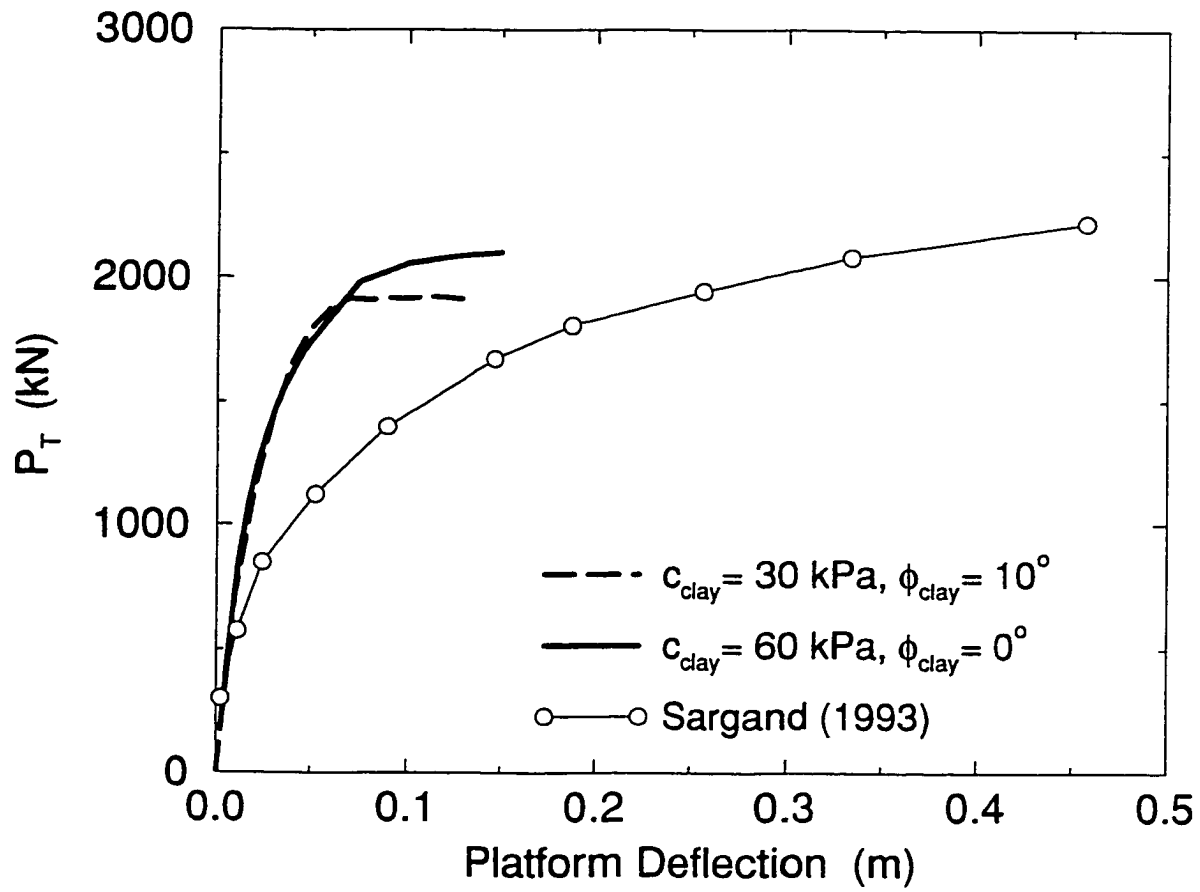


FIGURE AII.13 Effect of clay cohesion and angle of internal friction (c_{clay} , ϕ_{clay}) on load platform response.

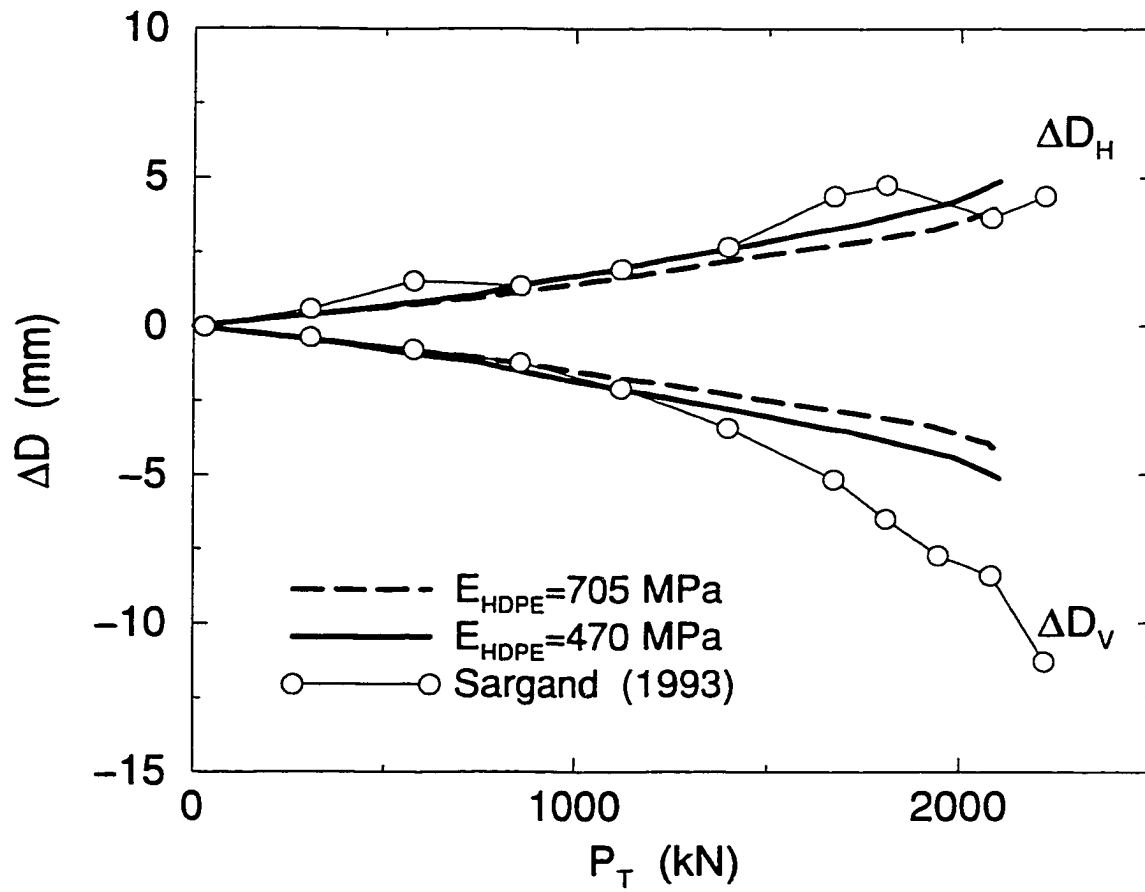


FIGURE AII.14 Effect of polyethylene modulus (E_{HDPE}) on pipe deflections.

APPENDIX III

Laboratory Results

Laboratory results from Tests P3a, P3b, P3c and P4 are appended. Measured pipe deflections, interior strains and exterior strains are given.

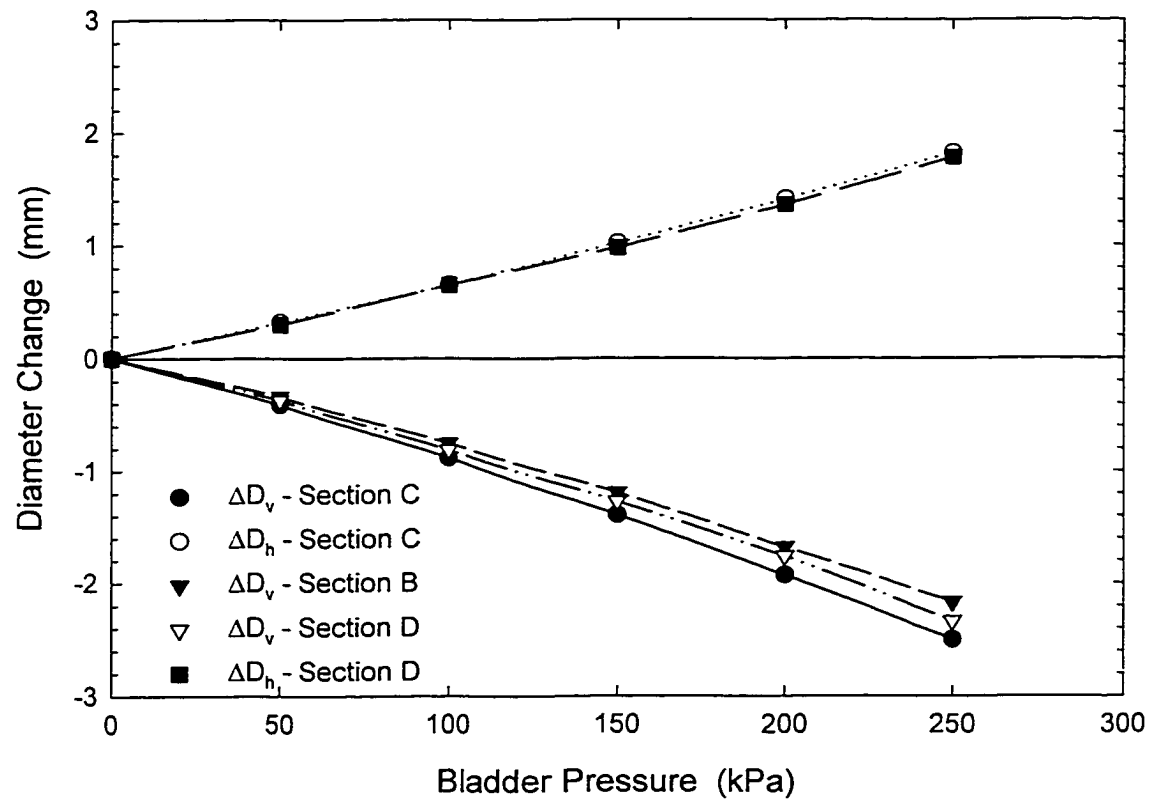


FIGURE AIII.1 Measured vertical ΔD_v and horizontal ΔD_h diameter change for test P3a.

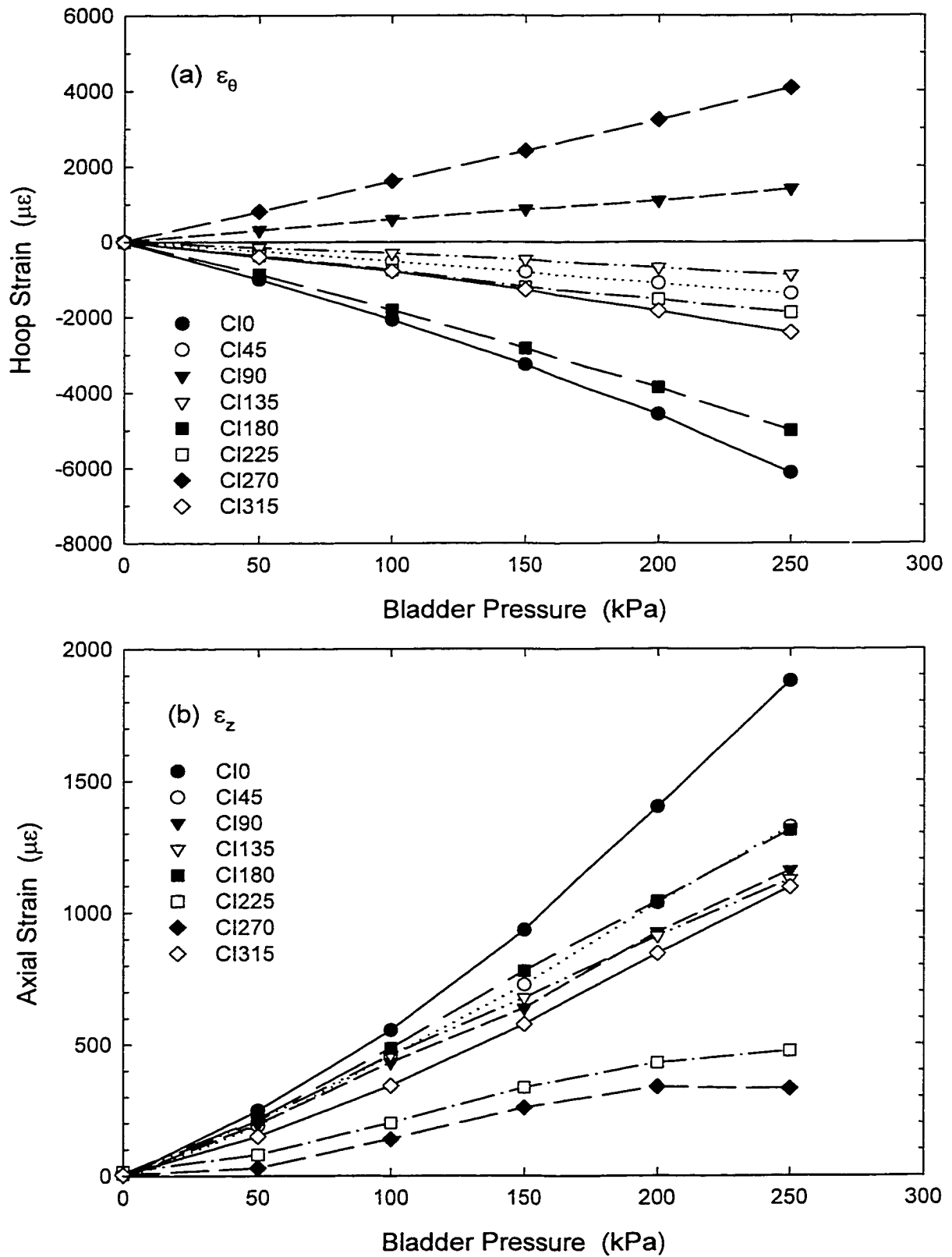


FIGURE AIII.2 Measured (a) hoop and (b) axial strains versus pressure at the interior of Sections C for Test P3a.

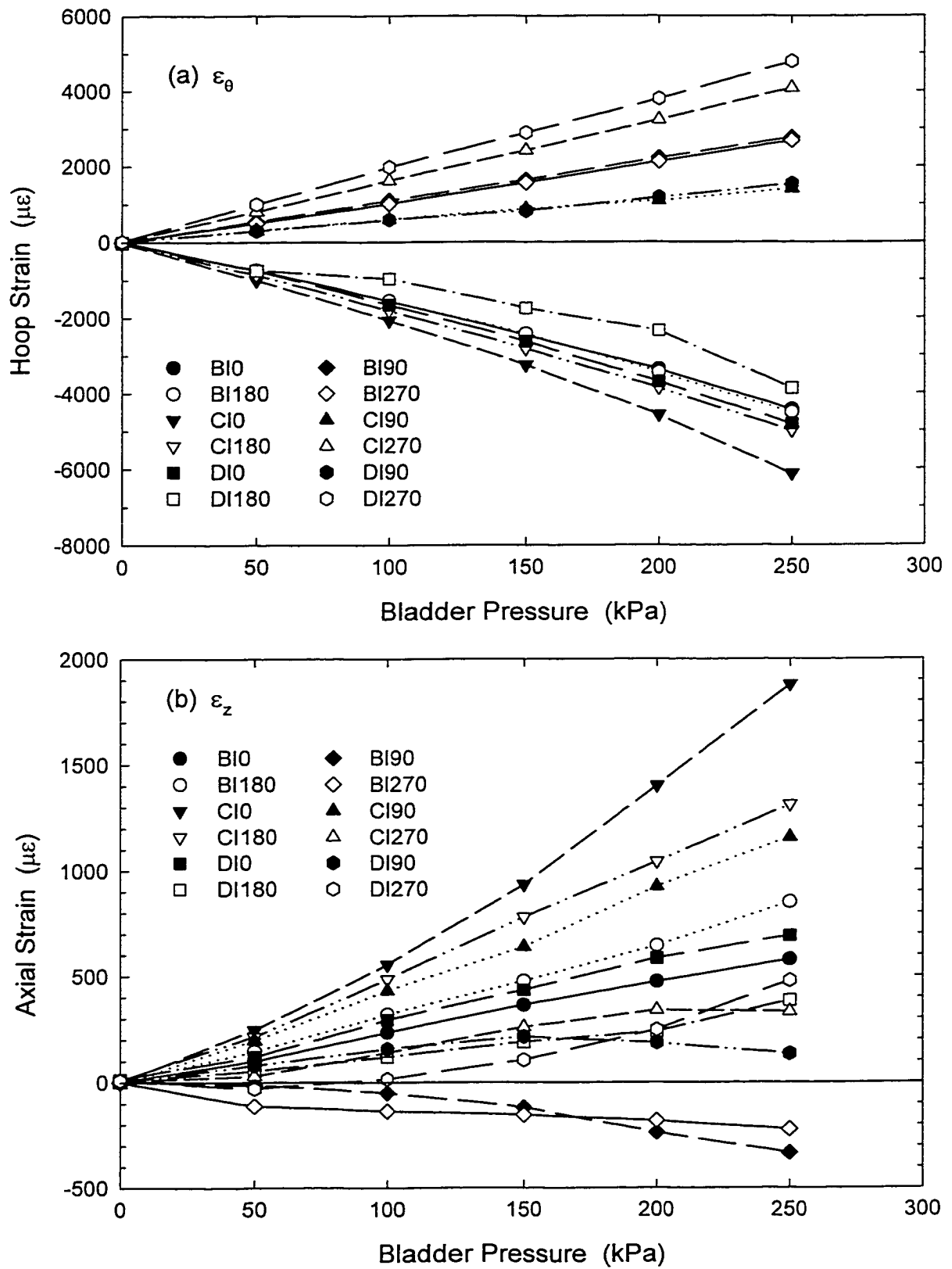


FIGURE AIII.3 Measured (a) hoop and (b) axial strains versus pressure at the interior crown, springline and invert locations at Sections B, C and D for Test P3a.

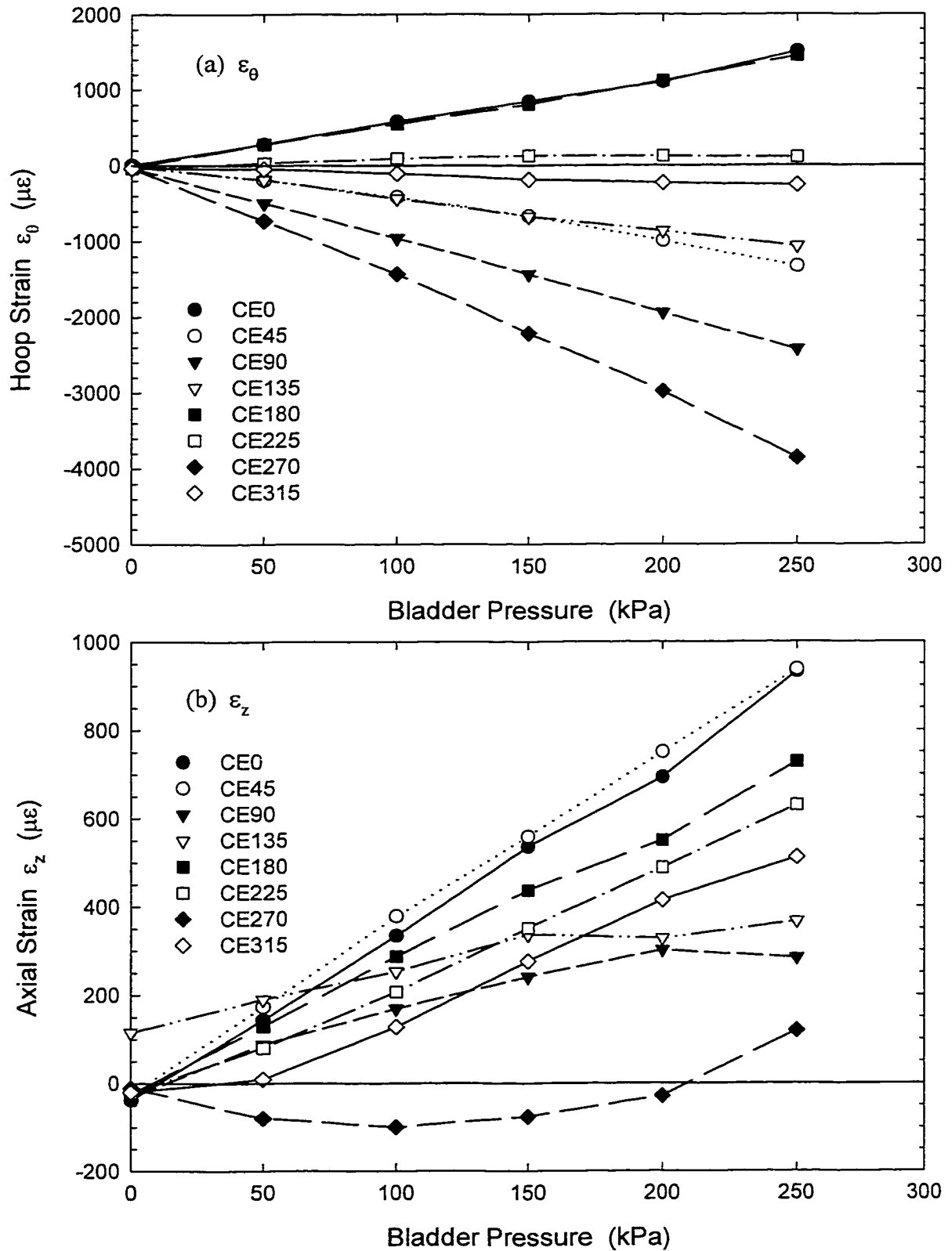


FIGURE AIII.4 Exterior strains ($\mu\epsilon$) versus applied bladder pressure (kPa) at Section C for Test P3a showing: (a) Hoop strains (ϵ_{θ}), and (b) Axial strain (ϵ_z).

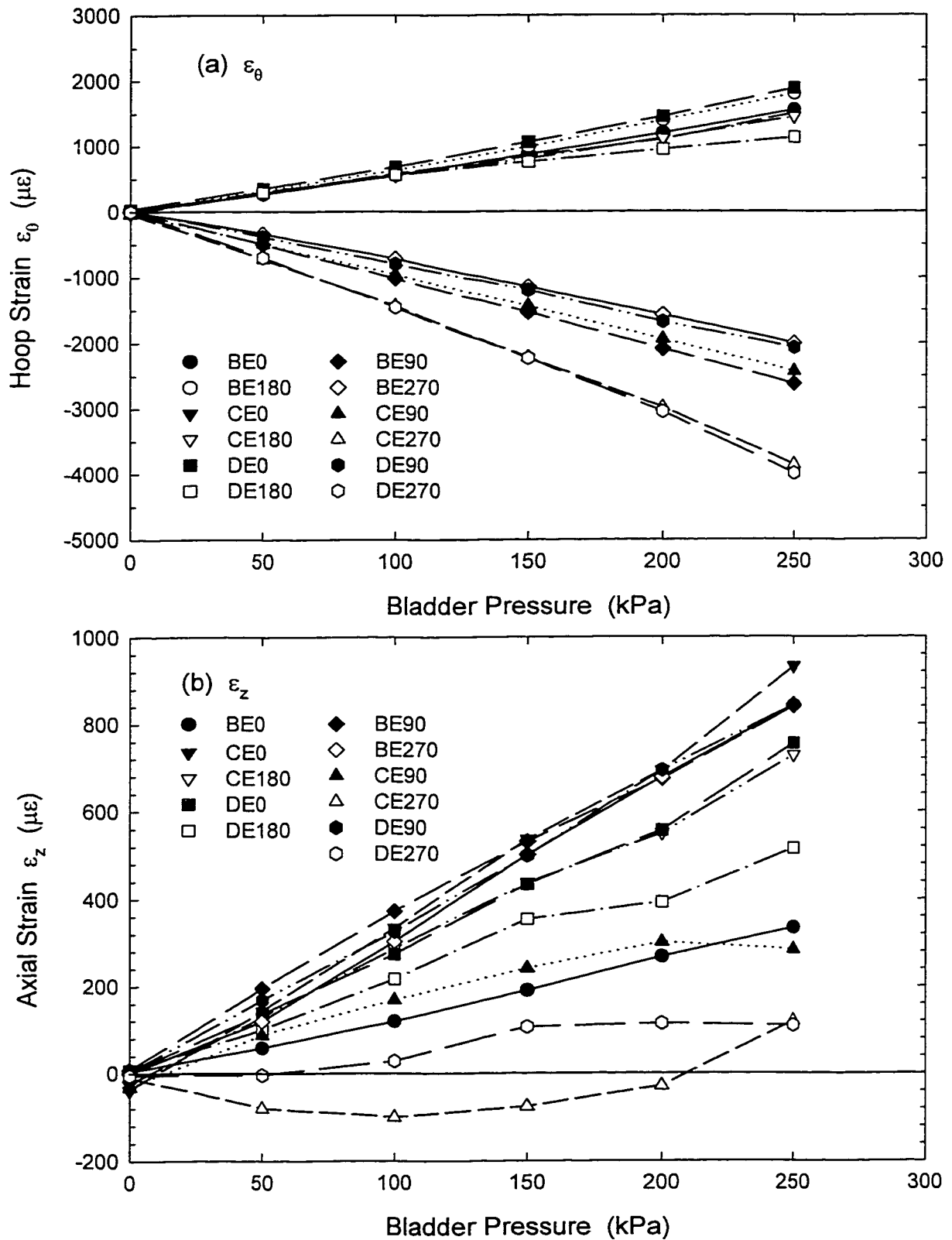


FIGURE AIII.5 Measured (a) hoop and (b) axial strains versus pressure at the exterior crown, springline and invert locations at Sections B, C and D for Test P3a.

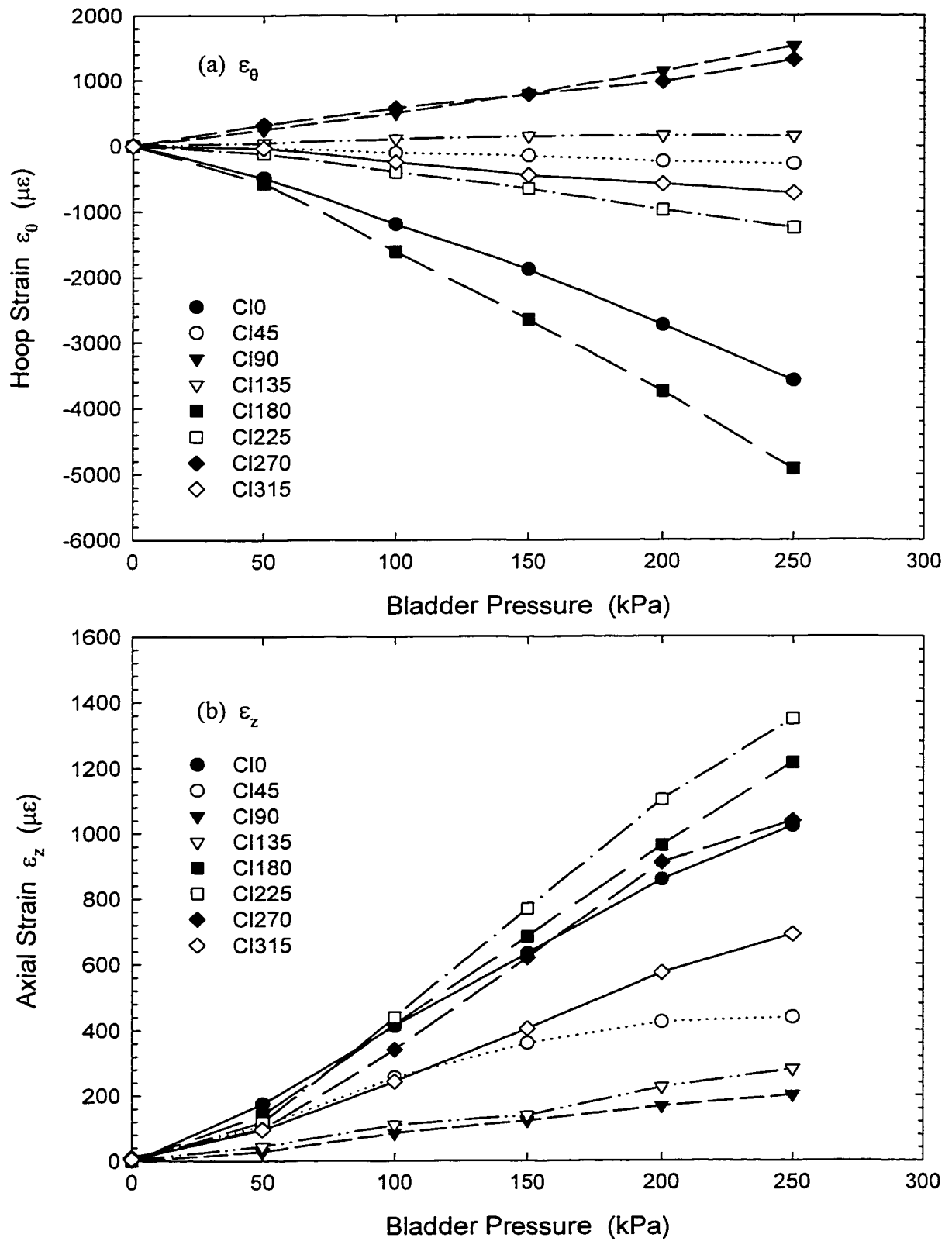


FIGURE AIII.7 Measured strains ($\mu\epsilon$) versus applied bladder pressure (kPa) at Section C for Test P3b showing: (a) Hoop strains (ϵ_θ), and (b) Axial strain (ϵ_z).

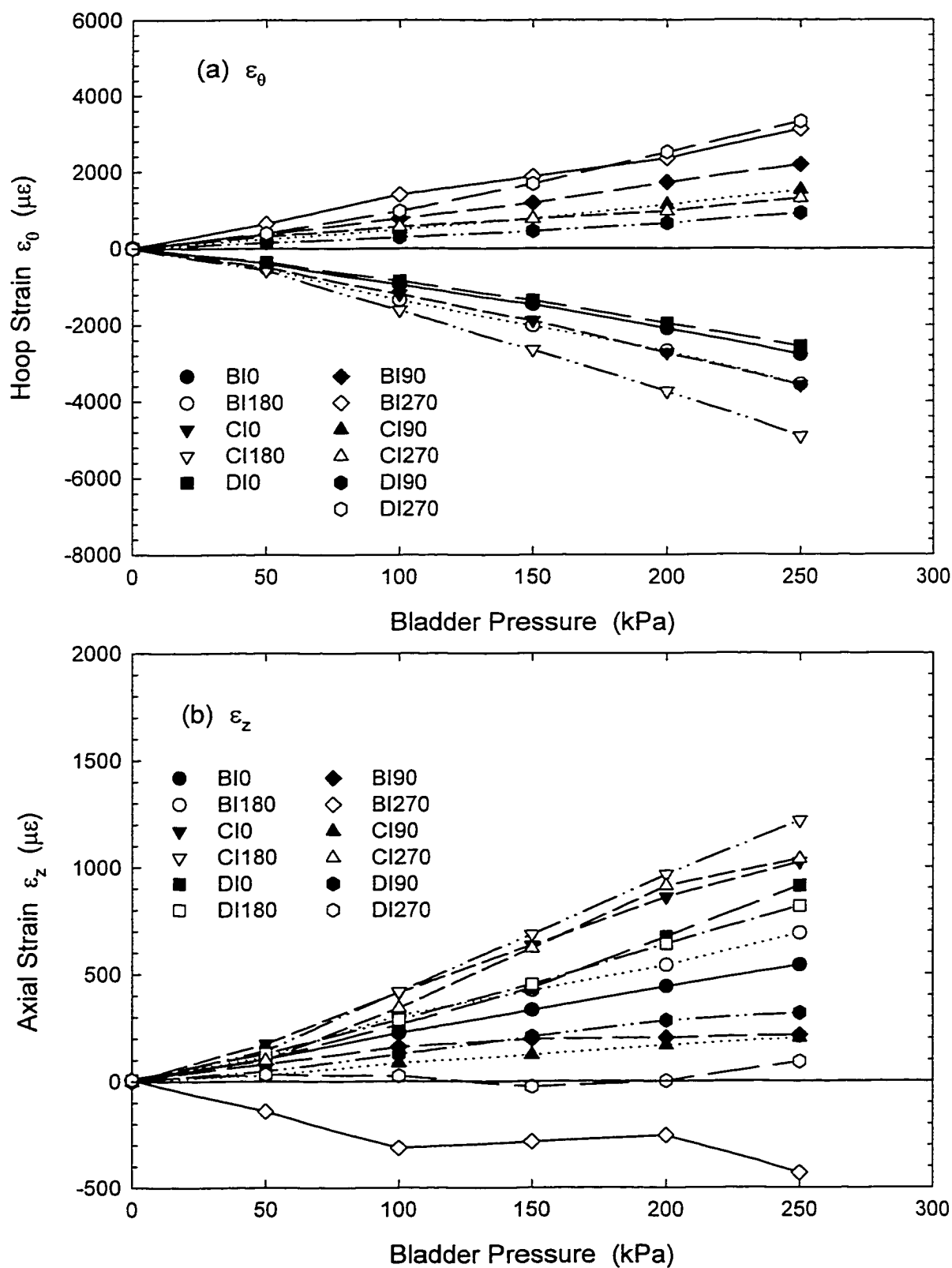


FIGURE AIII.8 Measured (a) hoop and (b) axial strains versus pressure at the interior crown, springline and invert locations at Sections B, C and D for Test P3b.

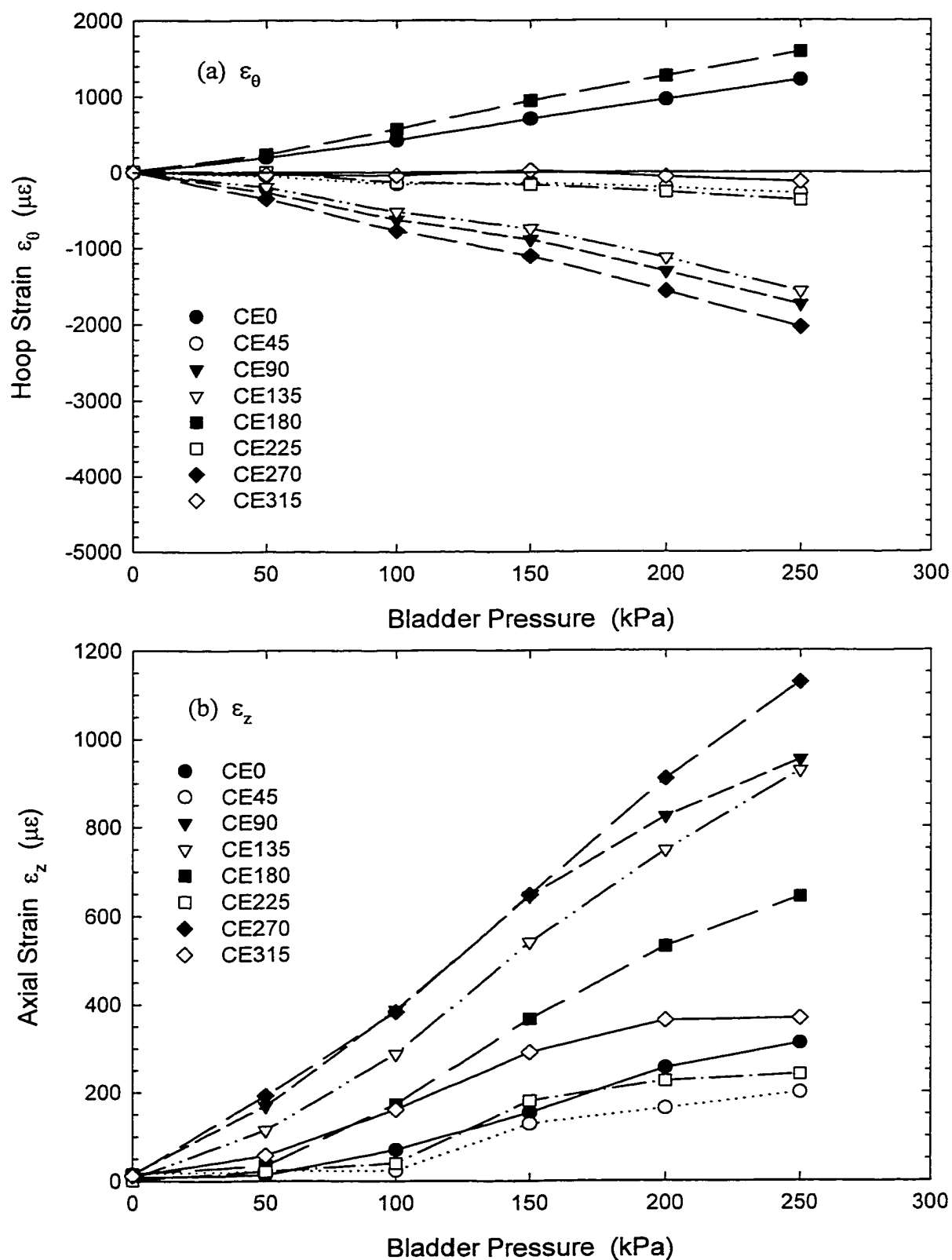


FIGURE AIII.9 Exterior strains ($\mu\epsilon$) versus applied bladder pressure (kPa) at Section C for Test P3b showing: (a) Hoop strains (ϵ_θ), and (b) Axial strain (ϵ_z).

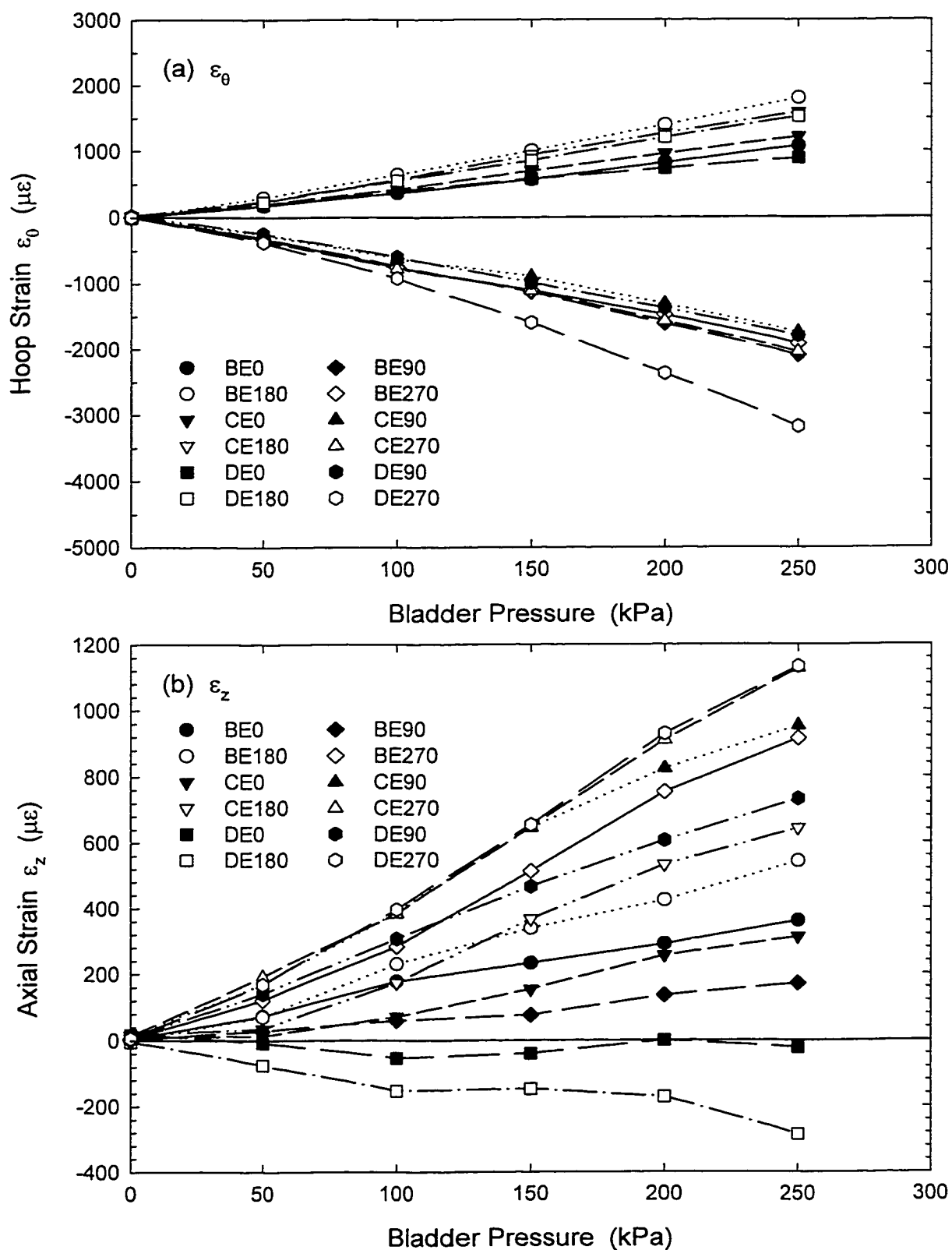


FIGURE AIII.10 Measured (a) hoop and (b) axial strains versus pressure at the exterior crown, springline and invert locations at Sections B, C and D for Test P3b.

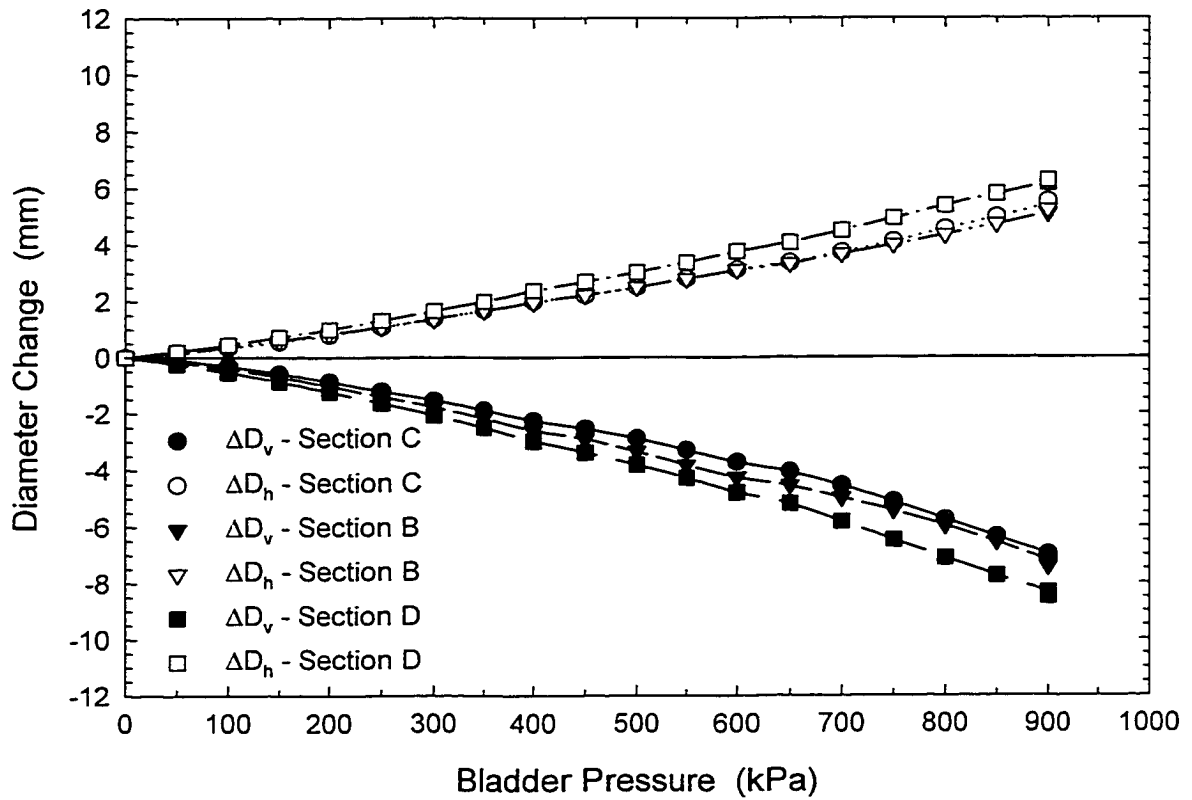


FIGURE AIII.11 Measured vertical ΔD_v and horizontal ΔD_h diameter change for test P3c.

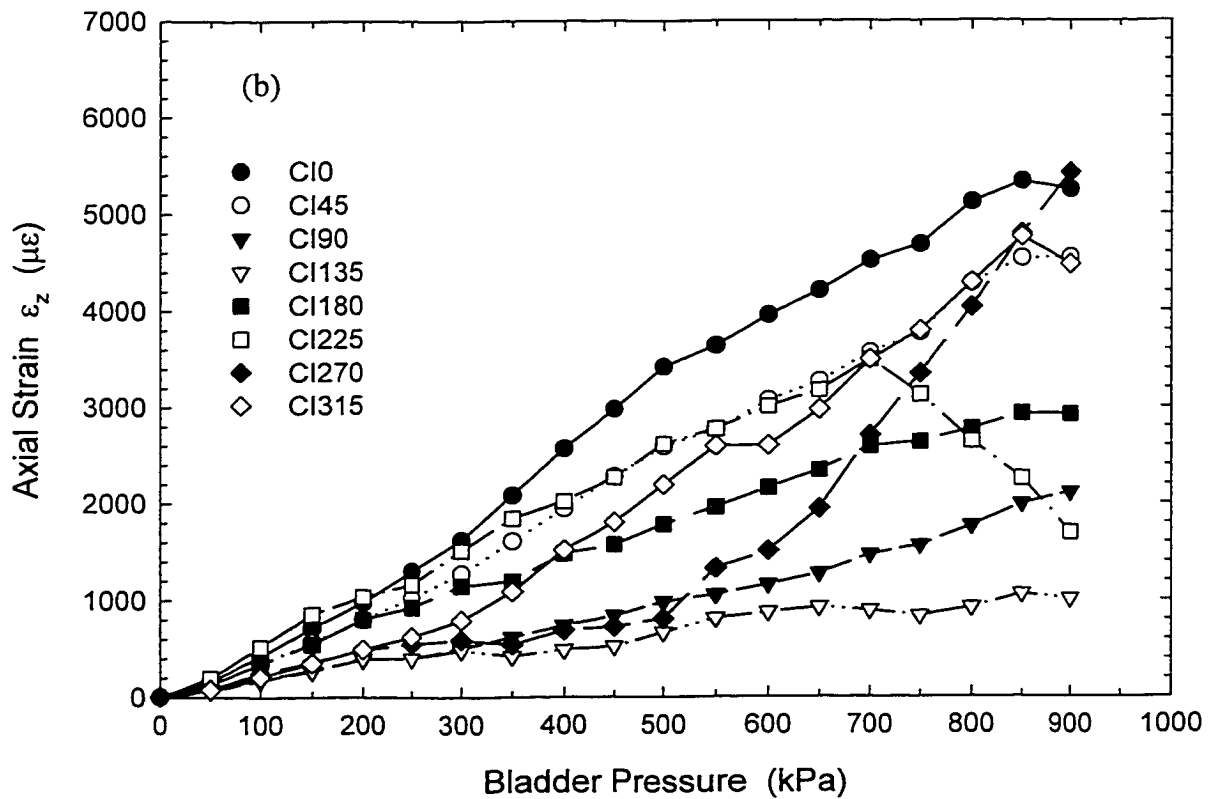
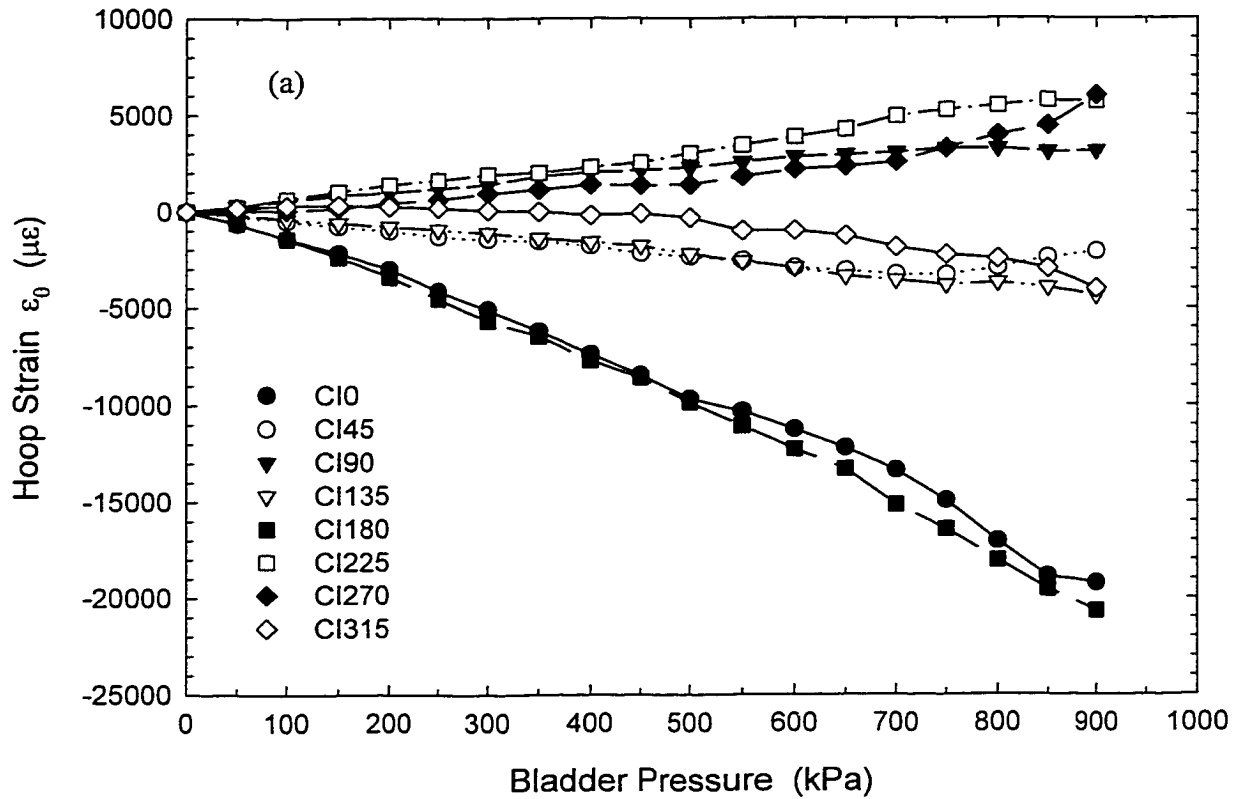


FIGURE AIII.12 Measured strains ($\mu\epsilon$) versus applied bladder pressure (kPa) for Test P3c showing: (a) Hoop strains (ϵ_0), and (b) Axial strain (ϵ_z).

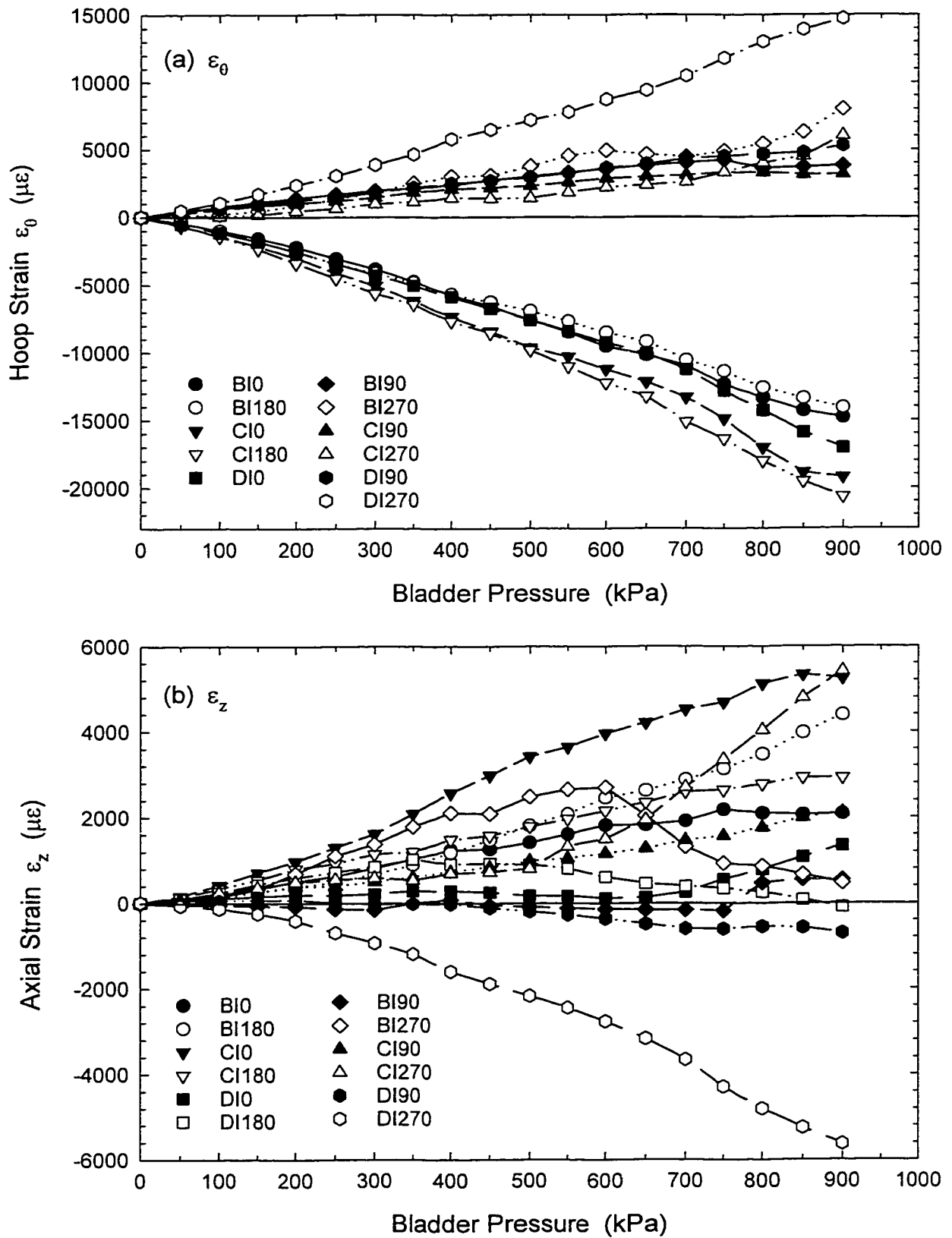


FIGURE AIII.13 Interior strains ($\mu\epsilon$) versus applied bladder pressure (kPa) for Test P3c: (a) Hoop strains (ϵ_{θ}), and (b) Axial strains (ϵ_z) measured at Sections B, C and D.

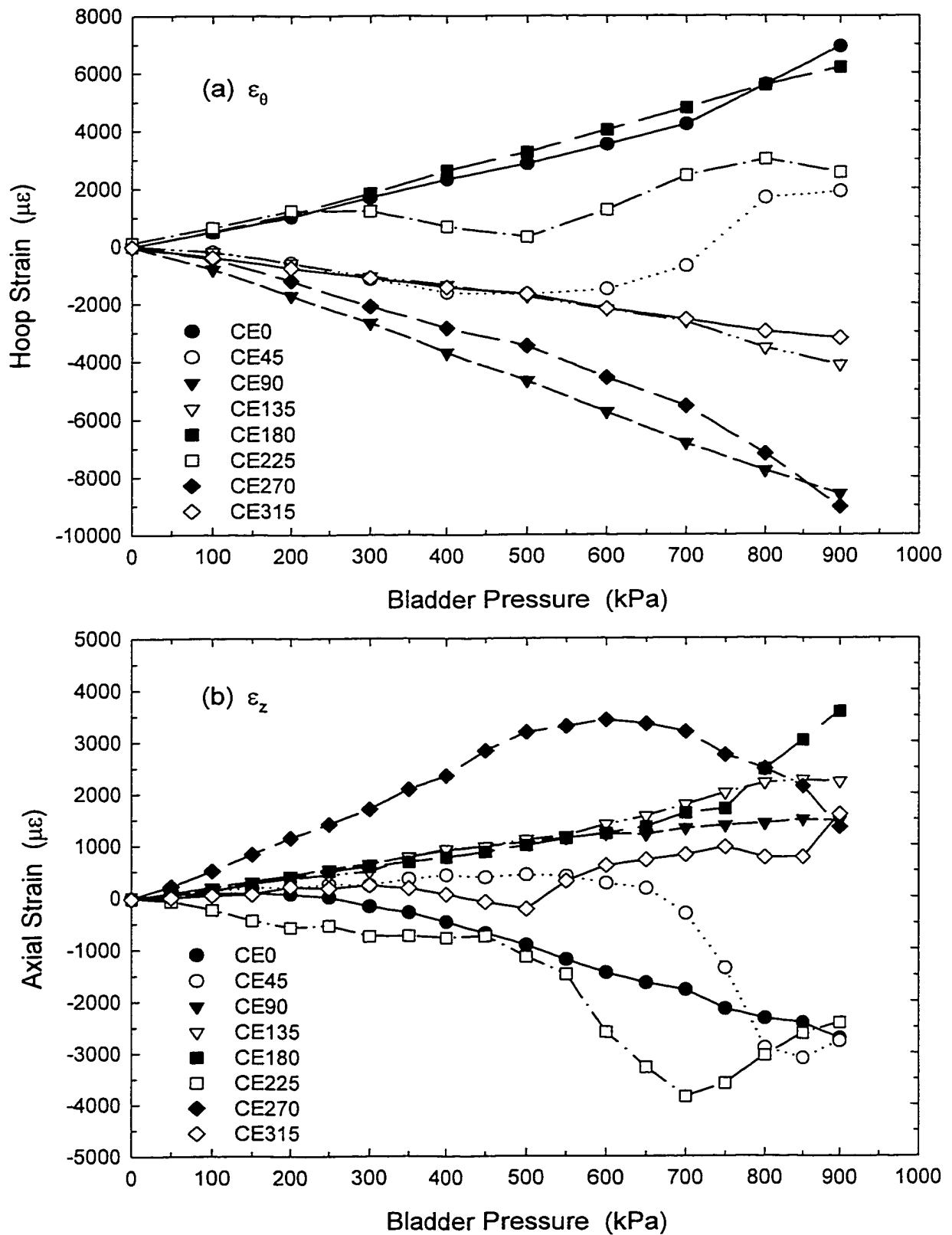


FIGURE AIII.14 Measured exterior (a) hoop and (b) axial strains versus pressure at Section C for Test P3c.

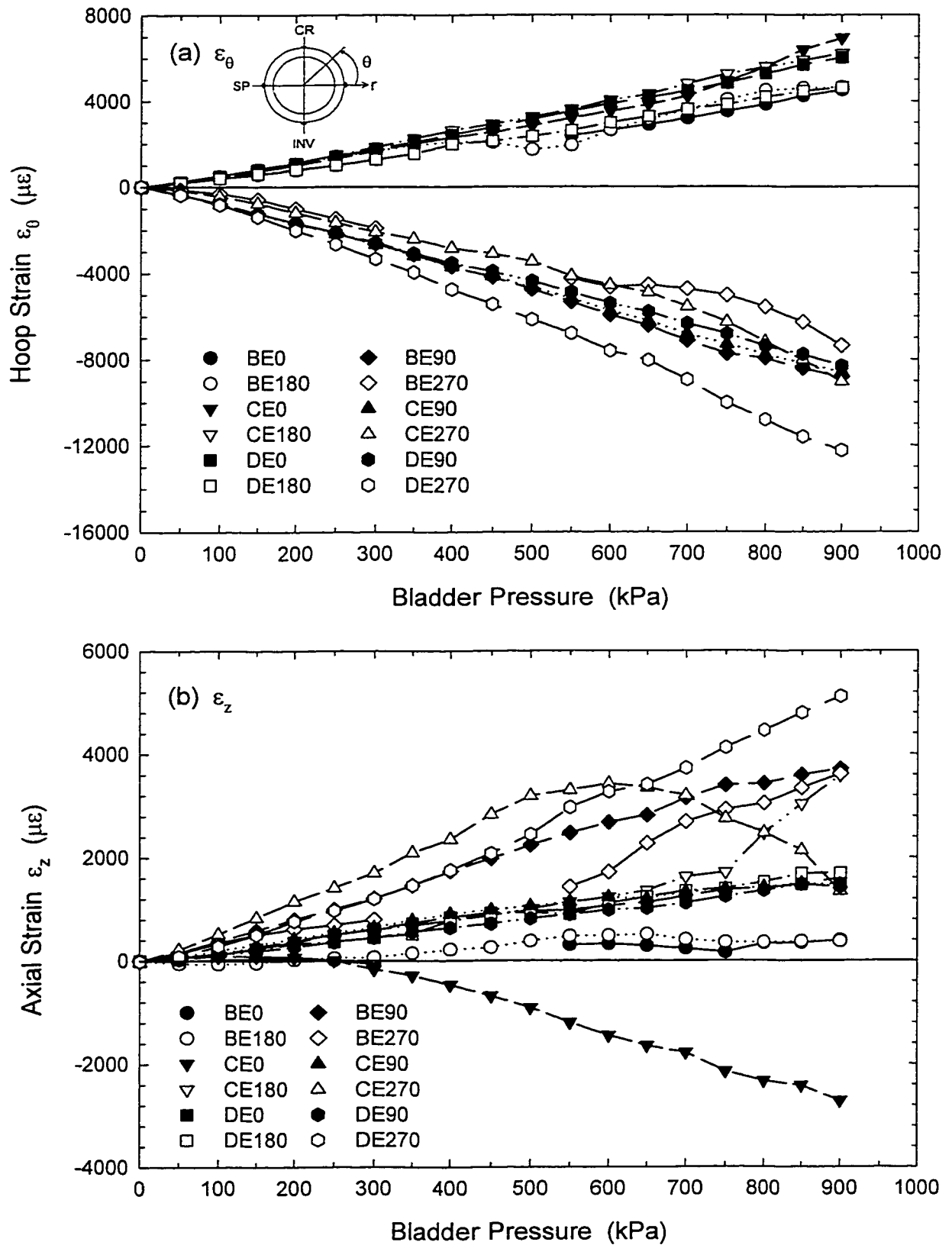


FIGURE AIII.15 Exterior strains ($\mu\epsilon$) versus applied bladder pressure (kPa) for Test P3c: (a) Hoop strains (ϵ_{θ}), and (b) Axial strains (ϵ_z) measured at Sections B, C and D.

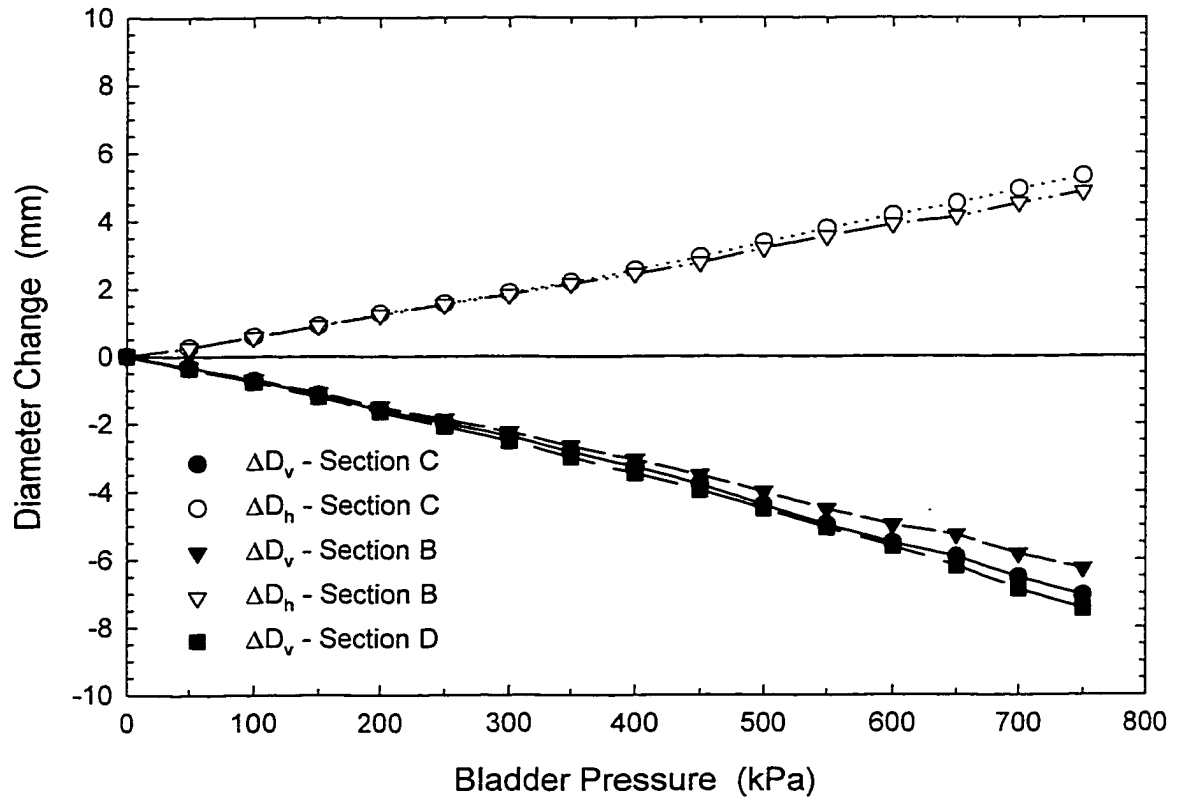


FIGURE AIII.16 Measured vertical ΔD_v and horizontal ΔD_h diameter change for test P4.

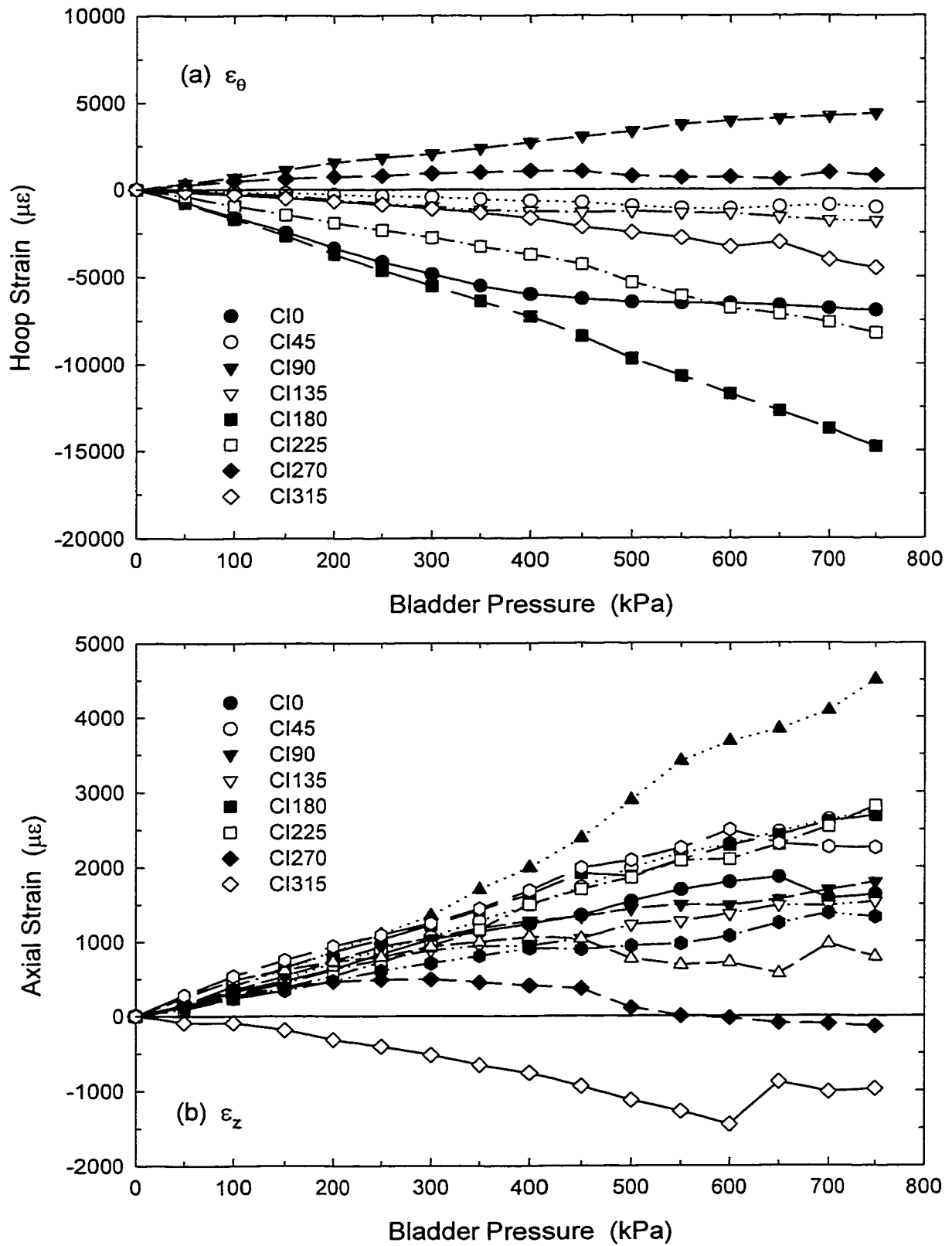


FIGURE AIII.17 Interior strains ($\mu\epsilon$) versus applied bladder pressure (kPa) at Section C for Test P4 showing: (a) Hoop strain (ϵ_{θ}), and (b) Axial strain (ϵ_z).

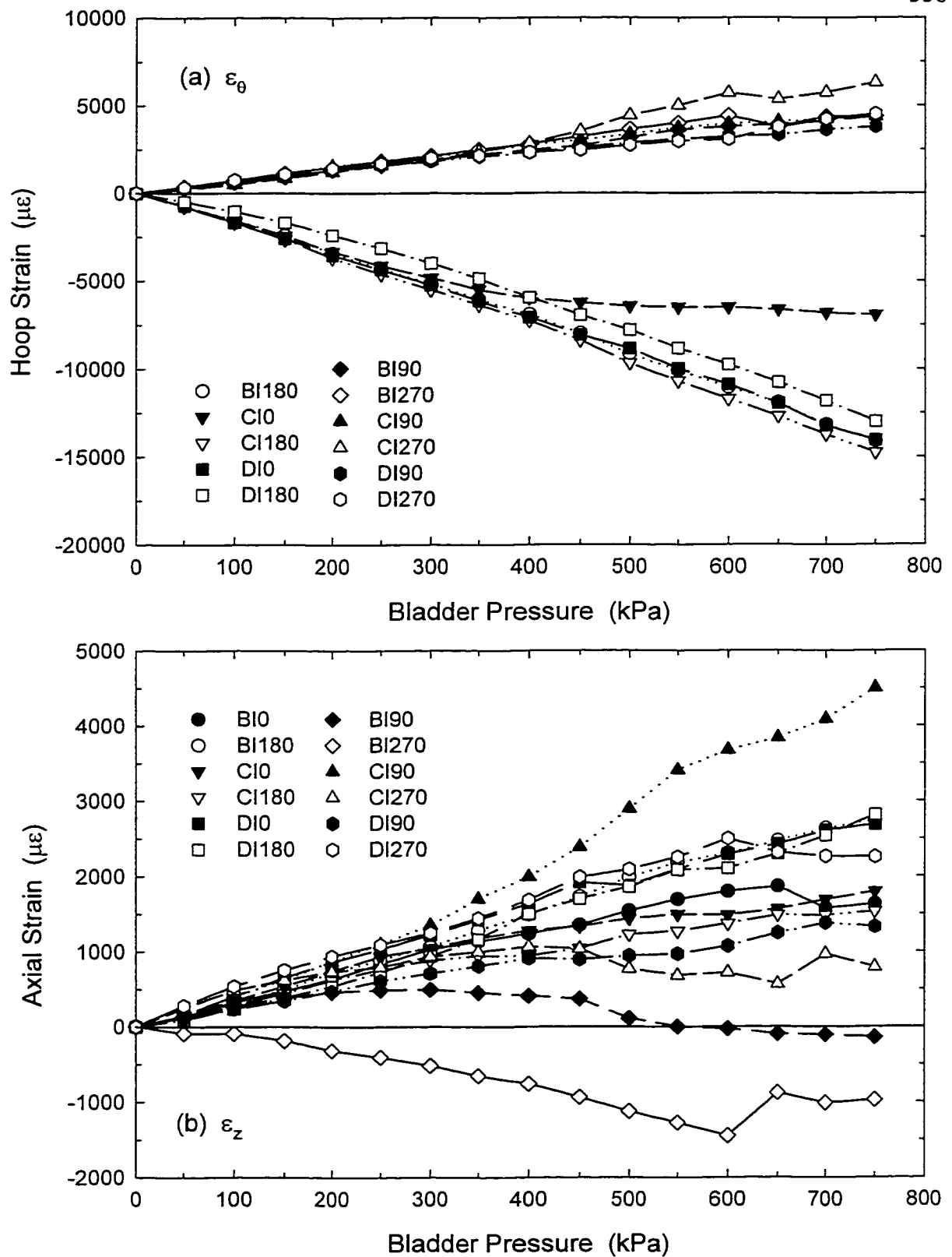


FIGURE AIII.18 Measured (a) hoop and (b) axial strains versus pressure at the interior crown, springline and invert locations at Sections B, C and D for Test P4.

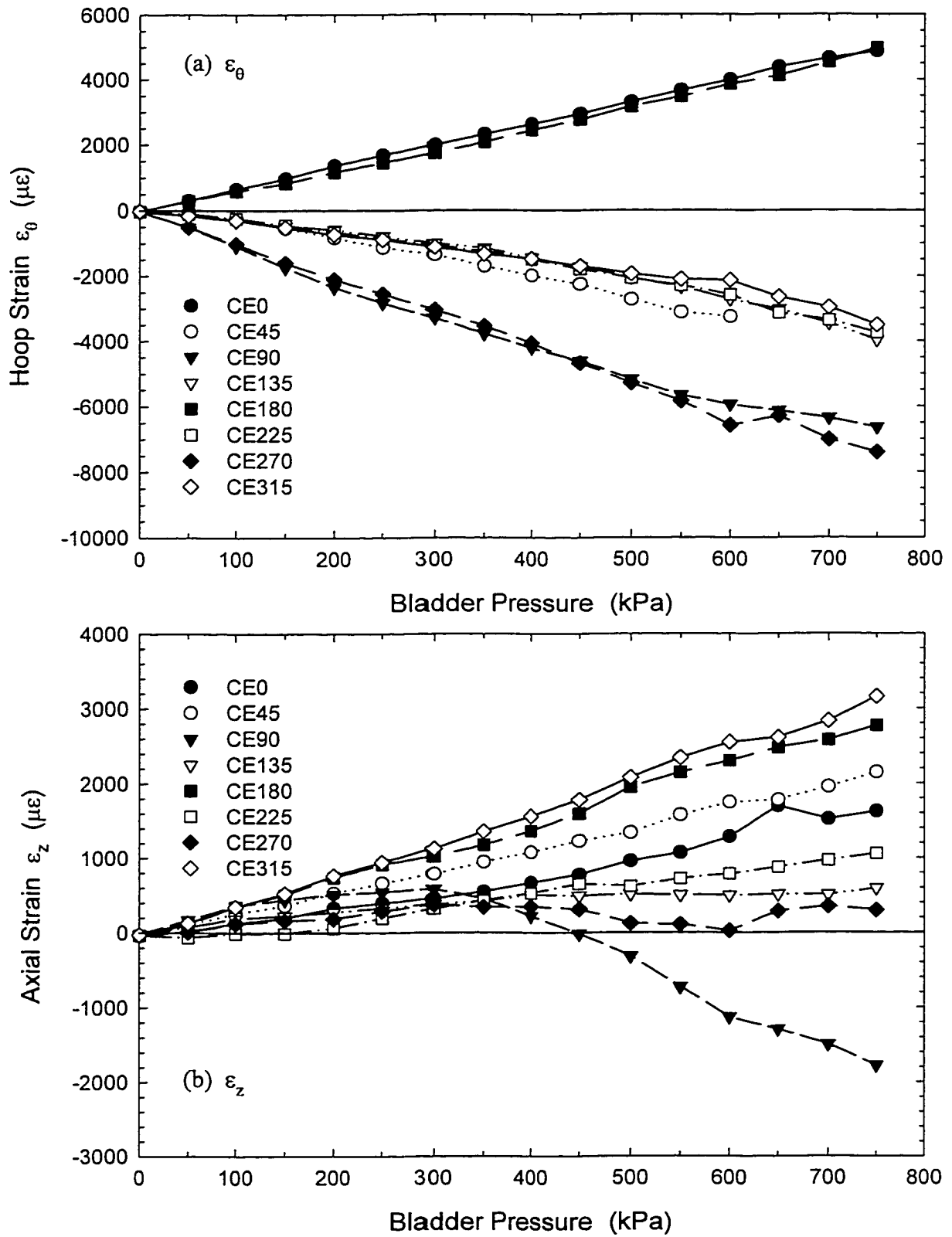


FIGURE AIII.19 Exterior strains ($\mu\epsilon$) versus applied bladder pressure (kPa) at Section C for Test P4 showing: (a) Hoop strains (ϵ_{θ}), and (b) Axial strain (ϵ_z).

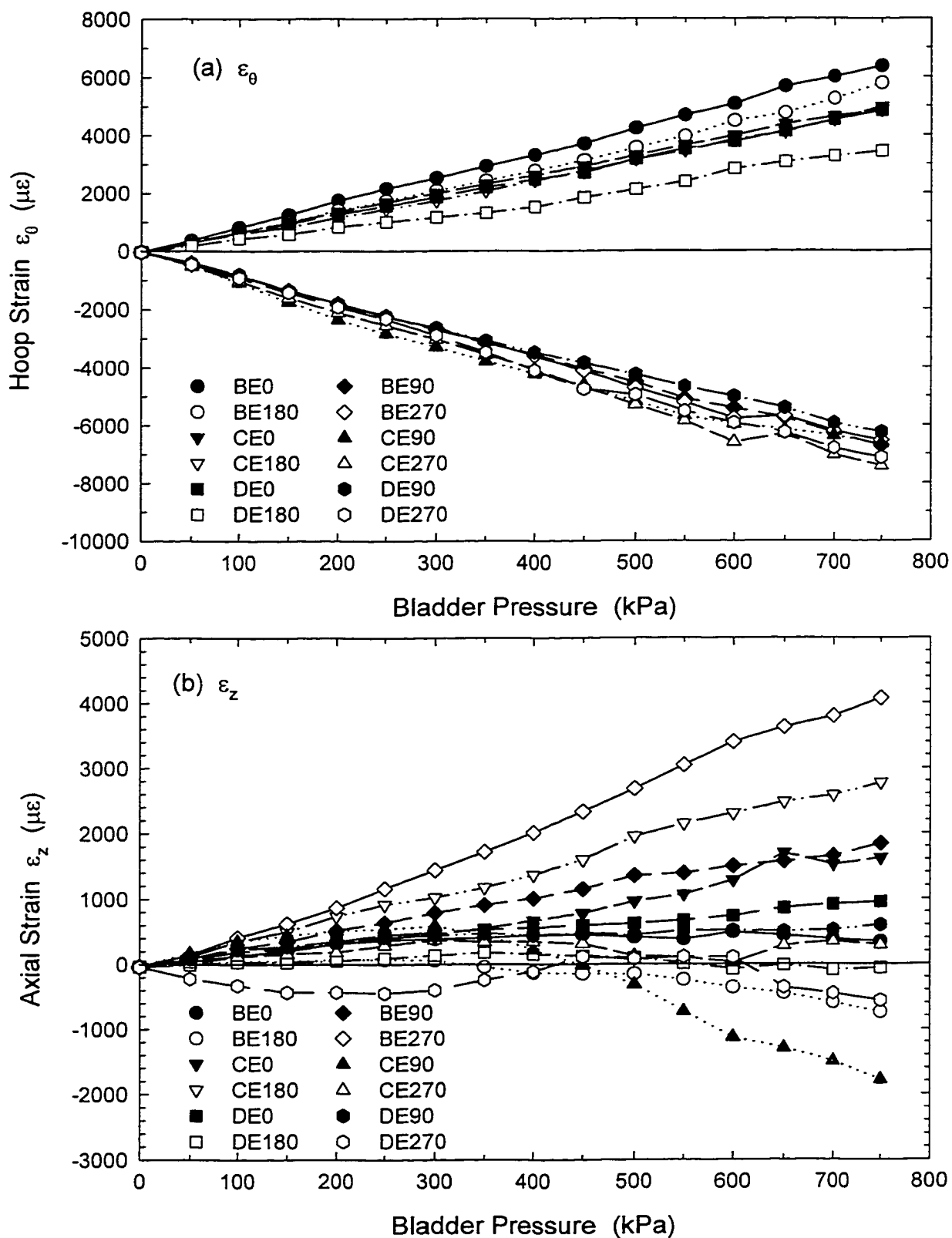


FIGURE AIII.20 Measured (a) hoop and (b) axial strains versus pressure at the exterior crown, springline and invert locations at Sections B, C and D for Test P4.

CURRICULUM VITAE

NAME Richard W.I. Brachman

PLACE AND YEAR OF BIRTH Sudbury, Ontario, 1970

EDUCATION

Bachelor of Engineering Science (B.E.Sc.) - Civil Engineering, 1989 - 1993
 Doctor of Philosophy (Ph.D.) - Geotechnical Engineering, 1993 - 1999
 The University of Western Ontario, London, Canada.

ACADEMIC AWARDS AND ACHIEVEMENTS

Natural Sciences and Engineering Research Council of Canada PGS-B Scholarship, 1995 to 1997
 Graduate Tuition Scholarship, 1995 - 1997
 North American Geosynthetics Society Student Paper Competition, Finalist, 1997
 L.G. Soderman Award, 1996
 Canadian Geotechnical Society Graduate Student Paper Competition, 1995
 Ontario Graduate Scholarship, 1994 - 1995
 Special University Scholarship, 1994
 Amway of Canada Environmental Engineering Scholarship, 1993
 Graduate Entrance Scholarship, 1993
 Canadian Geotechnical Society Undergraduate Thesis Competition, 1993
 Gold Medal in Civil Engineering, 1993
 Dean's Honour List, 1990 - 1993
 Canada Scholar, 1989 - 1993
 Governor General's Award in Environmental Engineering, 1992
 The Frederick Weijerman Memorial Award in Civil Engineering, 1991
 The University of Western Ontario In-Course Scholarship, 1991
 Alexander Spencer Entrance Scholarship in Engineering Science, 1989
 Ontario Scholar, 1989

JOURNAL PUBLICATIONS

Brachman, R.W.I., Moore, I.D., and Rowe, R.K., 1999. The Design of a Laboratory Facility for Evaluating the Structural response of Small Diameter Buried Pipes. *Canadian Geotechnical Journal*, Accepted 25/01/99.

Tognon, A.R.M., Rowe, R.K., and Brachman, R.W.I. 1999 Evaluation of Sidewall Friction for a Buried Pipe Testing Facility. *Geotextiles and Geomembranes*, 17 (4), (In Press).

Brachman, R.W.I., and Moore, I.D. 1998. Numerical Integration During Fourier Integral Analysis. *International Journal for Numerical and Analytical Methods in Geomechanics*, In Press, Accepted 7/16/98.

Brachman, R.W.I., Moore, I.D., and Rowe, R.K., 1996. Interpretation of a buried pipe test: Small diameter pipe in the Ohio University facility. *Transportation Research Record*, 1541, pp. 64 - 70.

VITA continued

JOURNAL PUBLICATIONS continued

- Moore, I.D., and Brachman, R.W.I., 1994. Three Dimensional Analysis of Flexible Circular Culverts, *Journal of Geotechnical Engineering*, **120** (10), pp. 1829-1844.
- Rowe, R.K., and Brachman, R.W.I., 1994. Geosynthetics in Waste Containment Applications, *Engineering Materials for Waste Isolation*, CSCE Special Publication of the Engineering Materials Division, Chapter 1, CSCE, pp. 1-36.

CONFERENCE PUBLICATIONS

- Brachman, R.W.I., Moore, I.D., Lo, K.Y., and Ansari, N., 1998. Performance of a Shoring System with Tie-Back Anchors, 51st Canadian Geotechnical Conference of the Canadian Geotechnical Society, Edmonton, Alberta, pp. 439-446.
- Moore, I.D., Brachman, R.W.I., Rowe, R.K., and Tognon, A., 1998. Analysis of Pipe Structures in Soil Test Cells - Biaxial Pipe Testing at The University of Western Ontario, Transportation Research Board Annual Meeting, Washington, DC, USA, January 1998.
- Brachman, R.W.I., Rowe, R.K., Moore, I.D., and Tognon, A., 1998. Laboratory Investigation of the Effect of Coarse Drainage Stone on the Performance of Leachate Collection Pipes, Sixth International Conference on Geosynthetics, Atlanta, GA, USA, pp. 191-196.
- Brachman, R.W.I. 1997. Hoop compression testing of HDPE leachate collection pipe. Geosynthetics '97, IFAI, Long Beach, CA, USA, pp. 337 - 350.
- Brachman, R.W.I., Rowe, R.K., and Moore, I.D., 1997. Laboratory testing of perforated leachate collection pipes. Proceedings of the 1997 Annual Conference of the Canadian Society for Civil Engineering, May 27-30, Sherbrooke, Quebec, pp. 113-122.
- Brachman, R.W.I., Moore, I.D., and Rowe, R.K., 1996. A new laboratory facility for evaluating the performance of small diameter buried pipes. Proceedings of the 1996 Annual Conference of the Canadian Society for Civil Engineering, Edmonton, Alberta, pp. 72 - 83.
- Moore, I.D., Laidlaw, T.C., and Brachman, R.W.I., 1996. Test cells for static pipe response under deep burial. 49th Canadian Geotechnical Conference of the Canadian Geotechnical Society, St. John's, Newfoundland, pp. 737 - 744.

RELATED WORK EXPERIENCE

- Department of Civil and Environmental Engineering, The University of Western Ontario
Lecturer, Sept.- Dec. 1997
Teaching Assistant, 1993 - 1998
- Department of Civil and Environmental Engineering, University of Alberta
Assistant Professor, Nov. 1998 - present